THE GEOLOGY AND GEOCHEMISTRY OF THE STERKSPRUIT INTRUSION, BARBERTON MOUNTAIN LAND, MPUMALANGA PROVINCE

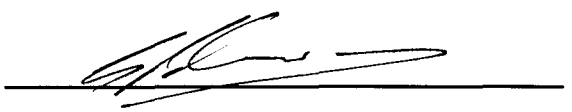
Gavin Patrick Conway

A dissertation submitted to the Faculty of Science, University of the Witwatersrand, Johannesburg, in fulfilment of the requirements for the degree of Master of Science.

Johannesburg, 1997

DECLARATION

I declare that this dissertation is my own, unaided work. It is being submitted for the Degree of Master of Science in the University of the Witwatersrand, Johannesburg. It has not been submitted before for any degree or examination in any other University.



14 day of August 19 97

ABSTRACT

The Sterkspruit Intrusion, in the south-western portion of the Barberton greenstone belt, is a sill-like body containing rocks of gabbroic to dioritic composition. It is hosted by a sequence of komatiitic basalts and komatiites of the Lower Onverwacht Group. The intrusion is considered unique in this area in that it lacks ultramafic components and has no affinities with the surrounding mafic- to- ultramafic lavas. The gabbroic suite also contains an unusual abundance of quartz, and the chill margin shows an evolved quartz-normative, tholeiitic parental magma. Based on petrographic and geochemical evidence, the intrusion can be subdivided into four gabbroic zones and a quartz diorite, which is an end product of a differentiating magma. The chill margin records an MgO content of 4.8%, an Mg# of 42, an SiO_2 value of 52.5% and a normative plagioclase composition of An_{44}. The sill-like nature of the body, indicated by geochemical trends, and the steep sub-vertical layering, point to a body that has been tilted along with the surrounding lavas. This constrains the relative age of the body to be older than the emplacement of the Kaap Valley and Nelshoogte Plutons, which caused the regional deformation observed in the Nelshoogte Schist Belt. A sequence of tholeiitic to andesitic basalts from the Kromberg Formation in the Upper Onverwacht Group, have compositions which can be correlated with the Sterkspruit Intrusion. It is possible that this body represents a subvolcanic magma chamber, which acted as a feeder to tholeiitic lavas higher up in the volcanic sequence. The Sterkspruit Mafic Dyke Swarm intruded the southern Nelshoogte Schist Belt and displays intra-dyke chemical variation.

DEDICATION

This work is dedicated to Julie, and Shona Gabriela

And for my parents, Bernie and Shirley Conway

ACKNOWLEDGEMENTS

I would like to acknowledge the support, guidance and encouragement from my supervisor, Professor Carl Anhaeusser. Thanks must also go to Dr. Michael Meyer, my co-supervisor early on in the project, and to Professor Grant Cawthorn for assistance with certain aspects of the project. Mrs Nellie Day at the RAU Geology Department assisted me with microprobe analyses. The Foundation for Research and Development is acknowledged for financial support. The support and assistance of Dr. Hannes Henckel is greatly appreciated, as is the assistance with mineralogy from Mr Gavin Martin and Mr Tom Evers at the Gold Fields Mineralogy Unit. Thanks must also go to Gold Fields of South Africa for providing logistical support during field work. Mr Frik Van der Merwe and Mrs Meyer at the Gold Fields Geological Centre drafting department, took care of all my drafting requirements for which I am most grateful. Finally, my thanks and appreciation must go to my wife Julie, for all her support and assistance during the course of this project.

CONTENTS

	Page
Declaration	ii
Abstract	iii
Dedication	iv
Acknowledgements	v
List of Figures	ix
List of Tables	xiii
List of Plates	xiv
List of Tables in Appendix A	xix
CHAPTER ONE - INTRODUCTION	1
1.1 Location of the Study Area	1
1.2 Previous Work	3
1.3 Physiography and Climate	5
1.4 Research Objectives	5
1.5 Research Methods	7
CHAPTER TWO - REGIONAL GEOLOGICAL DESCRIPTION	8
2.1 Geology of the Barberton Mountain Land	8
2.2 Metamorphism	15
CHAPTER THREE - GEOLOGY OF THE STERKSPRUIT INTRUSION AND MAFIC DYKE SWARM	16
3.1 Geology of the Nelshoogte Schist Belt	16
3.2 Description of the Geological Map	21
3.3 Geology of the Sterkspruit Intrusion	22
3.3.1 Morphology	22
3.3.2 Lithology	24
3.3.3 Structure	32
3.4 Geology of the Sterkspruit Mafic Dyke Swarm	38
CHAPTER FOUR - PETROGRAPHY	42
4.1 Introduction	42
4.2 Alteration	43
4.2.1 Saussuritisation	43
4.2.2 Albitisation	43
4.2.3 Uralitisation	44
4.2.4 Epidotisation	44
4.2.5 Chloritisation	44
4.2.6 Carbonation	45

Page

4.3 Petrography of the Sterkspruit Intrusion 45
4.3.1 Marginal Zone Gabbro 45
4.3.2 Lower Zone Gabbro 50
4.3.3 Central Zone Gabbro 52
4.3.4 Quartz Diorite 54
4.3.5 Upper Zone Gabbro 57
4.3.6 Gabbroic Lens 59
4.4 Petrography of the Sterkspruit Mafic Dyke Swarm 59

CHAPTER FIVE - GEOCHEMISTRY 63

5.1 Introduction 63
5.2 Sampling Method 63
5.2.1 Traverse 1 64
5.2.2 Traverse 2 64
5.2.3 Traverse 3 65
5.2.4 Mafic Dykes 65
5.3 Analytical Techniques 66
5.4 Alteration and Element Mobility 67
5.5 Mineral Chemistry 68
5.5.1 Plagioclase 68
5.5.2 Pyroxene 73
5.6 Whole-rock Geochemistry of the Sterkspruit Intrusion 75
5.6.1 Bulk Geochemistry 75
5.6.2 Classification 78
5.6.3 Major Oxide and Trace Element Variation 82
5.6.4 Rare Earth Element Geochemistry 98
5.6.5 Normalised Multi-element Diagrams (Spider Diagrams) 102
5.6.6 Trace-element Discrimination Diagrams - Tectonic Setting 105
5.7 Whole-rock Geochemistry of the Sterkspruit Mafic Dyke Swarm 109
5.7.1 Introduction 109
5.7.2 Classification 109
5.7.3 Binary Variation Diagrams 114
5.7.4 Trace-element Discrimination Diagrams - Tectonic Setting 115

CHAPTER SIX - COMPARISONS WITH OTHER MAFIC COMPLEXES 119

6.1 Description of Mafic Complexes 119
6.1.1 Southern Africa - Usushwana Complex 119
6.1.2 Western Australia - Mt Kilkenny Layered Sill 121
6.1.3 Greenland - Skaergaard Intrusion 122
6.1.4 Canada - Superior Province 123
6.1.5 United States - Midcontinent Rift, Duluth Complex 124
6.2 Comparison Between the Sterkspruit Intrusion and other Mafic Complexes 125

Page

CHAPTER SEVEN - COMPARISONS WITH VOLCANIC ROCKS FROM THE ONVERWACHT GROUP 131

7.1 Comparisons with Volcanic Rocks from the Nelshoogte Schist Belt 131
7.2 Comparisons with Tholeiitic Basalts from the Onverwacht Group 134

CHAPTER EIGHT - DISCUSSION 140

CHAPTER NINE - CONCLUSIONS 147

LIST OF REFERENCES 151

APPENDIX A

LIST OF FIGURES

		Page
Figure 1 :	Regional Geological Map of the Barberton Greenstone Belt, showing the locality of the Sterkspruit Intrusion and study area.	2
Figure 2 :	Geological map of the Sterkspruit Intrusion and Mafic Dykes, Barberton Mountain Land.	*
Figure 3 :	Geological outline of the Sterkspruit Intrusion and Mafic Dyke Swarm, showing sample localities.	*
Figure 4:	Sketch map of Traverse 1 across the Sterkspruit Intrusion showing geological descriptions and sample localities.	26
Figure 5 :	Sketch map of Traverse 2 across the Sterkspruit Intrusion showing geological descriptions and sample localities.	27
Figure 6 :	Sketch map of Traverse 3 across the northern portion of the Sterkspruit Intrusion showing geological descriptions and sample localities.	28
Figure 7 :	Cryptic variation in plagioclase with stratigraphic height in the Sterkspruit Intrusion - Traverse 1.	72
Figure 8 :	Cryptic variation in plagioclase with stratigraphic height in the Sterkspruit Intrusion - Traverse 2.	72
Figure 9 :	AFM (Na_2O+K_2O - $FeO+Fe_2O_3$ - MgO) diagram of the Sterkspruit Intrusion showing the gabbroic zones and Fe enrichment trend.	80
Figure 10 :	AFM (Na_2O+K_2O - $FeO+Fe_2O_3$ - MgO) diagram comparing the Sterkspruit Intrusion to trends from other layered complexes.	80
Figure 11 :	SiO_2 vs Total Alkali diagram for rocks from the Sterkspruit Intrusion showing the tholeiitic composition of the gabbro (after MacDonald and Katsura, 1964).	81
Figure 12 :	Cation ternary diagram ($Fe^{2+}+Fe^{3+}+Ti$ - Al - Mg) of the Sterkspruit Intrusion (after Jensen, 1976).	81

* Figures 2 and 3 are included in the back inside cover

		Page
Figure 13 :	Whole-rock compositional variations with stratigraphic height across the Sterkspruit Intrusion - Traverse 1. The base of the intrusion is on the NW side of the intrusion which youngs towards the SE.	90
Figure 14 :	Whole-rock compositional variations with stratigraphic height across the Sterkspruit Intrusion - Traverse 2. The base of the intrusion is on the NW side of the intrusion which youngs towards the SE.	91
Figure 15 :	Whole-rock compositional variations with stratigraphic height across the Sterkspruit Intrusion - Traverse 3. The base of the intrusion is on the NW side of the intrusion which youngs towards the SE.	92
Figure 16 :	Chemical variation diagrams of gabbroic rocks from the Sterkspruit Intrusion with SiO_2 plotted against (a) MgO, (b) Al_2O_3 and (c) TiO_2.	95
Figure 17 :	Chemical variation diagrams of gabbroic rocks from the Sterkspruit Intrusion with MgO plotted against (a) Al_2O_3, (b) P_2O_5 and (c) FeO/MgO.	96
Figure 18 :	Chemical variation diagrams of gabbroic rocks from the Sterkspruit Intrusion with Zr plotted against (a) Nb, (b) Ti/Zr and (c) Ni.	97
Figure 19 :	Chondrite normalised REE patterns of the (a) Marginal Zone, (b) Lower Zone, (c) Central Zone and (d) Upper Zone from the Sterkspruit Intrusion.	101
Figure 20 :	Chondrite normalised multi-element (spider diagram) of (a) gabbro samples SG25, SG31 and p1 from the Sterkspruit Intrusion, (b) average >3.0Ga and 2.5-3.0Ga greenstone belt basalts for the Archaean, after Condie (1990) and (c) average N-MORB, E-MORB and OIB after Floyd (1991).	104
Figure 21 :	Ti - Zr - Y discrimination diagram for the Sterkspruit Intrusion (after Pearce and Cann, 1973).	107

		Page
Figure 22 :	Ti - Zr discrimination diagram for the Sterkspruit Intrusion (after Pearce and Cann, 1973).	108
Figure 23 :	Zr/Y - Ti/Y discrimination diagram for the Sterkspruit Intrusion (after Pearce and Gale, 1977).	108
Figure 24 :	SiO_2 vs Total Alkali diagram for rocks from the Sterkspruit mafic dykes showing their subalkaline composition (after MacDonald and Katsura, 1964). A - D are the dyke groups referred to in the text.	111
Figure 25 :	Classification of the Sterkspruit mafic dykes according to their cation proportions of (Fe^{2+} + Fe^{3+} + Ti) - Al - Mg (after Jensen, 1976). A - D refer to the dyke groups.	113
Figure 26 :	AFM (Na_2O+K_2O - FeO+Fe_2O_3 - MgO) diagram of the Sterkspruit mafic dykes. The trend of the Sterkspruit Intrusion (s - s) is shown for comparison.	113
Figure 27 :	Major oxide binary plots showing intra-dyke swarm variation. A, B, C, D indicated on the diagrams refer to dyke groups as discussed in the text.	116
Figure 28 :	Trace-element binary plots showing intra-dyke swarm variation. A, B, C, D indicated on the diagrams refer to dyke groups as discussed in the text.	117
Figure 29 :	Ti - Zr - Y discrimination diagram for the Sterkspruit mafic dykes (after Pearce and Cann, 1973). A - D are the dyke groups referred to in the text.	118
Figure 30 :	Ti - Zr discrimination diagram for the Sterkspruit Mafic Dykes (after Pearce and Cann, 1973).	118
Figure 31 :	MgO - CaO - Al_2O_3 ternary diagram comparing gabbroic rocks from complexes on the Kaapvaal Craton with the Sterkspruit Intrusion gabbros. Data breaks separating komatiitic basalt fields after Viljoen *et al.* (1982).	130
Figure 32 :	Cation ternary diagram (Fe^{2+}+Fe^{3+}+Ti - Al - Mg) comparing gabbroic rocks from complexes on the Kaapvaal Craton with the Sterkspruit Intrusion (after Jensen, 1976).	130

		Page
Figure 33 :	MgO - CaO - Al_2O_3 ternary diagram comparing volcanic rocks from the Onverwacht Group with gabbroic rocks from the Sterkspruit Intrusion. Data breaks separating komatiitic basalt fields after Viljoen *et al.* (1982).	133
Figure 34 :	Cation ternary diagram (Fe^{2+}+Fe^{3+}+Ti - Al - Mg) comparing volcanic rocks from the Onverwacht Group with gabbroic rocks from the Sterkspruit Intrusion (after Jensen, 1976).	133
Figure 35 :	Bivariate diagrams of major oxides and trace elements plotted against (a) MgO and (b) Zr, comparing gabbros from the Sterkspruit Intrusion with tholeiitic basalts from the Onverwacht Group.	139

LIST OF TABLES

		Page
Table 1 :	Lithostratigraphy of the Barberton Sequence	14
Table 2 :	Microprobe analyses of plagioclase from Traverse 1	70
Table 3 :	Microprobe analyses of plagioclase from Traverse 2	71
Table 4 :	Microprobe analyses of plagioclase, clinopyroxene and orthopyroxene	74
Table 5 :	Comparison of chill margin and calculated bulk compositions of the Sterkspruit Intrusion	76
Table 6 :	Whole-rock geochemical data from the Sterkspruit Intrusion Marginal Zone	83
Table 7 :	Whole-rock geochemical data from the Sterkspruit Intrusion Lower Zone	84,85
Table 8 :	Whole-rock geochemical data from the Sterkspruit Intrusion Central Zone and Quartz Diorite	86
Table 9 :	Whole-rock geochemical data from the Sterkspruit Intrusion Upper Zone	87
Table 10 :	Average chondrite-normalised rare earth element abundances from the Sterkspruit Intrusion	99
Table 11 :	Average whole-rock geochemical data of dyke groups from the Sterkspruit Mafic Dyke Swarm in comparison with dykes of similar and younger age	110
Table 12 :	Selected whole-rock geochemical data of gabbroic rocks from the Stolzburg, Usushwana and Uitkomst Complexes	126
Table 13 :	Selected whole-rock geochemical data of komatiitic basalts and komatiites from the Nelshoogte Schist Belt	132
Table 14 :	Average whole-rock geochemical data of tholeiitic and andesitic basalts from the Onverwacht Group	135

LIST OF PLATES

		Page
Plate 1:	View of the eastern part of the Sterkspruit Intrusion. The northern margin forms the well-vegetated steep slope, extending to the upper left of the photograph. In the middleground, tailings from the Doyershoek asbestos mine can be seen hosted by the Stolzburg Complex which forms well-vegetated ridges.	19
Plate 2:	View of the Sterkspruit Intrusion (forming the middleground) looking west from Traverse 3 (shown on Figure 2). The Stolzburg Complex forms the vegetated ridge on the left of the photograph, and the Moodies sediments form the background on the left. Tailings from the Stolzburg asbestos mine are also visible.	19
Plate 3:	View of the Sterkspruit Intrusion looking west from Traverse 2 (shown in Figure 2), forming the smooth terrain in the central and right parts of the photograph. Komatiite rocks form prominent ridges on the left. The well-vegetated ridge in the middleground is a mafic dyke.	23
Plate 4:	View of the Sterkspruit Intrusion from the western end of the study area, looking northeast. Komatiitic basalts and komatiites form the prominent ridges.	23
Plate 5:	Weathered gabbro from the Sterkspruit Intrusion showing 'onion-skin' exfoliation.	25
Plate 6:	Contact between the Sterkspruit Intrusion (right) and komatiitic basalts (left), Traverse 2 (shown in Figure 2). The geological contact is demarcated by a shallow depression in the centre of the photograph.	25
Plate 7:	Fine-grained gabbro forming the chill margin to the Sterkspruit Intrusion, Traverse 2 (Figure 5).	30
Plate 8:	Close-up view of the medium-grained, massive, mesocratic gabbro from the Marginal Zone.	30

		Page
Plate 9:	Close-up view of the medium- to coarse-grained, leucocratic gabbro of the Lower Zone.	31
Plate 10:	Close-up view of the medium- to coarse-grained, meso- to leucocratic gabbro, with dark-green needles of amphibole, typical of the rocks in the Upper Zone.	31
Plate 11:	View (looking west) of the Lower Zone showing plagioclase-rich stringers dipping to the north (Traverse 3, Figure 6).	33
Plate 12:	Close-up view of the plagioclase-rich stringers in gabbro from the Lower Zone. (Traverse 3, Figure 6).	33
Plate 13:	Close-up view of rhythmic layering from the Lower Zone (Traverse 3, Figure 6).	34
Plate 14:	Close-up view of rhythmic layering from the Lower Zone (Traverse 3, Figure 6) showing gradational as well as sharp layer contacts.	34
Plate 15:	Deformation in the Sterkspruit Intrusion shown by shear foliation and flattening of gabbro from the Central Zone.	37
Plate 16:	Late veins, parallel to regional strike, containing fine-grained quartz and recrystallised gabbro occurring in a weathered portion of the Sterkspruit Intrusion.	37
Plate 17:	Close-up view of an intrusive contact, showing a fine-grained chilled margin, between a crosscutting mafic dyke (left) and gabbro (right) from the Sterkspruit Intrusion (Traverse 3, Figure 6).	41
Plate 18:	Photomicrograph of the fine-grained gabbroic chill margin in the Sterkspruit Intrusion. Intergrowth of actinolite, saussuritised plagioclase and quartz (Sample SG38; plane polarised light; 1 cm = 250 μm).	46

		Page
Plate 19:	Photomicrograph of the same sample shown in Plate 18 above, but observed under crossed nicols (Sample SG38, 1 cm = 250 μm).	46
Plate 20:	Photomicrograph of gabbro from the Marginal Zone within 5m of the intrusive contact. Subophitic textures occur with partly altered clinopyroxene, orthopyroxene and saussuritised plagioclase. Quartz is interstitial to plagioclase and occurs as subrounded grains (Sample SG39; plane polarised light; 1cm = 200 μm).	48
Plate 21:	Photomicrograph of the same sample shown in Plate 20 above, but observed under crossed nicols (Sample SG39; 1 cm = 200 μm).	48
Plate 22:	Photomicrograph of the gabbroic rocks from the Marginal Zone, showing typical subophitic textures with partly uralitised clinopyroxene oikocrysts enclosing plagioclase laths. The plagioclase retains subhedral shapes, but are clouded to a dark-brown colour due to the effects of saussuritisation (Sample SG22; plane polarised light; 1 cm = 200 μm).	49
Plate 23:	Photomicrograph of the same sample shown in Plate 22 above, but observed under crossed nicols (Sample SG22; 1 cm = 200 μm).	49
Plate 24:	Photomicrograph of the layered gabbro from the Lower Zone, showing orthocumulate clouded plagioclase with interstitial angular-shaped quartz. A clinopyroxene grain showing incipient uralitisation can be seen on the lower left side of the photograph (Sample SG24; plane polarised light; 1 cm = 200 μm).	51
Plate 25:	Photomicrograph of the same sample shown in Plate 24 above, but observed under crossed nicols (Sample SG24; 1 cm = 200 μm).	51

		Page
Plate 26:	Photomicrograph of the high-Ti ferrogabbro from the Central Zone, showing an intergrowth between fibrous actinolite, saussuritised plagioclase and quartz. Yellow-green epidote with bright interference colours is more prominent in the Central Zone. Opaque phases are leucoxene after Ti-ilmenite (Sample SG26; plane polarised light; 1 cm = 250 μm).	53
Plate 27:	Photomicrograph of the same sample shown in Plate 26 above, but with bright interference colours and observed under crossed nicols (Sample SG26; 1 cm = 250 μm).	53
Plate 28:	Photomicrograph of the Quartz Diorite, showing dark-green chlorite, large subhedral quartz grains, relatively unaltered plagioclase, carbonate, epidote and tiny biotite flakes (Sample SG28; plane polarised light; 1 cm = 200 μm).	55
Plate 29:	Photomicrograph of the same sample shown in Plate 28 above, but observed under crossed nicols (Sample SG28; 1 cm = 200 μm).	55
Plate 30:	Photomicrograph showing the amorphous nature of dark brown leucoxene. Also shown are partly uralitised clinopyroxene and subhedral plagioclase grains (Sample SG22; plane polarised light; 1 cm = 200 μm).	56
Plate 31:	Photomicrograph of the same sample shown in Plate 30 above, but observed under crossed nicols (Sample SG22; 1 cm = 200 μm).	56
Plate 32:	Photomicrograph of the quartz gabbro from the Upper Zone, showing intersertal textures with pleochroic green, acicular, actinolite needles partly enclosing epidotised plagioclase and quartz (Sample SG31; plane polarised light; 1 cm = 250 μm).	58
Plate 33:	Photomicrograph of the same sample shown in Plate 32 above, but observed under crossed nicols (Sample SG31; 1 cm = 250 μm).	58

		Page
Plate 34:	Photomicrograph of a mafic dyke from the western part of the study area. Intergranular textures with tabular clinopyroxene and clouded plagioclase grains are visible (Sample SD1; plane polarised light; 1 cm = 200 µm).	61
Plate 35:	Photomicrograph of the same sample shown in Plate 34 above, but observed under crossed nicols (Sample SD1; 1 cm = 200 µm).	61
Plate 36:	Photomicrograph of a sample from a mafic dyke intruded into the Nelshoogte trondhjemitic gneiss pluton. Right side of photograph shows plagioclase laths and interstitial quartz while the left side shows a uralitised pyroxene grain (Sample SD7; plane polarised light; 1 cm = 200 µm).	62
Plate 37:	Photomicrograph of the same sample shown in Plate 36 above, but observed under crossed nicols (Sample SD7; 1 cm = 200 µm).	62

LIST OF TABLES IN APPENDIX A

Table A1 : Whole-rock geochemical data of gabbros from the Sterkspruit Intrusion

Table A2 : Whole-rock geochemical data from the Sterkspruit Mafic Dyke Swarm

Table A3 : Whole-rock compositions of tholeiitic and andesitic basalts from the Kromberg Formation (Conway, 1985)

Table A4 : Average Rare Earth Element Abundances in C1 Chondritic Meteorites (Evensen *et al.*, 1978)

Table A5 : Chondrite-normalised data from Thompson (1982) and Hawkesworth *et al.* (1984), used in the calculation of spider-diagrams

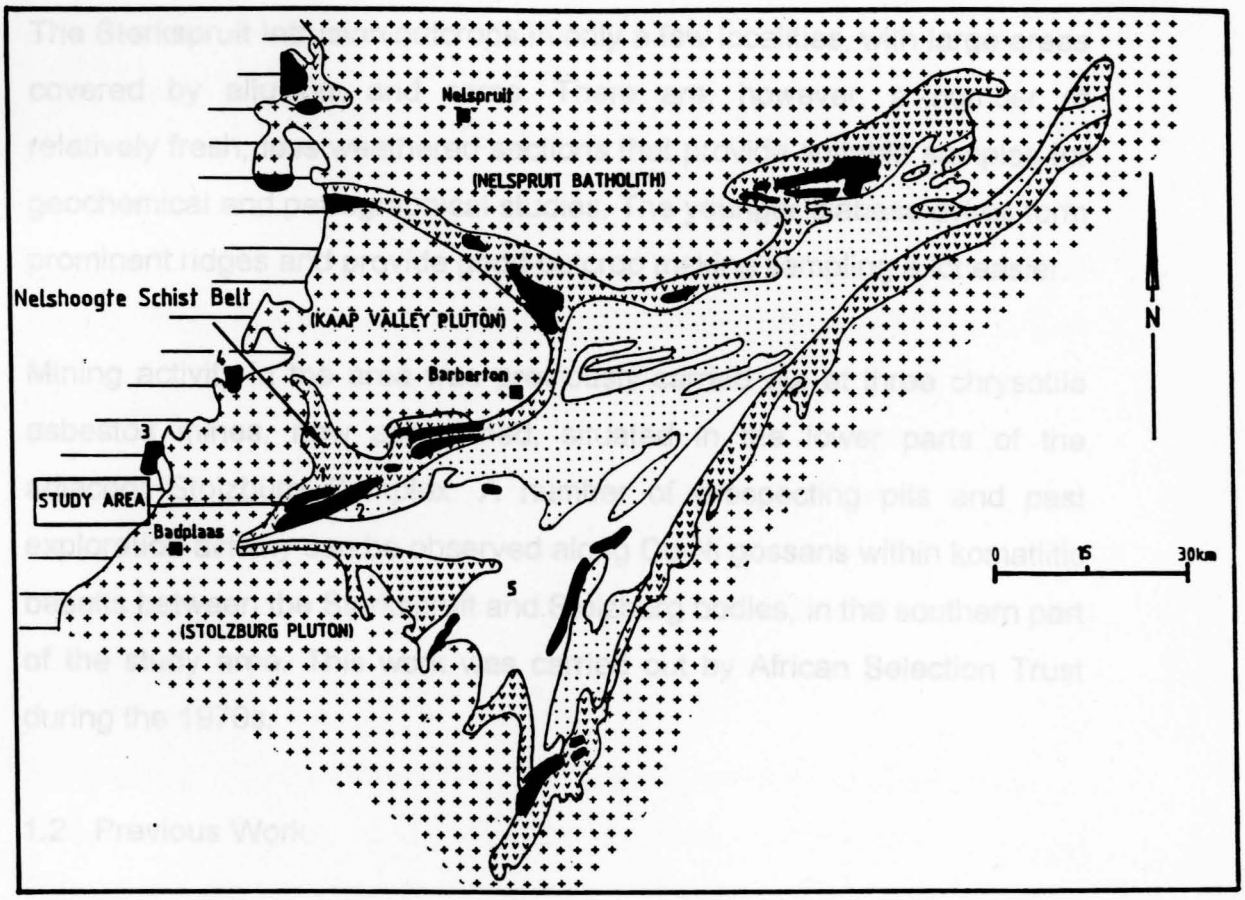
CHAPTER 1
INTRODUCTION

1.1 Location of the Study Area

The Sterkspruit Intrusion is situated in the southwestern region of the Barberton Mountain Land, Mpumalanga Province (formerly the Eastern Transvaal) (Figure 1). This east-northeast trending body, which is approximately 8 km in length and about 500 m wide, is geographically located about 20 km northeast of Badplaas, almost midway between Badplaas and Barberton. The intrusion is situated on the farms Sterkspruit 709 JT, Stolzburg 710 JT and Doyershoek 702 JT, and occupies an area of approximately 4.8 km^2, between latitudes 30°43' and 30°47' and longitudes 25° 54' and 25° 55'.

Geologically this intrusion is a massive (and in places layered) body of gabbroic to dioritic composition, located north of, and sub-parallel to, the Stolzburg Layered Ultramafic Complex. Both these intrusions are hosted by komatiites and komatiitic basalts forming the lower mafic to ultramafic unit of the Onverwacht Group and lying within the Nelshoogte Schist Belt. A number of younger diabase dykes, termed the Sterkspruit Mafic Dyke Swarm, are also located in the study area.

Access to the study area is via a dirt road to the (now defunct) Sterkspruit, Stolzburg and Doyershoek asbestos mines, or through the Nelshoogte Forest Reserve. Both roads lead off the main Badplaas to Barberton macadamised road. The quality of the dirt roads is generally very poor so that access is mostly restricted to four wheel drive vehicles. The area is, however, easily accessible on foot.



LEGEND

Proteozoic cover rocks

Intrusive granites

ARCHAEAN - SWAZILAND SUPERGROUP

Sediments - Fig Tree and Moodies Groups

Mafic-to-felsic volcanics - Onverwacht Group (Mafic to Felsic Unit)

Ultramafic-to-mafic volcanics - Onverwacht Group (Lower Ultramafic Unit)

Layered igneous complexes

1 Sterkspruit Intrusion
2 Stolzburg Complex
3 Kalkkloof Complex
4 Uitkomst Complex
5 Type section of Kromberg Formation

Figure 1: REGIONAL GEOLOGICAL MAP OF THE BARBERTON GREENSTONE BELT, SHOWING THE LOCALITY OF THE STERKSPRUIT INTRUSION AND STUDY AREA.

(Modified after Anhaeuser, 1985)

The Sterkspruit Intrusion outcrops in only a few localities, with large areas covered by alluvium and scree. There are, however, a number of relatively fresh, less weathered sections that provide suitable samples for geochemical and petrographical studies. The younger diabase dykes form prominent ridges and provide good outcrop making sampling a lot easier.

Mining activity in the area was previously carried out at three chrysotile asbestos mines, now abandoned, situated in the lower parts of the adjacent Stolzburg Complex. A number of prospecting pits and past exploration activity can be observed along Cu-Ni gossans within komatiitic basalts between the Sterkspruit and Stolzburg bodies, in the southern part of the study area. This work was carried out by African Selection Trust during the 1970s.

1.2 Previous Work

Visser *et al.* (1956) were the first investigators in the Barberton region to categorise the volcanic, sedimentary and basic to ultrabasic layered intrusive complexes. They classified these intrusive rocks as being part of the Jamestown Igneous Complex which intruded the Swaziland System comprising the Onverwacht, Fig Tree and Moodies Series. These authors further described granitic, syenitic and diabase dykes and sills invading the area and classified these as being either Post Jamestown, Pre- or Post-Transvaal System or Post-Karoo System in age.

Visser *et al.* (1956) also described sheet intrusions as having been injected parallel to the foliation of basic schists of the Jamestown Igneous Complex. They noted a thick intrusive sheet on the farms Sterkspruit, Stolzburg and Doyershoek in the southwestern portion of the Barberton area, and included this intrusion with those hypabyssal rocks older than the Godwan Formation. They also described diabase sheets at the

western end of the Jamestown Schist Belt, the latter associated with the Kaapsehoop Intrusive Body.

The Sterkspruit Intrusion was mapped by Anhaeusser in 1971, during regional mapping of the Nelshoogte Schist Belt. He produced a geological map entitled "Geological map of a portion of the Nelshoogte Schist Belt and the Stolzburg Layered Ultramafic Complex, Barberton Mountain Land.", which is included with an abstract on the Stolzburg Complex (Anhaeusser, 1974). Here mention was made of a massive layered diabase sheet or sill, lying conformably within the layered succession of basalts and peridotites. The map mentioned above was also included in a DSc thesis (Anhaeusser, 1983).

Anhaeusser (1976, 1985, 1986), in papers on the Archaean layered ultramafic complexes and chrysotile asbestos occurrences in South Africa, described a diabase sheet north of the Stolzburg Complex which intrudes komatiitic basalts and peridotites. He recorded mostly a massive gabbro with some vertical layering, which suggested that tilting may have occurred. He also suggested that there was no genetic relationship between the gabbro and the neighbouring komatiitic country rocks.

Pospisek (1991) undertook a geochemical study across a 100 m traverse of the gabbro body. She concluded that the Sterkspruit Intrusion is an Archaean, layered, sill-like body and described differentiation cycles and a zonation across the 100 m traverse.

Visser *et al.* (1956), Visser and Verwoerd (1960), Viljoen and Viljoen (1969a), Anhaeusser (1973), Robb (1977) and Wuth (1980) also described the dykes that are prolifically distributed throughout the Barberton area, in particular the northwest-trending set that is found traversing the study area.

1.3 Physiography and Climate

Geographically, the study area is situated between highveld and lowveld, east of the Transvaal escarpment, within the 'mist-belt'. The climate is warm to hot, with cooler weather recorded closer to the escarpment. Average temperatures vary between 18°C and 30°C in summer, and between 8°C and 23°C in winter.

Rainfall is seasonal with the summer months (October to March) recording an average of 92 mm per month and the winter months (April to September) recording 17 mm. The drainage of streams is mostly towards the south and west, eventually reaching the eastward flowing Komati River. In the study area, the Mawelawela and Sterkspruit streams are perennial with the remaining first and second order streams forming a dendritic drainage pattern.

The area is moderately hilly with some steep-sided valleys in places. Vegetation on the Sterkspruit Intrusion consists of grassland and a variety of scrub types. More dense bushes and trees are restricted to river courses and to crosscutting mafic dykes. The Nelshoogte Forestry Reserve occurs to the northeast of the study area where pine and gum tree plantations are located.

1.4 Research Objectives

The primary aim of this research is to characterise the Sterkspruit Intrusion. To accomplish this it will be necessary to establish whether this body has any similarities with other Archaean layered intrusions in the Barberton greenstone belt, particularly those within close proximity of the Sterkspruit Intrusion, or whether this body might be related to a younger (Proterozoic) basic intrusive event. A number of younger mafic intrusions

occur in the eastern Mpumalanga region, mostly in the form of sills and larger complexes. Examples include the Uitkomst Complex, approximately 20 km northwest of the study area, which is considered to be a satellite body of the Bushveld Complex (Kenyon *et al.*, 1986; Allen, 1990) ; the Usushwana Complex situated near Piet Retief in the southeastern part of Mpumalanga and in Swaziland, which contains a gabbroic suite within a broad magmatic cycle (Hammerbeck, 1982); and numerous sills, classified by Sharpe (1981) as being Pre-Bushveld in age, situated in the Lydenburg area.

It also needs to be established if this body intruded as a sill, or sheet and whether it was tilted along with the surrounding volcanic rocks into its present position, or whether it intruded as a dyke, thereby post-dating regional tectonism and deformation. If the body is a sill, then the base and top of the intrusion will have to be resolved, which will aid in establishing a regional younging direction for the southern portion of the Nelshoogte Schist Belt. To this end, the geochemical variation within the body will be investigated, in order to identify differentiation trends. If the body is a dyke-like feature, then the subvertical layering will have to be adequately explained.

It will also be necessary to ascertain whether the body consists of a single gabbroic rock type, or whether more than one variety of gabbro is present, which could represent a number of magmatic events. Associations between this intrusion and volcanic rocks in the Barberton region will also be investigated.

The numerous crosscutting diabase dykes, intrusive into the gabbroic body, will also be examined and compared with one another and the rocks of the Sterkspruit Intrusion, to determine any differentiation trends or similarities.

1.5 Research Methods

An initial reconnaissance investigation of the study area preceded two months of regional geological mapping using 1:10 000 scale aerial photographs. This was followed by detailed field investigations of outcrops, and the collection of a suite of rocks comprising some 95 samples from the Sterkspruit Intrusion, the surrounding volcanic rocks and the mafic dyke swarm.

The samples were analysed for major and trace element abundances in the Geology Department, and for rare earth elements at the Schonland Research Centre, both at the University of the Witwatersrand, Johannesburg. Thin sections were also prepared from these samples for petrographic investigations, and selected polished sections were used for electron microprobe analyses, undertaken in the Geology Department at Rand Afrikaans University, Johannesburg.

The samples from two complete traverses across the width of the gabbroic body, supplemented by samples used by Pospisek (1991) in her study on a portion of the intrusion, formed the basis for the geochemical investigation and characterisation of the Sterkspruit Intrusion.

Binary variation diagrams and ternary classification plots are presented in this study comparing the gabbroic suite from the Sterkspruit Intrusion with other gabbroic rock suites from intrusive sills, dykes and complexes in the Mpumalanga region. Samples from the crosscutting dykes were also investigated geochemically so as to relate them to the gabbroic intrusion and other dykes present in the Barberton area. Trace elements, including rare earth element variations were used to investigate geochemical differentiation trends within the intrusion and to compare the Sterkspruit body with patterns from other complexes.

CHAPTER 2
REGIONAL GEOLOGICAL DESCRIPTION

2.1 Geology of the Barberton Mountain Land

The Barberton Mountain Land, situated in the eastern portion of Mpumalanga Province and the western sector of Swaziland, comprises a rugged triangular-shaped tract of mountains elongated in a northeast - southwest direction. This mountainous terrain is comprised of 3.5 - 3.2 Ga Archaean greenstone volcanic and sedimentary rocks intruded by later granitic plutons and diabase dykes and sills.

Hall (1918), was the first investigator in the Barberton region to classify all the volcanic and sedimentary rocks into one system, which he called the Swaziland System. He defined a three-fold subdivision, viz.: the Onverwacht Volcanic Series for the volcanic rocks, the Jamestown Series for the serpentinites, basic schists, slates, quartzites and conglomerates and the Moodies Series for the sedimentary rocks occupying the central part of the Barberton greenstone belt.

The Geological Survey of South Africa remapped the Barberton area between 1937 and 1948. As a result of this work, Visser *et al.* (1956) redefined the Moodies Series and classified the upper, predominantly arenaceous rocks into the Moodies System, separated by an unconformity from the lower banded iron formations, shales and greywackes, which they termed the Fig Tree Series. This Series and the Onverwacht Series, which then comprised of basic and acid lavas, formed the Swaziland System. The Geological Survey further reclassified the ultramafic rocks of

the Jamestown Series as intrusive rocks belonging to the Jamestown Igneous Complex.

Visser *et al.* (1956) interpreted this Complex as being intrusive into both the Swaziland and Moodies Systems. It contained both basic and ultrabasic rocks as well as an acid phase (granodioritic in composition), which was termed the Kaap Valley Granite. The Barberton area was subsequently intruded by various granitic and syenitic rocks, and later by diabase dykes and sills of varying ages.

As part of the Upper Mantle Project, Viljoen and Viljoen (1969c,d), reclassified the rocks from Barberton into the Swaziland Sequence comprising the Onverwacht, Fig Tree and Moodies Groups. They, together with Anhaeusser and Viljoen (1965), also reinterpreted the Jamestown Igneous Complex as being the highly metamorphosed equivalents of the Onverwacht Group. Their investigations of the volcanic rocks of the 15 000 m thick Onverwacht Group led them to further classifying this succession into the Tjakastad Subgroup, consisting of basaltic to ultramafic lavas (Lower Ultramafic Unit), and the more felsic Geluk Subgroup towards the top (Upper Mafic to Felsic Unit). These two Subgroups are separated by the Middle Marker, a continuous sedimentary horizon which, according to Viljoen and Viljoen (1969c), heralded a change in the nature of the volcanic activity.

In the Tjakastad Subgroup, the Viljoens described both peridotitic komatiites and komatiitic basalts. Komatiites are ultramafic lavas with an MgO content greater than 18%, which are the products of liquids that, in turn, have an MgO content greater than 18% (Arndt and Nisbet, 1982). The early definitions of komatiites by Viljoen and Viljoen (1969c) included CaO/Al_2O_3 ratios greater than 1. However, these komatiites are now considered unique as the majority of komatiites in Archaean terrains

worldwide have CaO/Al_2O_3 ratios between 0.8 and 1. Higher CaO/Al_2O_3 results from Al depletion in komatiites, and are restricted to sequences older than 3.0 Ga (Cattell and Taylor, 1990).

Komatiitic basalts, on the other hand, erupted with MgO contents between 7-15 % (Cattell and Taylor, 1990). MgO may vary from 5%, in evolved gabbroic centres, to 18% in layered cumulate flows. In general, komatiitic basalts are relatively rich in silica and poor in aluminium compared to tholeiitic basalts. The komatiitic basalts in the lower Onverwacht Group (Tjakastad Subgroup) constitute the bulk of the Komati Formation, where they were originally subdivided into three varieties (Viljoen and Viljoen, 1969c), viz.:

1) the Barberton type, which is a tremolite-actinolite-plagioclase variety, having equal MgO, CaO and Al_2O_3 contents of about 10% each. Both pillowed and massive phases are developed;

2) the Badplaas type, which is a tremolite/actinolite variety with MgO contents between 14 and 18.5%, and the highest Ca/Al ratios of the three varieties (Ca/Al in the Badplaas type = 2.4 as opposed to 1.0 for the Barberton type and 1.2 for the Geluk type). Fewer pillow structures have been observed in this class, which mostly resemble massive gabbroic to pyroxenitic sills; and

3) the Geluk type, which is a tremolite-chlorite variety consisting of small, but well-formed pillow structures. MgO contents are between 19% and 24%, with SiO_2 averaging 47.4%, the lowest of the three basalt varieties.

Metatholeiites are also present in the Tjakastad Subgroup but are only sporadically developed, mainly associated with komatiitic basalts of the Barberton type (Viljoen and Viljoen, 1969c). The tholeiites have a high

content of sodium plagioclase with conspicuous chlorite and minor actinolite. They also have higher alumina (Al_2O_3 = 13.3%) and alkali contents (Na_2O = 2.9% and K_2O = 0.26%) than komatiitic basalts. In contrast to the Lower Onverwacht, Viljoen and Viljoen (1969d) and Smith (1980) considered the Geluk Subgroup to consist of a normal tholeiitic succession with lesser amounts of andesite, dacite and rhyodacite. They described pillowed tholeiites at the base of the sequence, which approximate to oceanic tholeiite compositions, while those towards the top of the sequence have affinities with continental tholeiites. MgO contents of these tholeiites vary from about 9% in massive, coarser-grained flow centres to 7.5% in pillowed, or finer-grained non-pillowed varieties (Viljoen and Viljoen, 1969d). Viljoen and Viljoen (1969a,d) and Anhaeusser (1971) also described cyclic volcanism, whereby cycles grade from tholeiitic lavas at the base through to rhyodacites at the top. Each cycle is often terminated by a chert horizon.

The interpretation of cyclic volcanism has been investigated by Ranson and Byerly (1983), who indicated that silicification of mafic flows accounts for the more felsic nature of these cycles. According to De Wit *et al.* (1987b), the felsic units in the Onverwacht Group do not form part of mafic-to-felsic volcanic cycles and are not related to mafic - ultramafic rocks of this group. Rather they interpreted these units as high-level equivalents of gneissic trondhjemite - tonalite plutons which intruded the greenstone belt and post-date the Onverwacht Group by 40-50 Ma.

In a study on the geochemistry of Lower Onverwacht Group lavas, Smith (1980) proposed a three-fold subdivision of komatiitic rocks:

1) ultramafic komatiites with MgO > 24%;
2) high-Mg mafic komatiites with MgO between 19 - 24%; and
3) low-Mg mafic komatiites with MgO between 8 - 16%.

Smith (1980) also identified three types of tholeiitic basalts in the Onverwacht Group, namely:

1) low-Ti tholeiites;
2) high-Ti tholeiites; and
3) high-Mg tholeiites.

The presently accepted stratigraphy of the volcano-sedimentary Barberton Sequence is the one adopted by the South African Committee for Stratigraphy (SACS, 1980), and proposed by Viljoen and Viljoen (1969a,b,c) and Anhaeusser (1975). Table 1 is a modified stratigraphic column after SACS (1980), and shows the dominantly volcanic Onverwacht Group overlain by the largely argillaceous sedimentary Fig Tree Group and the uppermost arenaceous sediments of the Moodies Group.

The lowermost formations of the Onverwacht Group (the Tjakastad Subgroup) are found around the periphery of the greenstone belt, with the Geluk Subgroup located in the southwestern parts (Tankard *et al.,* 1982). The Fig Tree and Moodies Groups are located mostly within the central core regions of the belt.

The lithostratigraphic sequence of units or 'layer cake' interpretation of the stratigraphic sequence has been questioned by more recent field investigations. The stratigraphy of the Onverwacht Group is considered by some to consist of several tectonic units that have been structurally duplicated by a mechanism of large-scale isoclinal folding combined with thrusting (De Wit, 1982; De Wit and Tredoux, 1987; De Wit *et al.*, 1983; 1987a,b; 1992; Williams and Furnell, 1979; Lowe *et al.*, 1985). Furthermore, De Wit *et al.* (1987a) proposed that the mafic-to-ultramafic rocks form a pseudostratigraphy comparable to Phanerozoic ophiolites.

A number of sill-like, differentiated, mafic-to-ultramafic layered complexes, of which there are about 27 (Anhaeusser, 1985), occur at various stratigraphic levels in the Onverwacht Group. The majority of these complexes are located along the northwestern to northern parts of the greenstone belt where they occur in the formations of the Tjakastad Subgroup. These complexes are considered to have intruded penecontemporaneously with the surrounding basaltic and komatiitic lavas (Viljoen and Viljoen, 1970; Anhaeusser, 1976, 1979, 1985; Wuth, 1980). As the bulk composition of these layered complexes approximate to the composition of komatiites from the Komati Formation, they are attributed to fractionation and magmatic differentiation of a similar komatiite magma (Wuth, 1980). In contrast, the basaltic-to-tholeiitic magma types are responsible for the larger differentiated gabbroic intrusions such as Stillwater, Skaergaard and the Bushveld Complex (Condie, 1981). De Wit *et al.* (1987a) interpreted the layered ultramafic intrusive complexes as representing peridotitic tectonites, similar to alpine peridotites which form the upper mantle base of the oceanic lithosphere.

Byerly *et al.* (1996) questioned the tectonic stacking model and suggested that the early Archaean crust developed slowly by episodic mafic and felsic igneous activity. This interpretation supports the hypothesis of a continuously evolving sequence, rather than a thin volcanic unit structurally duplicated several times. They also recorded an age of 3445 - 3452 Ma for the dacitic lavas from the upper Hooggenoeg Formation.

Table 1: Lithostratigraphy of the Barberton Sequence (after SACS, 1980)

Group	Subgroup	Formation	Description	(m)
MOODIES		Baviaanskop	sandstone, greywacke, grit, quartzite, conglomerate, shale	685
		Joe's Luck	shale, subgreywacke, grit, conglomerate, quartzite, jaspilites	740
		Clutha	shales, conglomerates, quartzites, jaspilites	1600
FIG TREE		Schoongezicht	agglomerates, tuffs, lava, chert breccia	550
		Belvue Road	banded ferruginous chert, tuff, shale	600
		Sheba	banded ferruginous chert, greywacke, shale	1000
ONVERWACHT	Geluk	Swartkoppie	mafic-felsic lavas, chert	915
		Kromberg	mafic-felsic lavas, agglomerates, banded cherts and carbonates	1920
		Hooggenoeg	mafic-felsic lavas, chert	4850
	Middle Marker		chert and carbonate	
	Tjakastad	Komati	ultramafic-mafic lavas, chert	3510
		Theespruit	ultramafic-mafic lavas, felsic tuffs, carbonaceous chert	1890
		Sandspruit	ultramafic lavas	2130

2.2 Metamorphism

The Barberton greenstone belt succession, especially the Onverwacht Group volcanics, has been influenced by regional low-grade greenschist facies metamorphism (Anhaeusser *et al.,* 1969; Viljoen and Viljoen, 1969b; Cloete, 1991; 1994; Ward, 1995). Earlier, Hall (1918) and Visser *et al.* (1956) had described contact metamorphic rocks along narrow contact aureoles surrounding granitic plutons. The metamorphic grade along these dynamic contact zones, ranges from upper greenschist to amphibolite facies (Viljoen and Viljoen, 1969b).

A chronological sequence of metamorphic events has been proposed by Cloete (1991, 1994), beginning with high- and low-temperature, sea-floor metamorphism. He described the high-temperature (spreading centre) type as having caused hydration and greenschist-grade metamorphism of the Komati Formation and Upper Onverwacht. Cloete associated this metamorphism with magmatically driven hydrothermal convection of heated seawater in the 1-3 km levels of an oceanic crust. The low temperature type (or shallow subaerial/submarine variety) is associated with pervasive silicification which according to Cloete (1991) occurs only in rocks of the Upper Onverwacht Group.

Superimposed on this earlier sea-floor metamorphism was a regional burial metamorphism (Cloete, 1990, 1991, 1994), also described as a static style of metamorphism. The origin of this metamorphism variety is not well understood but is believed to result from volcano-sedimentary loading and/or low-angle tectonic duplication. The last metamorphic episode, according to Cloete (1991, 1994), is dynamothermal contact metamorphism confined to intrusive contact zones of early granitic plutons.

CHAPTER 3
GEOLOGY OF THE STERKSPRUIT INTRUSION AND MAFIC DYKE SWARM

3.1 Geology of the Nelshoogte Schist Belt

The Nelshoogte Schist Belt consists of a triangular-shaped area underlain mostly by rocks of the Lower Onverwacht Group (Tjakastad Subgroup) with Moodies Group sediments, granitic rocks and hypabyssal diabase dykes present in the surrounding region (Figures 1 and 2). The schist belt mainly comprises komatiitic basalts, including both pillowed and variolitic varieties, metatholeiites, mafic-to-ultramafic tuffs, cherty-quartzitic sediments and ultramafic komatiites. The sequence of alternating komatiitic basalts and komatiites are highly visible features to the north and south of the Sterkspruit Intrusion, with the komatiites forming prominent ridges.

Visser *et al.* (1956) referred to this large triangular area of basic rocks as part of the Jamestown Igneous Complex. They also described a differentiated green and blue serpentinite in contact with basic schists and sediments of the Moodies System.

This area, now known as the Nelshoogte Schist Belt, was mapped in detail by Anhaeusser (1973, 1974, 1983). The mafic-to-ultramafic volcano-sedimentary rocks were interpreted as forming a triangular or funnel-shaped synclinal fold structure with axes trending southwest, northeast and northwest. The schist belt conforms to the schistose synclinal belts or arcuate tongues of Onverwacht volcanics described by Viljoen and Viljoen (1969a).

The Nelshoogte Schist Belt is buttressed by the trondhjemitic Nelshoogte pluton to the west and the tonalitic Kaap Valley pluton to the north. These plutons represent part of the oldest granitic intrusive events in the area which commenced at approximately 3500 Ma (Anhaeusser and Robb, 1981). The Nelshoogte pluton has yielded U - Pb ages of 3220 Ma (Oosthuyzen, 1970) , while the Kaap Valley pluton has been dated at 3227 Ma (Kamo and Davis, 1991). The area has also been intruded by a swarm of predominantly northwest-striking, crosscutting mafic dykes, thought to be of Proterozoic age.

The greenstone belt successions resemble the Theespruit and Sandspruit Formations of the Lower Onverwacht Group (Anhaeusser, 1974). These successions include komatiitic basalts, komatiites and subordinate siliceous marker horizons. A variety of volcanic and pyroclastic textures and structures are displayed including pillow lavas, flow breccias, mafic tuffs, agglomerates and spherulites.

Van Berkel (1977) identified komatiitic basalts and komatiites in the eastern part of the Nelshoogte Schist Belt, thus confirming the earlier mapping and interpretation of Anhaeusser (1973, 1974, 1983). The geochemistry of these volcanics show the komatiitic basalts to have $CaO/Al_2O_3 > 1$, $MgO > 9$, $K_2O < 0.9$ and $TiO_2 > 0.9$. The tholeiitic basalts in contrast have $CaO/Al_2O_3 = 0.7$. (Wuth, 1980). Observations by Wuth (1980) on the basalts of the Oorschot-Weltevreden Schist Belt to the northeast of the Nelshoogte Schist Belt, show them to have compositions intermediate between Barberton type komatiitic basalts and metatholeiites.

The Sterkspruit and Stolzburg bodies are two mafic-to-ultramafic intrusions situated along the southern portion of the Nelshoogte Schist Belt (Plates 1 and 2). They are aligned sub-parallel to each other and to the volcanic rocks into which they are intruded and are orientated in an east-northeast direction (Figure 2). A thin sliver of Onverwacht Group komatiitic basalts and komatiites separate the two intrusive bodies and varies in width from a few metres to about 300 m.

The southern margin of the Stolzburg Complex is juxtaposed by a major strike fault against the Moodies Group rocks comprising quartzites, sandstones, conglomerates and shales. Evidence of a faulted contact in the south is provided by intense shearing and schistosity, and the transgressive nature of the fault, which is seen cutting across the layering in the Complex. The Stolzburg Complex has a western portion comprising lower division rocks and an eastern portion comprising both lower and upper division rock types. These terms were coined by Anhaeusser (1976, 1985), to describe the repetitive cycles of dunite and orthopyroxenite which form the lower division of the Complex and the upper division cycles of harzburgite, websterite and gabbro. Rodingites, which occur as dykes and as a calcium metasomatised zone, are an integral feature of the upper division and have been described by Anhaeusser (1979) and Rodel (1993).

The nature of the northern contact of the Stolzburg Complex with komatiitic basalts is less well defined, but has been described by Anhaeusser (1976, 1985, 1986) as being faulted. There are indications however, that this is an intrusive contact, as evidenced by the conformable relationship along strike, the absence of shear zones and the presence of possible chill margins in the vicinity of the Stolzburg asbestos mine (Rodel, 1993).

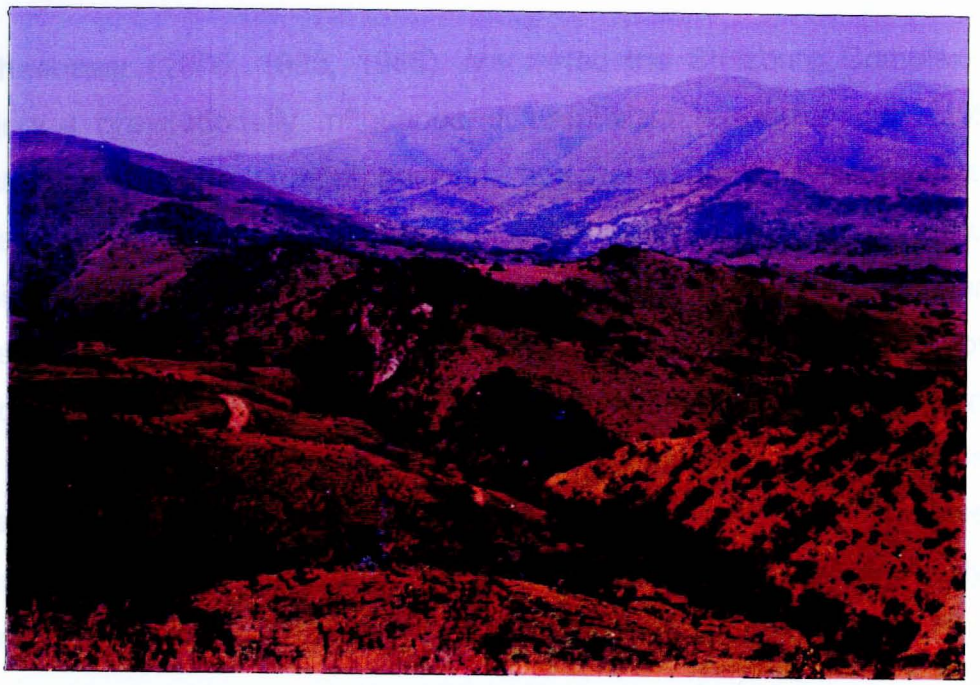


Plate 1.
View of the eastern part of the Sterkspruit Intrusion. The northern margin forms the well-vegetated steep slope, extending to the upper left of the photograph. In the middleground, tailings from the Doyershoek asbestos mine can be seen hosted by the Stolzburg Complex which forms well-vegetated ridges.



Plate 2
View of the Sterkspruit Intrusion (forming the middleground) looking west from Traverse 3 (shown on Figure 2). The Stolzburg Complex forms the vegetated ridge on the left of the photograph, and the Moodies sediments form the background on the left. Tailings from the Stolzburg asbestos mine are also visible.

Anhaeusser (1976, 1985, 1986) interpreted the Stolzburg Complex as being a gravitationally influenced differentiated layered body, rotated tectonically to the vertical position, and younging in a southeasterly direction. He described localised folding developed due to cross faults which offset the stratigraphy. De Wit *et al.* (1987a), on the other hand, interpreted the lower division of the Complex as being a tectonic peridotite body which intruded the rocks of the upper division (which they regarded as not representing part of the Complex). They described isoclinal folds in the layering as well as steeply plunging fold cores in the southwest. These structures, they maintained, resemble folding in Alpine-type ultramafic complexes in the Pyrenees.

Rodel (1993) pointed to a genetic link between the Stolzburg Complex and ultramafic flows in the Barberton Greenstone Belt and provided two alternative origins for the Stolzburg Complex. Firstly, she proposed a subvolcanic sill model whereby the complex formed a high-level magma chamber from which lavas were extruded. Secondly, she considered a lava river model, with the complex forming a coarse-grained lateral equivalent of the volcanics.

In the west, the Stolzburg Complex appears to pinch out and is covered by agricultural land and alluvium. In the east, the Complex continues beneath the Nelshoogte Forest Reserve and can possibly be linked to other ultramafic complexes such as Morgenzon, Sawmill, Emmenes and Pioneer, described by Wuth (1980).

Mining activity in the area is restricted to chrysotile asbestos deposits located within the 'ore-zone' serpentinised dunites of the Stolzburg Complex (Anhaeusser, 1976, 1986). Numerous prospecting pits and boreholes can also be found in the vicinity of the Sterkspruit Intrusion, especially within sheared and gossanous komatiitic basalts separating

this body from the Stolzburg Complex. Exploration carried out by African Selection Trust in the Nelshoogte Schist Belt during the 1970s investigated signs of copper-nickel mineralisation identified by Anhaeusser in 1971.

3.2 Description of the Geological Map

The 1:20 000 scale geological map of the Sterkspruit Intrusion and crosscutting dykes, was produced following regional 1:10 000 scale aerial photograph interpretation and more detailed field mapping (Figures 2 and 3). The geological map of a portion of the Nelshoogte Schist Belt and the Stolzburg Complex, compiled by Anhaeusser (1974, 1983), was used as a base map onto which details of the geology of the Sterkspruit Intrusion was superimposed.

The map depicts the gabbroic intrusion, the surrounding mafic to ultramafic volcanic rocks into which it intruded, the Stolzburg Complex, the Nelshoogte trondhjemite pluton and the crosscutting mafic dykes. The purpose of the map is to show :

1) the locality of the study area, the access routes and the three defunct chrysotile asbestos deposits;

2) the position or setting of the gabbroic intrusion with respect to the surrounding geology, and in particular the contact relationship of this intrusion with the mafic and ultramafic rocks;

3) the distribution and relationships of the major rock types in this part of the Barberton area, including the lower Onverwacht Group

volcanics, the Stolzburg Complex, the Moodies Group sediments, the Nelshoogte granitic intrusion and later hypabyssal intrusives;

4) the major structural features including regional lineaments, faults and localised shear zones; and

5) the gabbroic and dyke sample positions and the locations of the three traverses across the gabbroic intrusion selected for the geochemical investigation.

These traverses, labelled 1, 2 and 3, are represented in Figures 4 - 6, which show the sample localities and geological descriptions of the gabbro in more detail.

3.3 Geology of the Sterkspruit Intrusion

3.3.1 Morphology

The Sterkspruit intrusive body measures approximately 8 km in length and averages about 500 m in width (Plate 3). This sheet-like body has an overall elongated shape orientated in an east-northeast direction. It is generally conformable with the surrounding mafic and ultramafic volcanic rocks, with only a few marginally crosscutting and indented sections (Figure 2).

At the western end of the study area the intrusion thins and bifurcates into two "fingers" before disappearing beneath a cover of alluvium and agricultural land (Plate 4). At the eastern extremity the intrusion appears to be abruptly truncated by a wide crosscutting diabase dyke which forms part of the mafic dyke swarm in the study area. Abundant scree from this dyke made observations of the gabbroic body very difficult.



Plate 3
View of the Sterkspruit Intrusion looking west from Traverse 2 (shown in Figure 2), forming the smooth terrain in the central and right parts of the photograph. Komatiite rocks form prominent ridges on the left. The well-vegetated ridge in the middleground is a mafic dyke.



Plate 4
View of the Sterkspruit Intrusion from the western end of the study area, looking northeast. Komatiitic basalts and komatiites form the prominent ridges.

The northern margin of the body, which is in contact with komatiitic basalts, can be clearly traced in the field and has a definite chill zone exposed in at least two localities. The southern edge of the body is less well defined. The approximate contact can, nevertheless, be determined in most places along strike from the position of gabbroic boulders and scree. There is a section in the centre of the study area, north of the Stolzburg asbestos mine, where a large area of alluvium obscures the southern contact. The shape of the Sterkspruit Intrusion is unclear at this point. Most of the intrusion is poorly exposed with outcrops consisting mainly of weathered gabbro boulders, the latter displaying 'onion-skin'-type exfoliation (Plate 5). The remainder of the intrusion is covered by transported overburden in the form of scree and alluvium.

3.3.2 Lithology

The two localities along the northern edge of the intrusion, where a chilled margin can be observed, were sampled and included in detailed Traverses 2 and 3 (Figure 3). The intrusion at this margin (Plate 6) is fine grained and is in contact with spinifex-textured and pillowed komatiitic basalts. Based on field observations of the intrusion and supported by textural, mineralogical and chemical variations, the body can be subdivided into five zones. Moving from north to south across the body, the following zones are recognised: a Marginal Zone, a Lower Zone, a Central Zone, a Quartz Diorite and an Upper Zone (Figures 4, 5 and 6). The Marginal Zone includes the chill margin on Traverses 2 and 3. The exact contacts of these zones cannot be delineated with accuracy due to constraints imposed by lack of outcrop, but a broad correlation between Traverses 1 and 2, a distance of 900 m apart, can be seen. The Marginal and Lower Zones of Traverse 3, 1200 m to the east of Traverse 2, can also be clearly correlated with those from Traverses 1 and 2.



Plate 5
Weathered gabbro from the Sterkspruit Intrusion showing spheroidal weathering.



Plate 6
Contact between the Sterkspruit Intrusion (right) and komatiitic basalts (left), Traverse 2 (shown in Figure 2). The geological contact is demarcated by a shallow depression in the centre of the photograph.

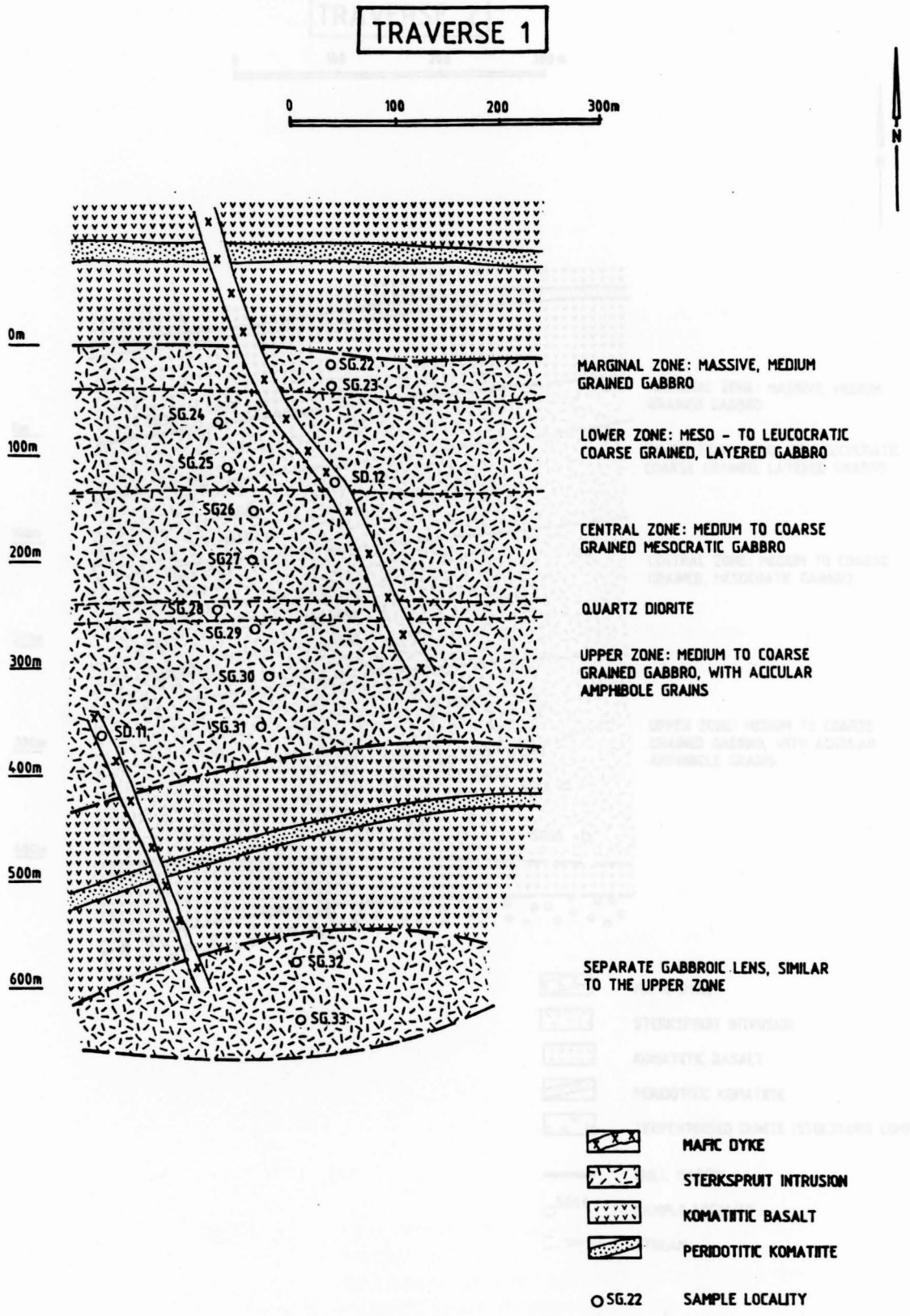


FIGURE 4: SKETCH MAP OF TRAVERSE 1 ACROSS THE STERKSPRUIT INTRUSION SHOWING GEOLOGICAL DESCRIPTION AND SAMPLE LOCALITIES.

(SEE FIGURE 3 FOR REGIONAL POSITION OF TRAVERSE 1)

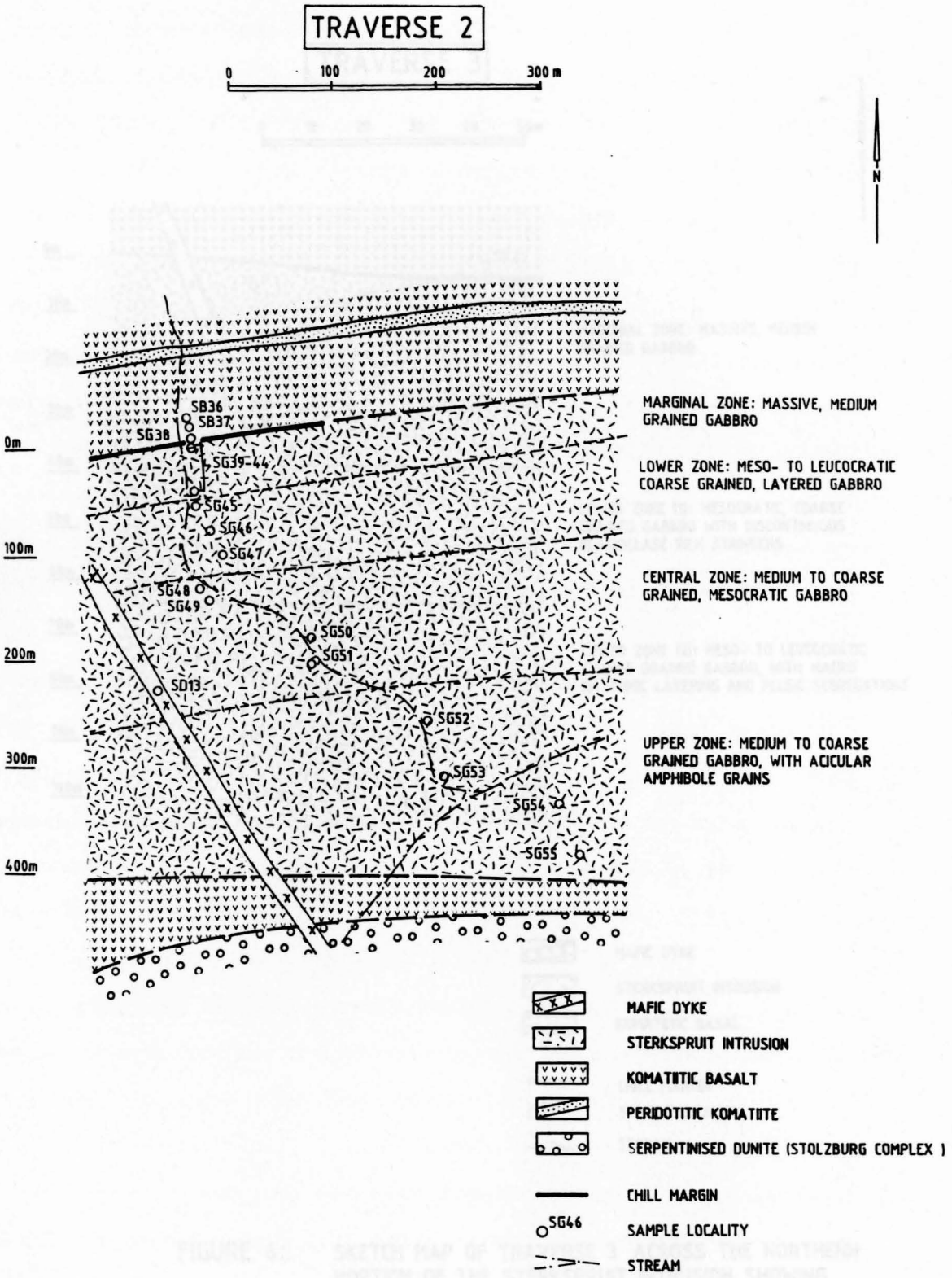


FIGURE 5: SKETCH MAP OF TRAVERSE 2 ACROSS THE STERKSPRUIT INTRUSION SHOWING GEOLOGICAL DESCRIPTIONS AND SAMPLE LOCALITIES.

(SEE FIGURE 3 FOR REGIONAL POSITION OF TRAVERSE 2)

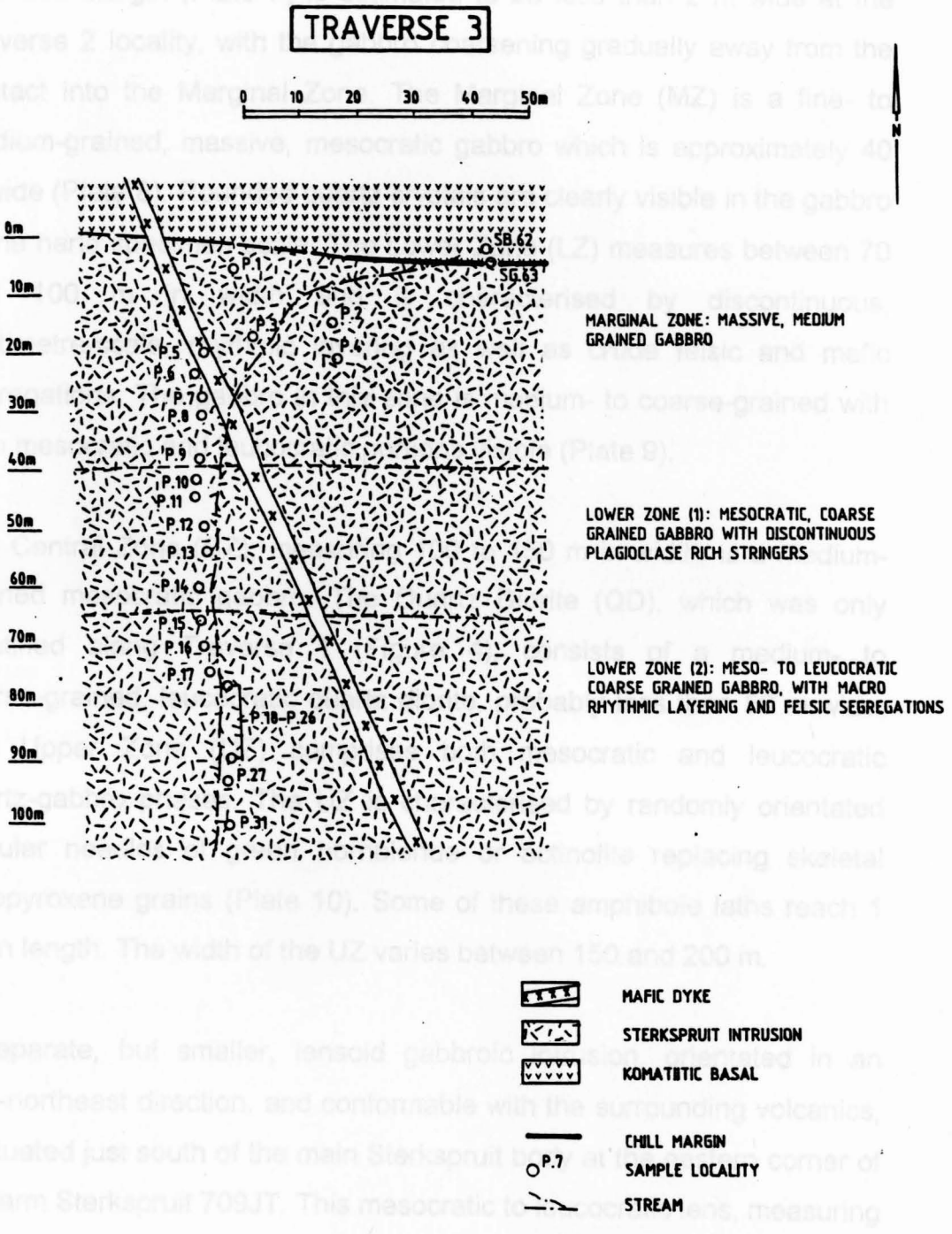


FIGURE 6: SKETCH MAP OF TRAVERSE 3 ACROSS THE NORTHERN PORTION OF THE STERKSPRUIT INTRUSION SHOWING GEOLOGICAL DESCRIPTION AND SAMPLE LOCALITIES.
(SAMPLES LABLED 'P' FROM POSPIŠEK, 1991)

(SEE FIGURE 3 FOR REGIONAL POSITION OF TRAVERSE 3)

The chill margin (Plate 7) is estimated to be less than 2 m wide at the Traverse 2 locality, with the gabbro coarsening gradually away from the contact into the Marginal Zone. The Marginal Zone (MZ) is a fine- to medium-grained, massive, mesocratic gabbro which is approximately 40 m wide (Plate 8). Rounded quartz crystals are clearly visible in the gabbro at the hand specimen scale. The Lower Zone (LZ) measures between 70 and 100 m in width and is characterised by discontinuous, centimetre-scale, rhythmic layering as well as crude felsic and mafic segregations. The gabbro in this zone is medium- to coarse-grained with both mesocratic and leucocratic portions visible (Plate 9).

The Central Zone (CZ), measuring 100 to 150 m in width, is a medium-grained mesocratic gabbro. The Quartz Diorite (QD), which was only identified along Traverse 1 (Figure 4), consists of a medium- to coarse-grained, leucocratic quartz diorite, probably less than 50 m wide. The Upper Zone (UZ) comprises both mesocratic and leucocratic quartz-gabbro phases. The UZ is characterised by randomly orientated acicular needles of green hornblende or actinolite replacing skeletal clinopyroxene grains (Plate 10). Some of these amphibole laths reach 1 cm in length. The width of the UZ varies between 150 and 200 m.

A separate, but smaller, lensoid gabbroic intrusion, orientated in an east-northeast direction, and conformable with the surrounding volcanics, is situated just south of the main Sterkspruit body at the eastern corner of the farm Sterkspruit 709JT. This mesocratic to leucocratic lens, measuring 150m x 600m, is texturally and mineralogically similar to the Upper Zone of the main gabbroic body, and contains similar green acicular hornblende needles.

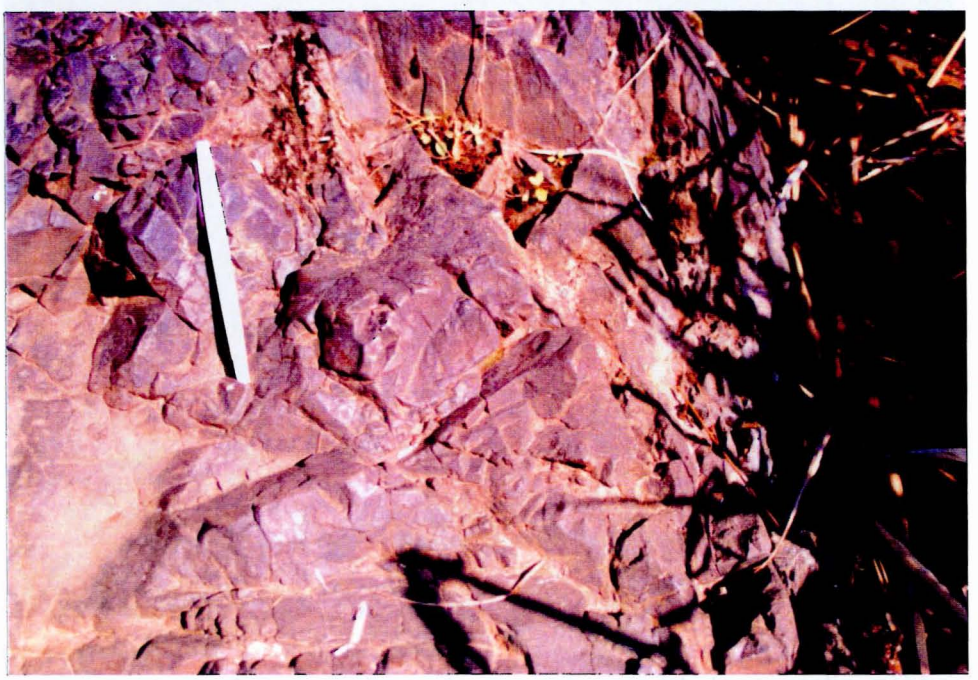


Plate 7
Fine-grained gabbro forming the chill margin to the Sterkspruit Intrusion, Traverse 2 (Figure 5).

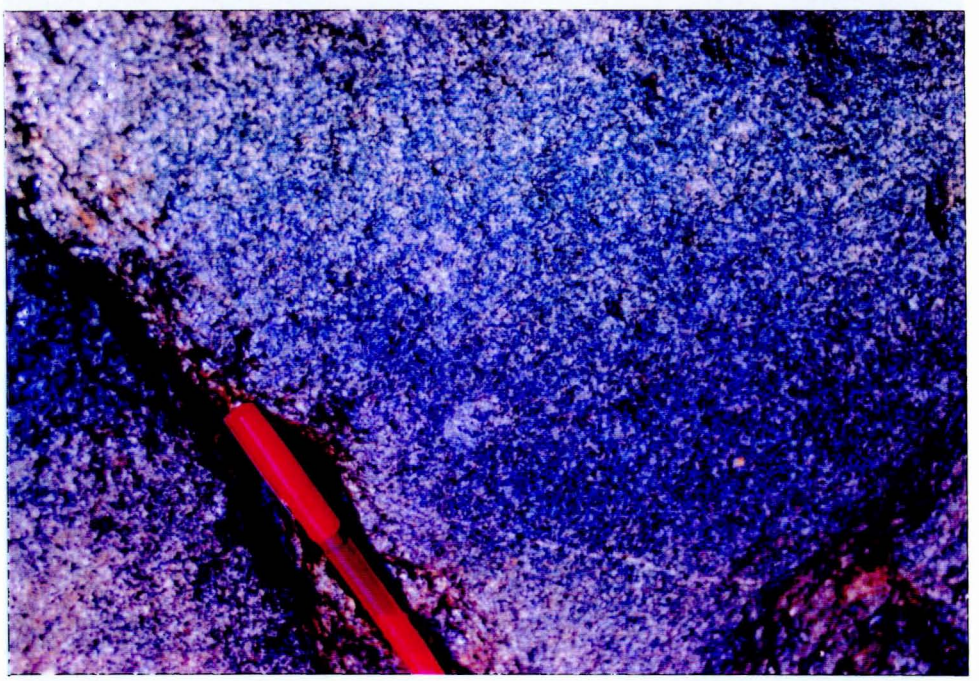


Plate 8
Close-up view of the medium-grained, massive, mesocratic gabbro from the Marginal Zone.

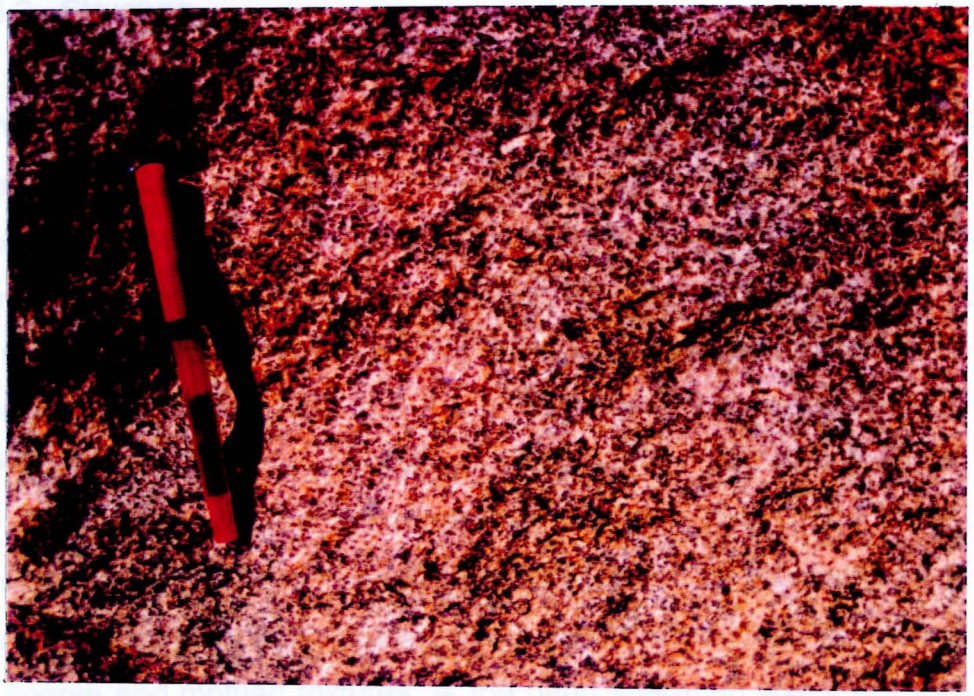


Plate 9
Close-up view of the medium- to coarse-grained, leucocratic gabbro of the Lower Zone.



Plate 10
Close-up view of the medium- to coarse-grained, meso- to leucocratic gabbro, with dark-green needles of amphibole, typical of the rocks in the Upper Zone.

3.3.3 Structure

Structurally, the Sterkspruit gabbroic intrusion is mostly massive except in the Lower Zone where discontinuous, steeply subvertical to northerly dipping stringers and layering are evident. The lower portion of this zone consists of gabbros with plagioclase-rich stringers <5 cm in width (Figure 6, Plates 11 and 12). The rhythmic layering found higher up in the Lower Zone is conformable with the intrusive contact, and consists of diffuse lighter and darker mineral phases representing altered plagioclase and ferromagnesian (altered pyroxene) phases respectively (Plate 13). Strike continuity of these layers is difficult to assess due to poor outcrop, but in places, layers disappear within a single outcrop. The grain size is medium to coarse and mottled textures, at the hand specimen scale, are features of this zone. Contacts between predominantly white feldspar-rich zones and mafic zones are mostly diffuse and gradational, but in many places sharp contacts are also visible (Plate 14). A usually encountered gradation is from a predominantly mafic, mineral-rich base, to a coarser-grained plagioclase-rich top. Similar rhythmic layering is not evident in the marginal, central and upper zones of the body.

The type of layering found in the Lower Zone conforms best to rhythmic or microrhythmic modal layering as described by Irvine (1982). Layering is formed by alternating modally graded and more uniform layers, but in places a continuous succession of modally graded layers is observed. Each individual layer measures less than 30 cm in width and a zone of these graded layers does not exceed 2 or 3 m before more uniform layers are again encountered.



Plate 11
View (looking west) of the Lower Zone showing plagioclase-rich stringers dipping to the north (Traverse 3, Figure 6).



Plate 12
Close-up view of the plagioclase-rich stringers in gabbro from the Lower Zone (Traverse 3, Figure 6).

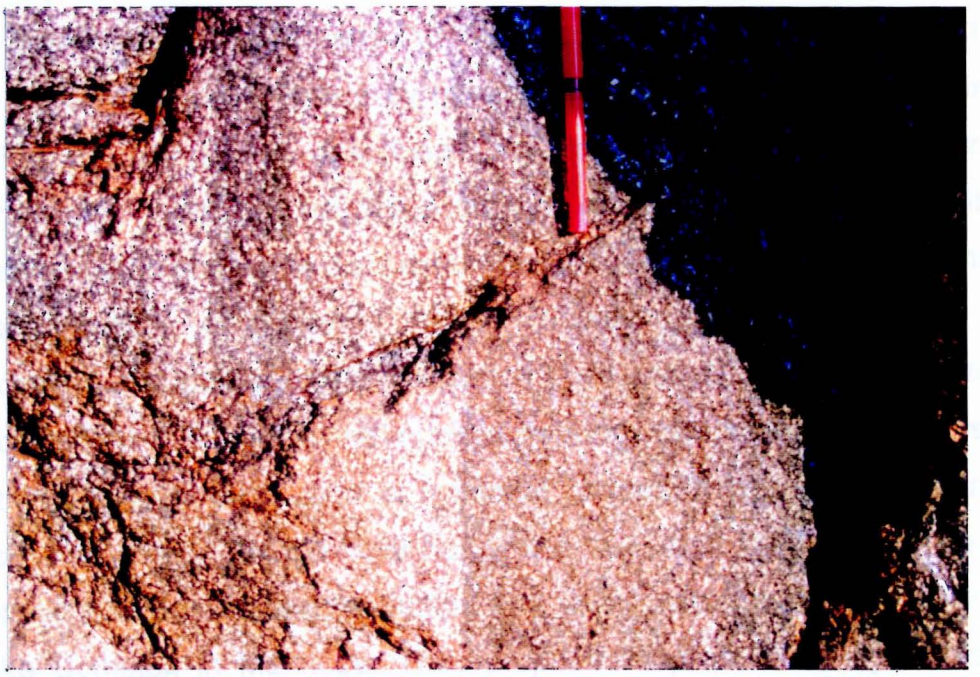


Plate 13
Close-up view of rhythmic layering from the Lower Zone (Traverse 3, Figure 6).

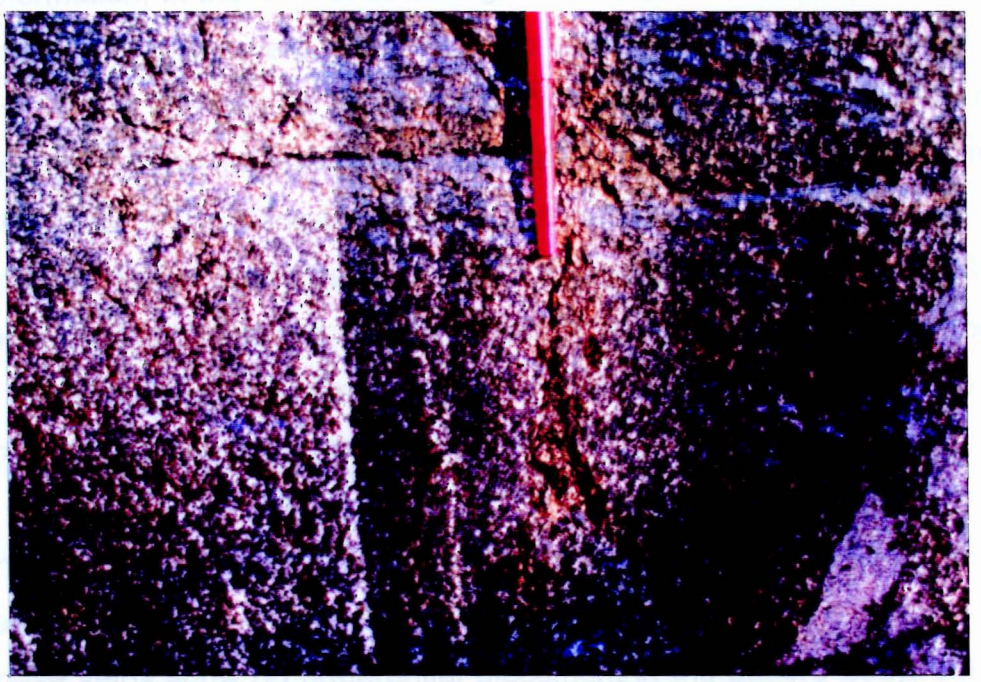


Plate 14
Close-up view of rhythmic layering from the Lower Zone (Traverse 3, Figure 6) showing gradational as well as sharp layer contacts.

Layering in the Sterkspruit Lower Zone Gabbro can also be described as density sorted, whereby the more dense pyroxenes accumulated towards the floor of the chamber, and the less dense plagioclase accumulated in the upper portions of layers by means of a flotation mechanism (Irvine, 1982). Goode (1976) described similar layering in the Kalka layered intrusion in Australia. He proposed that density-sorted layers resulted from repeated phases of discontinuous nucleation, followed by differential gravity settling of pyroxene relative to plagioclase. Factors such as thickness and height of the nucleation zone above the nucleation front and the time interval between nucleation bursts, control differential crystal settling and the production of isomodal or graded layers (Naslund and McBirney, 1996). On the other hand, Mandziuk *et al.* (1989), described a genetic link between magmatic flow and layer development in the Falcon Lake Complex in Manitoba. They proposed a process of crystal-liquid separation, stimulated by laminar flow.

Deformation, in the form of flattening and shear foliation, is evident in the gabbro and in the field takes the form of both 'dog-tooth' type outcrops and sets of sub-parallel fractures, both dipping steeply to the north and having an east-northeast direction parallel to the gabbro-basalt contact (Plate 15). The 'dog-tooth' outcrops are similarly located in the surrounding komatiitic basalts, but at a smaller scale. These localised shears within the gabbro are not widespread and are separated by zones of more massive, unsheared gabbro. The absence of shearing is also not uncommon in the surrounding schist belt.

Shearing is also evident in dilational veins, varying in width from a few centimetres to more than a metre wide, but averaging 50 cm (Plate 16). These veins show no preferential placement in the gabbro body, but are discontinuous and never more than a few metres in length. These thin zones of deformation are replaced by quartz and fine-grained

recrystallised gabbro and resemble isolated shear zones with sub-parallel foliation developed locally in the surrounding gabbro. The orientation of these veins and shear fabric is generally east-west, dipping steeply to the north. This direction is parallel to the rhythmic layering in the Lower Zone gabbro as well as the regional strike direction of the rocks in the southern portion of the Nelshoogte Schist Belt.

The lack of more widespread deformation in the gabbro body is probably due to its greater width in comparison to the thinner, layered komatiitic basalt flow units, both massive and pillowed, as well as the interlayered komatiites and cherty and ferruginous sediments. These units, constituting part of the Nelshoogte Schist Belt, acted as zones of preferential movement during deformation.

On a larger scale, towards the west side of the intrusion, the body displays gentle open folding, with the strike changing from east-northeast to northeast, concordant with the surrounding volcanic rocks and the Stolzburg Complex.

Lineaments, forming regional features, can be clearly seen on aerial photographs as evidenced by abundant vegetation growth and where many streams have taken advantage of fractures. The general trend of these lineaments is northwest, with faults and fractures commonly providing tensional zones of weakness that appear to have controlled the emplacement of diabase dykes.



Plate 15
Deformation in the Sterkspruit Intrusion shown by shear foliation and flattening of gabbro from the Central Zone.



Plate 16
Late veins, parallel to regional strike, containing fine - grained quartz and recrystallised gabbro occurring in a weathered portion of the Sterkspruit Intrusion.

3.4 Geology of the Sterkspruit Mafic Dyke Swarm

Hypabyssal rocks in the form of dykes and to a lesser extent, sills, are prolifically distributed over the entire Barberton area (Visser *et al.*, 1956; Visser and Verwoerd, 1960; Viljoen and Viljoen, 1969a; Anhaeusser, 1973; Robb, 1977). Establishment of dyke emplacement ages is based mainly on field observations. From their relationship with the volcano-sedimentary sequences comprising the Barberton Mountain Land and the granites, as well as relationships with the stratigraphic sequences present along the Transvaal Drakensberg escarpment to the west, the relative ages of these dykes can be determined. Visser *et al.* (1956), proposed a four-fold subdivision of the dykes as follows:

1) dykes older than the Moodies System (now Moodies Group);
2) dykes and sills older than the Godwan Formation;
3) dykes and sills younger than the Transvaal System (now Transvaal Supergroup); and
4) later dykes of Karoo dolerite age.

Visser and Verwoerd (1960) also recognised three ages of dykes north of Nelspruit which they termed:

1) pre-Godwan intrusions;
2) post-Transvaal intrusions; and
3) post Karoo doleritic intrusions.

The lack of geochronological data on Archaean and Proterozoic dykes in Southern Africa was highlighted by Hunter and Reid (1987) as constraining the identification of their extent and distribution. They also based the relative ages of dykes on field criteria. An Archaean age can be inferred where it can be demonstrated that dykes predate the deposition

of sediments correlated with the ~ 2.8 Ga Witwatersrand Supergroup. Hunter and Reid (1987) considered there was sufficient evidence of dyke emplacement in the Archaean and Early Proterozoic at ~3.0 Ga, ~2.8 Ga, ~2.2 Ga and ~1.9 Ga. Dykes from these time periods were shown to be orientated in northwesterly or northeasterly directions.

In the study area, approximately 15 crosscutting mafic dykes were found intruded into the Sterkspruit body and surrounding volcanic and granitic rocks. These dykes were mapped and sampled (Figure 3). The majority of these dykes, forming the Sterkspruit dyke swarm, conform to the most common northwest or 30 to 35° west of north direction, which is the prominent strike direction in the Barberton area (Visser *et al.*, 1956; Wuth, 1980). The Sterkspruit dykes do not appear to intrude either the Godwan Beds, or the sediments of the Transvaal Supergroup and therefore correspond to dykes older than the Godwan Formation (Visser *et al.*, 1956) and to pre-Godwan intrusions (Visser and Verwoerd, 1960). The dykes are also similar to the majority of dykes and sills studied by Robb (1977) in the region north of Nelspruit, between Hazyview and Bushbuckridge. These dykes, which Robb (1977) interpreted to be pre-Godwan in age, are predominantly diabasic in composition consisting of sericitised plagioclase and uralitised pyroxene. The petrological and geochemical characteristics of these dykes compare favourably with those of the Sterkspruit dyke swarm and will be discussed further in Chapters 4 and 5.

A variety of diabase and dolerite dykes and sills of different ages have also been reported by Menell *et al.* (1986) which intrude the Kalkkloof Complex which lies within a greenstone remnant west of the Nelshoogte Schist Belt. They described a set of dykes and sills which are post Transvaal Supergroup in age and which they associate with the igneous activity that led to the emplacement of the Bushveld Igneous Complex.

This relationship between diabase dykes and the Bushveld Complex was also proposed by Anhaeusser (1978) for a set of medium-grained diabase dykes crosscutting the Johannesburg Dome and the western parts of the Muldersdrif Ultramafic Complex.

The dykes which intruded into the Nelshoogte Schist Belt are generally steeply dipping and form prominent ridges, especially in the lower-lying granitic terrains. The majority of the dykes also support abundant vegetation growth, making them highly visible features. Most of the dykes tend to terminate against the Stolzburg Complex. Where they do intrude this Complex, they generally form negative weathering depressions relative to the more resistant ultramafic rocks. Within the Sterkspruit Intrusion, these dykes form piles of weathered boulders and contact relationships are rarely visible.

The dykes vary in thickness from a few metres to about 50 m. Closely spaced parallel dykes commonly coalesce or split and form thinner dykes before dying out completely. A variety of shapes occur, including wider sections where the dykes appear to form large bulbous masses. The most common dyke form, however, is the linear, subvertical variety which often follow (or are intruded into) earlier fault or shear zones. Many of these dykes have been displaced by later faulting. In places the dykes also appear to have been deflected by the komatiitic lava units that appear to have undergone shearing rather than fracturing, making it more difficult for the magma to intrude the strongly foliated or anisotropic successions. More rarely, finer-grained, narrow sheet intrusions (sills) can be observed interlayered with the surrounding volcanics.

All of the dykes in the study area appear to be younger than the Sterkspruit Intrusion. Clear evidence of an intrusive relationship can be demonstrated by a fine-grained chilled contact on both sides of a 5 m

wide diabase dyke crosscutting the gabbro body in the stream traverse labelled Traverse 3 in Figure 6 (Plate 17).

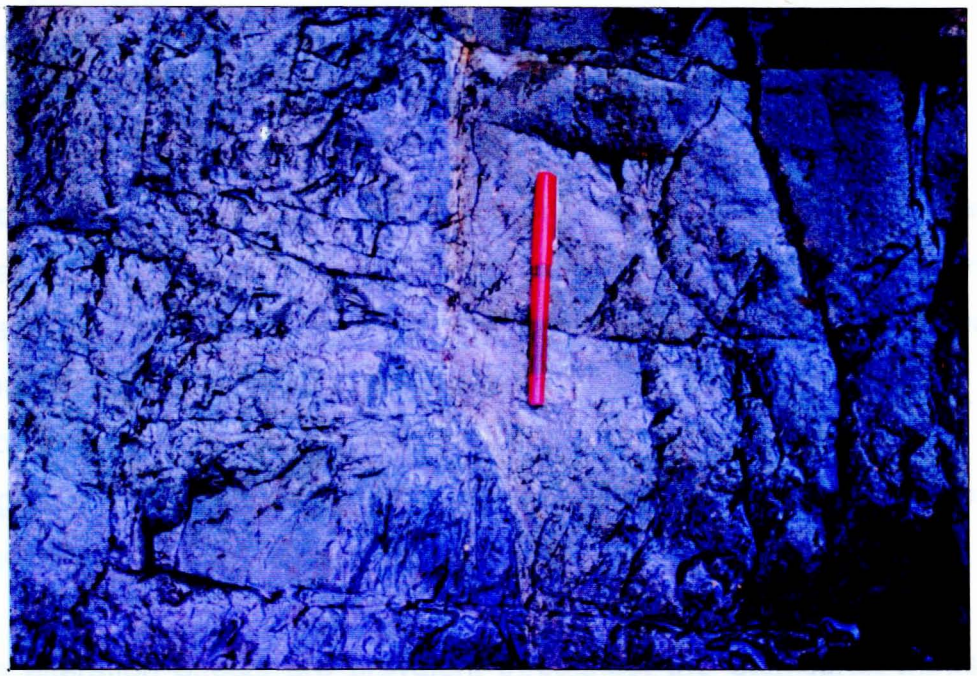


Plate 17
Close-up view of an intrusive contact, showing a fine-grained chilled margin, between a crosscutting mafic dyke (left) and gabbro (right) from the Sterkspruit Intrusion (Traverse 3, Figure 6).

CHAPTER 4
PETROGRAPHY

4.1 Introduction

The mineralogical description of the Sterkspruit gabbro samples has been restricted to two main sample traverses across the body, namely Traverse 1 and Traverse 2 (Figures 3 - 5). The overall petrography of the gabbroic intrusion is relatively uniform between the two sections which can be used as type localities for describing the intrusion as a whole. In addition, samples collected by Pospisek (1991) for a study of a portion of the intrusion were used to supplement those collected by the writer.

Along both sample sections the compositions of some of the least altered plagioclase grains were determined using a microprobe analyser. Depending on the locality within the body, the composition was found to vary between oligoclase in the Marginal Zone to albite in the Central and Upper Zones. The plagioclase grains from the Lower Zone gabbro are highly altered and are unsuitable for analysis (see Chapter 5.3 on mineral chemistry).

As alteration effects are prevalent throughout the Sterkspruit Intrusion, only a general description of the main alteration types is included. Each of the main zones delineated across the width of the intrusion is described in detail (viz: the Marginal Zone, the Lower Zone, the Central Zone, the Quartz Diorite and the Upper Zone).

4.2 Alteration

All samples investigated are highly altered, with ferromagnesian minerals (clinopyroxene and orthopyroxene) partly or completely uralitised and the plagioclase phases having undergone saussuritisation, albitisation, epidotisation and sericitisation to varying degrees. Due to the lack of penetrative deformation fabric in the gabbroic rocks, this alteration assemblage possibly results more from high temperature deuteric alteration shortly after or during emplacement of the body (Cloete, 1991, 1994). However, it is likely that burial metamorphism caused greenschist facies overprinting to take place. The mineral assemblage, comprising actinolite, chlorite, epidote, zoisite, albite and leucoxene, are typical of greenschist facies metamorphism. However, the presence of pyroxenes in the Marginal and Lower Zones, discussed later on in sections 4.1.3 and 4.1.4, does not indicate a stable metamorphic assemblage. The following descriptions are of the most common types of alteration found in the Sterkspruit gabbroic rocks.

4.2.1 Saussuritisation

Saussuritisation is the replacement of plagioclase, especially noted in basalts and gabbros, by a fine-grained aggregate of zoisite, epidote, albite, calcite, sericite and zeolites (Bates and Jackson, 1980). This alteration is considered to be a metamorphic or deuteric process and is often accompanied by chloritisation of ferromagnesian minerals.

4.2.2 Albitisation

Albitisation is a process whereby albite is introduced and replaces more calcic plagioclase. This type of alteration is associated with low-

temperature metamorphic rocks (greenschist facies), but is also deposited from hydrothermal solutions (Bates and Jackson, 1980; Deer *et al.*, 1982).

4.2.3 Uralitisation

Uralitisation is the alteration process whereby primary pyroxenes are converted to fibrous amphibole. This process is ascribed to both the action of circulating hydrothermal solutions during late-stage crystallisation of the igneous rocks, or to regional metamorphism (Deer *et al.*, 1982). Uralite is a green, fibrous, acicular variety of secondary amphibole occurring as pseudomorphs after pyroxene.

4.2.4 Epidotisation

Epidotisation is the hydrothermal introduction of epidote into rocks, or the alteration of rocks in which plagioclase is albitised, freeing the anorthite molecules for the formation of epidote and zoisite. Epidote is, therefore, associated with albite and chlorite in low-grade metamorphic rocks. Zoisite (part of the epidote group) is an essential constituent of saussurite in low-grade metamorphic rocks, especially calcium-rich phases.

4.2.5 Chloritisation

Chloritisation is the replacement or conversion of ferromagnesian minerals into chlorite (Bates and Jackson, 1980) and is a product of hydrothermal processes.

4.2.6 Carbonation

This process involves the transformation of minerals containing Ca, Mg, K, Na and Fe into carbonates or bi-carbonates of these metals by CO_2 in circulating water (Bates and Jackson, 1980). In the Barberton sequence, Viljoen and Viljoen (1969b), described carbonate occurring as scattered grains or as small crosscutting veinlets close to shear zones. Elements lost during carbonation include SiO_2, Al_2O_3, MgO, CaO and K_2O while FeO, Na_2O and TiO_2 increase.

4.3 Petrography of the Sterkspruit Intrusion

4.3.1 Marginal Zone Gabbro

A fine-grained chill zone, measuring less than 2 m in width, marks the intrusive contact along the northern margin of the intrusion at Traverse 2 and at Traverse 3 (Figures 5 and 6). In thin section the chill margin is a fine-grained rock and, due to rapid cooling, shows in situ nucleation and growth. The chill margin consists of fibrous pleochroic green actinolite/tremolite showing low to moderate birefringence, a mass of highly saussuritised plagioclase of oligoclase composition and quartz (Plates 18 and 19). This mineralogical assemblage suggests low-grade greenschist facies metamorphism. Due to the fine-grained nature of this chill margin and the absence of cumulates, the whole-rock composition from this chilled zone could possibly be used as an indication of the parental magma to the gabbroic intrusion as a whole. The normative plagioclase composition for the chill zone is An_{29-44} indicating a dioritic liquid. This observation is supported by its evolved chemistry to be discussed in Chapter 5.

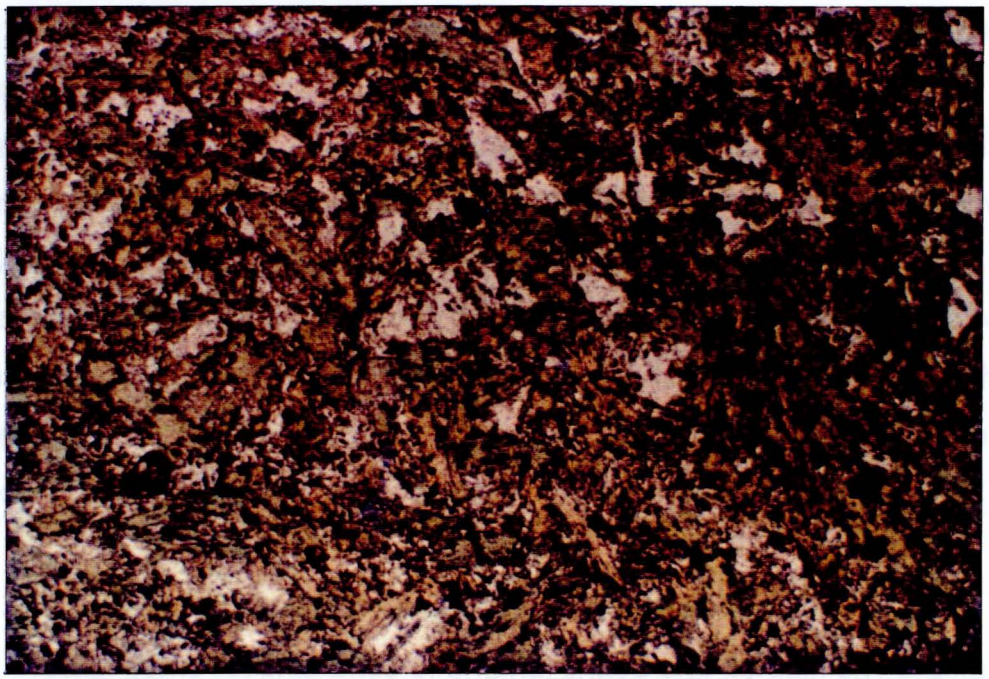


Plate 18
Photomicrograph of the fine-grained gabbroic chill margin in the Sterkspruit Intrusion. Intergrowth of actinolite, saussuritised plagioclase and quartz (Sample SG38; plane polarised light; 1 cm = 250 µm).

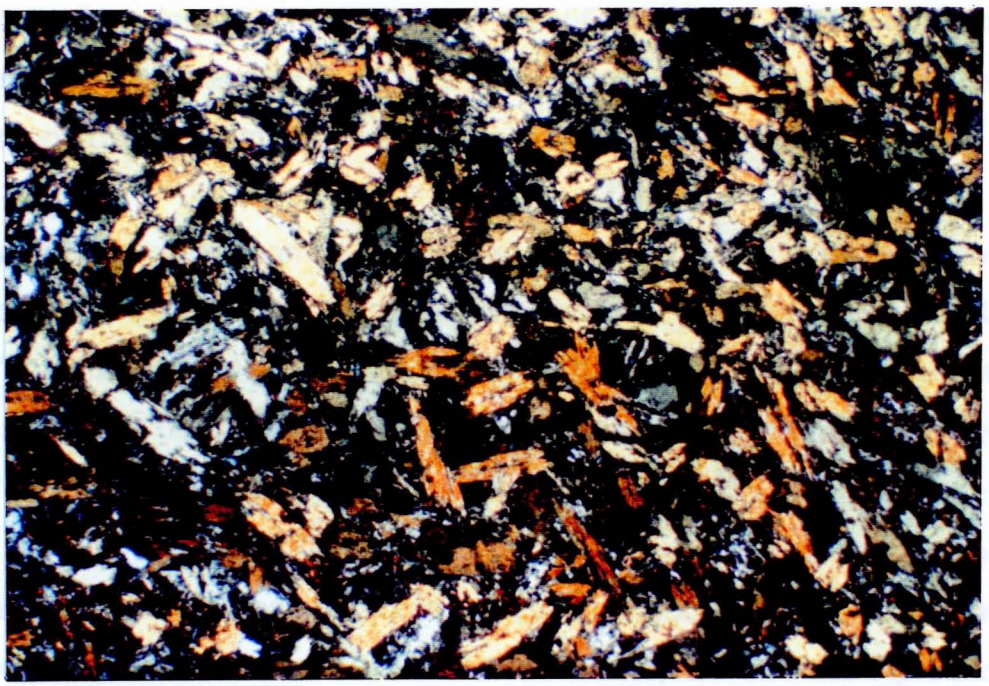


Plate 19
Photomicrograph of the same sample shown in Plate 18 above, but observed under crossed nicols (Sample SG38; 1 cm = 250 µm).

Away from the chill margin, the gabbro shows a progressive increase in grain size, but within 15 m of the contact retains the same minerals and texture as the fine-grained chill margin (Plates 20 and 21). Further into the intrusion, various textures are observed, including poikilitic clinopyroxenes enclosing plagioclase laths in a subophitic arrangement (Plates 22 and 23) and pyroxenes forming minor adcumulate to mesocumulate textures without the presence of plagioclase. Relatively fresh remnants of pyroxene are still visible in some grains, but all show some degree of alteration and conversion to uralite and amphibole. In general the pyroxene grains are either:

1) completely uralitised, having fibrous anhedral shapes or;
2) retain some resemblance of original shape and contain tiny uralite needles or;
3) are completely pseudomorphed by amphibole.

Simple twinning can be observed in the fresher clinopyroxene grains. Although alteration makes the identification of minerals difficult, clinopyroxene appears to be the most common pyroxene with orthopyroxene estimated to form less than 10% of the sample.

Plagioclase grains can be recognised in places by their equant subhedral tabular shapes, but are extremely clouded as a result of saussuritisation. Of particular note is the greater presence of zoisite in the alteration assemblage over epidote, associated with anorthite-rich plagioclase and probably controlled by iron activity and changes in oxygen fugacity in this part of the intrusion. Quartz is abundant and is interstitial to plagioclase forming characteristic angular infill shapes. Accessory mineral phases include leucoxene, an alteration product of titanium rich phases such as ilmenite, which occurs as a light brown mineral surrounding a dark brown core. Chlorite can be found mostly in the altered groundmass, along with zoisite.

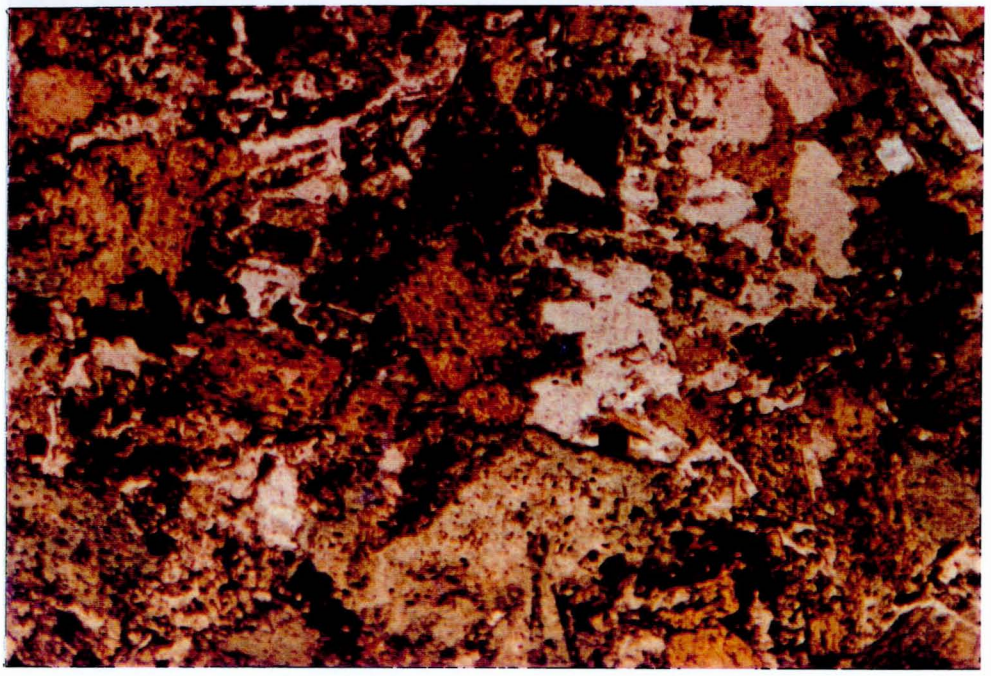


Plate 20
Photomicrograph of gabbro from the Marginal Zone within 5m of the intrusive contact. Subophitic textures occur with partly altered clinopyroxene, orthopyroxene and saussuritised plagioclase. Quartz is interstitial to plagioclase and occurs as subrounded grains (Sample SG39; plane polarised light; 1cm = 200 µm).

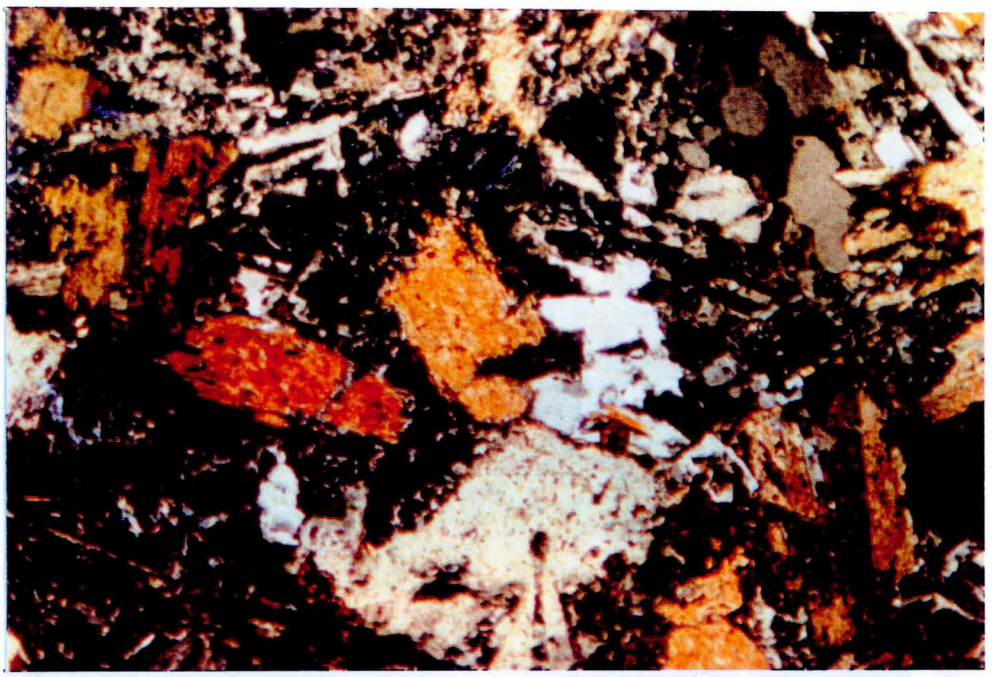


Plate 21
Photomicrograph of the same sample shown in Plate 20 above, but observed under crossed nicols (Sample SG39; 1 cm = 200 µm).

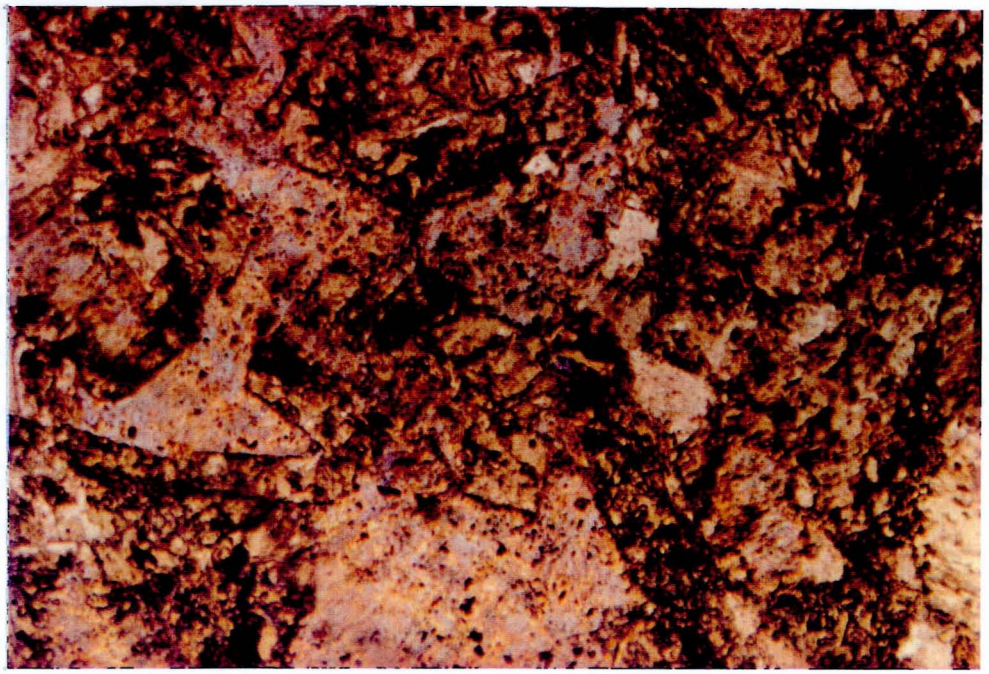


Plate 22
Photomicrograph of the gabbroic rocks from the Marginal Zone, showing typical subophitic textures with partly uralitised clinopyroxene oikocrysts enclosing plagioclase laths. The plagioclase retains subhedral shapes, but are clouded to a dark-brown colour due to the effects of saussuritisation (Sample SG22; plane polarised light; 1 cm = 200 µm).

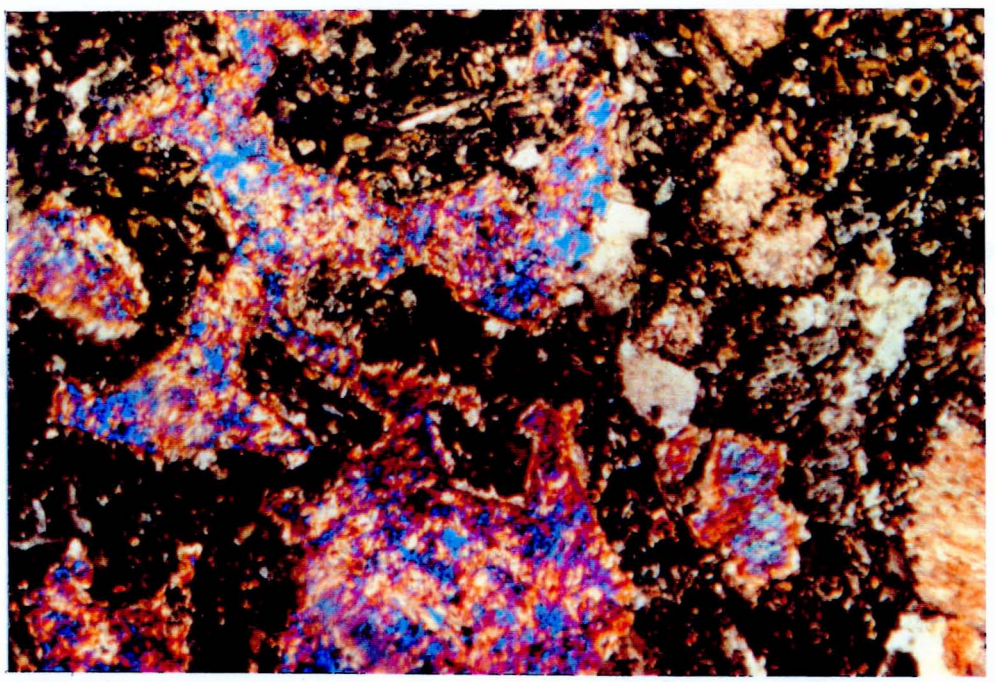


Plate 23
Photomicrograph of the same sample shown in Plate 22 above, but observed under crossed nicols (Sample SG22; 1 cm = 200 µm).

4.3.2 Lower Zone Gabbro

The rhythmically layered Lower Zone gabbro occurring on the northern portion of the intrusion displays both plagioclase and plagioclase - clinopyroxene cumulate textures (Plates 24 and 25). The more felsic layers and segregations consist of plagioclase orthocumulate textures with quartz forming the interstitial phase. The more mafic portions of the layers consist of cumulate plagioclase and clinopyroxene which nucleated together. Subhedral, lath-like plagioclase grains are partly enclosed by altered clinopyroxene in an ophitic to subophitic texture.

The lath-like plagioclase grains are clouded, as a result of saussuritisation, to a mixture of zoisite, albite, chlorite, sericite and epidote. Some grains still show evidence of polysynthetic twinning. As in the Marginal Zone, the intercumulate quartz forms typical angular shapes. The primary pyroxenes have either been altered to a medium-grained fibrous mass comprising incipient actinolite and chlorite needles, or are completely pseudomorphed by crystals of actinolite or hornblende. These latter amphiboles are generally subhedral in shape, but in places the mafic phases consist of highly altered masses of uralite with fibrous and very indistinct boundaries. In places, remnant simple twinning in pyroxenes is preserved. In addition to the above-mentioned altered mafic and felsic minerals there are also accessory amounts of dark, red-brown rutile together with leucoxene.

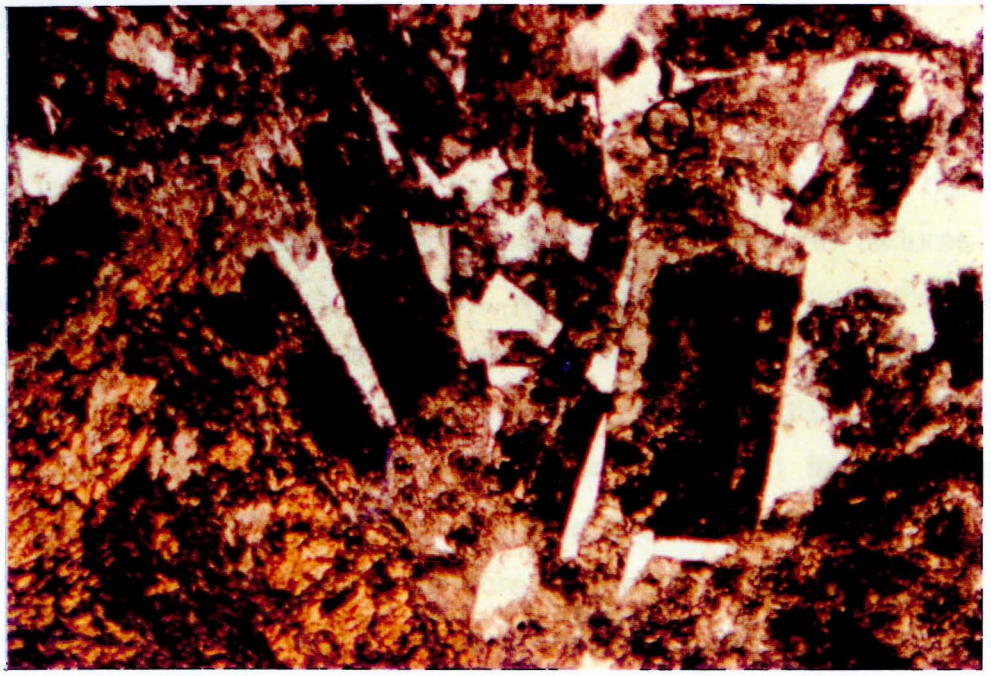


Plate 24
Photomicrograph of the layered gabbro from the Lower Zone, showing orthocumulate clouded plagioclase with interstitial angular-shaped quartz. A clinopyroxene grain showing incipient uralitisation can be seen on the lower left side of the photograph (Sample SG24; plane polarised light; 1 cm = 200 µm).



Plate 25
Photomicrograph of the same sample shown in Plate 24 above, but observed under crossed nicols (Sample SG24; 1 cm = 200 µm).

4.3.3 Central Zone Gabbro

This rather non-descript zone is gradational between the Lower Zone and the Quartz Diorite (Traverse 1, Figure 4). The rocks consist of a high-Ti ferrogabbro and display similar plagioclase orthocumulate textures as seen lower down in the sequence, with quartz occurring as the main intercumulus phase. In addition, plagioclase and actinolite display an intergranular texture. These dark-green, extremely pleochroic amphiboles have fibrous shapes and show complete conversion from pyroxene (Plates 26 and 27). The plagioclase phases are also highly saussuritised, but show epidote alteration to be more common than zoisite. In this zone there is a high proportion (~15%) of amorphous leucoxene (after ilmenite) which increases in amount towards the Quartz Diorite horizon. This increase in leucoxene is reflected chemically in the TiO_2 abundance in this zone which reaches 2.2%.

The upper portion of the Central Zone shows a gradational change, and has textures which are similar to the Quartz Diorite horizon. Intergranular textures comprising plagioclase, quartz and amphibole (actinolite/hornblende) are features of this part of the Central Zone. The plagioclase laths show less clouding than in the Lower Zone and are not as intensely saussuritised. Abundant epidote alteration occurs around the margins and replaces cores of plagioclase grains. Polysynthetic twinning in some of these grains is common. A number of the dark-green amphibole grains show alteration to chlorite.

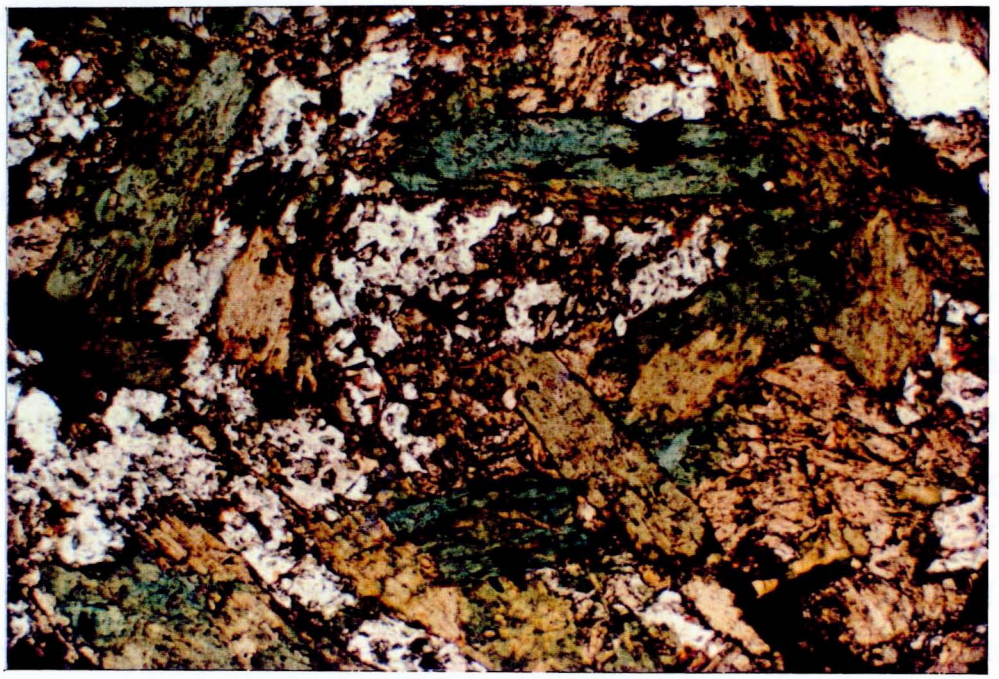


Plate 26
Photomicrograph of the high-Ti ferrogabbro from the Central Zone, showing an intergrowth between fibrous actinolite, saussuritised plagioclase and quartz. Yellow-green epidote with bright interference colours is more prominent in the Central Zone. Opaque phases are leucoxene after Ti-ilmenite (Sample SG26; plane polarised light; 1 cm = 250 μm).

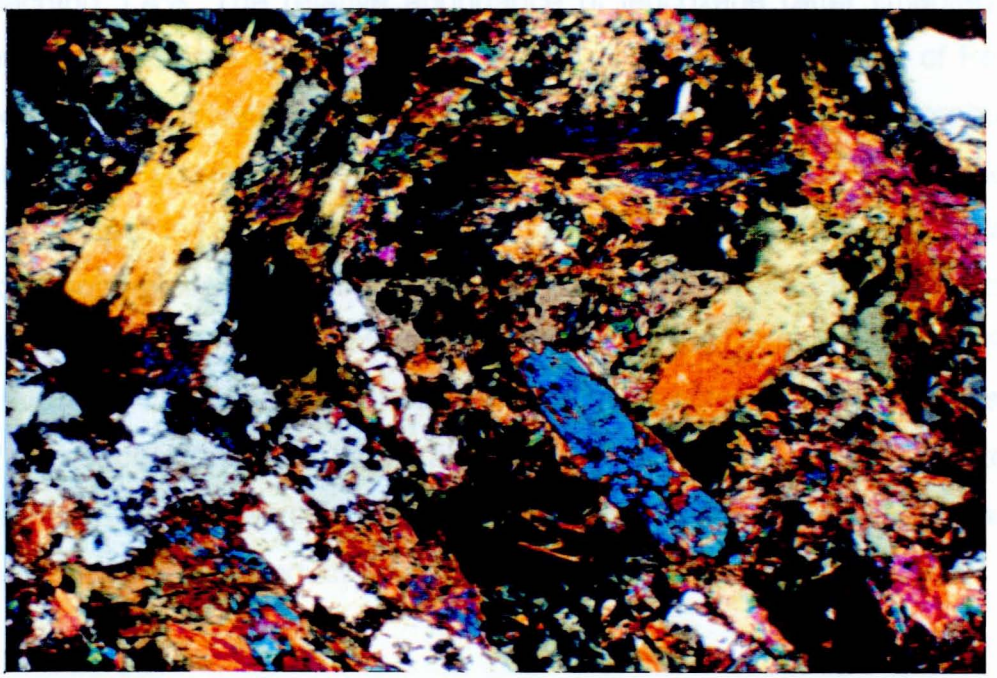


Plate 27
Photomicrograph of the same sample shown in Plate 26 above, but with bright interference colours and observed under crossed nicols (Sample SG26; 1 cm = 250 μm).

4.3.4 Quartz Diorite

This zone, which appears to be less than 50 m in width, is comprised of a medium- to coarse-grained, leucocratic, quartz-rich diorite with quartz (up to 25%), plagioclase (up to 25%), chlorite (20%) and carbonate (15%) forming the major constituents of the rock (Plates 28 and 29). The plagioclase is much less saussuritised than lower down in the body and displays polysynthetic twinning. It typically has epidote forming around the edges of grains or replacing the interior of grains. The quartz forms large, anhedral, subrounded grains and shows undulose extinction. The amphibole has been completely altered to chlorite and minor biotite. The chlorite forms amorphous fibrous masses, while the biotite forms tiny grains between the quartz and plagioclase grains.

An unidentified opaque phase (probably ilmenite) and leucoxene are abundant, forming about 15% of the rock. TiO_2 in this zone is high, reaching 1.4%. The relative abundance of leucoxene (after ilmenite) in this horizon and in the underlying Central Zone, is an indication of Fe-Ti oxides forming late in the crystallisation sequence The amorphous leucoxene shown in Plates 30 and 31, has dark-brown interiors surrounded by a lighter-brown rim. Carbonate is also an important accessory mineral replacing primary mineral phases rather than occurring in proximity to veins or fractures. De Wit *et al.* (1987b) and Cloete (1991) interpreted the carbonate alteration in the mafic volcanics to be the result of syndepositional sea-floor alteration. This Quartz Diorite horizon, although only observed in one locality on Traverse 1 (Figure 4), could represent the end product of a differentiating magma body.

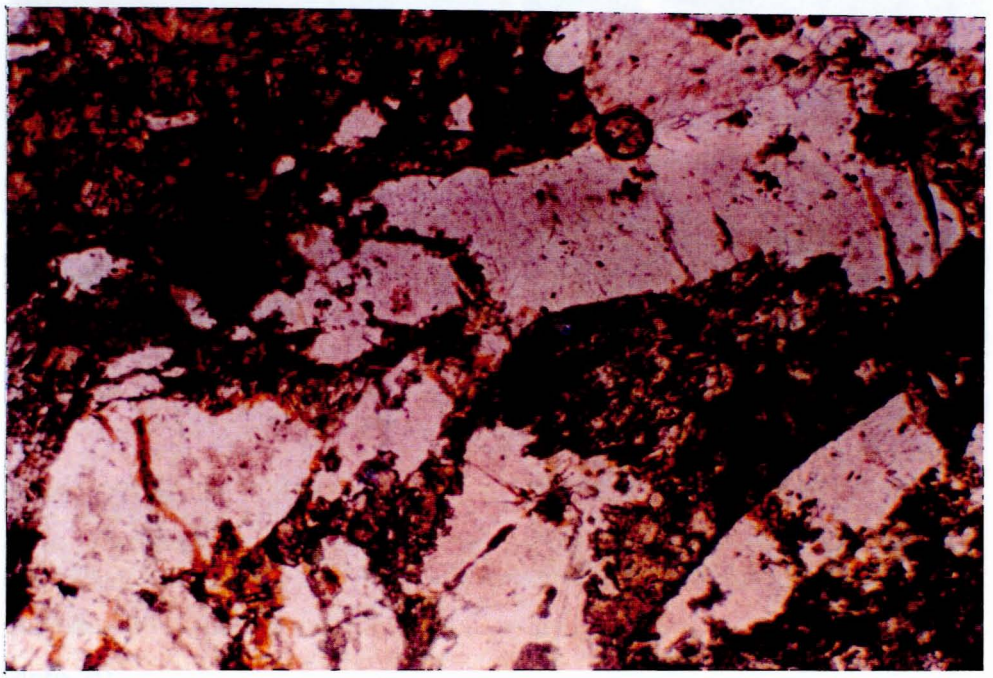


Plate 28
Photomicrograph of the Quartz Diorite, showing dark-green chlorite, large subhedral quartz grains, relatively unaltered plagioclase, carbonate, epidote and tiny biotite flakes (Sample SG28; plane polarised light; 1 cm = 200 μm).

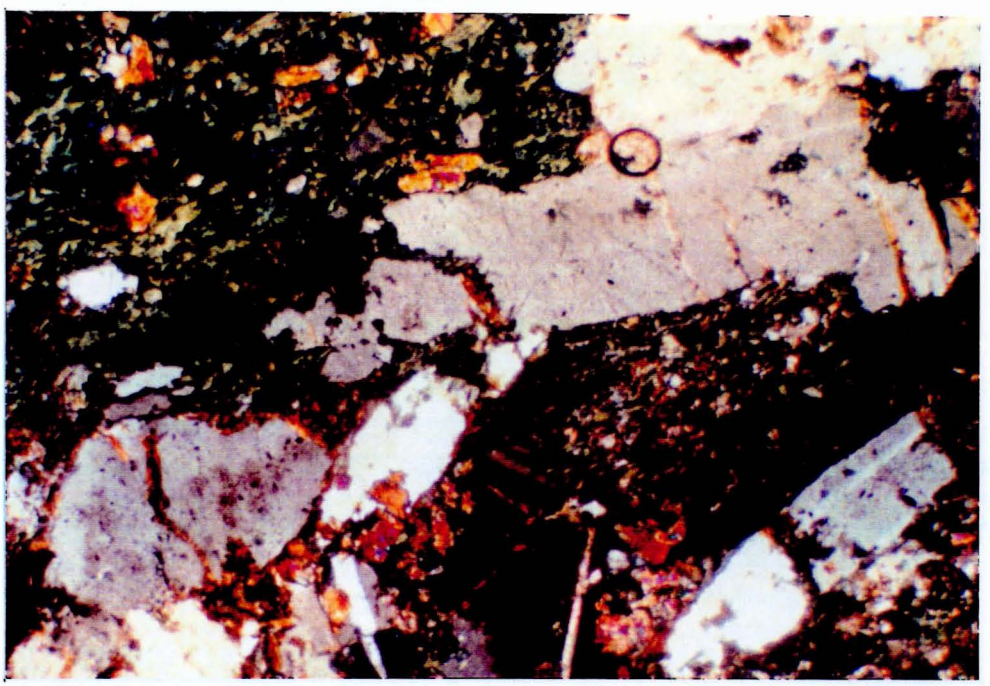


Plate 29
Photomicrograph of the same sample shown in Plate 28 above, but observed under crossed nicols (Sample SG28; 1 cm = 200 μm).

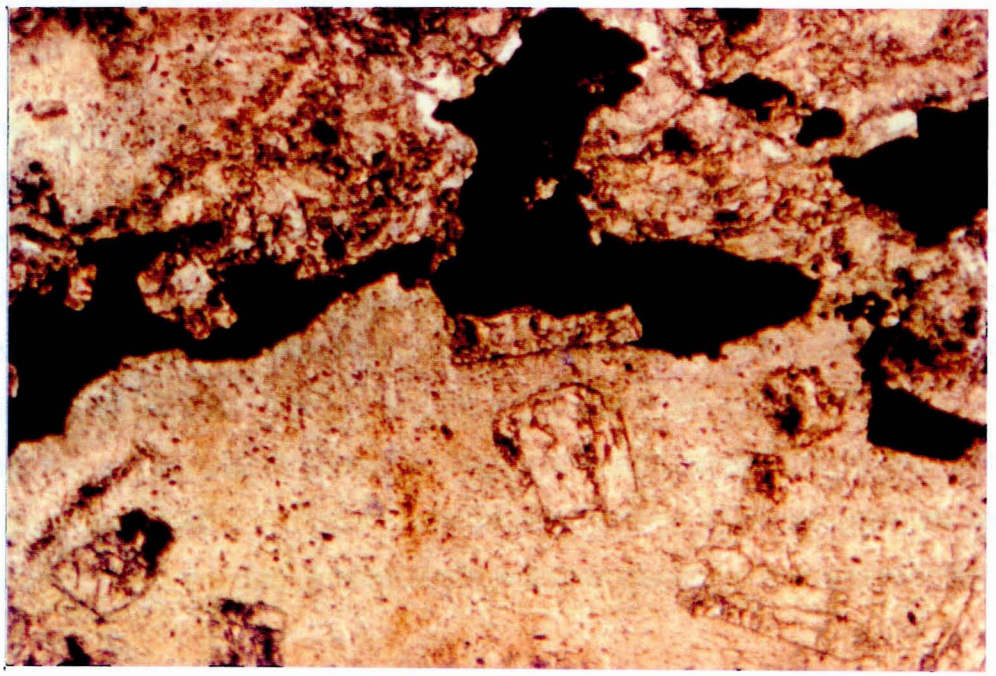


Plate 30
Photomicrograph showing the amorphous nature of dark brown leucoxene. Also shown are partly uralitised clinopyroxene and subhedral plagioclase grains (Sample SG22; plane polarised light; 1 cm = 200 μm).

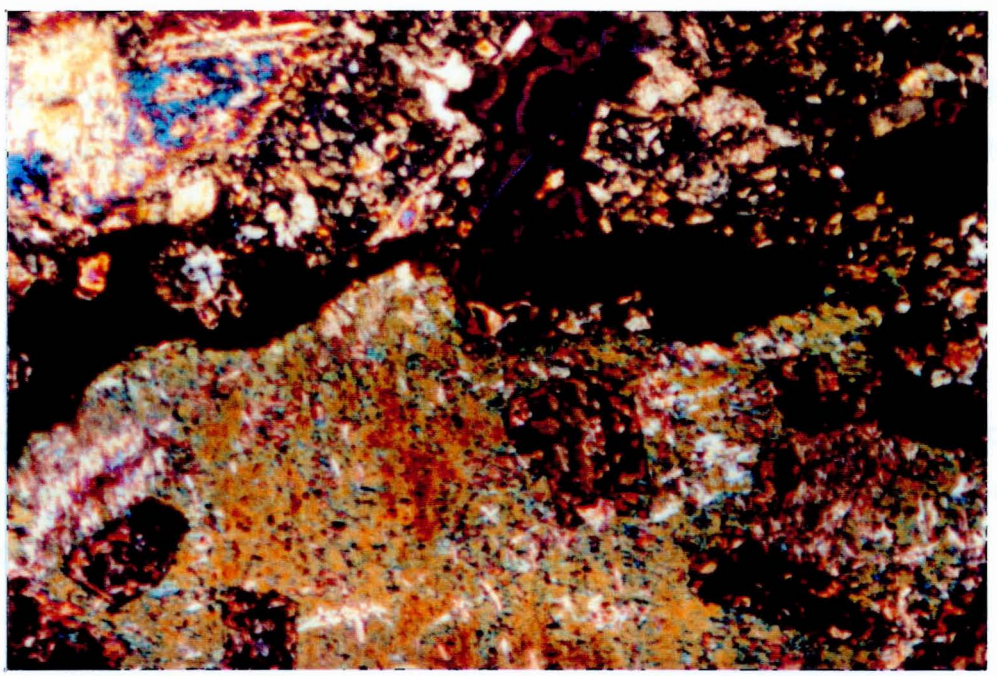


Plate 31
Photomicrograph of the same sample shown in Plate 30 above, but observed under crossed nicols (Sample SG22; 1 cm = 200 μm).

4.3.5 Upper Zone Gabbro

The lower portions of the Upper Zone (Figure 4) have many similarities with the Quartz Diorite and a gradational contact between the two horizons is assumed. In this part of the sequence, plagioclase, quartz, amphibole, epidote and chlorite are the main constituents, while biotite and leucoxene are accessory phases. Significantly, carbonate is almost completely absent. The amphiboles are partly or completely altered to chlorite, while epidote replaces plagioclase around the edges and within the cores of grains. The complete saussuritisation of plagioclase, as seen lower down in the gabbro sequence, was not observed in the Upper Zone.

The remainder of the Upper Zone gabbro, towards the southern margin, is texturally distinct from the remainder of the gabbro body in that bladed, epidotised plagioclase laths form an interlocking, granular texture with light to dark-green, needle-like hornblende and actinolite crystals (Plates 32 and 33). The amphiboles are generally equant in size and shape, but some anhedral grains occur, often with jagged rims where complete alteration to chlorite has taken place. Some acicular amphibole needles characteristically reach 1 cm in length. Epidote is more common in this part of the body, as opposed to zoisite in the lower portions. Overall, the plagioclase appears less altered in the Upper Zone.

Closer to the upper contact (southern margin), subophitic textures can be observed, together with plagioclase laths partly enclosed by fibrous hornblende. In contrast to the lower parts of the intrusion, quartz does not appear to be a late infilling stage in rocks of the Upper Zone.

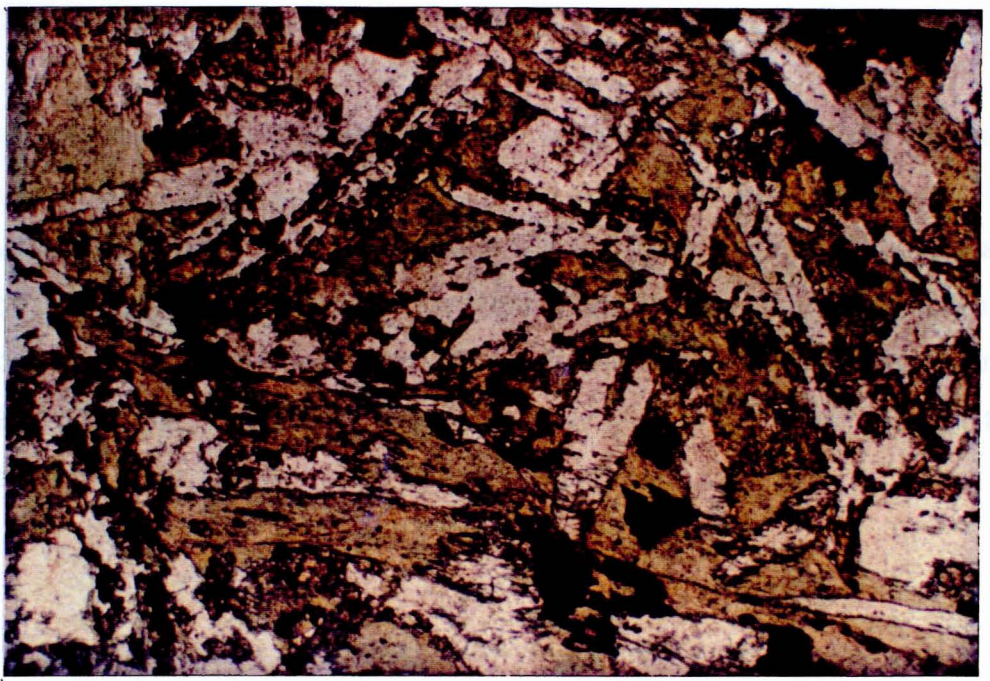


Plate 32
Photomicrograph of the quartz gabbro from the Upper Zone, showing intersertal textures with pleochroic green, acicular, actinolite needles partly enclosing epidotised plagioclase and quartz (Sample SG31; plane polarised light; 1 cm = 250 µm).

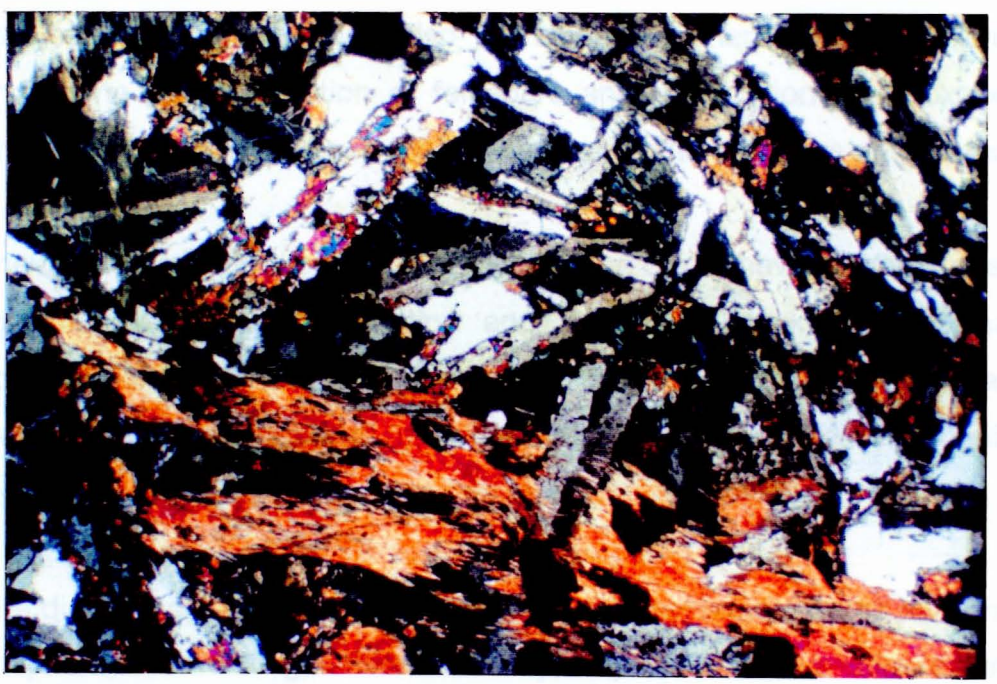


Plate 33
Photomicrograph of the same sample shown in Plate 32 above, but observed under crossed nicols (Sample SG31; 1 cm = 250 µm).

4.3.6 Gabbroic Lens

A small intrusive lens to the south of the main Sterkspruit body and seen in Traverse 1 (Figure 4) displays typical subophitic textures with lath-like plagioclase grains enclosed by large clinopyroxenes altered to uralite and hornblende. These textures show similarities to those seen in the Upper Zone of the main gabbroic body. The textures observed are in accordance with a magma body that has cooled rapidly, and the small size of this satellite intrusive body supports this interpretation.

4.4 Petrography of the Sterkspruit Mafic Dyke Swarm

Texturally, all the dykes in the study area are very similar and they can generally be described as medium-grained hypabyssal mafic dykes. The dykes are usually referred to as diabases, a term synonymous with dolerite, but generally considered to be older or pre-Tertiary in age (Bowes, 1989). They are also more altered than dolerites, having undergone saussuritization of feldspars and uralitization of pyroxenes. The use of the term diabase will be retained for the purposes of this study.

The outer, weathered portions, of the diabase dykes have a characteristic light-brown to cream coloration and are often speckled with small, positively weathered, quartz grains. The fresh rock is equigranular and medium grained, green to grey-green in colour, with ferromagnesian mineral phases plus plagioclase and quartz.

The diabase dykes are highly altered, but original rock textures and grain shapes can be distinguished microscopically and show variable textures and intergrowths of plagioclase, clinopyroxene, orthopyroxene and quartz (Plates 34 and 35). The most common texture displayed by these rocks is

intergranular, with subophitic textures showing plagioclase partly enclosed by pyroxenes also evident in many places. The plagioclase crystals are mostly tabular in form and appear cloudy due to the effects of saussuritization.

The pyroxenes are also highly altered and are replaced by actinolite or hornblende or altered to a fibrous uralite mass comprising amphibole and chlorite. Some crystals of pyroxene are altered around the edges to amphibole, biotite and chlorite. Sphene is present as an accessory mineral in some samples. In places, patches of plagioclase intergrown with quartz form a myrmekitic texture.

Sample SD7 is from a dyke that intruded into the trondhjemitic gneisses forming the Nelshoogte pluton northwest of the Sterkspruit Intrusion (Figure 3). Texturally, this dyke sample differs from the other mafic dykes forming the Sterkspruit mafic dyke swarm in that typical subophitic textures are rare, and felsic segregations more common. Plates 36 and 37 show what has been interpreted as a cumulate plagioclase texture with interstitial quartz in contact with a large crystal of fibrous, highly uralitised pyroxene. Assimilation of the granitic rock by the intruding magma could explain this textural difference.

Dyke sample SD8 (Figure 3) is a fine-grained, 2 m-wide dyke striking almost east-west. This dyke differs from the northwest-trending dykes in that it intruded along weaknesses in the gabbro, resulting from shearing parallel to the length of the Sterkspruit body. The dyke consists of a mass of fibrous amphiboles forming long acicular needles as well as radiating fibres. The rock also contains fine-grained altered pyroxene remnants in a groundmass consisting of chlorite, biotite and epidote.

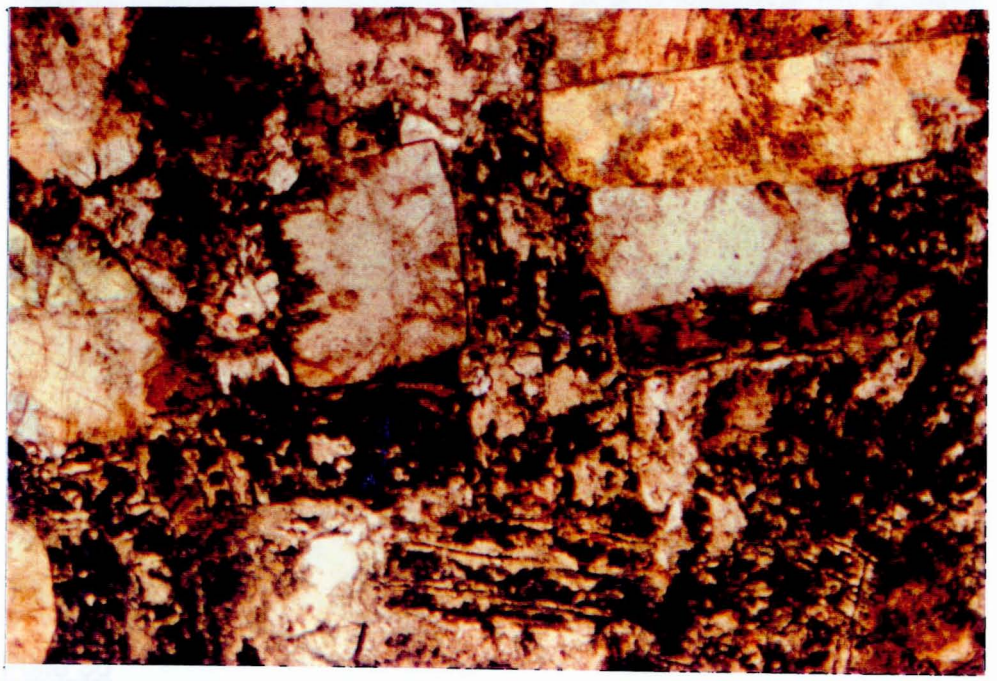


Plate 34
Photomicrograph of a mafic dyke from the western part of the study area. Intergranular textures with tabular clinopyroxene and clouded plagioclase grains are visible (Sample SD1; plane polarised light; 1 cm = 200 µm).

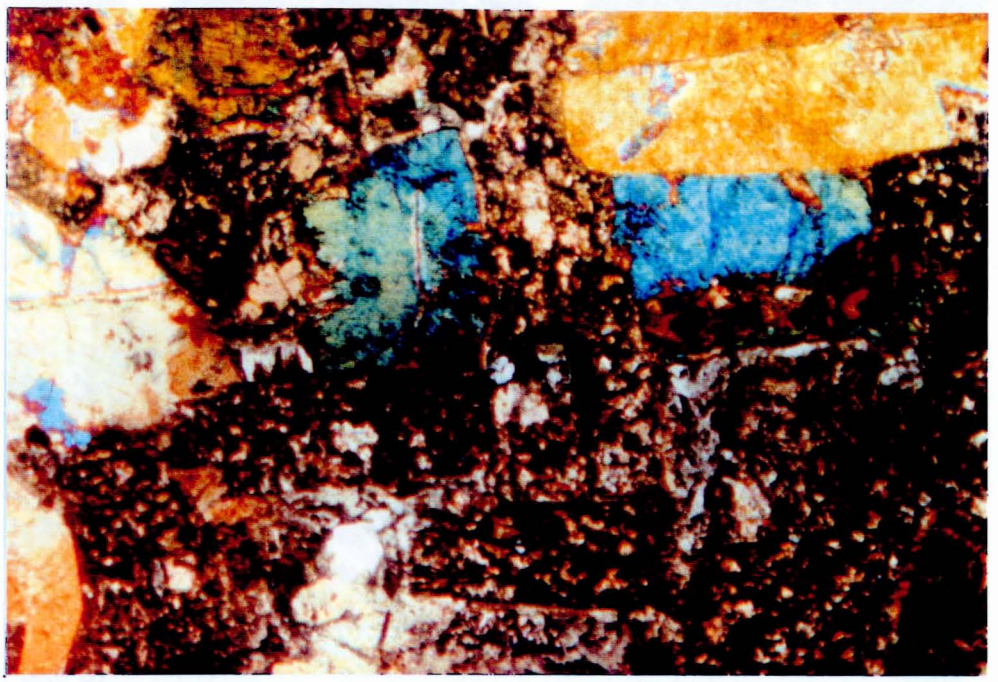


Plate 35
Photomicrograph of the same sample shown in Plate 34 above, but observed under crossed nicols (Sample SD1; 1 cm = 200 µm).

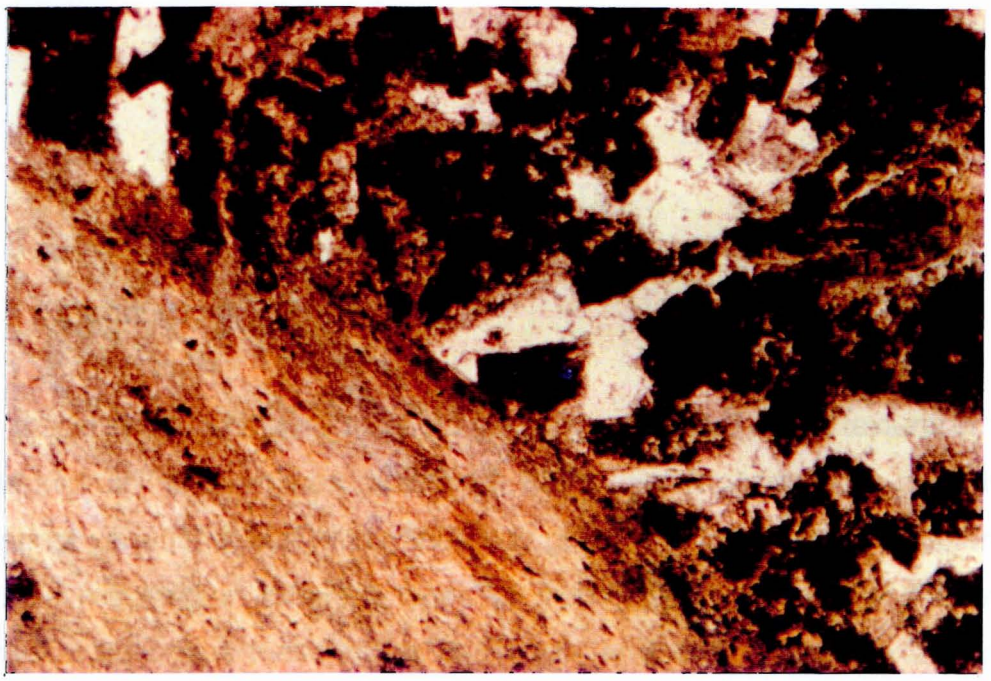


Plate 36
Photomicrograph of a sample from a mafic dyke intruded into the Nelshoogte trondhjemitic gneiss pluton. Right side of photograph shows plagioclase laths and interstitial quartz while the left side shows a uralitised pyroxene grain (Sample SD7; plane polarised light; 1 cm = 200 µm).

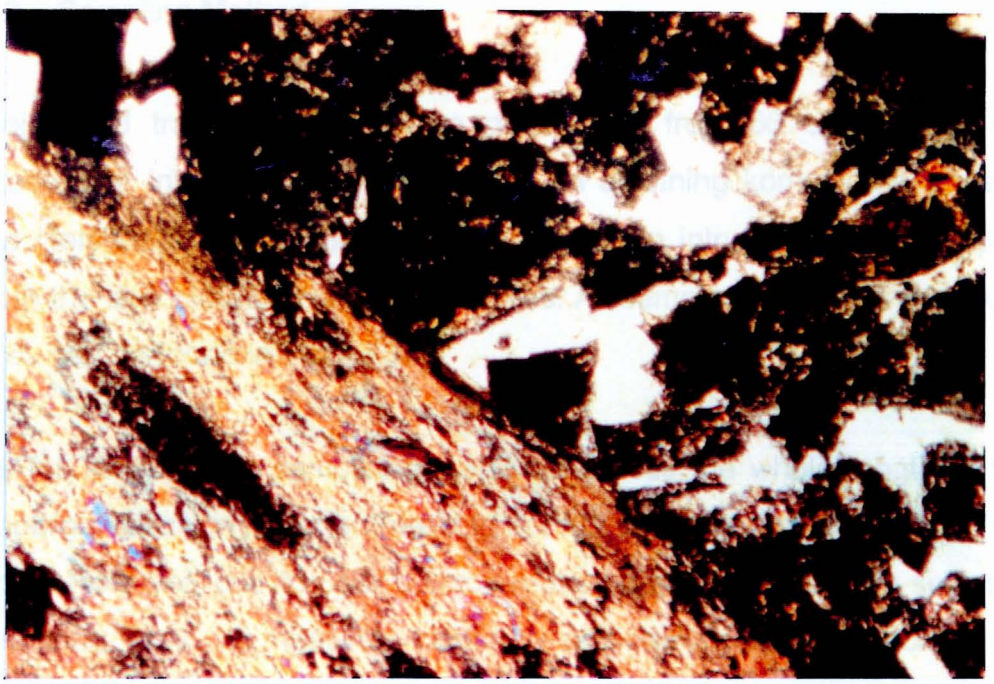


Plate 37
Photomicrograph of the same sample shown in Plate 36 above, but observed under crossed nicols (Sample SD7; 1 cm = 200 µm).

CHAPTER 5
GEOCHEMISTRY

5.1 Introduction

In the previous chapters the field geology, mineralogy and texture of the Sterkspruit Intrusion was described. From this evidence, it is clear that distinct variations exist within the body giving rise to at least five different zones resulting in different types of diorite and gabbro. The following chapter describes these zones chemically and enables more exact zone boundaries to be defined. The gabbroic rocks of the intrusion will be classified geochemically and compared to other mafic complexes. Variations across the body will also be described.

5.2 Sampling Method

Major and trace elements were determined from 66 samples of the Sterkspruit Intrusion, 5 samples from the adjoining komatiitic basalts in the Nelshoogte Schist Belt to the north of the intrusion and 2 samples from the associated komatiite extrusives. All sample localities in the study area can be found in Figure 3.

As far as possible, samples were taken across the whole length of the gabbroic intrusion from southwest to northeast and across the width of the body. However, due to poor outcrop restraints which resulted in selective sampling, only two relatively complete sections or traverses across the width of the intrusion could be used to investigate the geochemical trends. These traverses, labelled Traverse 1 and 2, are located towards the centre of the intrusion and are about 1 km apart (Figure 3). Traverse 3,

sampled by Pospisek (1991), and used to describe a portion of the Sterkspruit body, is located east of Traverse 2 (Figure 3). Samples from this traverse, although representing only a part of the gabbroic body extending southwestwards for approximately 100 m from the northern contact with the komatiitic basalt, have been used to investigate the geochemistry of this part of the intrusion.

5.2.1 Traverse 1

The northern and southern contacts of the Sterkspruit Intrusion with the adjacent komatiitic basalts are not visible as they are both covered by soil and scree. The width of the intrusion in the vicinity of Traverse 1 is approximately 400 m (Figure 3). Variations in major and trace element geochemistry are described from north to south across the gabbro body. Ten samples (SG 22 - SG 31) were collected at intervals of between 30 and 50 m. Sample SG 22 was collected about 20 m from the northern edge of the gabbroic body, while sample SG 31 is located about 30 m from the gabbro-basalt contact in the south. The sampling therefore does not reflect the geochemistry of the margins of the intrusion.

Samples SG 32 and SG 33 were collected from the small satellite gabbro intrusion located approximately 180 m south of the main Sterkspruit Intrusion (Figures 3 and 4).

5.2.2 Traverse 2

Eighteen samples from Traverse 2 (SG. 38 - SG. 55) were collected along a stream cutting diagonally through the gabbroic body from northwest to southeast (Figure 5). The northern contact of the body with the basalt is clearly seen forming a chilled margin, while the southern contact is again not visible due to soil and scree cover. The width of the gabbroic body in

the vicinity of Traverse 2 is approximately 450 m with the variation in geochemistry again being described from north to south across the body.

Sample SG 38 was taken from the chilled margin with an additional 6 samples being spaced at 5 m intervals within the first 40 m of the base of the intrusion. Thereafter, to the south, the sample spacing becomes more erratic because of poor exposure and varies from a few metres to 30 m. The last sample from this traverse (SG 55) is located approximately 20 m from the southern gabbro-basalt contact (Figures 3 and 5).

5.2.3 Traverse 3

As part of an earlier study of the Sterkspruit Intrusion, Pospisek (1991) collected 24 samples along a 100 m river traverse east of Traverse 2. The sampling included rocks from the chilled margin in the north at the contact with the komatiitic basalts of the adjacent schist belt, the Marginal Zone and part of the layered Lower Zone gabbro found towards the centre of the intrusion (Figures 3 and 6). The analytical results from these samples, which have a spacing of a few metres, were used in this investigation to describe the lower portions of the Sterkspruit body.

5.2.4 Mafic Dykes

Major and trace element concentrations were determined for 18 samples from selected mafic dykes crosscutting the Sterkspruit gabbroic intrusion (Figures 2 and 3). Each major dyke was sampled where it occurred within the Sterkspruit gabbro body. Some dykes were also sampled where they intruded both the surrounding komatiitic lavas and the Nelshoogte granitic pluton. In this way, any alteration by, or assimilation of, the country rock that might have influenced the composition of the dykes could be investigated. The composition of each dyke is compared to that of the

other dykes in the study area, as well as to the Sterkspruit Intrusion and the komatiitic basalts. Comparison are also made between the Sterkspruit Mafic Dykes and diabase sills which intruded the Uitkomst Complex, situated approximately 18 km northwest of the study area. Comparisons with these sills are made because of their close proximity to Sterkspruit and because their ages have been constrained to being younger than the 2025 Ma Uitkomst Complex (Kenyon *et al.*, 1986).

5.3 Analytical Techniques

Whole-rock and trace element analyses were determined in the Geology Department of the University of the Witwatersrand, Johannesburg. Samples from the study area were crushed using a steel jaw crusher and ground to a fine powder (-300 mesh size) in a tungsten sieb mill. The major oxides (SiO_2, TiO_2, Al_2O_3, FeO, Fe_2O_3, MnO, MgO, Ca_2O, K_2O and P_2O_5) were determined on a Phillips PW1400 X-Ray Fluorescence Spectrometer, on fusion discs prepared using the method described by Norrish and Hutton (1969).

The trace elements (Rb, Sr, Y, Zr, Nb, Co, Ni, Cu, Zn, Cr and Ba, as well as Na_2O) were also determined using X-Ray fluorescence techniques, but on pressed powder pellets. Full analytical results can be found in Appendix A, Tables A1 and A2, while analyses of rocks of the main zones, the mafic dyke groups and surrounding volcanics, can be found listed in this chapter under Tables 5, 6, 7, 8, 9, 11 and 13.

Major oxide and cation compositions of plagioclases found in the gabbroic rocks were determined using an Electron Microprobe Analyser at the Geology Department of Rand Afrikaans University, Johannesburg. Analyses are listed in Tables 2 and 3.

The Rare Earth Element (REE) abundances were determined using Instrumental Neutron Activation Analysis (INAA) at the Schonland Research Centre for Nuclear Sciences at the University of the Witwatersrand. A list of selected chondrite normalised REE from Sections 1, 2 and 3 appears in Table 10.

5.4 Alteration and Element Mobility

Element mobility and superimposed secondary element redistributions, especially that of major elements, is an important consideration in Archaean rocks when interpreting geochemical data. Rocks from the Barberton greenstone belt and other Archaean-to-Proterozoic volcanic terrains have been subjected to sea-water alteration, low-grade metamorphism and surface weathering which has affected the element distributions to varying degrees (Viljoen and Viljoen, 1969b; Condie *et al.*, 1977; Sun and Nesbitt, 1978; Jahn *et al.*, 1982; Smith and Erlank, 1982; Viljoen *et al.*, 1982; Anhaeusser, 1985).

Due to the expected alteration, an Fe_2O_3/FeO ratio of 0.20 is used to eliminate these alteration effects as much as possible. This ratio is considered typical for Archaean mafic rocks (Smith and Erlank, 1982; MacLachlan and Helmstaedt, 1995). All whole rock analyses presented in this study express total Fe as $Fe_2O_3(t)$, with FeO and Fe_2O_3 values calculated using Fe_2O_3/FeO = 0.20.

Sun and Nesbitt (1978) have shown that elements such as Ti, Y, Zr, Hf, Sc, Nb, P and the REE are fairly immobile during alteration, metamorphism and weathering. They also demonstrated, however, that crystalline Archaean basalts may show an increase in LREE, with HREE patterns remaining flat, along with Eu mobilisation. O'Nions and Pankhurst (1978), following studies of early Archaean rocks,

demonstrated that the abundances of large ion lithophile trace elements are modified by alteration. Beswick (1982) demonstrated widespread redistribution of Na_2O and K_2O in komatiitic suites, with no major redistribution of SiO_2, Al_2O_3, TiO_2, FeO, MgO and CaO. In contrast, Condie (1981) showed significant changes in K_2O, SiO_2, CaO, Al_2O_3, MgO, Ba, Rb and Cs, from Archaean greenstone belts in general.

Closer to the study area, Jahn *et al.* (1982) studied secondary element redistribution patterns in the Onverwacht volcanics. They found that, in general, the alkali (Na, K, Rb, Cs and Li) and alkaline earth elements (Mg, Ca, Sr, Ba and Be) were more prone to alteration effects. The less mobile elements include high field strength elements - REE, Y, Zr, Nb, Hf, P, Ti and some ferromagnesian elements - Ni, Co, Cr and Sc.

In this study of the Sterkspruit Intrusion, Na_2O and K_2O, along with Sr, Rb, Ba, Cu and Zn, show widespread scatter of data points, indicating element mobility. The major oxides such as MgO, SiO_2, TiO_2, FeO and Al_2O_3 and trace elements such as Zr, Y, Nb, Ni and V, can, however, be used with a certain amount of confidence for geochemical interpretation and petrogenetic modelling.

5.5 Mineral Chemistry

5.5.1 Plagioclase

The compositions of individual plagioclase grains were determined from samples collected along the two main sample traverses, Traverses 1 and 2 described earlier. The highly altered state of most of the plagioclase crystals, especially in the Marginal and Lower Zones, often made identification difficult, but suitable material was available to provide an average plagioclase composition for each sample. Tables 2 and 3 list the

plagioclase compositions in the gabbro samples from Traverse 1 and Traverse 2 respectively.

From the data provided in the tables, it can be seen that the plagioclase feldspars range in composition from oligoclase (An_{15-30}) in the chill margin and Marginal Zone forming the base of the intrusion, to albite (An_{0-7}) in the Central and Upper Zone gabbros towards the southern side of the body. No analyses from the Lower Zone were possible due to the highly turbid and altered nature of the plagioclase grains in these rocks. The more calcic plagioclase in the Marginal Zone, are also the ones showing strong saussuritisation.

The CaO concentrations in plagioclase from both Traverses 1 and 2 show a marked increase towards the northern contact (Figures 7 and 8). Values range from less than 0.5% in the Central and Upper Zones to over 3.0% in the Marginal Zone. This increase towards the base of the intrusion is matched by increased amounts of Al_2O_3. The Na_2O concentration, by contrast, shows the opposite trend, decreasing towards the Marginal Zone and the chill margin, a trend matched also by SiO_2. The Na_2O values range from between 10.5 and 12.0% in plagioclase from the Central and Upper Zones, to less than 10.0% in the Marginal Zone.

Table 2 : Microprobe analyses of plagioclase from Traverse 1

Sample	SG 22	SG 27	SG 28	SG 29	SG 30	SG 31
Zone	MZ	CZ	GG	UZ	UZ	UZ
wt %						
SiO_2	62.98	66.90	67.03	67.34	67.83	65.86
TiO_2	nd	nd	nd	nd	nd	nd
Al_2O_3	23.69	20.84	21.17	20.63	21.40	21.57
FeO	0.24	0.21	0.07	0.16	0.10	0.27
MnO	0.02	0.04	0.01	0.00	0.02	0.03
MgO	0.02	0.01	0.01	0.00	0.00	0.00
CaO	3.31	0.29	0.12	0.05	0.19	0.18
Na_2O	9.76	11.36	11.38	11.86	10.88	10.98
K_2O	0.07	0.05	0.04	0.06	0.05	0.11
Total	100.1	99.70	99.83	100.1	100.47	99.00
No. of Ions on the basis of 32 oxygens						
Si	11.12	11.75	11.74	11.78	11.77	11.64
Ti	nd	nd	nd	nd	nd	nd
Al	4.93	4.31	4.37	4.25	4.38	4.49
Fe	0.04	0.03	0.01	0.02	0.02	0.04
Mn	0.00	0.01	0.00	0.00	0.01	0.00
Mg	0.00	0.00	0.00	0.00	0.00	0.00
Ca	0.63	0.06	0.02	0.01	0.04	0.03
Na	3.34	3.87	3.87	4.02	3.67	3.76
K	0.02	0.01	0.01	0.01	0.01	0.02
Total	20.09	20.04	20.02	20.11	19.88	20.00
Z	16.06	16.06	16.11	16.03	16.15	16.13
X	4.03	3.98	3.01	4.06	3.74	3.85

Z = Si+Al

X = Na+Mg+Fe+Mn+K+Ca

Table 3 : Microprobe analyses of plagioclase from Traverse 2

Sample	SG 38	SG 40	SG 48	SG 49	SG 50	SG 53	SG 55
Zone	chill margin	MZ	CZ	CZ	CZ	UZ	UZ
wt %							
SiO_2	66.19	66.32	64.92	66.64	66.77	66.85	66.20
TiO_2	nd	nd	nd	nd	nd	nd	nd
Al_2O_3	22.26	22.23	20.99	21.43	20.93	20.94	21.08
FeO	1.30	0.28	0.19	0.22	0.17	0.17	0.17
MnO	0.00	0.01	0.00	0.01	0.03	0.00	0.01
MgO	0.38	0.00	0.01	0.00	0.00	0.00	0.01
CaO	2.20	1.06	0.25	0.26	0.10	0.15	0.27
Na_2O	8.95	11.27	11.26	11.37	11.27	11.51	11.75
K_2O	0.06	0.06	0.10	0.06	0.45	0.69	0.04
Total	100.32	101.24	97.72	99.97	99.72	100.32	100.53
No. of Ions on the basis of 32 oxygens							
Si	11.49	11.51	11.65	11.67	11.74	11.71	11.72
Ti	nd	nd	nd	nd	nd	nd	nd
Al	4.56	4.55	4.44	4.43	4.34	4.32	4.33
Fe	0.19	0.04	0.03	0.03	0.03	0.02	0.03
Mn	0.00	0.00	0.00	0.00	0.00	0.00	0.00
Mg	0.10	0.00	0.00	0.00	0.00	0.00	0.00
Ca	0.41	0.20	0.05	0.05	0.02	0.03	0.05
Na	3.01	3.80	3.92	3.87	3.84	3.91	3.97
K	0.01	0.01	0.02	0.01	0.10	0.16	0.01
Total	19.75	20.11	20.10	20.05	20.06	20.16	20.11
Z	16.04	16.06	16.09	16.10	16.07	16.04	16.05
X	3.72	4.05	4.02	3.95	3.99	4.12	4.06

Z = Si+Al

X = Na+Mg+Fe+Mn+K+Ca

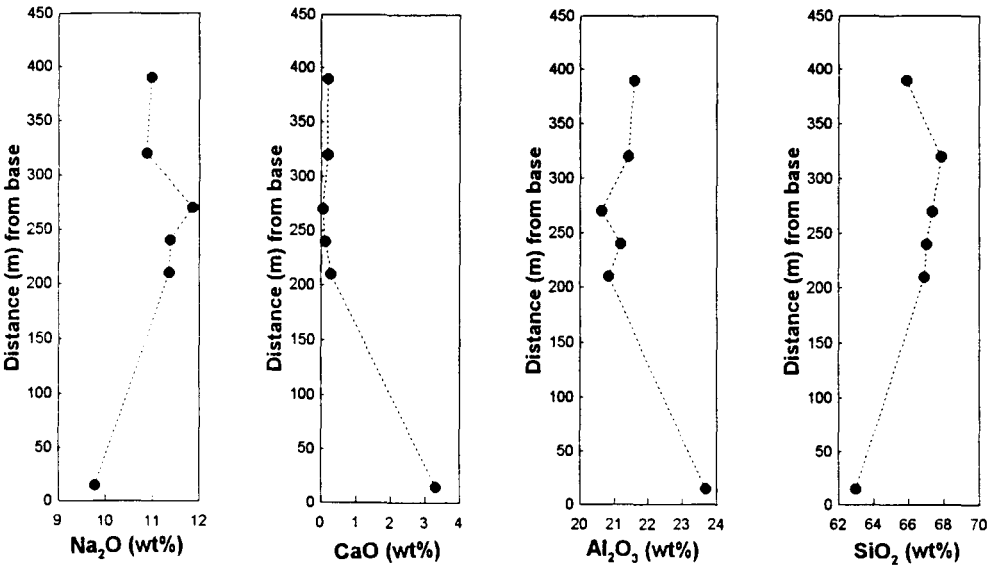


Figure 7: Cryptic variation in plagioclase with stratigraphic height in the Sterkspruit Intrusion - Traverse 1.

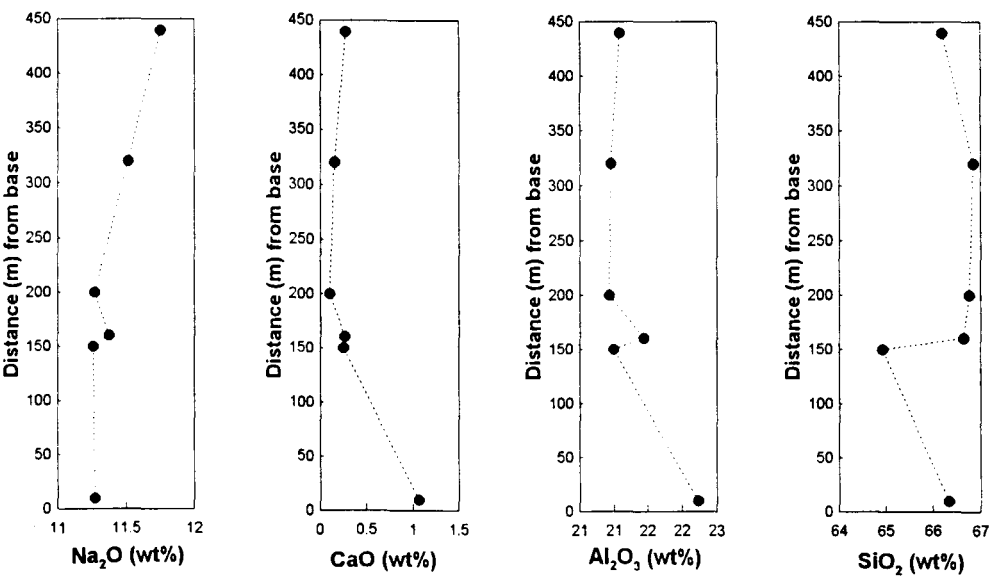


Figure 8: Cryptic variation in plagioclase with stratigraphic height in the Sterkspruit Intrusion - Traverse 2.

The trends shown by major oxides in plagioclase is consistent with a magma body cooling and crystallising from the base and roof of the magma chamber, with the lowermost marginal zones crystallising more Ca-rich plagioclase which then becomes more albite rich upwards in the sequence. The roof crystallisation process would also initially crystallise more Ca-rich plagioclase, with the composition becoming albitic downwards towards the Quartz Diorite in the centre of the magma chamber. This upwards cryptic variation shown by plagioclase is in accordance with similar trends seen in the Mt. Kilkenny tholeiitic sill in Australia (Jaques, 1976), where fractional crystallisation from a single magma pulse is suggested. The Skaergaard Intrusion also shows decreasing An content of plagioclase with height (Maaloe, 1976).

In order to model chemical differentiation in the cooling magma chamber using binary diagrams, a plagioclase composition of An_{61} was used, calculated from the normative data from the Sterkspruit gabbro samples. This approximates to a composition for labradorite which is common in gabbroic bodies in general (Bowes, 1989). This plagioclase composition (Deer *et al.*, 1982) is listed in Table 4.

5.5.2 Pyroxene

The pyroxene phases over most of the Sterkspruit Intrusion have been altered to fine, fibrous uralite or are completely converted to amphiboles such as actinolite. The altered state of these minerals thus prevented the determination of pyroxene mineral compositions. In order to model chemical trends in the gabbro, compositions of clinopyroxene from the Kromberg Formation (UMFU) were used (Conway, 1985). The orthopyroxene compositions were derived from the Stolzburg Complex (Rodel, 1993). Table 4 lists the average compositions from each of these sources.

Table 4 : Microprobe analyses of plagioclase, clinopyroxene and orthopyroxene

Sample	plagioclase	cpx 1	cpx 2	cpx 3	opx
wt %					
SiO_2	52.96	51.6	52.4	51.4	56.11
TiO_2	--	1.4	0.3	0.4	0.06
Al_2O_3	29.72	2.6	1.8	1.6	0.86
FeO	--	5.8	5.8	11.8	8.98
MnO	nd	0.19	0.18	0.24	0.17
MgO	--	16.3	17.2	15.1	33.14
CaO	12.28	21.3	20.0	18.5	1.39
Na_2O	4.21	0.35	0.18	0.18	0.02
K_2O	0.13	nd	nd	nd	0.01

plagioclase : Labradorite (Deer *et al.*, 1982)

cpx 1 : High-Ti clinopyroxene from the Kromberg Fm (Conway, 1985)

cpx 2 : Clinopyroxene from the Kromberg Fm (Conway, 1985)

cpx 3 : High-Fe clinopyroxene from the Kromberg Fm (Conway, 1985)

opx : Stolzburg Complex - bronzite sample DH8a (Rodel, 1993)

5.6 Whole-rock Geochemistry in the Sterkspruit Intrusion

5.6.1 Bulk Geochemistry

In many instances, the parent compositions of magmas forming mafic- to-ultramafic layered complexes are used to formulate petrogenetic ideas on the origins of these complexes and to compare them with similar intrusions worldwide. The parent compositions are in many instances taken as the composition of the chill margin of the intrusions. The bulk composition of the body can also be expressed by calculating the average weighted composition for the intrusion as a whole.

In the case of the Sterkspruit Intrusion, the parent composition was derived using the following approach:

Firstly, the compositions of the two chill margin samples, SG38 from Traverse 2 and SG63 from Traverse 3 were averaged. Secondly, the bulk composition of the body was calculated using a weighted average method. The average composition of samples from each of the main zones was calculated and an overall weighted average expressed using the following estimated percentages: MZ (9%), LZ (23%), CZ (24%) and UZ (44%). The shortcomings in this method include the inaccuracy in locating exact contacts between zones, the uncertainty in assigning to a zone a particular composition and the inhomogeneous sampling method. Possible shortcomings using the chill margin composition concern whether or not the fine-grained gabbro represents a primary liquid or a cumulate. Nevertheless, despite these uncertainties, the average chill zone composition (X), shows a good correlation with the calculated bulk composition (B), both of which are listed in Table 5. This compositional consistency suggests that the chill margin gabbro can be used as an indication of the parental magma composition.

Table 5 : Comparison of chill margin and calculated bulk compositions of the Sterkspruit Intrusion

	Chill Sample SG.38	Chill Sample SG.63	Average Chill (X)	Calculated Bulk Composition (B)
wt %				
SiO_2	52.82	52.26	52.54	52.55
TiO_2	1.34	1.37	1.36	1.39
Al_2O_3	13.81	13.43	13.62	13.61
Fe_2O_3(t)	15.38	16.00	15.69	13.70
MnO	0.22	0.17	0.20	0.19
MgO	4.84	4.82	4.83	5.42
CaO	7.21	7.26	7.24	8.29
Na_2O	3.39	2.24	2.82	2.15
K_2O	0.09	0.10	0.10	0.16
P_2O_5	0.16	0.16	0.16	0.14
FeO	11.74	12.21	11.98	10.46
Fe_2O_3	2.35	2.44	2.39	2.09
ppm				
Rb	14	14	14	14
Sr	91	117	104	98
Y	35	29	32	33
Zr	102	100	101	83
Nb	6	7	7	6
Co	26	33	30	39
Ni	55	64	60	58
Cu	53	105	79	46
Zn	69	92	81	83
Ba	8	4	6	18
Ti	1	1	1	1
V	371	364	368	421
Cr	55	61	58	64
Ti/Zr	79	82	81	100
Ti/Y	231	282	254	255
mg#	42	41	42	48

Fe_2O_3(t) : Total Fe as Fe_2O_3

FeO and Fe_2O_3 calculated using Fe_2O_3/FeO ratio = 0.2

Using the above approach, the parental magma composition of the Sterkspruit Intrusion has MgO values between 4.8 and 5.4%, consistent with that of normal to iron-rich tholeiites (Jensen, 1976; Viljoen *et al.*, 1982). By comparison, the average MgO contents in gabbros, quartz gabbros and ferrogabbros from the Usushwana Complex, southeast of the Sterkspruit Intrusion, range between 3.4 and 5.4% (Hammerbeck, 1982). The MgO contents in bulk compositions from the Skaergaard Intrusion range between 7.2 and 8.6% (McBirney, 1996), for the Bushveld Complex, 12% (Davies *et al.*, 1980) and for the Mt Kilkenny tholeiitic sill in Australia, between 7.7 and 8.2% (Jaques, 1976).

The parental composition of the Sterkspruit Intrusion differs markedly, however, from that of the neighbouring Stolzburg Complex, which has a calculated MgO composition of 33.8% (Rodel, 1993). This falls within the range of other layered complexes in the Barberton greenstone belt of between 29.4 and 34.1% MgO (Viljoen and Viljoen, 1970; Anhaeusser, 1976; Wuth, 1980). A single, relatively unaltered gabbro sample from Stolzburg does, however, compare favourably with Sterkspruit, having an MgO value of 5.9%. These gabbro units were however, considered by Anhaeusser (1985) to represent residual liquids left over after the crystallisation of earlier-formed phases and were derived from primary komatiitic basalt liquids. Wuth (1980) confirmed this view by showing the existence of geochemical similarities between gabbroic phases of layered complexes in the Oorschot-Weltevreden schist belt and Barberton-type komatiitic basalts. The average MgO content in komatiitic basalts from the Nelshoogte Schist Belt is 15% ('SB' samples, Table 13), while tholeiitic basalts from the Hooggenoeg Formation at Barberton have MgO contents of 7.3% (Viljoen and Viljoen, 1969d).

5.6.2 Classification

A composite ternary plot of A (Na_2O+K_2O) - F ($FeO+Fe_2O_3$) - M (MgO) (AFM diagram), shows the Sterkspruit gabbroic suite forms an overall linear Fe- enrichment trend typical of the initial differentiation trend shown by some tholeiitic suites (Viljoen and Viljoen, 1970; Jaques, 1976; Sharpe, 1981; Hammerbeck, 1982; Hunter and Sparks, 1987). The main zones comprising the gabbroic intrusion plot as distinct, though in places, overlapping fields (Figure 9). The Marginal and Lower Zones plot in fields closest to the MgO apex, which is consistent with the northwestern section forming the base of the intrusion, with a differentiation trend towards the Central and Upper Zones in the southeast. The Lower Zone gabbros, in addition, form a much tighter grouping and plot closest to the MgO apex. The Marginal Zone samples display a spread of points from the chill zone (X) towards the Lower Zone.

The overlapping Upper Zone and Central Zone fields plot towards the $FeO+Fe_2O_3$ apex. The quartz diorite sample (SG28) lies on an Fe-enrichment trend closer to the $FeO+Fe_2O_3$ - Na_2O+K_2O tie line than the Central and Upper Zones, and is consistent with this unit being a late stage, more differentiated portion of the intrusion. The average chill zone composition (X) plots within the Central and Upper Zone fields.

The marked Fe-enrichment trend shown by the Sterkspruit Intrusion has close similarities with the trends of the Usushwana Complex (Hammerbeck, 1982), the Skaergaard Intrusion, and the Mt Kilkenny Intrusion (Jaques, 1976) (Figure 10). These trends indicate tholeiitic affinities and similarities between them will assist in modelling the origin and crystallisation sequence of the Sterkspruit body.

The complete suite of samples from the Sterkspruit Intrusion have also been plotted on a silica (SiO_2) vs total alkali (Na_2O + K_2O) diagram (Figure 11). The gabbroic rocks shows a subalkaline, tholeiitic character, consistent with the composition of some gabbros from Barberton layered complexes and Archaean basic volcanic and intrusive rocks elsewhere in the world (Viljoen and Viljoen, 1969c; Anhaeusser, 1985).

On the Kaapvaal Craton, basic-to-ultrabasic intrusions having the same tholeiitic nature as the Sterkspruit Intrusion (as shown by the silica vs total alkali diagrams), include the Pre-Bushveld and Waterberg sills (Sharpe, 1981), the Usushwana Complex in Mpumalanga and Swaziland (Hammerbeck, 1982), and gabbros from the Upper Division of the Stolzburg Complex (Rodel, 1993). The Uitkomst Complex, however, which is situated on the edge of the Transvaal Escarpment close to Badplaas is comprised of gabbros and diabase sills, more alkaline in character than the rocks of the Sterkspruit Intrusion (Allen, 1990).

A Jensen (1976) cation plot was also used to classify the subalkaline gabbroic rocks from the Sterkspruit Intrusion. The proportions of the cations (Fe^{2+} + Fe^{3+} + Ti), Al and Mg were recalculated to 100% and plotted on a triangular diagram (Figure 12). The liquid composition of the body, represented by the chill margin, as well as the rocks from the Central and Upper Zones, fall in the field of high-Fe tholeiites. The quartz diorite sample, significantly, plots in the andesite-tholeiite field and is consistent with this rock being a late-stage differentiate. The gabbro from the Marginal and Lower Zones form a distinct grouping within the high-Mg tholeiite field, but this relationship is ambiguous as these compositions are cumulate enriched, and hence higher MgO contents are to be expected.

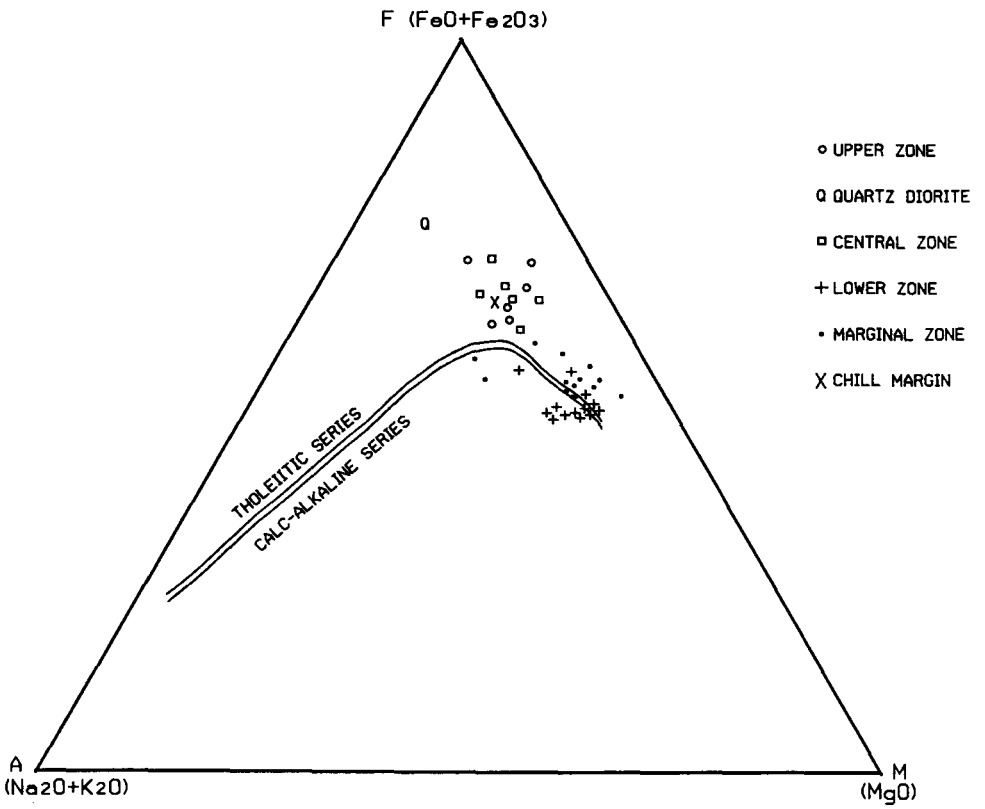


Figure 9 : **AFM (Na_2O+K_2O - $FeO+Fe_2O_3$ - MgO) diagram of the Sterkspruit Intrusion showing the gabbroic zones and Fe enrichment trend.**

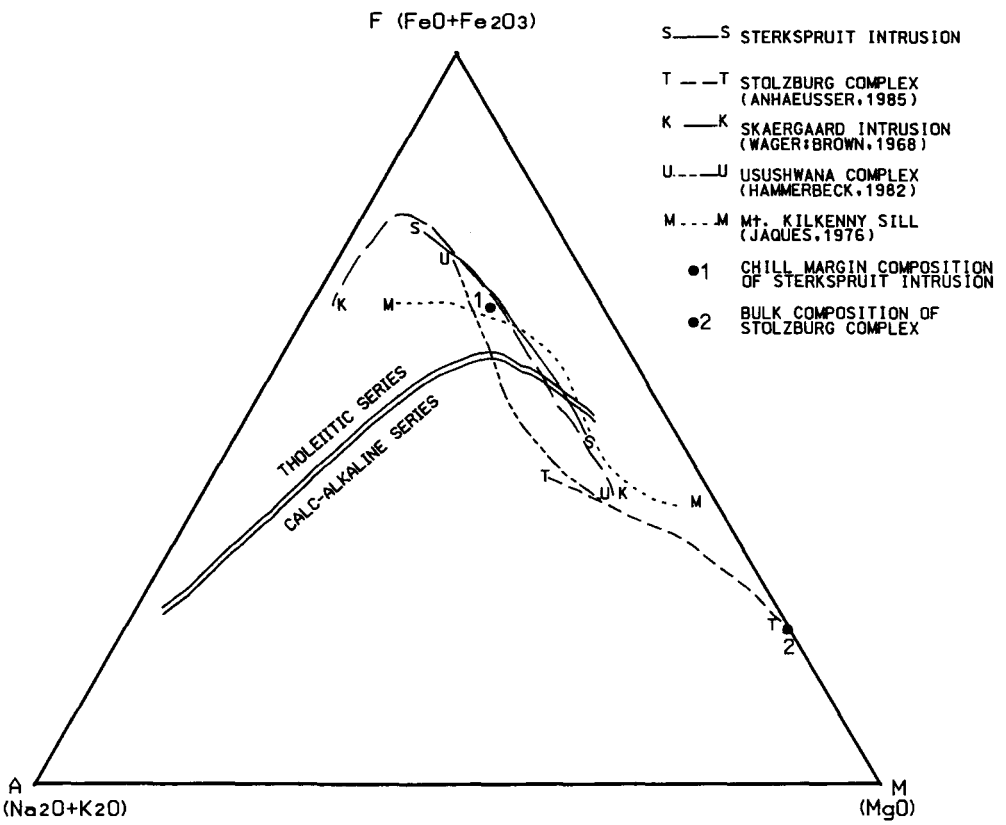


Figure 10 : **AFM (Na_2O+K_2O - $FeO+Fe_2O_3$ - MgO) diagram comparing the Sterkspruit Intrusion to trends from other layered complexes.**

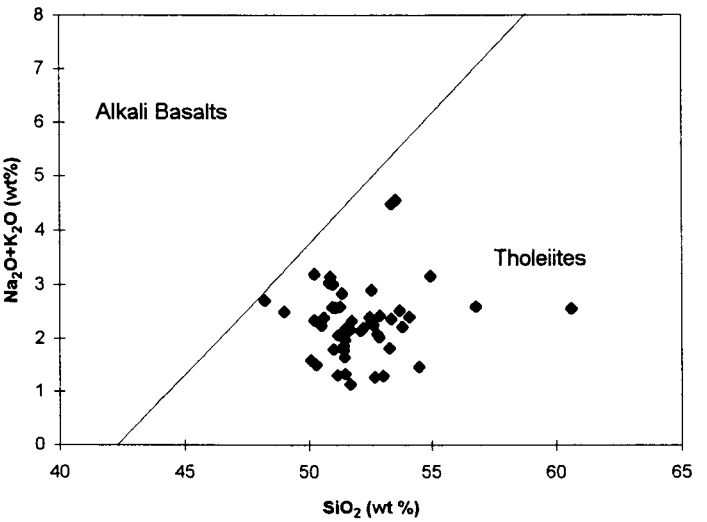


Figure 11 **SiO_2 vs Total Alkali diagram for rocks from the Sterkspruit Intrusion showing the tholeiitic composition of the gabbro (after MacDonald and Katsura, 1964).**

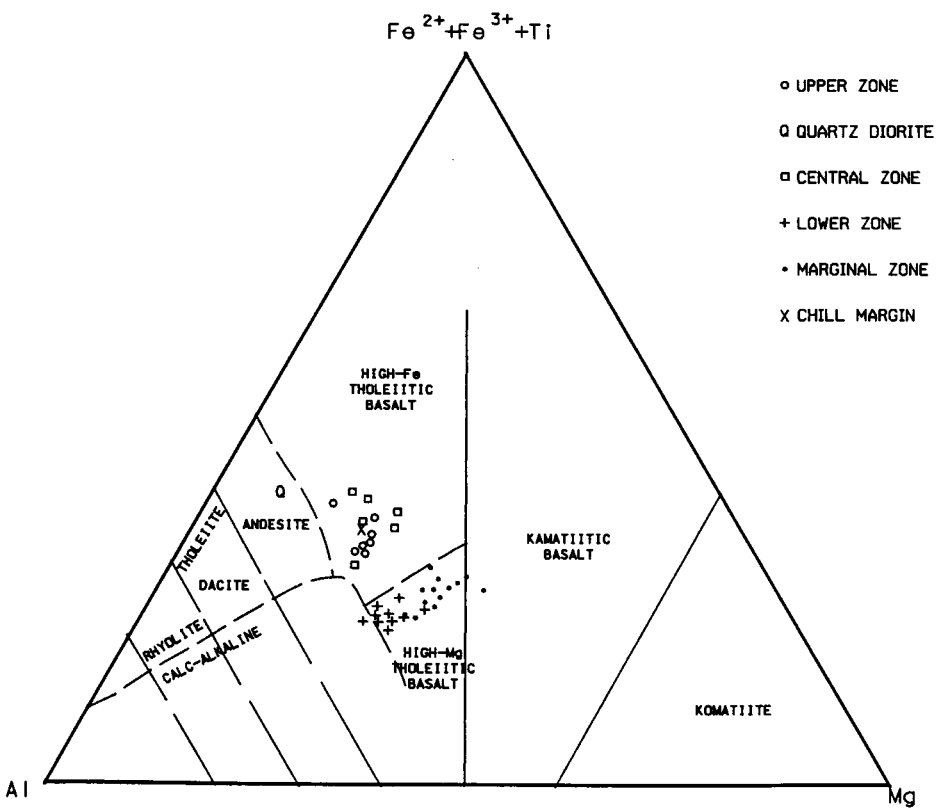


Figure 12 : **Cation ternary diagram ($Fe^{2+}+Fe^{3+}+Ti$ - Al - Mg) of the Sterkspruit Intrusion (after Jensen, 1976).**

5.6.3 Major Oxide and Trace Element Variation

The whole-rock geochemistry of the Sterkspruit Intrusion has been used to separate the body into a number of zones. These zones, which were described petrographically in an earlier section, can be more accurately subdivided on the basis of geochemical variations. The whole-rock analytical data from the Marginal Zone (MZ), Lower Zone (LZ), Central Zone (CZ), Quartz Diorite (QD) and Upper Zone (UZ) is listed in Tables 6 to 9. Based on chemical differences the body can be subdivided into cumulate-textured gabbros forming the LZ and parts of the MZ, Ti-rich ferro-gabbros forming the CZ, quartz-gabbros forming the UZ and a quartz diorite horizon (QD), only observed on Traverse 1 between the CZ and UZ (Figure 4).

SiO_2 and TiO_2 show similar chemical trends in the lower and upper sectors of the gabbroic body, with both having overall higher contents in the upper zones as compared to lower in the sequence. SiO_2 varies between 50.5 - 53.5% in the MZ and LZ, and between 53.0 - 56.7% in the UZ. As well as increasing upwards from the lower margin, SiO_2 also increases from the upper margin downwards towards the QD horizon which is located approximately two thirds of the way up the body. The SiO_2 content in the QD is 60.6%. TiO_2 values are between 0.8 - 1.3% in the MZ and LZ and average 1.5% in the UZ. The Central Zone is enriched in TiO_2 (1.3 - 2.2%) as well as in Fe (average 16.6% $Fe_2O_{3(T)}$), which distinguishes this zone from the rest of the body.

Al_2O_3 remains constant throughout the gabbroic body with concentrations between 11.5 - 14.8%, except in the case of the LZ, where it reaches 13.7- 17.2%, in response to the cumulate development and the more felsic portions of the layering.

Table 6 : Whole-rock geochemical data from the Sterkspruit Intrusion - Marginal Zone

sample	SG22	SG23	SG39	SG40	SG41	SG42	SG43	SG44	P1	P2	P3	P4	P5	P6	P7	P9
Traverse	1	1	2	2	2	2	2	2	3	3	3	3	3	3	3	3
wt %																
SiO_2	52.63	51.17	53.54	53.36	52.84	52.10	52.67	51.48	53.36	52.77	53.26	52.89	51.68	52.19	51.48	50.51
TiO_2	0.99	0.72	1.32	1.27	1.07	0.89	0.87	0.76	1.14	0.89	1.15	0.93	0.90	0.91	0.88	0.80
Al_2O_3	11.89	15.31	13.16	13.30	12.47	12.65	13.73	14.60	13.33	12.88	13.33	12.13	11.49	13.30	13.87	14.78
$Fe_2O_3(t)$	13.95	11.76	14.11	13.17	13.66	12.88	12.41	11.47	13.47	12.87	13.83	13.08	13.02	13.00	12.38	12.60
MnO	0.20	0.15	0.20	0.22	0.21	0.22	0.19	0.15	0.20	0.18	0.20	0.19	0.19	0.16	0.15	0.14
MgO	8.92	8.07	5.12	5.75	7.35	8.40	7.66	7.88	6.09	8.10	6.16	8.73	9.70	7.96	8.13	8.78
CaO	7.08	8.64	7.56	7.17	7.91	7.27	7.76	8.42	7.77	7.41	7.91	7.51	8.92	7.16	8.22	7.35
Na_2O	2.04	1.17	4.50	4.39	1.98	2.05	1.14	1.20	2.20	1.85	1.73	2.28	1.04	2.01	2.02	2.04
K_2O	0.22	0.15	0.07	0.10	0.05	0.10	0.14	0.14	0.17	0.24	0.10	0.15	0.11	0.20	0.17	0.21
P_2O_5	0.11	0.07	0.20	0.22	0.13	0.12	0.12	0.09	0.13	0.11	0.12	0.10	0.10	0.10	0.10	0.11
LOI	2.30	2.89	1.43	1.42	2.30	2.75	2.46	2.68	1.98	2.17	2.04	2.19	2.49	2.34	2.33	2.86
Total	100.32	100.10	101.20	100.36	99.96	99.40	99.14	98.86	99.83	99.46	99.83	100.17	99.64	99.32	99.73	100.16
FeO	10.65	8.98	10.77	10.05	10.43	9.83	9.47	8.76	10.28	9.82	10.56	9.98	9.94	9.92	9.45	9.62
Fe_2O_3	2.13	1.80	2.15	2.01	2.09	1.97	1.89	1.75	2.06	1.96	2.11	2.00	1.99	1.98	1.89	1.92
ppm																
Rb	16	12	12	11	12	10	14	14	9	11	6	8	8	10	9	14
Sr	72	94	93	88	88	89	91	97	96	85	96	94	130	91	128	89
Y	25	18	39	44	31	26	24	19	31	25	28	25	22	23	20	20
Zr	61	49	101	93	79	62	64	53	85	85	78	61	67	59	52	53
Nb	6	5	7	6	6	5	6	5	6	5	6	5	5	6	6	5
Co	52	44	35	34	44	47	48	42	55	52	50	53	53	56	51	53
Ni	133	122	66	67	106	128	121	125	86	120	82	129	138	121	119	132
Cu	82	69	43	51	69	93	54	53	62	86	59	82	82	52	48	28
Zn	118	126	92	93	107	98	87	84	93	116	96	181	87	91	80	101
Ba	32	11	14	15	11	15	20	26	36	48	28	34	25	30	30	33
Ti	0.8	0.6	1.0	1.0	0.8	0.8	0.7	0.7	0.9	0.8	0.9	0.8	0.7	0.8	0.7	0.7
V	278	214	347	363	284	261	250	228	318	266	304	277	273	269	245	248
Cr	282	246	74	88	204	265	250	256	137	257	144	296	295	251	249	299
Ti/Zr	97	89	79	82	81	87	81	86	80	63	88	92	80	93	102	91
Ti/Y	242	235	202	173	207	209	215	234	222	218	248	227	242	235	268	239
Zr/Y	2	3	3	2	3	2	3	3	3	3	3	2	3	3	3	3
Zr/Nb	11	10	14	15	14	14	12	11	15	16	13	13	13	10	9	11
mg#	60	62	46	50	56	60	59	62	51	60	51	61	64	59	61	62
distance m	15	40	2	5	13	19	24	29	2	3	5	13	20	25	28	36

$Fe_2O_3(t)$: Total Fe as Fe_2O_3 FeO and Fe_2O_3 calculated using Fe_2O_3/FeO ratio = 0.2

mg# : 100 [Mg^{2+}/ Mg^{2+} + Fe^{2+}]

distance m : Distance in metres from the base of the intrusion

Table 7 : Whole-rock geochemical data from the Sterkspruit Intrusion - Lower Zone

sample	SG24	SG25	SG45	SG46	SG47	P10	P11	P12	P13	P14
Traverse	1	1	2	2	2	3	3	3	3	3
wt %										
SiO_2	51.26	52.45	51.43	51.44	50.31	51.47	51.69	51.34	50.82	50.87
TiO_2	0.73	0.92	0.67	0.82	0.76	0.76	0.73	0.72	0.76	0.69
Al_2O_3	16.09	16.68	15.61	15.53	16.02	13.77	14.04	16.05	15.81	15.90
$Fe_2O_3(t)$	10.52	9.73	10.71	10.85	10.53	12.02	11.55	10.70	11.10	10.45
MnO	0.17	0.14	0.16	0.18	0.15	0.14	0.15	0.15	0.13	0.15
MgO	7.23	4.88	7.87	7.53	6.53	9.00	8.88	7.38	7.94	7.39
CaO	9.16	11.47	8.37	8.78	9.30	7.06	7.35	7.85	7.80	7.67
Na_2O	2.47	2.27	1.64	1.54	1.48	1.69	1.88	2.66	2.82	2.97
K_2O	0.13	0.14	0.15	0.12	0.03	0.29	0.30	0.19	0.23	0.18
P_2O_5	0.10	0.13	0.07	0.07	0.10	0.09	0.08	0.09	0.09	0.09
LOI	2.73	1.72	2.82	2.85	3.91	3.07	2.84	2.86	2.89	3.75
Total	100.60	100.52	99.48	99.71	99.11	99.33	99.48	99.97	100.39	100.11
FeO	8.03	7.43	8.18	8.28	8.04	9.18	8.82	8.17	8.47	7.98
Fe_2O_3	1.61	1.49	1.64	1.66	1.61	1.84	1.76	1.63	1.69	1.60
ppm										
Rb	10	9	12	11	9	13	14	10	13	10
Sr	97	114	107	102	111	74	85	108	102	92
Y	17	23	18	19	24	16	14	17	19	16
Zr	42	51	39	49	50	45	46	45	52	45
Nb	4	4	4	5	5	2	1	3	3	4
Co	35	29	43	36	37	49	48	41	46	41
Ni	103	69	122	109	97	134	163	108	123	110
Cu	13	36	31	18	9	28	38	9	10	14
Zn	72	57	88	85	67	87	84	76	81	83
Ba	17	10	24	16	7	38	40	34	38	35
Ti	0.6	0.8	0.6	0.7	0.6	0.7	0.6	0.7	0.6	0.6
V	213	258	211	244	230	244	225	239	239	233
Cr	189	123	249	197	158	286	287	243	268	221
Ti/Zr	105	107	102	100	91	101	95	96	89	91
Ti/Y	262	240	226	262	189	280	306	250	235	263
Zr/Y	2	2	2	3	2	3	3	3	3	3
Zr/Nb	11	12	9	10	11	22	39	16	20	11
mg#	62	54	63	62	59	64	64	62	63	62
distance m	80	110	50	85	125	45	46	49	51	55

$Fe_2O_3(t)$: Total Fe as Fe_2O_3 FeO and Fe_2O_3 calculated using Fe_2O_3/FeO ratio = 0.2

mg# : 100 $[Mg^{2+}/ Mg^{2+} + Fe^{2+}]$

distance m : Distance in metres from the base of the intrusion

Table 7 (continued...) : Whole-rock geochemical data from the Sterkspruit Intrusion - Lower Zone

sample	P15	P16	P17	P19	P21	P24	P26	P27	P31
Traverse	3	3	3	3	3	3	3	3	3
wt %									
SiO_2	50.97	50.61	50.94	50.96	51.09	51.43	51.48	51.19	51.00
TiO_2	0.69	0.66	0.67	0.78	0.67	0.70	0.79	0.79	0.70
Al_2O_3	16.03	16.00	17.23	16.39	16.48	14.19	14.06	15.01	14.30
$Fe_2O_3(t)$	11.10	10.42	10.17	10.07	9.90	11.87	11.67	11.46	11.76
MnO	0.13	0.13	0.12	0.11	0.14	0.17	0.15	0.16	0.18
MgO	7.84	7.49	6.85	6.95	7.07	8.90	8.54	7.98	9.03
CaO	7.24	8.78	8.61	8.83	8.85	8.04	8.29	8.38	8.46
Na_2O	2.78	2.05	2.74	2.06	2.06	1.58	1.92	1.85	1.67
K_2O	0.24	0.35	0.28	0.53	0.52	0.30	0.17	0.22	0.13
P_2O_5	0.03	0.08	0.08	0.07	0.08	0.09	0.10	0.09	0.04
LOI	2.93	2.73	2.64	2.76	2.74	2.77	2.81	2.80	2.94
Total	99.96	99.31	100.34	99.51	99.59	100.01	99.97	99.92	100.19
FeO	8.47	7.95	7.76	7.69	7.56	9.06	8.91	8.75	8.98
Fe_2O_3	1.69	1.59	1.55	1.54	1.51	1.81	1.78	1.75	1.80
ppm									
Rb	13	17	14	21	24	15	9	12	7
Sr	85	114	126	113	119	81	92	98	73
Y	13	18	15	18	19	18	14	15	14
Zr	41	51	41	47	47	50	41	45	40
Nb	3	4	3	4	5	3	4	4	2
Co	52	47	39	42	41	49	50	46	50
Ni	108	110	99	97	103	129	122	114	132
Cu	10	14	12	22	16	7	6	8	1
Zn	91	79	98	79	79	111	91	96	87
Ba	32	42	38	63	64	39	27	34	30
Ti	0.6	0.6	0.6	0.7	0.6	0.6	0.7	0.7	0.6
V	190	220	225	234	215	229	249	252	222
Cr	226	218	191	189	202	246	229	202	250
Ti/Zr	100	77	97	99	85	84	116	105	106
Ti/Y	308	221	275	261	214	240	330	322	297
Zr/Y	3	3	3	3	3	3	3	3	3
Zr/Nb	15	12	14	13	9	18	12	11	18
mg#	62	63	61	62	63	64	63	62	64
distance m	63	67	71	74	77	81	84	95	100

$Fe_2O_3(t)$: Total Fe as Fe_2O_3 FeO and Fe_2O_3 calculated using Fe_2O_3/FeO ratio = 0.2

mg# : 100 $[Mg^{2+}/ Mg^{2+} + Fe^{2+}]$

distance m : Distance in metres from the base of the intrusion

Table 8 : Whole-rock geochemical data from the Sterkspruit Intrusion - Central Zone and Quartz Diorite

sample	SG26	SG27	SG48	SG49	SG50	SG51	SG28 Quartz Diorite
Traverse	1	1	2	2	2	2	1
wt %							
SiO_2	49.00	50.21	48.20	51.74	50.09	50.23	60.60
TiO_2	1.73	2.21	1.72	1.31	1.85	1.92	1.43
Al_2O_3	13.92	12.95	13.55	14.33	12.70	13.14	11.55
$Fe_2O_3(t)$	16.37	16.80	16.98	12.93	15.98	16.85	12.68
MnO	0.17	0.20	0.17	0.17	0.20	0.21	0.18
MgO	4.93	4.11	5.76	5.15	5.78	4.66	1.36
CaO	10.13	9.21	7.83	9.21	8.63	7.86	5.93
Na_2O	2.40	2.28	2.50	2.22	1.42	3.08	2.51
K_2O	0.11	0.07	0.22	0.12	0.18	0.12	0.06
P_2O_6	0.09	0.14	0.12	0.13	0.12	0.11	0.31
LOI	2.16	1.91	1.93	1.88	2.04	2.10	3.63
Total	101.01	100.09	98.97	99.20	98.99	100.28	100.23
FeO	12.50	12.82	12.96	9.87	12.20	12.86	9.68
Fe_2O_3	2.50	2.56	2.59	1.97	2.44	2.57	1.94
ppm							
Rb	15	16	17	12	17	18	12
Sr	87	85	81	125	74	91	84
Y	24	32	27	29	27	27	68
Zr	55	74	60	77	59	67	161
Nb	5	6	5	6	5	5	10
Co	46	47	55	31	46	40	13
Ni	57	0	62	47	85	5	1
Cu	219	71	182	44	127	92	29
Zn	83	101	95	77	107	102	52
Ba	9	4	14	8	15	27	8
Ti	1.4	1.7	1.2	1.0	1.4	1.5	1.1
V	881	562	949	402	700	663	28
Cr	0	0	0	9	4	0	0
Ti/Zr	188	178	171	102	189	173	53
Ti/Y	429	418	386	274	411	419	127
Zr/Y	2	2	2	3	2	2	2
Zr/Nb	12	12	11	14	12	13	17
mg#	41	36	44	48	46	39	20
distance m	170	210	150	160	200	220	240

$Fe_2O_3(t)$: Total Fe as Fe_2O_3 FeO and Fe_2O_3 calculated using Fe_2O_3/FeO ratio = 0.2

mg# : 100 $[Mg^{2+}/ Mg^{2+} + Fe^{2+}]$

distance m : Distance in metres from the base of the intrusion

Table 9 : Whole-rock geochemical data from the Sterkspruit Intrusion - Upper Zone

sample	SG29	SG30	SG31	SG52	SG53	SG54	SG55
Traverse	1	1	1	2	2	2	2
wt %							
SiO_2	56.76	53.00	53.68	54.08	54.94	54.47	53.80
TiO_2	1.69	1.47	1.49	1.48	1.44	1.50	1.34
Al_2O_3	12.42	12.98	13.17	12.88	12.95	13.14	13.08
$Fe_2O_3(t)$	14.46	15.17	12.89	14.10	13.27	13.76	12.83
MnO	0.20	0.24	0.25	0.20	0.17	0.20	0.15
MgO	3.02	4.56	4.83	4.76	4.66	4.73	5.09
CaO	7.21	8.88	9.23	8.05	7.29	7.70	7.69
Na_2O	2.51	1.23	2.31	2.33	3.05	1.39	1.92
K_2O	0.09	0.07	0.22	0.08	0.12	0.08	0.31
P_2O_6	0.22	0.17	0.18	0.20	0.19	0.17	0.15
LOI	1.85	2.04	2.02	2.00	2.28	2.03	2.35
Total	100.44	99.81	100.28	100.14	100.36	99.16	98.70
FeO	11.04	11.58	9.84	10.76	10.13	10.50	9.79
Fe_2O_3	2.21	2.32	1.97	2.15	2.03	2.10	1.96
ppm							
Rb	13	15	15	13	13	11	14
Sr	107	123	122	93	94	83	82
Y	50	40	44	39	42	42	37
Zr	122	105	106	107	115	105	99
Nb	8	7	7	7	7	7	6
Co	35	39	34	35	30	33	35
Ni	11	40	45	37	39	46	52
Cu	23	2	5	33	5	14	32
Zn	42	86	91	91	74	81	71
Ba	8	7	28	1	21	16	10
Ti	1.3	1.2	1.2	1.2	1.1	1.1	1.1
V	314	413	387	393	386	392	350
Cr	0	3	23	7	14	23	53
Ti/Zr	83	84	84	83	75	85	81
Ti/Y	202	219	205	226	206	213	217
Zr/Y	2	3	2	3	3	2	3
Zr/Nb	15	16	15	16	17	16	17
mg#	33	41	47	44	45	45	48
distance m	270	320	390	280	320	370	440

$Fe_2O_3(t)$: Total Fe as Fe_2O_3 FeO and Fe_2O_3 calculated using Fe_2O_3/FeO ratio = 0.2

mg# : 100 $[Mg^{2+}/ Mg^{2+} + Fe^{2+}]$

distance m : Distance in metres from the base of the intrusion

MgO values are higher in the MZ and LZ where they range from 5.0 - 9.7 %, falling drastically to 1.3% in the QD. The high values in the lower portions of the body are again a reflection of the cumulate processes as well as the presence of more orthopyroxene in the assemblage than higher up in the gabbro series. MgO values in the upper zones are generally lower than the MZ and LZ, with the CZ and UZ recording values of between 3.0 and 5.8%. CaO remains constant throughout the body at around 7.0 - 11.0%, except in the QD zone where it drops to 5.9%.

The above major oxide variations are mirrored by the Mg#. The magnesium number (Mg#) is an index using the MgO-FeO ratio to measure fractionation during the evolution of an igneous sequence (Rollinson, 1993). The Mg# for the Sterkspruit gabbroic rocks has been calculated (as an atomic fraction) as $100[Mg^{2+}/Mg^{2+} + Fe^{2+}]$. The MZ and LZ have Mg# of about 60, reflecting the cumulate processes that took place lower down in the body. The Mg# drops to about 42 in the CZ and UZ and 20 in the QD reflecting the more fractionated nature of this zone. The low values from the CZ and UZ match that from the chill margin (Mg# composition 42 - Table 5) and confirm the evolved nature of the parent magma.

In the case of trace elements, a slightly different variation can be seen. The lowest Zr concentrations (46 ppm) are reached in the cumulate LZ, while average Zr contents of about 64 ppm are recorded in the MZ and CZ. The UZ is enriched in Zr, averaging 108 ppm, while the QD records the highest concentrations of 161 ppm. This behaviour of Zr is matched by the other incompatible trace elements, Y and Nb. The low incompatible trace element values in the cumulate LZ are typical of rocks formed by cumulate processes. These elements are excluded from the plagioclase and pyroxenes, which are the main cumulate phases and are enriched in the liquid squeezed out from the crystallising cumulates. The Ti/Zr ratio of

82 in the UZ and 81 in the average chill margin composition (Table 5), is in agreement with Archaean age greenstone belt volcanic rocks > 3.0 Ga, as recorded by Condie (1990). The similarity in this ratio attests to an Archaean age for the Sterkspruit Intrusion, to be discussed in Chapters 6 to 8.

Compositional variations with stratigraphic height are shown in Figures 13, 14 and 15. Trends are best shown by SiO_2, Al_2O_3, MgO, Mg#, Zr and Yb. The variations displayed by these elements are typical of those encountered across layered sill-like intrusions. The variation, especially apparent across Traverse 1, shows a fractionation trend from the floor of the magma chamber upwards and from the roof of the chamber inwards. These fractionating fronts converge at the most evolved composition, the quartz diorite, located approximately 60% of the way up the body. This trend, however, is not symmetrical due to the cumulate zone which formed on the floor of the chamber, some 50 m into the crystallising body. Note that incompatible trace element abundances initially decrease steadily over the lower 50 m (MZ), attain their minimum values in the cumulate LZ and then increase upwards, reaching a maximum in the QD zone. The element abundances also increase from the upper margin of the UZ towards the QD, and show an overall higher abundance than lower in the sequence.

The low concentration of Zr and other incompatible elements in the cumulate LZ is consistent with a similar association in the Kamiskotia gabbroic complex in western Abitibi Subprovince, Canada, described by Barrie *et al.* (1991). According to them, incompatible element variations are ascribed to changes in the mode of cumulus and intercumulus phases. The increasing concentration of these elements up-section in the Sterkspruit Intrusion is attributed partly to a decrease in the cumulus phases.

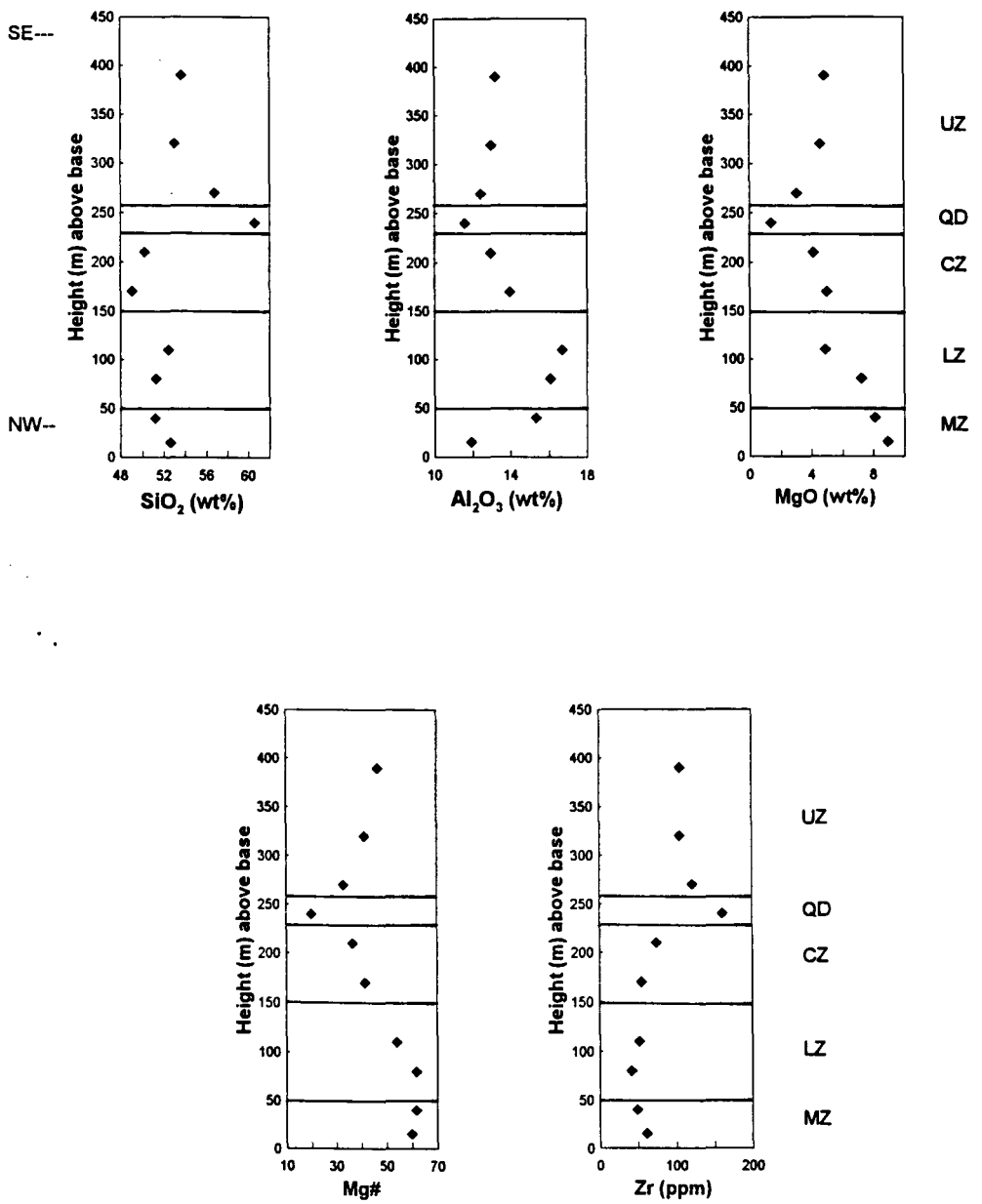


Figure 13: **Whole-rock compositional variation with stratigraphic height across the Sterkspruit Intrusion - Traverse 1. The base of the intrusion is on the northwest side of the body which youngs towards the southeast.**

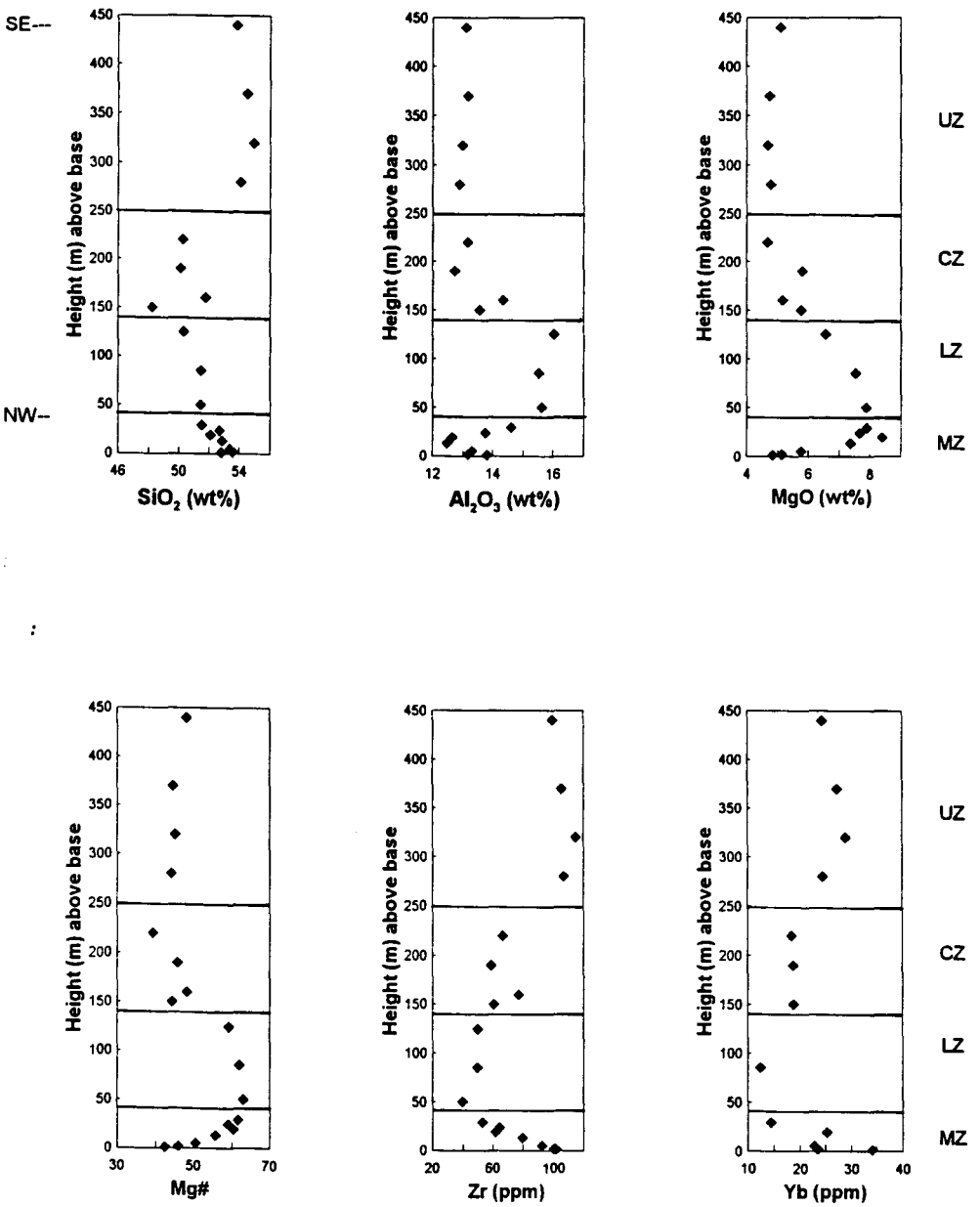


Figure 14: **Whole-rock compositional variation with stratigraphic height across the Sterkspruit Intrusion - Traverse 2. The base of the intrusion is on the northwest side of the body which youngs towards the southeast.**

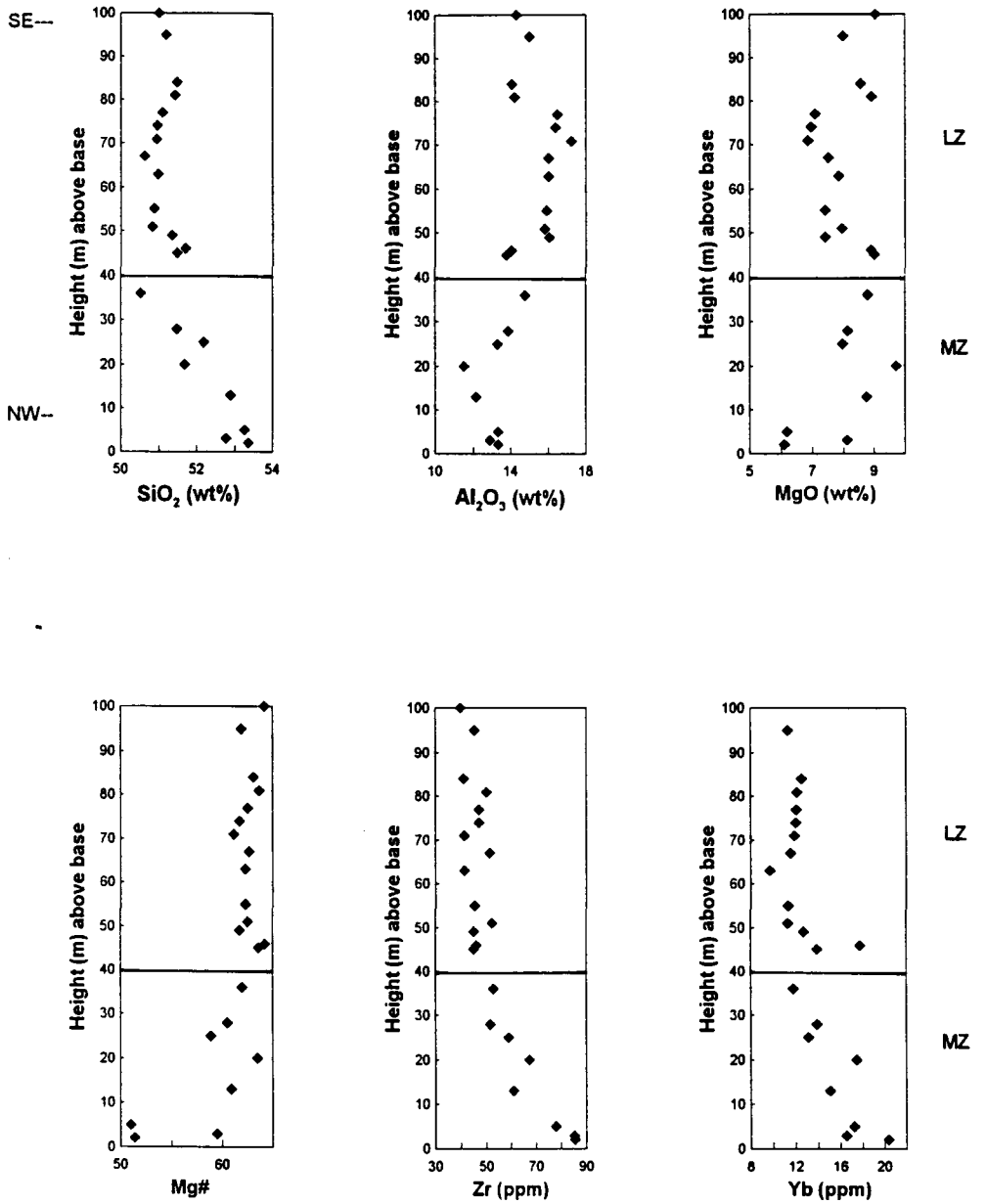


Figure 15: **Whole-rock compositional variation with stratigraphic height across the Sterkspruit Intrusion - Traverse 3. The base of the intrusion is on the northwest side of the body which youngs towards the southeast.**

MgO, Al_2O_3 and the Mg#, all display a reverse trend to the incompatible elements. They increase to the top of the MZ, reach their highest values in the LZ and then decrease towards the QD. They also decrease down-section, through the UZ, from the upper margin towards the QD. The trend shown by MgO, Al_2O_3 and Mg#, mirrors the 'S'-shaped variation of modal olivine with height in some basic sills (Gibb and Henderson, 1992). They ascribed this trend to gravity settling.

In the Mt Kilkenny sill in Western Australia, the MgO content also decreases sharply at the top of the Lower Zone, a trend which Jaques (1976) attributed to the cessation of olivine crystallisation. Rodel (1993) also described an initial increase in the MgO content in the basal dunites of the Stolzburg Complex, prior to the development of a normal fractionation trend. This she attributed to the initial 'filling-effect' of the magma chamber in a subvolcanic sill setting. In addition, the MgO content in olivine cumulates at the base of the Rozentuin body initially increases upwards, before decreasing as in a normal fractionation trend (Rodel, 1993).

The variations of selected major oxides can be demonstrated on bivariate plots with firstly SiO_2 (Harker diagrams) and MgO plotted on the x-axis (Figures 16 and 17). Chemical variations are also shown on trace element bivariate diagrams, with Zr plotted on the x-axis (Figure 18). For some of the major oxide diagrams the composition of pyroxene and plagioclase are also shown to provide clarification on the fractionation processes that have taken place. The source of these mineral compositions to be used for modelling purposes has already been described in section 5.5.2, and are listed in Table 4.

On all the bivariate diagrams the separation of the gabbroic rocks into zones is clearly evident. Fractionation paths, or liquid lines of descent, are best demonstrated by the Marginal, Central and especially the Upper Zones, which display strong geochemical coherence between the major elements. The LZ, being comprised of cumulate plagioclase and pyroxene, rarely forms distinct trends and is excluded from modelling processes.

A point of inflection, marking the apparent change in direction of the liquid path, can be seen on the variation diagrams between the MZ and UZ rocks. This trend, best seen on the SiO_2 plots (Figure 16a-c) and on the MgO vs Al_2O_3 plot (Figure 17a), is attributed to changing proportions of the fractionating mineral assemblages. The MZ crystallised equal amounts of pyroxene and plagioclase, while the UZ crystallised more plagioclase than pyroxene (in the proportion of approximately 60 - 40%). A definite path can be observed in the UZ rocks, from the chill margin composition towards the QD. This confirms the postulated fractionation trend seen on the height variation diagram (Figures 13 and 14) whereby the UZ gabbros crystallised (and the composition evolved) downwards towards the QD zone. The Zr vs Nb incompatible element variation diagram also demonstrates this trend (Figure 18a).

The Ti-rich ferrogabbros from the CZ form a discrete group on bivariate plots of SiO_2 vs TiO_2 (Figure 16c), Zr vs Ti/Zr and Zr vs Ni (Figures 18b,c). This zone could reflect the late stage crystallisation of Ti-rich pyroxenes and Ti-rich oxides or could be unrelated to the rest of the gabbroic body, forming a separate influx of magma. It has been observed petrographically that leucoxene, an alteration product of Ti-ilmenite, is abundant in this zone.

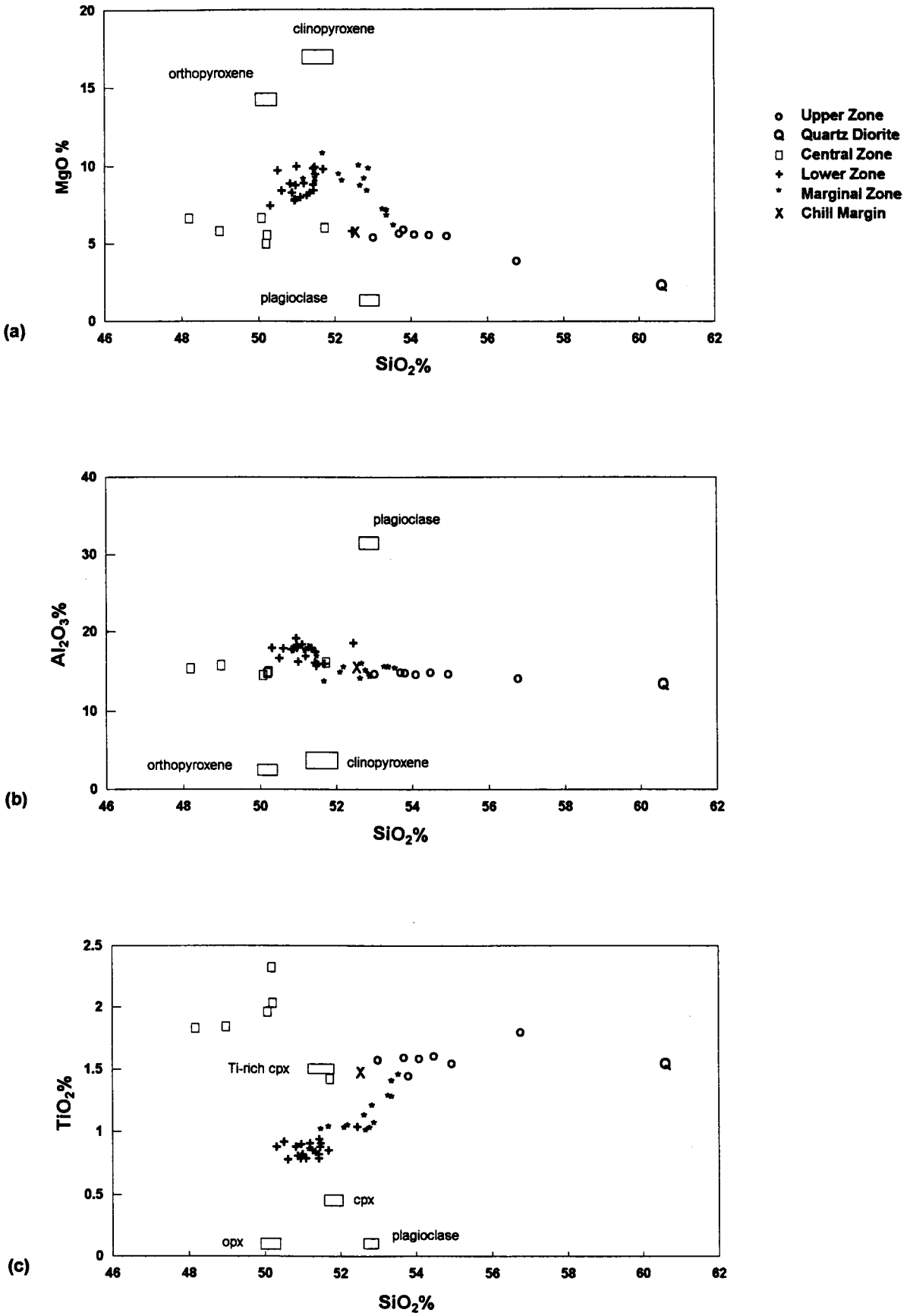


Figure 16 : Chemical variation diagrams of gabbroic rocks from the Sterkspruit Intrusion with SiO_2 plotted against (a) MgO, (b) Al_2O_3 and (c) TiO_2.

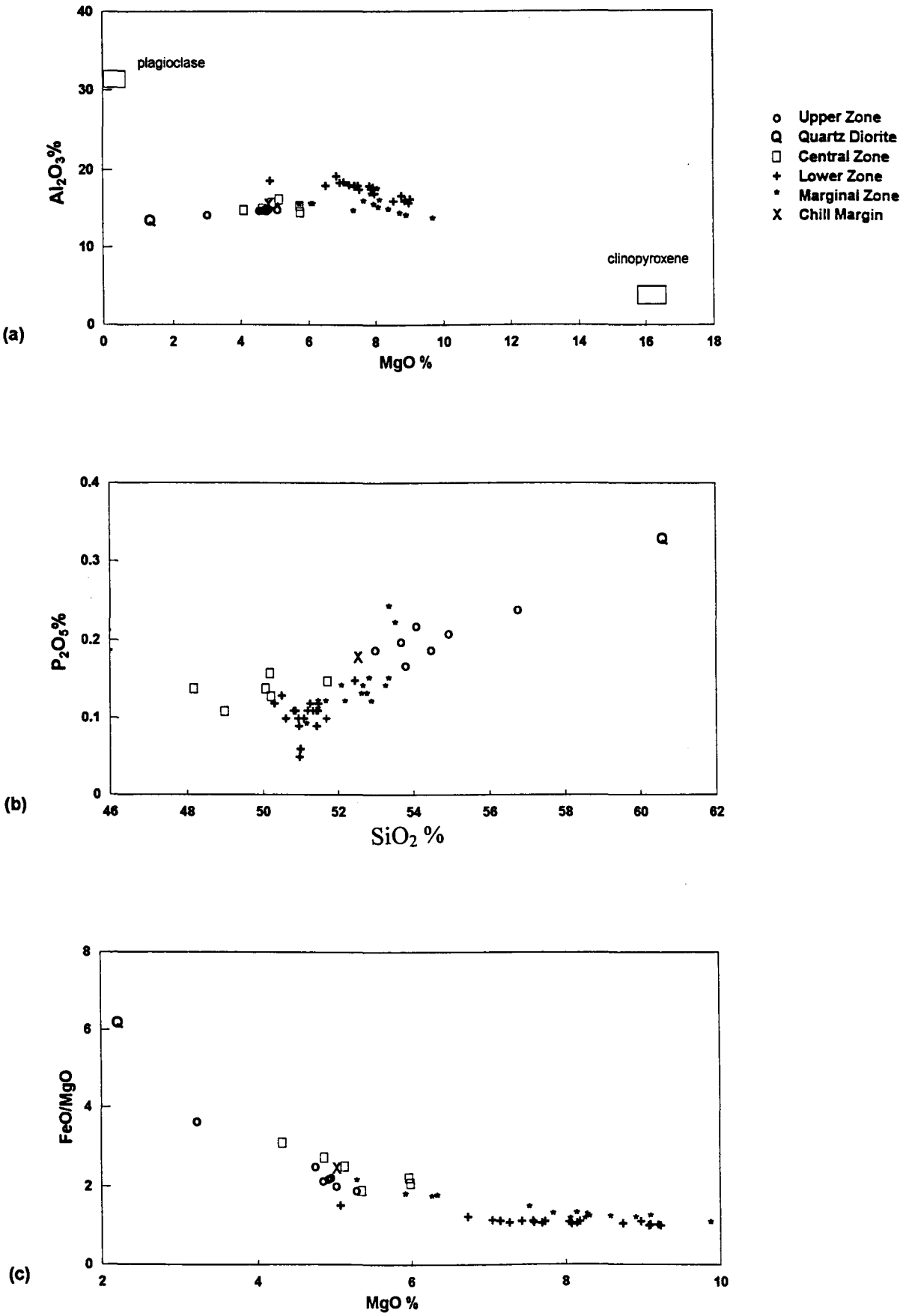


Figure 17 : Chemical variation diagrams of gabbroic rocks from the Sterkspruit Intrusion with MgO plotted against (a) Al_2O_3, (b) P_2O_5 and (c) FeO/MgO.

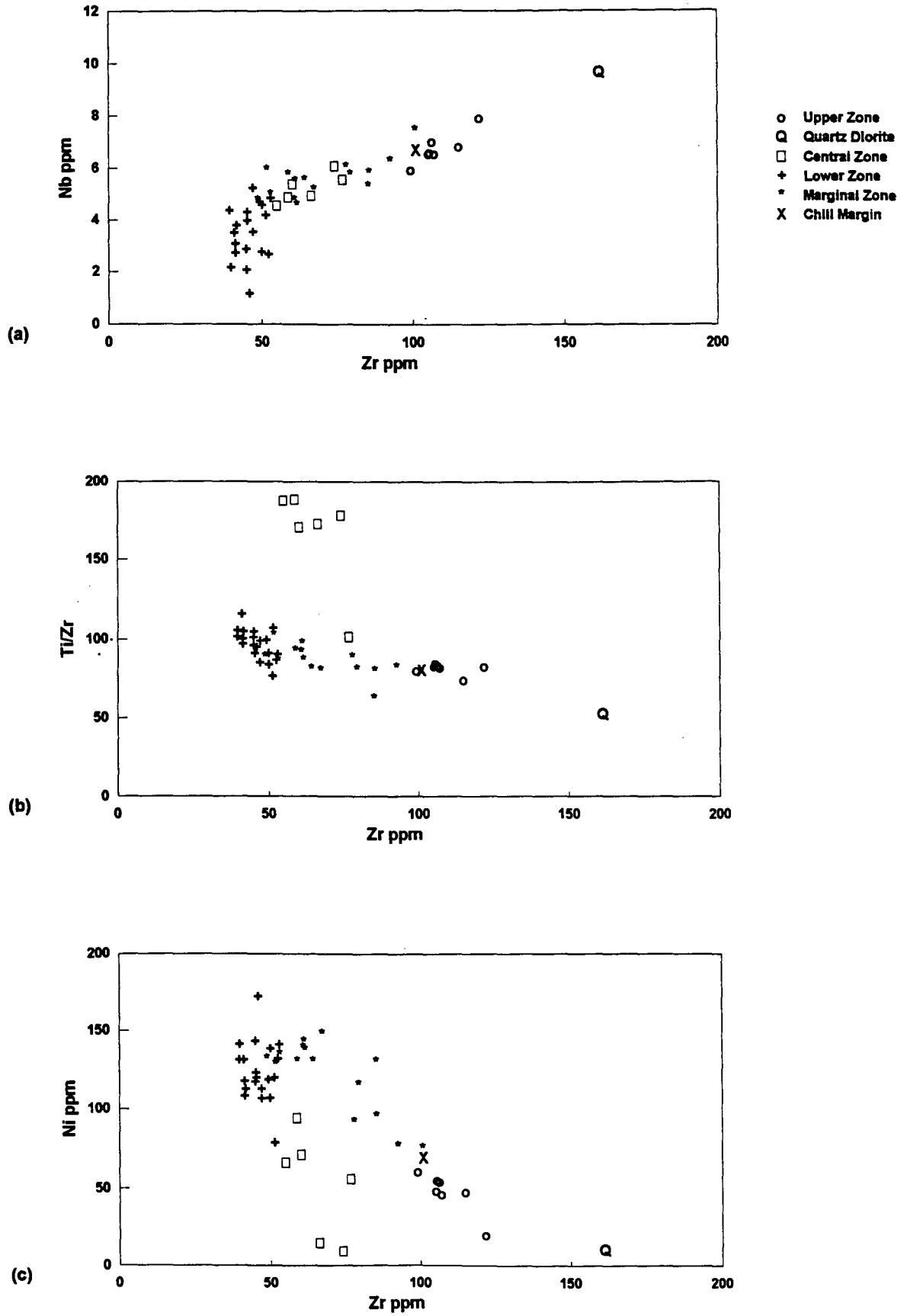


Figure 18: Chemical variation diagrams of gabbroic rocks from the Sterkspruit Intrusion with Zr plotted against (a) Nb, (b) Ti/Zr and (c) Ni.

5.6.4 Rare Earth Element Geochemistry

Rare Earth Element (REE) concentrations were determined for a suite of samples from the Sterkspruit Intrusion, using instrumental neutron activation techniques. Selected samples, which in outcrop were the least altered, are located along Traverses 1 and 2 and include a sample from the chilled margin (SG38) at the base of the intrusion in Traverse 2. Three more sample sites are located towards the eastern portion of the intrusion, with a further sample having being taken from the chilled margin east of Traverse 3 (Figure 3). In addition, the REE values from Traverse 3, reported by Pospisek (1991), were used in this investigation. The REE concentrations were normalised to chondrite abundances using the REE abundances in chondritic meteorites as provided by Evensen *et al.* (1978) (Appendix A, Table A4).

The REE abundances from the Marginal, Lower, Central and Upper Zone gabbros are listed in Table 10 and show a clear variation across the intrusion. Typical REE patterns from gabbro samples in each of the major zones are discussed using chondrite-normalised diagrams. These REE patterns will also be compared to gabbro lithotypes from other layered complexes in the Barberton area and with Onverwacht volcanic rocks. The europium (Eu) anomaly discussed in this section refers to the plotted position of Eu which sometimes lies away from the trend defined by the other REE on a chondrite-normalised diagram (Henderson, 1984). The anomaly is expressed as follows:

$$Eu/Eu^* = Eu_N / \sqrt{(Sm)_N \times (Gd)_N}$$

Eu* is the value obtained at the europium position by straight line interpolation between the plotted points for Sm and Gd.

Table 10 : Average chondrite normalised rare earth element abundances from the Sterkspruit Intrusion

Sample No.	Zone	La	Ce	Nd	Sm	Eu	Gd	Tb	Ho	Yb	Lu	La/Yb	Eu/Eu*
SG38	**CH**	29.94	29.22	27.54	26.50	26.77	26.44	26.71	30.66	34.06	34.89	0.88	1.01
p2	**MZ**	17.38	17.56	17.28	16.44	16.83	17.02	16.96	16.71	16.55	16.43	1.05	1.01
p9	**MZ**	20.99	20.01	18.40	17.72	15.02	15.56	14.51	13.23	11.75	11.53	1.79	0.90
p10	**LZ**	8.19	9.91	11.43	11.78	17.47	13.35	14.74	14.15	13.88	12.80	0.59	1.39
p11	**LZ**	9.98	11.22	11.82	11.36	22.03	13.56	15.84	17.31	17.78	17.91	0.56	1.77
p27	**LZ**	8.34	8.62	8.73	9.77	12.92	10.63	11.28	11.75	11.30	11.21	0.74	1.27
SG50	**CZ**	19.88	19.66	17.73	16.39	15.86	16.03	17.47	18.41	18.84	19.09	1.06	0.98
SG51	**CZ**	15.22	15.37	15.23	14.45	13.11	16.00	16.99	18.30	18.36	18.39	0.83	0.86
SG28	**QD**	19.14	18.57	16.34	14.41	11.50	14.29	16.58	16.32	17.24	nd	1.11	0.80
SG30	**UZ**	42.28	46.14	49.92	45.90	48.24	45.12	43.29	47.88	54.70	54.98	0.77	1.06
SG53	**UZ**	21.90	23.42	23.98	23.01	24.14	23.07	23.59	27.02	29.06	0.00	0.75	1.05

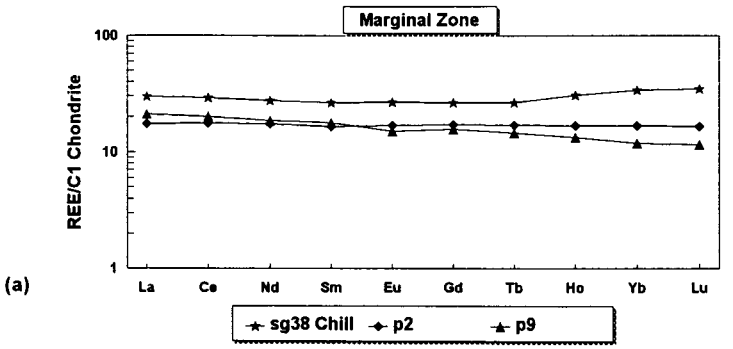
CH - Chill Margin
MZ - Marginal Zone gabbro
LZ - Lower Zone cumulate gabbro
CZ - Central Zone Ti-rich ferrogabbro
QD - Quartz Diorite
UZ - Upper Zone quartz-rich gabbro

The Marginal Zone gabbro is characterised by flat to slightly light rare earth element (LREE) enriched patterns, with REE abundances between 20 and 30x C1 chondrite values (Figure 19a). The average $(La/Yb)_N$ ratio is 1.08. Small negative and positive Eu anomalies that are found (average Eu/Eu* = 0.96), are produced by either plagioclase fractionation or alteration at shallow depths (Condie, 1981).

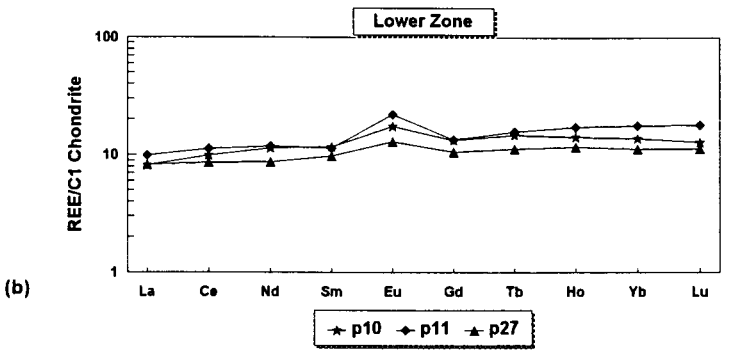
The Lower Zone gabbro, by contrast, displays slightly LREE depleted, sloping patterns with positive Eu anomalies (Figure 19b). The Eu/Eu* averages 1.3, varying between 1.04 and 1.77. The concentrations of these REE vary between 10 and 20x C1 chondrite abundances and the $(La/Tb)_N$ ratio averages 0.72. Petrographical evidence from this zone, which shows plagioclase cumulates in diffuse layering and segregations, suggests that plagioclase fractionation is the cause of the positive Eu anomalies. This zone, compared to the rest of the gabbro, displays the greatest degree of REE fractionation as well as the lowest element abundances.

The Central Zone gabbro is characterised by flat, slightly convex upwards patterns with REE abundances averaging about 20x chondritic. The Eu/Eu* anomaly is about 0.92 while the $(La/Tb)_N$ ratio averages 0.9 (Figure 19c). Lastly, the Upper Zone gabbro has flat REE patterns with REE abundances between 20 and 40x C1 chondrite values. The ratios are very similar to the Central Zone, Eu/Eu* = 0.97 and $(La/Tb)_N$= 0.92 (Figure 19d).

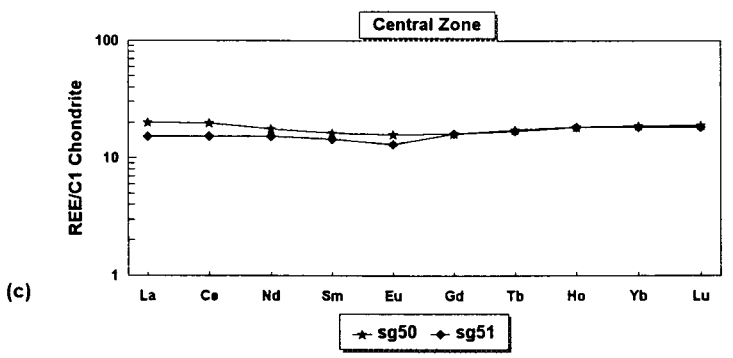
The patterns observed in the Sterkspruit gabbroic rocks compare favourably with those of Archaean komatiitic and tholeiitic basalts. O'Nions and Pankhurst (1978) found that tholeiitic volcanics from early Archaean terrains have low incompatible element contents and LREE depleted or flat REE patterns.



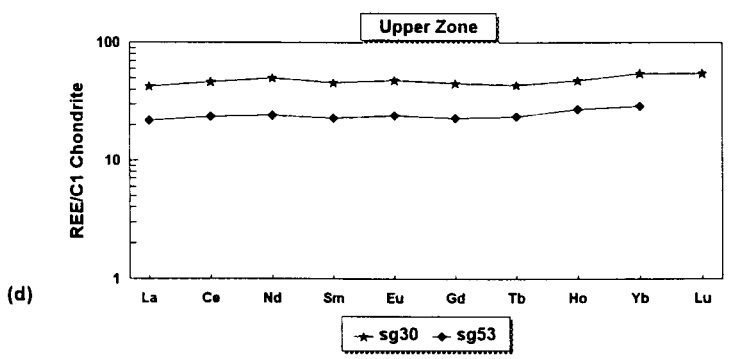
(a)



(b)



(c)



(d)

Figure 19 : Chondrite normalised REE patterns of the (a) Marginal Zone, (b) Lower Zone, (c) Central Zone and (d) Upper Zone from the Sterkspruit Intrusion.

Condie (1981) proposed a two-fold classification of Archaean tholeiites based on REE patterns. Firstly, TH1 (originally termed DAT) is characterised by flat REE patterns with or without small Eu anomalies. Abundances are about 10x chondritic. The TH2 group by comparison (originally termed EAT) is characterised by LREE enriched, sloping patterns between 10 - 40x chondritic. According to Condie (1981), TH1 is the most common tholeiitic rock type in most greenstone belts with TH2 becoming more abundant at higher stratigraphic levels.

Both these types of REE patterns were observed in tholeiites from the Onverwacht Group by Condie *et al.* (1977) who studied the effects of alteration on element distributions. These authors found different patterns between relatively unaltered flows and those flows displaying epidotisation and carbonation. The unaltered flows display LREE enriched, sloping patterns (10 - 50x chondritic), typical of TH2 tholeiites of Condie (1981), while the epidotised and carbonatised flows are characterised by flat to slightly LREE enriched paterns (10 - 29x chondritic).

5.6.5 Normalised Multi-element Diagrams (Spider Diagrams)

Normalised multi-element diagrams, more commonly called spider diagrams, provide a graphical representation of incompatible elements, and are useful for depicting basalt chemistry and for comparing rocks with each other. They are also used to measure deviations from primitive compositions. The incompatible trace elements are plotted in order of decreasing incompatibility and are conventionally normalised to either chondritic, MORB or primitive mantle values.

The trace-element concentrations form the Sterkspruit Intrusion have been normalised to the composition of chondritic meteorites and are

plotted from left to right in order of increasing compatibility in a small fraction melt of the mantle, as described by Rollinson (1993). The normalising values used (listed in Appendix A, Table A5) are those of Thompson (1982) with modifications for the Ba value from Hawkesworth *et al.* (1984). To overcome erratic patterns, due to the effects of fractional crystallisation in different basalts of varying MgO content, Thompson *et al.* (1983) recalculated the normalised trace-element data to make $(Yb)_N$ = 10.

The incompatible element contents of the gabbroic rocks from the Sterkspruit Intrusion are shown on a chondrite-normalised multi-element diagram (Figure 20). Overall the elements are enriched at about 10x chondrite abundances and show flat patterns. Also plotted are the average patterns from >3.0 Ga and 3.0 - 2.5 Ga greenstone belt basalts, as calculated by Condie (1990), average ocean island basalts (OIB), and E- and N-type MORB from Floyd (1991). The Sterkspruit rocks show similar flat patterns to the average greenstone belt basalts except for a slight enrichment in elements Ba, Rb, Th and K in the basalts. These latter rocks are also more enriched at about 10 - 20x chondrite. The mobility of Ba is indicated by their low values in the Sterkspruit gabbro samples.

The multi-element patterns do not show any similarity with average N-MORB and seem to lie midway between the E-MORB and ocean island basalt (OIB) patterns. Floyd (1991) pointed out that the OIB have a wide range of compositions that actually encompass E-MORB, making them difficult to distinguish.

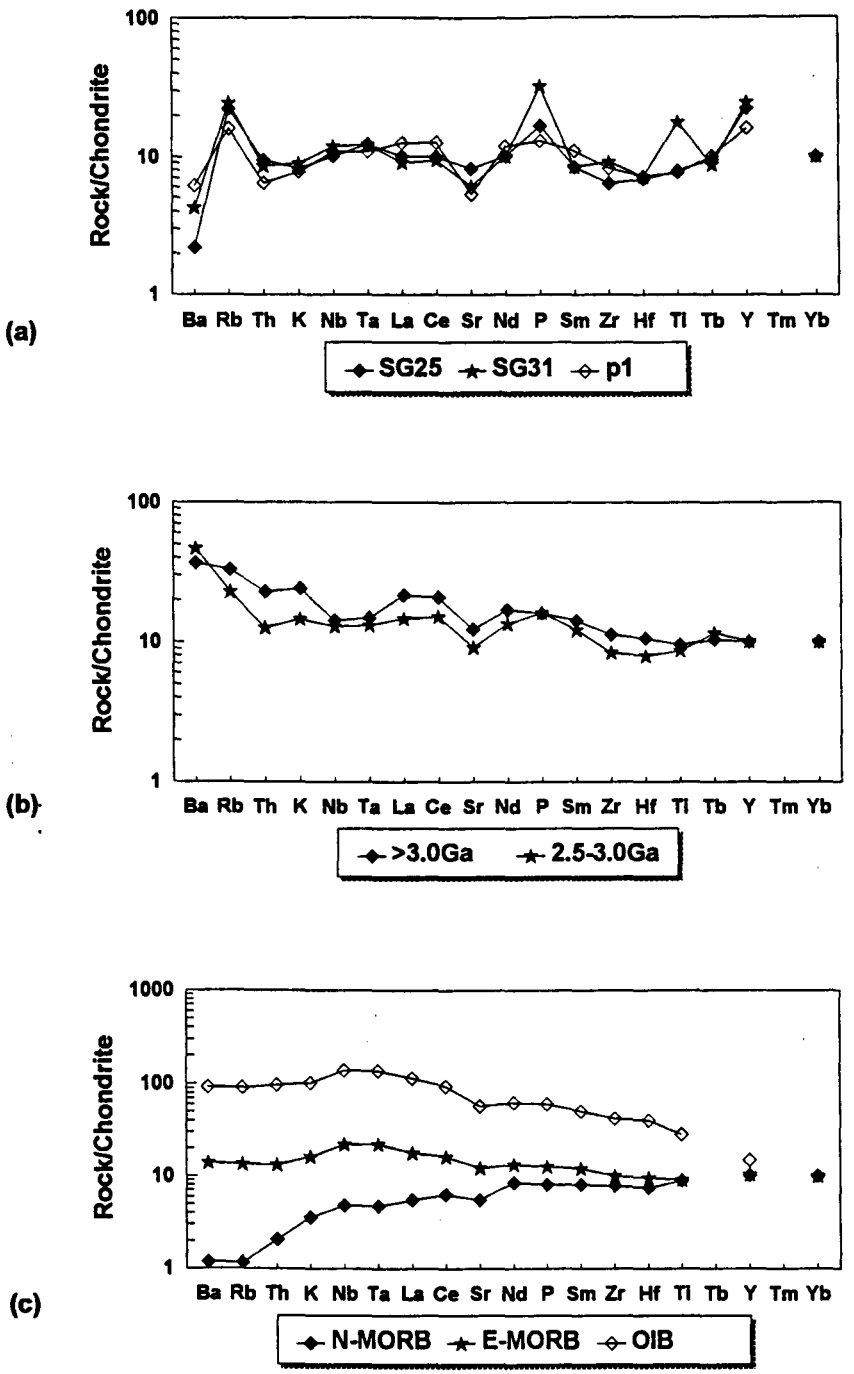


Figure 20: **Chondrite normalised multi-element diagram (spider diagram) of (a) gabbro samples SG25, SG31 and p1 from the Sterkspruit Intrusion, (b) average >3.0Ga and 2.5-3.0Ga greenstone belt basalts for the Archaean, after Condie (1990) and (c) average N-MORB, E-MORB and OIB after Floyd (1991).**

5.6.6 Trace-element Discrimination Diagrams - Tectonic Setting

Trace-element discrimination diagrams are commonly used during petrogenetic modelling to infer the original tectonic setting of a particular suite of basaltic lavas. Due to their relative immobility, elements such as Ti, Zr, Y and Nb are found to be the most effective discriminants between basalts erupted in differing tectonic environments (Rollinson, 1993). Smith (1980) alluded to certain assumptions which must be made when using geochemical parameters for modern tectonic environments and adapting them to infer Archaean environments. These assumptions include:

1) similar mineralogical and chemical source compositions;
2) melting conditions through time were similar;
3) a particular geochemical feature is generated by a single process which is diagnostic of a specific environment; and
4) plate tectonic processes were in operation in the Archaean.

Rocks containing cumulus phases may give erroneous results, so only the chill margin composition and that of the quartz gabbro from the Upper Zone of the Sterkspruit Intrusion have been included in the interpretation. Further limitations, according to Pearce and Cann (1973), for tholeiitic basalts is that they fall in the compositional range 20% > CaO + MgO > 12%. On the Ti - Zr - Y discrimination ternary diagram after Pearce and Cann (1973), the Sterkspruit data plots in the field assigned to MORB, island-arc tholeiites and calc-alkali basalts (Figure 21). Rocks plotting in this field, however, give an ambiguous result and can be further subdivided on their Ti - Zr relationships (Pearce and Cann, 1973). On the Ti - Zr diagram (Figure 22), the Chill Zone and Upper Zone quartz gabbro compositions of the Sterkspruit Intrusion, representing magmatic liquids, plot in the field for modern day MORB. According to Smith (1980) who studied the tectonic setting of tholeiites from the Onverwacht Group, the

Ti - Zr and Ti - Zr - Y relationship indicates an association of these gabbroic rocks with ocean floor basalts and low-K tholeiites. Exceptions include the Central Zone Ti-rich ferrogabbroic rocks which plot as a separate group not related to any reported specific tectonic setting. The Sterkspruit gabbroic compositions also show an affiliation with plate margin basalts on a Zr/Y - Ti/Y discrimination diagram (Pearce and Gale, 1977) as opposed to within plate basalts (Figure 23).

The trace element associations from the Sterkspruit body are comparable to the tholeiitic and andesitic basalt trace element relationships from the Kromberg Formation (Conway, 1985) as well as the high-Ti basalts from the Lower Onverwacht Group (Smith, 1980). Smith (1980) also drew an analogy between the Onverwacht lavas and back-arc basin lavas, pointing to similarities in their chemistry. Exceptions include higher K, Rb, Cs, Sr, Ba and REE's in the arc-related basalts, which he felt could be related to sea-water contamination.

In a description of the geochemical characteristics of Precambrian basaltic greenstones, Condie (1990) concluded that basalts with island-arc affinities are dominant in the Archaean and that basalts with MORB or within-plate geochemical characteristics are rare in Precambrian sequences of all ages.

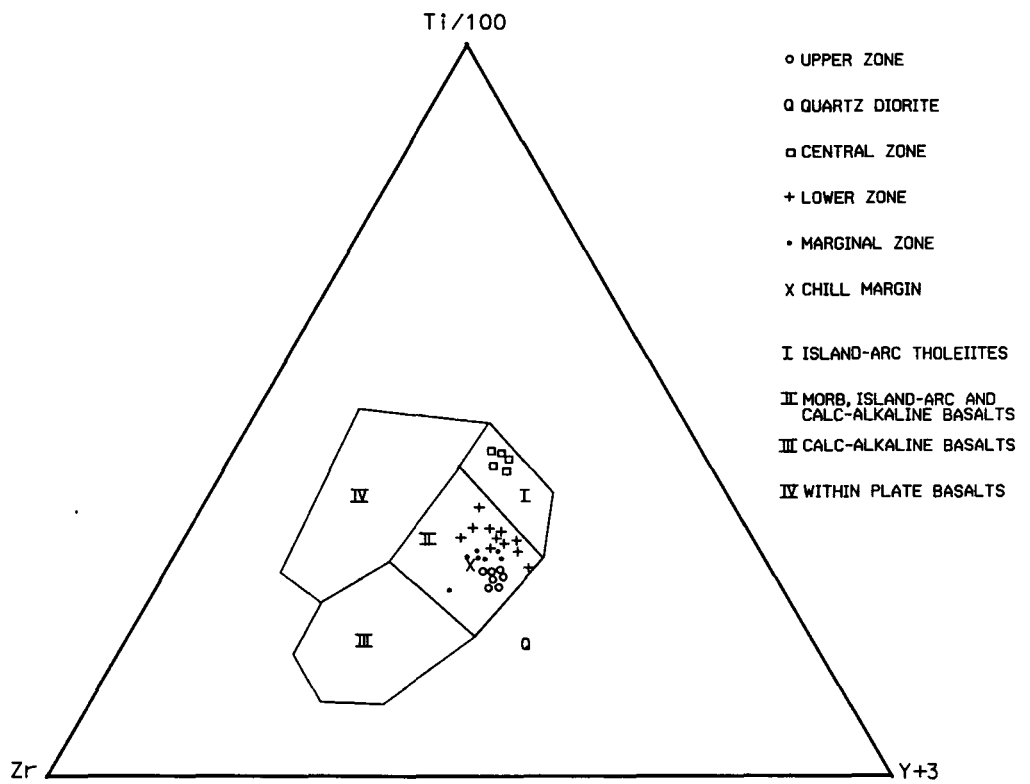


Figure 21 : **Ti - Zr - Y discrimination diagram for the Sterkspruit Intrusion (after Pearce and Cann, 1973).**

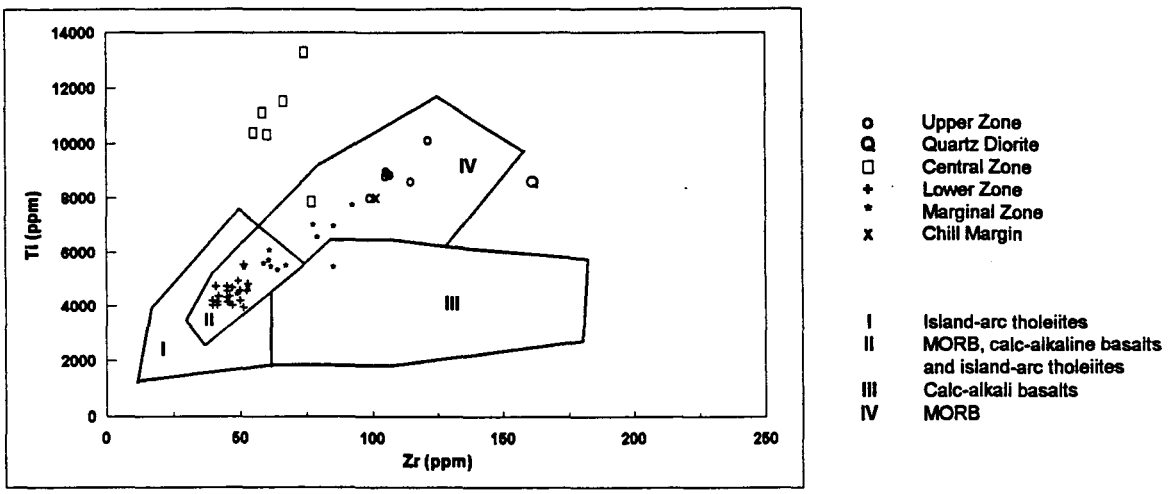


Figure 22: Ti - Zr discrimination diagram for the Sterkspruit Intrusion (after Pearce and Cann, 1973).

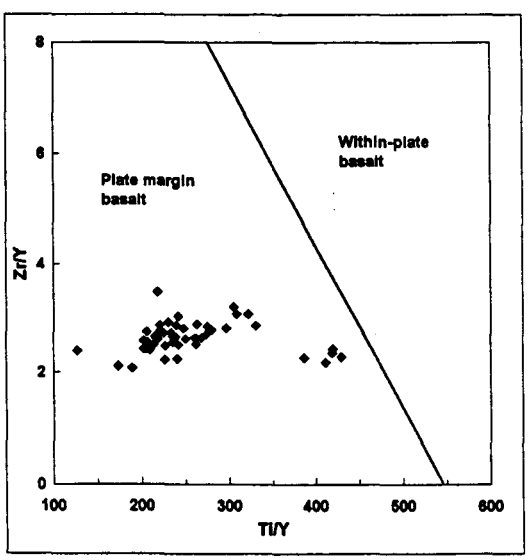


Figure 23: Zr/Y - Ti/Y discrimination diagram for the Sterkspruit Intrusion (after Pearce and Gale, 1977).

5.7 Whole-rock Geochemistry of the Sterkspruit Mafic Dyke Swarm

5.7.1 Introduction

The northwest-trending dykes which make up the Sterkspruit mafic dyke swarm can be classified into four main groups (A - D) based on differences in their chemistry (Table 11). Figure 3 shows the localities of the dyke samples and a complete list of whole-rock analyses appears in Appendix A, Table A2. The dyke samples forming these groups are as follows:

Group A : samples SD.1, 2, 3 and 7
Group B : samples SD. 4, 5, 6, 9, 10, 11, 12, 13 and 14.
Group C : samples SD. 15 and 16
Group D : samples SD. 17 and 18

5.7.2 Classification

On a silica - total alkalis (SiO_2 vs Na_2O+K_2O) major oxide diagram (Figure 24) the Sterkspruit mafic dykes all plot in the subalkaline field below the MacDonald and Katsura (1964) line. The dykes show a wide range in SiO_2 and, to a lesser extent, alkali concentrations. Groups A to D can be clearly distinguished on this diagram, with Group A plotting at the high SiO_2 end and Group C at the low end. Also plotted for comparison are the average compositions of the pre-Godwan, post-Transvaal and Karoo age dykes after Robb (1977). The Sterkspruit Intrusion is also indicated.

Table 11 : Average whole-rock geochemical data of dyke groups from the Sterkspruit Mafic Dyke Swarm in comparison with dykes of similar and younger age

Dyke Group	A	B	C	D	Pre Godwan	Post Transvaal	Karoo
Sample No.	1, 2, 3, 7	4, 5, 6 9 - 14	15, 16	17, 18	H.V.2	P.T.1	ODS.1
wt %							
SiO_2	54.8	52.6	49.1	52.3	55.8	53.2	51.4
TiO_2	0.4	0.4	0.3	1.1	1.2	0.6	0.5
Al_2O_3	16.4	12.9	11.9	9.7	14.2	6.8	7.9
Fe_2O_3(t)	8.0	8.8	9.5	11.9	10.4	9.6	11.2
MnO	0.1	0.1	0.2	0.2	0.4	0.2	0.2
MgO	5.7	10.9	14.3	10.5	4.1	18.9	19.6
CaO	8.8	8.0	9.0	9.1	6.2	5.1	7.1
Na_2O	2.0	1.3	0.5	1.2	4.4	1.0	1.1
K_2O	1.9	1.5	0.8	0.9	0.9	0.9	0.3
P_2O_5	0.1	0.09	0.07	0.13	0.26	0.11	0.06
ppm							
Rb	72	55	41	36			
Sr	254	135	87	202			
Y	19	18	14	21			
Zr	95	87	47	130			
Nb	7	7	4	8			
Co	32	49	58	58			
Ni	126	419	591	466			
Cu	26	29	36	117			
Zn	64	67	62	78			
Ba	300	233	111	270			
Ti	0	0	0	1			
V	103	126	126	199			
Cr	213	1203	2024	1041			
Ti/Zr	24	26	36	52			
Ti/Y	122	128	124	316			
Zr/Y	5.1	4.9	3.5	6.1			
Zr/Nb	13.1	11.9	11	16.5			
mg#	62	74	78	67			

Fe_2O_3(t) : Total Fe as Fe_2O_3

H.V.2 : Pre-Godwan diabase dyke, Hazyview area (Robb, 1977)

P.T.1 : Post-Transvaal intrusion, south of White River (Robb, 1977)

ODS.1 : Karoo-age dolerite sill, west of Sabie Sands (Robb, 1977)

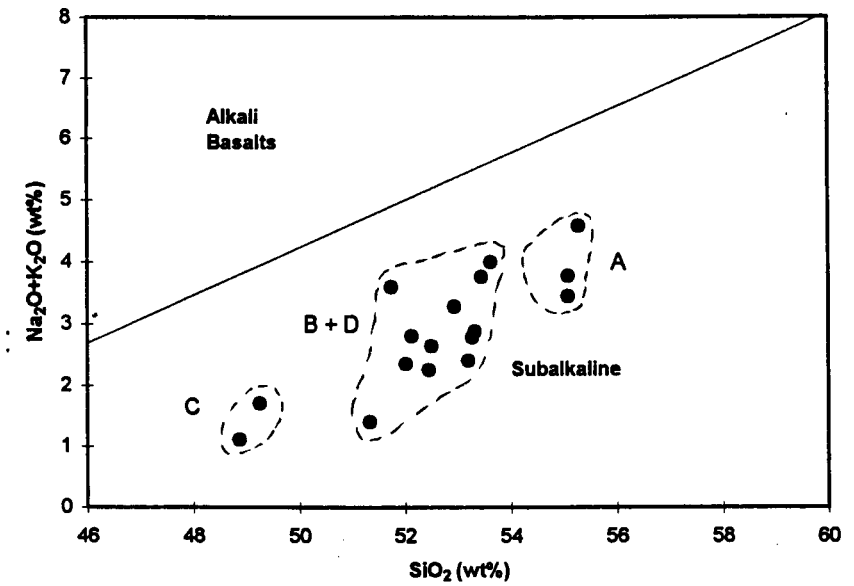


Figure 24 : SiO_2 Vs Total Alkali diagram for rocks from the Sterkspruit mafic dykes showing their subalkaline composition (after MacDonald and Katsura, 1964). A - D are the dyke groups referred to in the text.

The mafic dykes are also plotted on a Jensen (1976) diagram based on the proportions of the cations (Fe^{2+} + Fe^{3+} + Ti), Al and Mg. Figure 25 shows the wide range in compositions of these dykes, with the different groups clearly differentiated. Group A dykes plot in the field for calc-alkaline basalts while group B dykes straddle the boundary between high-Mg tholeiitic basalts and komatiitic basalts. The samples from groups C and D plot in the komatiitic basalt field with group C closer towards the Mg apex and group D closer towards the Fe+Ti apex reflecting their high Ti contents.

The dyke compositions are clearly different to the gabbroic compositions from the Sterkspruit Intrusion, which range from high-Mg to high-Fe tholeiites (Figure 12). Some dykes from Group B are similar to the Precambrian dyke swarms reported by Sial *et al.* (1987) who investigated the differences between dykes from this time period and dykes in the Phanerozoic. The Precambrian dyke swarms have affinities with Mg-tholeiites while the Phanerozoic are similar to Fe-tholeiites.

On an AFM (Na_2O+K_2O - FeO+Fe_2O_3 - MgO) ternary diagram (Figure 26) the mafic dyke data show a broad differentiation curve and plot in the calc-alkaline field as defined by Kuno (1968). The Fe-enrichment trend of the Sterkspruit gabbroic rocks is plotted for comparison. The clear separation of the data points from the trend line of the Sterkspruit Intrusion suggests there is no genetic link between the magma types responsible for the intrusions.

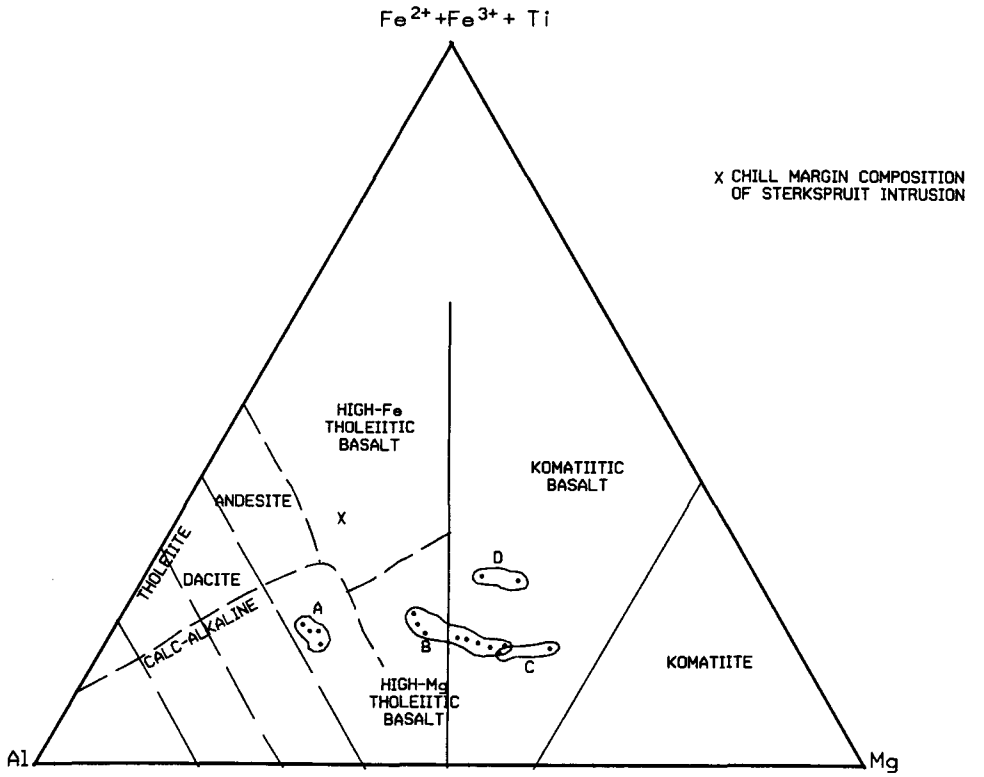


Figure 25 : **Classification of the Sterkspruit mafic dykes according to their cation proportions of (Fe^{2+} + Fe^{3+} + Ti) - Al - Mg (after Jensen, 1976). A - D refer to the dyke groups.**

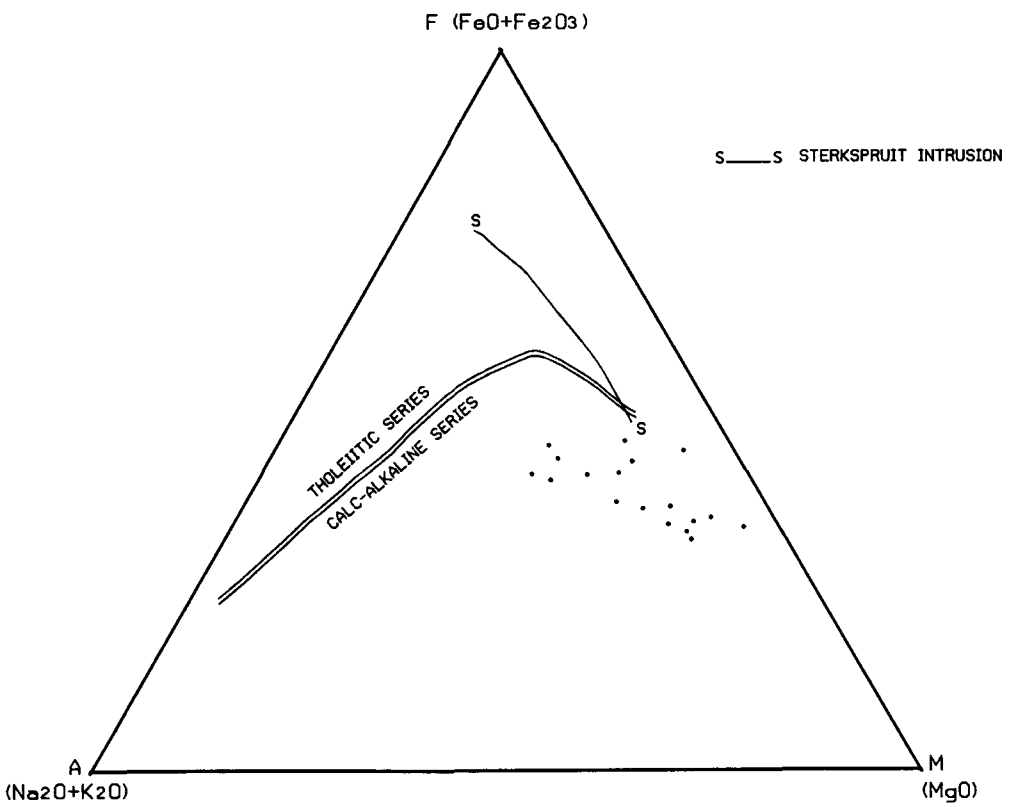


Figure 26 : **AFM (Na_2O+K_2O - $FeO+Fe_2O_3$ - MgO) diagram of the Sterkspruit mafic dykes. The trend of the Sterkspruit Intrusion (s -- s) is shown for comparison.**

5.7.3 Binary Variation Diagrams

As mentioned in the introduction, the mafic dykes from Sterkspruit show clear intra-swarm chemical variation. The dykes are numbered generally from west to east across the study area and show, in this direction, a steady increase in MgO and FeO and a decrease in SiO_2 and Al_2O_3. The average compositions from each of the four groups is listed in Table 11. Group A dykes, intruded into the western end of the study area, have high SiO_2 (54.8%), Al_2O_3 (16.4%) and low MgO (5.6%). These dykes are in close proximity to the trondhjemitic gneisses of the Nelshoogte pluton, with sample SD7 located in a dyke hosted by this gneiss. The effects of assimilation of the granitic material by the intruding melt are thought to be the cause of the high SiO_2 and Al_2O_3 contents in these dykes. A dyke located nearby, and seen cutting the main Badplaas - Barberton road, is full of granitic inclusions that have spalled off the sidewalls to the dyke and provide support for the assimilation argument (C.R. Anhaeusser, pers. commun.).

Group C dykes are characterised by low SiO_2 (49.1%) and high MgO (14.3%). They also have the lowest incompatible element contents between the groups with Zr and Nb concentrations of 47 ppm and 4.3 ppm respectively. Group D dykes, adjacent to those of group C (Figure 3), are TiO_2 rich (1.12%), low in Al_2O_3 (9.7%) and have the highest Zr concentrations (130 ppm) of all the dykes.

These intra-dyke swarm compositional differences are highlighted in the major oxide and trace element binary diagrams shown in Figures 27 and 28. A number of processes could be responsible for the differences seen in dykes having the same orientation. These include emplacement of magma at different times, crystal fractionation, variable degrees of partial melting, crustal contamination and a heterogeneous mantle source.

Condie *et al.* (1987), following a study of the geochemistry of Precambrian mafic dykes from the Southern Superior Province in Canada, suggested that variations in incompatible element abundances within dyke swarms resulted from a heterogeneous mantle source. These authors further suggested that the enrichment of highly incompatible elements reflects enriched mantle or crustal contamination. However, constraints imposed on crustal contamination by Condie *et al.* (1987) include the requirement of at least 20% contamination to explain enrichments of LIL. Such levels of contamination, however, would change the bulk composition of the dyke to andesite, which is not the case.

In a geochemical study of the Mackenzie dyke swarm in Canada, Gibson *et al.* (1987) also described inter-dyke chemical variation and included processes such as crystal fractionation as well as the dykes being fed from several different high-level magma chambers, possibly of slightly different ages and each having different magma chemistry. They also considered possible crustal contamination of basaltic magmas and both selective and/or wholesale assimilation of gneissic country rocks. Further examination of the effects of contamination on the Sterkspruit dykes would require studying samples from the chill margins and comparing them with the compositions from the dyke interiors, which is beyond the scope of the present investigation.

5.7.4 Trace-element Discrimination Diagrams - Tectonic Setting

On the Ti - Zr - Y ternary discrimination diagram after Pearce and Cann (1973), the Sterkspruit mafic dykes plots in the field assigned to calc-alkali basalts (Figure 29). This setting is confirmed by the Ti (ppm) - Zr (ppm) diagram after Pearce and Cann (1973) (Figure 30). In both diagrams the Sterkspruit gabbroic rocks are plotted for comparison and show the completely dissimilar source and tectonic setting.

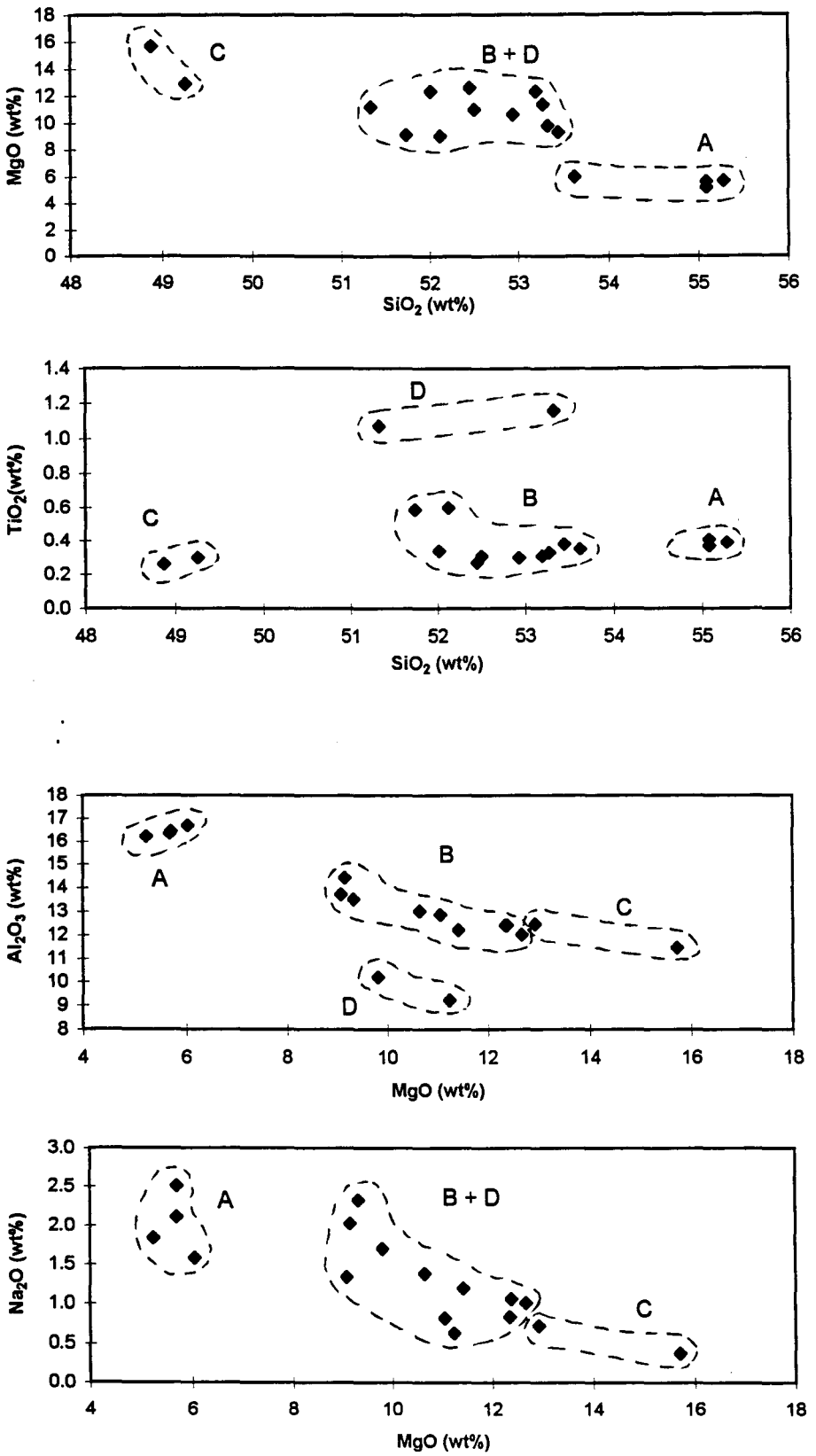


Figure 27 : Major oxide binary plots showing intra-dyke swarm variation. A, B, C, D indicated on the diagrams refer to dyke groups as discussed in the text.

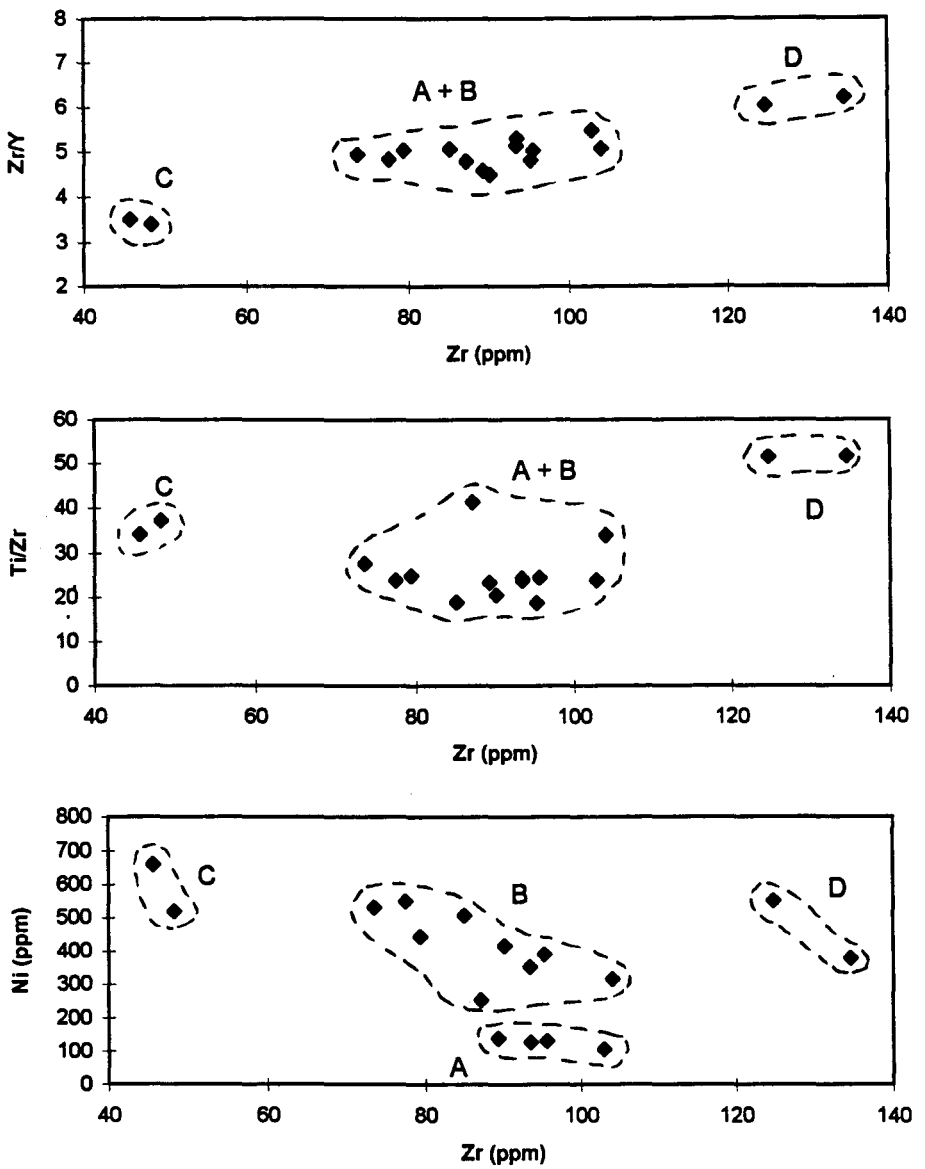


Figure 28 : Trace element binary plots showing intra-dyke swarm variation. A, B, C, D indicated on the diagrams refer to dyke groups as discussed in the text.

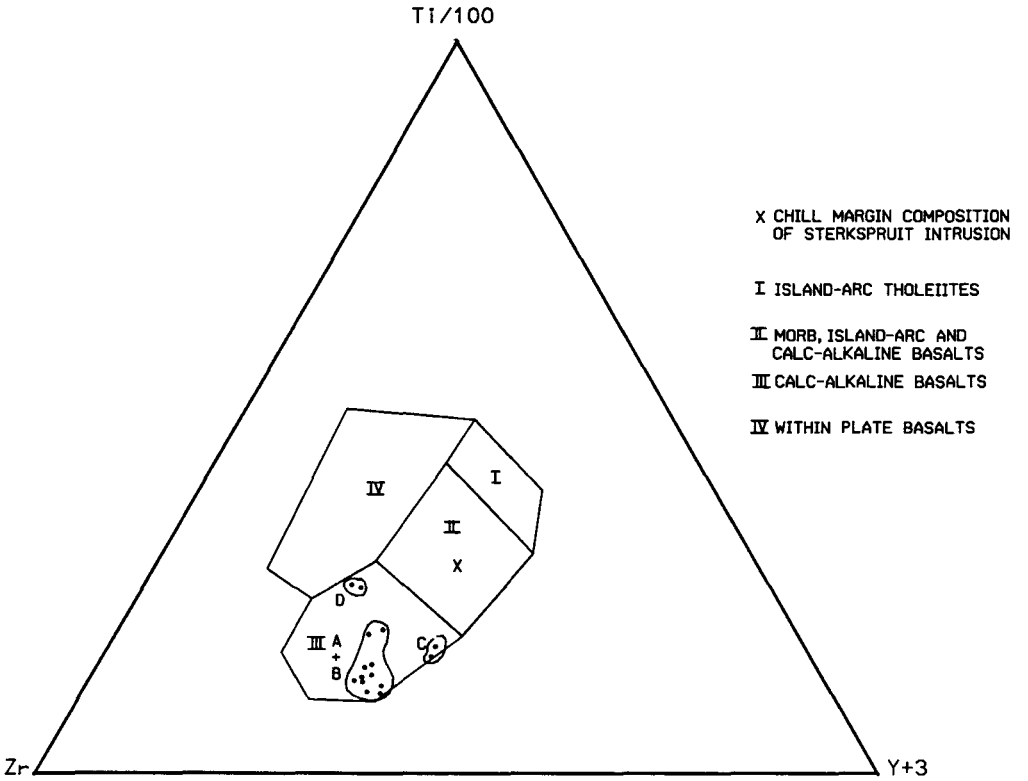


Figure 29 : **Ti - Zr - Y discrimination diagram for the Sterkspruit mafic dykes (after Pearce and Cann, 1973). A - D are the dyke groups referred to in the text.**

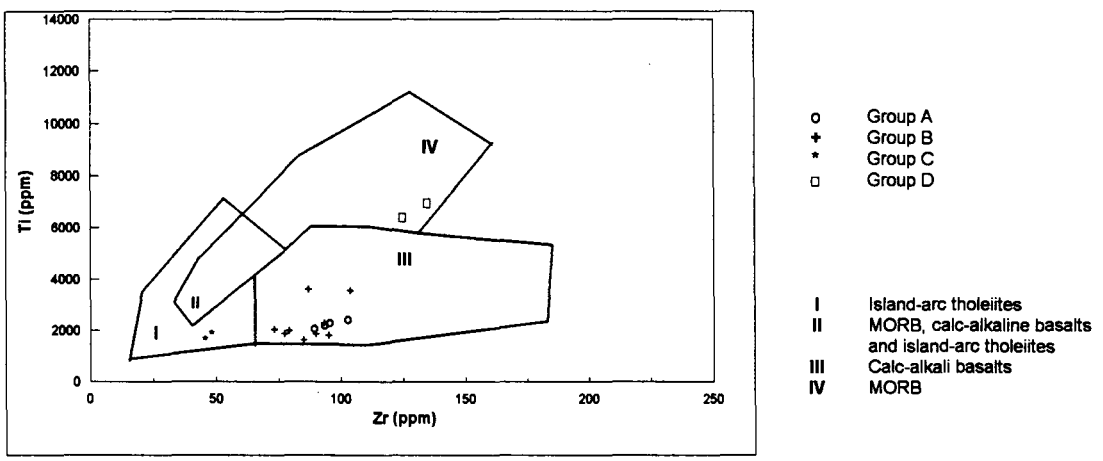


Figure 30: TI - Zr discrimination diagram for the Sterkspruit Mafic Dykes (after Pearce and Cann, 1973).

CHAPTER SIX
COMPARISONS WITH OTHER MAFIC COMPLEXES

6.1 Description of Mafic Complexes

Mafic-to-ultramafic layered complexes have been described from many Archaean terrains including South Africa, Australia and Canada. Mafic or gabbroic intrusions, which are distinct from typical layered complexes having komatiitic affinities, have also been described from the Archaean through to the Tertiary. Many of these intrusions lack ultramafic lithologies (such as dunites, pyroxenites and peridotites) and can be associated with tholeiitic rock suites (Condie, 1981). The smaller complexes are generally lensoid and conformable with the sediments and volcanic rocks into which they intrude (Condie, 1981), and many appear to be closely related to volcanism. Jolly (1977) suggested that layered intrusive bodies represent fractionated holding chambers from which volcanics were erupted. The following is a brief description of some selected mafic intrusions from different Precambrian Shields that could have some bearing on the characterisation of the Sterkspruit Intrusion.

6.1.1 Southern Africa - Usushwana Complex

The Usushwana Complex is located in the southeastern part of the Kaapvaal Craton, in Mpumalanga Province, between Piet Retief and Amsterdam, extending into neighbouring Swaziland. The Complex, which has the shape of an inverted 'h', extends in a northwesterly-southeasterly direction for approximately 100 km. Hammerbeck (1982), described the progression of events leading to the emplacement of the Complex as follows:

1) deposition of sediments and basic volcanics of the Pongola Sequence;
2) emplacement of the Thole ultramafic sills;
3) extrusion of rhyolites and dacites of the Amsterdam Formation; and
4) intrusion of the gabbroic and acidic rocks of the Usushwana Complex.

The igneous rocks of the Usushwana intrusive suite represent a case of late Archaean continental magmatism (Hegner *et al.*, 1984). Using Sm-Nd whole rock data, they interpreted an apparent age of ~ 3.1Ga for the gabbros as a mixing line between 2.87Ga old magma and older continental crust.

The intrusive rocks of the Usushwana Complex are subdivided into the gabbroic Piet Retief Suite and the acidic Hlelo Suite, both forming the two outer limbs of the Complex. The western limb, reaching 4000 m in width, is more continuous and extends as a narrow belt for about 90 km. The main mafic rock types from the Piet Retief Suite are quartz gabbro, ferrogabbro, gabbro and hyperite (Hammerbeck, 1982). Quartz gabbro is the most common type in which quartz is a conspicuous constituent. Weakly developed layering is displayed in the ferrogabbro which contains high-Ti contents. Magnetite layers form discontinuous lenses at several localities in the ferrogabbro. The gabbro unit is considered to be more mafic than the other gabbroic types but shows distinctive uralitisation of the ferromagnesian components. The hyperite (comparable to hypersthene gabbro) is intermediate in composition between the sills of the Thole ultramafics and the gabbroic rocks of the Piet Retief Suite.

The granodiorite from the more acidic Hlelo Suite, occurring intermittently along strike of the Piet Retief Suite, is considered to be partly a differentiation product of the gabbroic rocks outlined above with assimilation of rhyolitic roof rocks also a possibility.

Hammerbeck (1982) related the mafic rocks of the Piet Retief Suite to a tholeiitic parentage which originated from a magma source that was re-activated from time to time. He also described sills of the Thole ultramafics, and compared the parental magma to komatiitic basalts of the Geluk type from the Barberton Sequence.

6.1.2 Western Australia - Mt Kilkenny Layered Sill

The Mt Kilkenny intrusion is a small (600m wide) metamorphosed layered gabbroic sill of Archaean age, situated in the Eastern Goldfields of Western Australia. This intrusion was emplaced into a lower mafic - ultramafic volcanic sequence which forms the lower unit of a basic to acid volcanic cycle (Jaques, 1976). The parent magma is thought to be a high-alumina tholeiite which gave rise to an intrusion consisting of non-cumulate marginal portions, cumulate gabbroic zones and a simple layered sequence. A small amount of granophyre was produced as an end stage differentiate. Based on a steady cryptic variation with height shown by plagioclase and augite, Jaques (1976) suggested fractional crystallisation from a single magma pulse by gravity settling.

Geochemically, the Mt Kilkenny gabbroic rocks are hypersthene or quartz normative indicating a saturated, non-alkaline magma type. Plots of oxide variation with height in the sill show an 'S'-type pattern, similar to that seen in the Sterkspruit Intrusion. MgO increases to the top of the Lower Zone and then decreases steadily following a normal fractionation trend. Jaques (1976) attributed this decrease in MgO at the top of the Lower Zone to the cessation of olivine crystallisation. TiO_2 and Fe are enriched in the late-stage cumulate rocks of Mt Kilkenny, a feature also seen in the Central Zone of the Sterkspruit Intrusion. This increase is attributed to the late formation of intercumulus titanomagnetite.

6.1.3 Greenland - Skaergaard Intrusion

One of the best described examples of a shallow, differentiated layered complex, formed from a tholeiitic magma, is the Skaergaard Intrusion on the east coast of Greenland (Wager and Brown, 1968; Hess, 1989; McBirney, 1996). Even though the Skaergaard Intrusion is much larger than the Sterkspruit Intrusion, measuring 6 by 11 km, and is associated with a much younger magmatic event at 55 Ma, their exist many similarities between these two igneous intrusions which can be used for petrogenetic modelling of the Sterkspruit Intrusion.

The gabbroic Skaergaard Intrusion was emplaced into Archaean gneisses and Tertiary basalts as a moderately evolved tholeiitic magma in a single, prolonged pulse (McBirney, 1996). The original magma followed a differentiation trend characterised by strong Fe-enrichment and a late-stage split into two liquids, one rich in Fe, the other rich in silica. The intrusion is subdivided into three major units: A Layered Series, an Upper Border Series and a Marginal Border Series. The Layered Series is made up of medium- to coarse-grained gabbros that can be subdivided into three zones, each of which, in turn, is also subdivided into units based on mineralogical differences. Layering is prevalent throughout most of this Series. The Upper Border Series is also subdivided into three subzones based mostly on plagioclase composition. The Marginal Border Series is a sequence of gabbros that crystallised on the walls of the chamber.

The Skaergaard Intrusion displays differentiation mechanisms which may have some relevance to the Sterkspruit Intrusion. Crystallisation processes occur from the floor of the magma chamber upwards, forming the Layered Series, from the roof downwards, forming the Upper Border Series and from the walls inwards, resulting in the development of the Marginal Border Series. The plagioclase, olivine and pyroxene in the

Skaergaard Intrusion become compositionally more evolved inwards from the floor, roof and walls, culminating at the Sandwich Horizon, which is a unit located at the interface of the upper part of the Layered Series and the lower reaches of the Upper Border Series. McBirney (1996) suggested that the Sandwich Horizon represents a zone of convergence for the fronts of crystallisation from the floor up and from the roof down. The Quartz Diorite zone in the Sterkspruit Intrusion may have a similar setting and origin to that described for the Sandwich Horizon.

Trace element variations with height in the Skaergaard Intrusion are also similar to those of the Sterkspruit Intrusion. Incompatible elements initially decrease in abundance across the lower Layered Series, then strongly increase to reach maximum concentrations in the Sandwich Horizon. Above this horizon the abundances again decrease into the Upper Border Series, but overall abundances remain higher than in the Layered Series. McBirney (1996) attributed this to compaction processes operating in the Layered Series, whereby only small proportions of segregating late interstitial liquids (residual liquids) were retained. In contrast the Upper Border Series lacked significant compaction and therefore retained larger proportions of late interstitial liquids leading to higher element abundances.

6.1.4 Canada - Superior Province

Intrusions in the Superior Province of Canada, described as normal gabbroic bodies by Irvine and Ridler (1972), are distinctive in that they are composed essentially of gabbro with only minor ultramafic or anorthositic components. They are described as tholeiitic bodies with the only common acidic differentiate being small amounts of granophyre. Most ultramafic and gabbroic bodies in the Superior Province are closely associated with volcano-sedimentary belts and have the following

characteristics (Irvine and Ridler, 1972): they are pre-orogenic and underwent the same regional deformation and metamorphism as the related stratified rocks; they rarely show close relationships to faults; and they have subalkaline affinities, with the gabbroic rocks having modal hypersthene and quartz.

6.1.5 United States - Midcontinent Rift, Duluth Complex

The Duluth Complex in northeastern Minnesota is composed of numerous individual mafic layered intrusions of tholeiitic affinity (Miller and Ripley, 1996). The complex was emplaced into comagmatic volcanics during the development of the 1.1 Ga Midcontinent Rift in North America. Miller and Ripley (1996) summarised the geological setting and the cumulate stratigraphy and cryptic variation of six of these intrusions located in the layered series comprising the Duluth Complex. These intrusions, although formed from similar tholeiitic basaltic magmas, differ fundamentally in their openness to magmatic recharge, eruption, and assimilation during crystallisation. The Sonju Lake Intrusion displays features consistent with a nearly closed magmatic system, wherein cumulus augite crystallised before ilmenite. The Partridge River and South Kawishiwi Intrusions show evidence of frequent magmatic recharge and country rock assimilation. The Layered Series at Duluth shows a cyclical progression of cumulates and features strong crystallisation differentiation interrupted by recharge and eruption events. The Wilder Lake Intrusion differs from the other intrusions in that cumulus ilmenite appears before augite and that olivine and augite compositions define an inverted cryptic variation. Lastly, the Bald Eagle Intrusion is considered unique in that Fe-Ti oxide did not appear as a cumulus phase despite crystallisation of cumulus augite.

6.2 Comparison Between the Sterkspruit Intrusion and other Mafic Complexes

Comparisons are made between the compositions of gabbro rocks from the Sterkspruit Intrusion and gabbroic suites from intrusions in Mpumalanga Province. These include the Stolzburg, Usushwana and Uitkomst Complexes, as well as smaller pre-Bushveld sills. A comparison is also made with the Insizwa Complex, a younger Karoo age intrusion.

A direct comparison of major element oxides in gabbros from both the Sterkspruit and Stolzburg bodies, initially shows them to be quite similar, with the exception of MgO and TiO_2. MgO has a higher range (5 - 11 %) in the Stolzburg Complex (Table 12) compared to the 3 - 5% in the Sterkspruit rocks, while TiO_2 is considerably lower (average 0.55%) compared to the 1.4% in Sterkspruit. However, differences in composition are seen on major element classification diagrams. It has already been shown that a distinct tholeiitic Fe-enrichment trend is displayed by the Sterkspruit Intrusion on an AFM diagram (Na_2O+K_2O - $FeO+Fe_2O_3$ - MgO) (Figure 10), which has no resemblance to the more ultramafic tendency of the Stolzburg Complex. Gabbro samples from Stolzburg have a wide scatter (not shown) on an AFM diagram, probably the result of the alteration that is prevalent in that Complex.

The wide scatter of the gabbro samples from Stolzburg are highlighted on an MgO-CaO-Al_2O_3 (MCA) ternary diagram (Figure 31) and a cation plot of (Fe^{2+}+Fe^{3+}+Ti)-Al-Mg (FAM) (Figure 32). On the MCA diagram, the gabbroic rocks plot between the Sterkspruit gabbro field and the field for the Barberton type komatiitic basalt. On the cation plot, the gabbroic rocks from Stolzburg fall in the komatiitic basalt, high-Mg tholeiite and calc-alkaline field. In contrast, the Sterkspruit Intrusion parental magma falls in the high-Fe tholeiitic basalt field.

Table 12 : Selected whole-rock geochemical data of gabbroic rocks from the Stolzburg, Usushwana and Uitkomst Complexes

	1 DH14B	2 DH22	3 DH85	4 Qtz. gab	5 Fer. Gab	6 Gabbro	7 Gabbro	8 Gabbro
wt %								
SiO_2	54.3	54.8	54.9	53.5	51.1	51.6	44.9	51.9
TiO_2	0.3	0.7	0.7	0.4	1.6	0.2	1.0	1.7
Al_2O_3	12.5	12.2	15.3	17.2	13.9	18.7	5.6	15.1
FeO	8.9	10.1	8.9	7.5	11.2	5.5	--	--
Fe_2O_3	0.0	0.0	0.0	1.4	3.9	1.2	22.9	11.8
MnO	0.07	0.1	0.1	--	--	--	0.2	0.2
MgO	11.1	8.7	5.9	4.3	3.4	5.4	11.1	6.1
CaO	11.5	8.7	7.9	10.3	9.1	12.3	7.6	6.5
Na_2O	2.7	3.1	5.7	2.7	3.1	2.4	2.2	4.9
K_2O	0.2	0.2	0.1	0.6	0.8	0.3	1.0	0.8
P_2O_5	0.03	0.06	0.05	--	--	--	0.1	0.2
ppm								
Rb	<10	<10	<10	--	--	--	47	25
Sr	237	116	142	--	--	--	111	364
Y	<10	16	10	--	--	--	24	21
Zr	24	54	30	--	--	--	110	108
Nb	<10	<10	<10	--	--	--	7	6
Co	38	47	38	--	--	--	331	34
Ni	251	87	56	--	--	--	5608	105
Cu	13	86	11	--	--	--	6391	239
Zn	27	52	20	--	--	--	72	76
Ba	207	79	34	--	--	--	--	--
V	204	254	277	--	--	--	--	--
Cr	623	434	50	--	--	--	--	--

1. DH14B - Altered gabbro, Stolzburg Complex (Rodel, 1993)
2. DH22 - Altered gabbro, Stolzburg Complex (Rodel, 1993)
3. DH85 - Altered gabbro, Stolzburg Complex (Rodel, 1993)
4. Qtz. Gab. - Av. quartz-gabbro from Usushwana Complex (Hammerbeck, 1982)
5. Fer. Gab. - Av. ferro-gabbro from Usushwana Complex (Hammerbeck, 1982)
6. Qtz. Gab. - Av. gabbro from Usushwana Complex (Hammerbeck, 1982)
7. G68/20 - Gabbro from Uitkomst Complex (Allen, 1990)
8. G43/12 - Gabbro from Uitkomst Complex (Allen, 1990)

Significant distinctions in trace element contents are a better reflection of the differences in the chemistry of these two intrusions. Incompatible elements such as Zr and Y are much lower in the gabbro layers from the Stolzburg Complex, while Cr, Ni and Sr contents are higher than in the gabbroic rocks from the Sterkspruit Intrusion. The REE from both intrusions display flat, chondrite normalised patterns, with no REE fractionation. The Stolzburg gabbros have average $(La/Tb)_N = 0.9$ (Rodel, 1993), similar to the Central and Upper Zones of Sterkspruit, but REE abundances are much lower, varying between 3 - 16x chondritic abundances (10 - 40x chondritic in the Sterkspruit body).

From the above descriptions, gabbroic rocks occurring in the upper divisions of the Stolzburg Complex (Anhaeusser, 1985; Rodel, 1993) are difficult to interpret and are not readily comparable with the Sterkspruit gabbros. The fundamental difference between the Sterkspruit and Stolzburg Intrusions is that the gabbros from the upper parts of the Stolzburg body are essentially late-stage differentiation products of an ultramafic layered complex, with a parental komatiitic composition (Anhaeusser, 1985), while the Sterkspruit gabbroic rocks were derived from an evolved tholeiitic magma.

The average quartz gabbro, ferrogabbro and gabbro from the Usushwana gabbroic suite are plotted on both the MCA and cation diagrams (Figures 31 and 32). In contrast to Stolzburg, these gabbroic rocks show a close affinity, on the MCA diagram, with the Sterkspruit Intrusion parental magma composition. On the cation plot, however, the quartz gabbro and gabbro fall in the calc-alkaline field while the ferrogabbro falls in the high-Fe tholeiite field. This calc-alkaline composition of the quartz gabbro and gabbro from Usushwana is a feature also shown on the AFM diagram (Figure 10). The majority of the chemical, Fe-enrichment trend, falls in the calc-alkaline field with only the ferrogabbro extending across the divide

into the field for tholeiitic series. The ferrogabbro compares most favourably with the Sterkspruit chill margin (parental magma) composition (Table 12), while the quartz gabbro and gabbro have much higher Al_2O_3 (18.7%) compared to the 13.6% for Sterkspruit.

Gabbroic rocks from the Uitkomst Complex are clearly different to those from the Sterkspruit Intrusion, in that they are alkaline in composition as compared to the subalkaline nature of the Sterkspruit gabbroic suite. Table 12, which lists typical gabbro compositions from the Uitkomst Complex, shows the high Na_20 and K_20 contents, and relatively low SiO_2 of these rocks. On both the MCA and cation diagrams (Figures 31 and 32), the samples from the Uitkomst Complex display a wide scatter of points and do not fall into any one field. This large variation in composition, which makes direct comparisons between the intrusions difficult, is confirmed in Table 12.

Sharpe (1981) studied the chemistry of pre-Bushveld sills which intruded into the Transvaal Supergroup in eastern Mpumalanga. He described these sills as gabbros, norites and pyroxenites, possessing tholeiitic affinities. The average MgO contents in these sills is 8.7%; higher than in the gabbros from the Sterkspruit Intrusion. On an AFM diagram, these sills lack the pronounced Fe-enrichment trend displayed by the Sterkspruit rocks. Average SiO_2 values are 53.0%, with Al_2O_3 and CaO contents of 12.9 and 8.0% respectively.

The Insizwa Complex is included to demonstrate the clear difference in composition between this Karoo age intrusion, associated with continental flood basalts (Lightfoot and Naldrett, 1984), and the much older Precambrian bodies. In general, on both the MCA and cation diagrams, the Insizwa gabbros and picrites plot towards the Mg apex indicating their high MgO contents. Lightfoot and Naldrett (1984) argued for a low-Mg

parentage for the marginal gabbro and picrite units, which were subsequently enriched in Mg due to the addition of cumulus olivine. These rocks are still, however, much more enriched in Mg than the cumulus Lower Zone gabbros from the Sterkspruit Intrusion which fall in the high-Mg tholeiitic field, as opposed to the komatiitic basalt field for the Insizwa rocks.

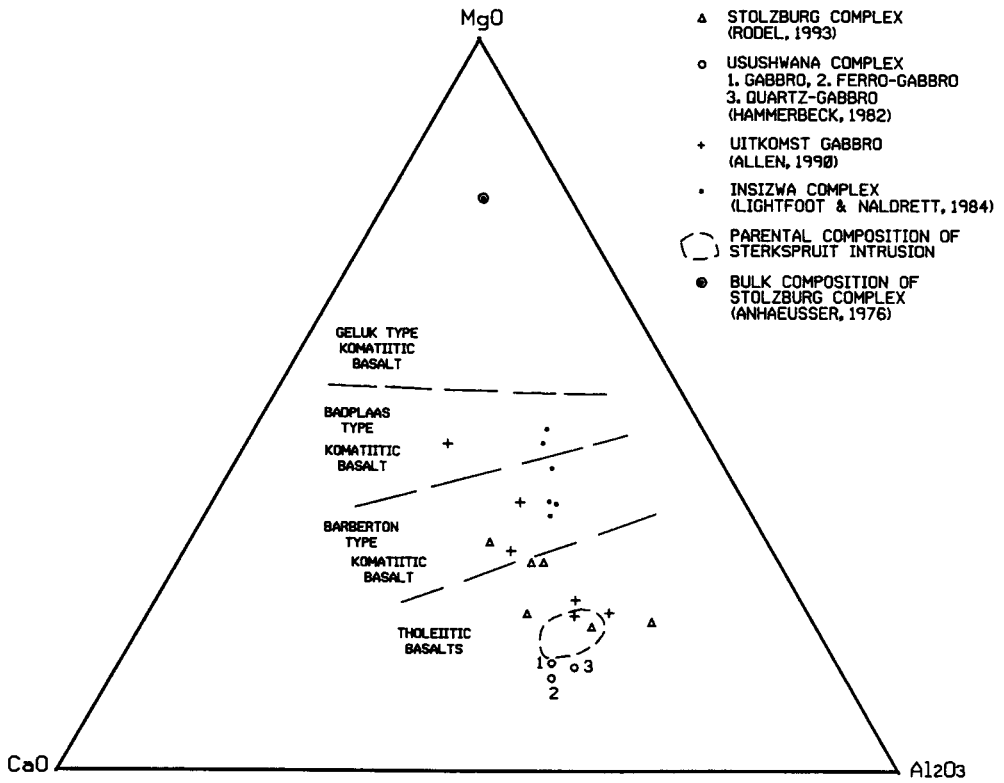


Figure 31 : **MgO - CaO - Al_2O_3 ternary diagram comparing gabbroic rocks from complexes on the Kaapvaal Craton with the Sterkspruit Intrusion gabbros. Data breaks separating komatiitic basalt fields after Viljoen *et al.* (1982).**

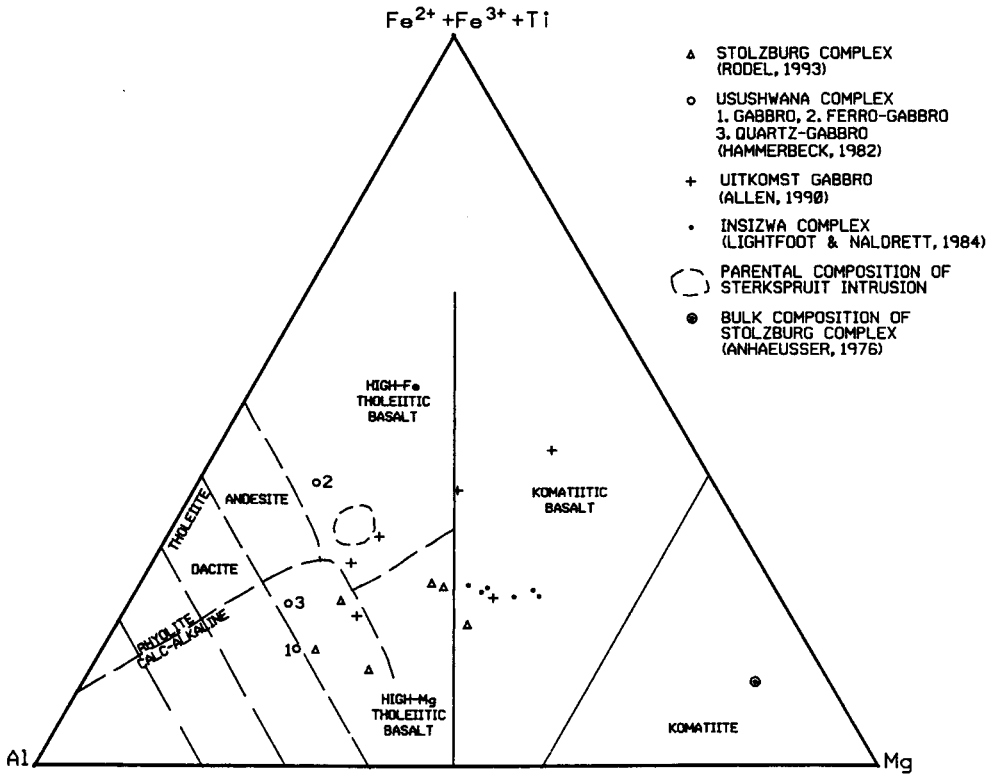


Figure 32 : **Cation ternary diagram (Fe^{2+}+Fe^{3+}+Ti - Al - Mg) comparing gabbroic rocks from complexes on the Kaapvaal Craton with the Sterkspruit Intrusion (after Jensen, 1976).**

CHAPTER SEVEN
COMPARISONS WITH VOLCANIC ROCKS FROM THE ONVERWACHT GROUP

7.1 Comparisons with Volcanic Rocks from the Nelshoogte Schist Belt

The geology of the Sterkspruit Intrusion has been described earlier in Chapter 3, as well as its setting within the southern part of the Nelshoogte Schist Belt. The composition of the surrounding komatiitic basalts and komatiites are listed in Table 13 and show no similarity to the gabbroic suite from the Sterkspruit Intrusion. The komatiitic basalts share some chemical affinities with both the Barberton- and Badplaas-type komatiitic basalts, as classified by Viljoen and Viljoen (1969c). MgO contents range from 10 to 17%, while SiO_2 and CaO contents average 50.8 and 12% respectively. The komatiites have average MgO values of 32%. These ultramafic lavas, as expected, have much lower incompatible trace element concentrations than the more evolved tholeiitic magma that gave rise to the gabbroic rocks of the Sterkspruit Intrusion.

The komatiitic basalts and komatiites are compared to the Sterkspruit Intrusion parental magma composition on an MCA diagram (Figure 33) and on a cation plot (Figure 34). These diagrams demonstrate the difference in composition between the Sterkspruit Intrusion and the effusive mafic-to-ultramafic rocks into which it was emplaced. The bulk composition of the Stolzburg Complex is also shown for comparison. The close affinity between the peridotitic parental magma composition of this Complex and the komatiitic rocks is indicated.

Table 13 : Selected whole-rock geochemical data of komatiitic basalts and komatiites from the Nelshoogte Schist Belt

Sample	SB 7	SB 10	SB 36	SB 37	SK 6	SK 9
	komatiitic basalt				komatiite	
wt %						
SiO_2	51.6	48.9	51.5	51.1	40.6	40.4
TiO_2	0.4	0.6	0.4	0.6	0.2	0.2
Al_2O_3	3.1	5.1	9.6	11.9	2.3	2.3
FeO	6.9	12.5	7.9	9.2	9.4	9.7
Fe_2O_3	1.4	2.5	1.6	1.9	1.9	1.9
MnO	0.2	0.2	0.1	0.1	0.3	0.2
MgO	17.6	13.8	13.1	10.4	32.2	32.3
CaO	15.7	12.2	10.9	9.1	1.2	0.9
Na_2O	0.08	0.29	1.3	1.8	0	0
K_2O	0.05	0.16	0.35	0.07	0	0
P_2O_5	0.03	0.05	0.05	0.07	0.03	0.03
ppm						
Rb	12	18	14	10	3	2
Sr	5	11	23	46	1	1
Y	6	11	15	24	4	5
Zr	17	25	36	57	12	11
Nb	4	3	3	5	3	4
Co	54	76	45	48	130	137
Ni	386	317	341	184	2762	2613
Cu	74	208	5	9	86	154
Zn	121	71	94	95	274	188
Ba	8	21	47	6	--	--
V	148	241	222	295	76	78
Cr	3097	60	1283	869	2	1002

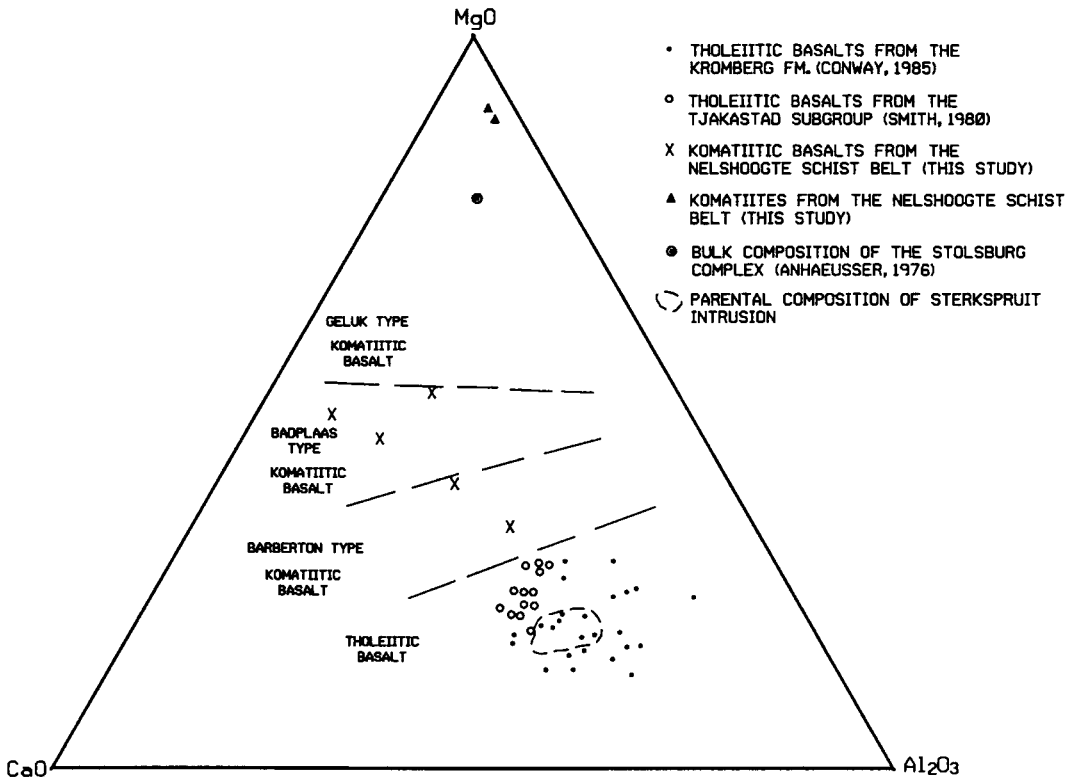


Figure 33 : **MgO - CaO - Al_2O_3 ternary diagram comparing volcanic rocks from the Onverwacht Group with gabbroic rocks from the Sterkspruit Intrusion. Data breaks separating komatiitic basalt fields after Viljoen *et al.* (1982).**

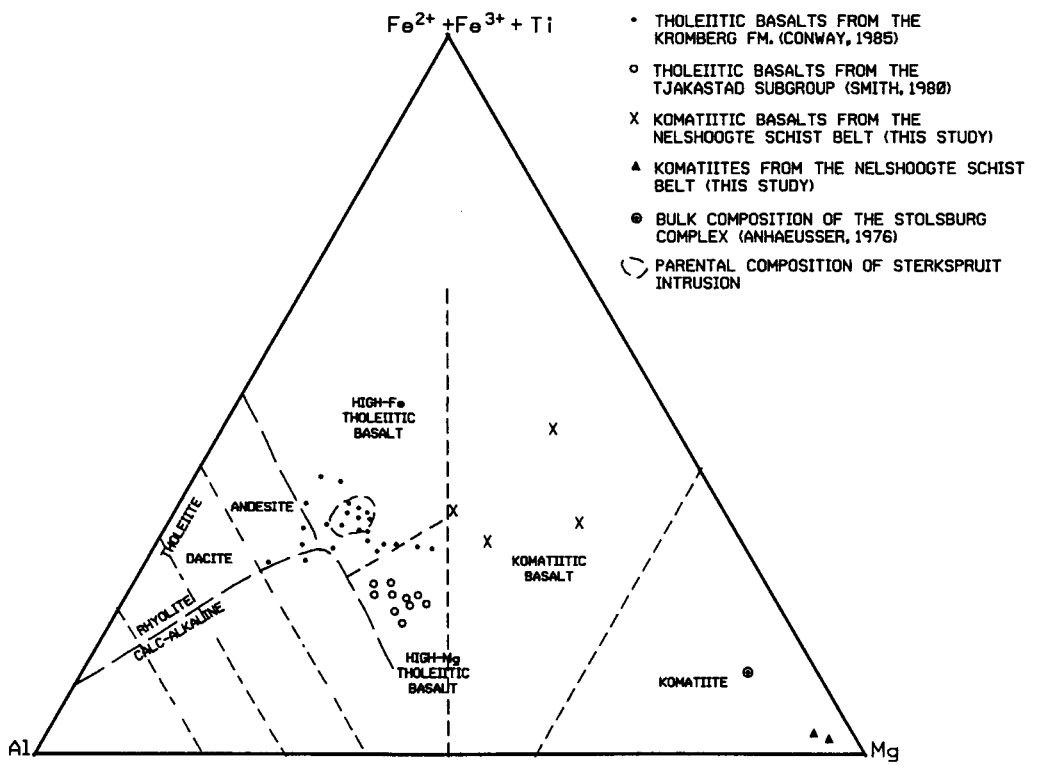


Figure 34 : **Cation ternary diagram (Fe^{2+}+Fe^{3+}+Ti - Al - Mg) comparing volcanic rocks from the Onverwacht Group with gabbroic rocks from the Sterkspruit Intrusion (after Jensen, 1976).**

7.2 Comparisons with Tholeiitic Basalts from the Onverwacht Group

It has been established that the gabbroic rocks from the Sterkspruit Intrusion were derived from a magma which was tholeiitic in composition. It is therefore pertinent that comparisons be made with tholeiitic basalts from the Onverwacht Group volcanics. As has been mentioned in the description of the regional geology of the Barberton Mountain Land (Chapter 2), tholeiitic basalts are more common in the Upper Mafic-to-Felsic Unit (Geluk Subgroup) of the Onverwacht sequence than in the Lower Ultramafic Unit (Tjakastad Subgroup). Comparisons will be made with tholeiites from both these subgroups, the average compositions of which are listed in Table 14.

Smith (1980) studied tholeiitic basalts from the Tjakastad Subgroup and identified three types, which he believed to be similar in composition to boninites, viz.:

1) a low-Ti basalt;
2) a high-Ti basalt; and
3) a high-Mg basalt.

According to Smith (1980) none of these basalt types are related to each other, or to low-Mg mafic komatiitic rocks, by crystal fractionation or accumulation processes.

The tholeiites from the Kromberg and Hooggenoeg Formations in the Geluk Subgroup show some similarities with tholeiites from lower in the sequence, but those from the Kromberg Formation, although mineralogically similar to those from the Hooggenoeg Formation, have significant chemical differences (Viljoen and Viljoen, 1969d). These authors noted that some of the Kromberg Formation rocks contain more plagioclase than normal and possibly represent basaltic andesites.

Table 14 : Average whole-rock geochemical data of tholeiitic and andesitic basalts from the Onverwacht Group

	Tholeiite	Andesite	Low-Ti Tholeiite	High-Ti Tholeiite
	1	2	3	4
wt %				
SiO_2	51.5	58.1	51.6	51.1
TiO_2	1.4	1.5	0.6	1.4
Al_2O_3	14.2	13.1	15.1	14.0
FeO	9.6	7.8	8.2	11.4
Fe_2O_3	3.0	2.4	1.6	2.3
MnO	--	--	0.2	0.2
MgO	5.5	3.8	8.7	7.0
CaO	7.2	5.5	10.8	9.8
Na_2O	2.6	3.6	2.4	2.2
K_2O	0.8	0.3	0.6	0.5
P_2O_5	0.2	0.4	--	--
ppm				
Rb	15	4	22	10
Sr	142	80	148	118
Y	30	54	16	34
Zr	100	224	40	106
Nb	4	11	1	4
Co	--	--	--	--
Ni	84	24	176	99
Cu	--	--	--	--
Zn	--	--	--	--
Ba	--	--	--	--
V	--	--	--	--
Cr	87	10	--	--
Mg#	50	46	51	38

1 : Average tholeiitic basalt - Kromberg Formation (Conway, 1985)

2 : Average andesitic basalt - Kromberg Formation (Conway, 1985)

3 : Average low-Ti tholeiitic basalt - Tjakastad Subgroup (Smith, 1980)

4 : Average high-Ti tholeiitic basalt - Tjakastad Subgroup (Smith, 1980)

The Kromberg Formation conformably overlies the Hooggenoeg Formation and is developed predominantly in the southern portion of the Mountain Land. The type section is located along the Komati River gorge on the west limb of the Kromberg syncline (Figure 1). A geochemical study of volcanic lavas from this section was carried out by Conway (1985). These lavas were found to range in composition from komatiitic basalt to tholeiitic basalt to andesitic basalt. Whole rock geochemical analyses from this area have been used to compare the compositions of tholeiitic basalts with gabbroic rocks studied in the Sterkspruit Intrusion. Average geochemical analyses from these tholeiites and andesites are listed in Table 14, while a more complete list of analyses is included in Appendix A, Table A3.

The tholeiitic basalts from the Kromberg Formation have MgO contents ranging from 2.7 to 9.3%, averaging 5.5%. This compares with the 4.8% from the Sterkspruit Intrusion chill margin composition. The andesitic basalts average 3.8% MgO. The SiO_2 content in the tholeiitic basalts ranges from 45.5 to 60.0%, averaging 51.5%, while the andesitic basalts average 58%. The tholeiites compare favourably with the 52.5% SiO_2 in the Sterkspruit Intrusion chill margin. TiO_2 contents average 1.3% in both tholeiitic basalts and the Sterkspruit Intrusion chill margin, and 1.5% in the andesitic basalts. The lower MgO, and higher SiO_2 and TiO_2 contents in the andesitic basalts are also a feature of the Quartz Diorite from the Sterkspruit Intrusion. The Ca/Al ratio in the tholeiitic basalts averages 0.46 compared to 0.48 for the Sterkspruit Intrusion chill margin.

Trace element data from the Kromberg Formation are also similar to the Sterkspruit Intrusion. Unusually low Sr values in tholeiitic basalts range from 36 to 507 ppm, averaging 142 ppm, compared to 104 ppm from the chill margin of the Sterkspruit Intrusion. Zr contents average 100 ppm for tholeiites and 224 ppm for andesites compared to 102 ppm for the chill

margin and 161 ppm for the Quartz Diorite from the Sterkspruit Intrusion. Ti/Zr ratios from the tholeiites averages 82 compared to the 79 for the Sterkspruit Intrusion. The average Ti/Zr ratio of the andesites is 43 corresponding to the 53 from the Quartz Diorite from Sterkspruit.

The similarities between the Kromberg Formation tholeiites and the parental (liquid) composition of the Sterkspruit Intrusion can be shown graphically. On an MCA (MgO-CaO-Al_2O_3) ternary classification diagram (Figure 33), the data from the Sterkspruit Intrusion is plotted along with tholeiites from the Kromberg Formation (Conway, 1985) and tholeiites from the Tjakastad Subgroup (Smith, 1980). The bulk composition of the Stolzburg Complex is also shown for comparison. This diagram clearly shows the close affinity between the liquid composition (Upper Zone and chill margin) of the Sterkspruit Intrusion and the tholeiites from the Kromberg Formation. The tholeiites from the Tjakastad Subgroup have lower Al_2O_3 and higher MgO contents than the tholeiites from higher in the Onverwacht sequence, and plot in the high-Mg tholeiite field.

The cation ternary diagram (Fe^{2+}+Fe^{3+}+Ti)-Al-Mg (Figure 34), also demonstrates the very close correlation between the tholeiites from the Kromberg Formation and the parental composition of the Sterkspruit Intrusion. This diagram also shows the disparity between different tholeiite types from the Onverwacht Group.

An examination of the REE in tholeiitic basalts from the Kromberg Formation by Glikson and Jahn (1985), showed them to have similar flat patterns to some gabbroic rocks of the Sterkspruit Intrusion. As previously mentioned, the Marginal Zone and Upper Zone gabbroic rocks display flat to very slightly LREE-enriched patterns at about 10 to 20x chondritic abundances. The REE from the Kromberg Formation, although reported by Glikson and Jahn (1985) to have suffered alteration effects, likewise

have abundances of between 12 and 20x chondritic. These authors also showed that the composition of the tholeiites from the Geluk Subgroup differs from those of the tholeiites from the Lower Ultramafic Unit (Tjakastad Subgroup).

In addition, Glikson and Jahn (1985) reported magnesium numbers (Mg#) to be lower (49 - 54) in the Kromberg Formation tholeiites compared to values of 67 in the underlying Hooggenoeg Formation and 56 - 61 in the Komati Formation. These low values in the Kromberg Formation were confirmed by Conway (1985) who reported average Mg# of 50 for tholeiitic basalts and 46 for andesitic basalts. The low Mg# values in the Kromberg Formation correspond closely with the values from the Sterkspruit Intrusion chill margin and calculated bulk composition. Here values of 42 and 48, respectively, were calculated.

Major oxide and trace element variations in both the gabbroic rocks from the Sterkspruit Intrusion and the tholeiites from the Onverwacht Group, are depicted on bivariate diagrams (Figure 35). Plots with MgO and Zr on the x-axis, demonstrate the geochemical overlap between the gabbroic suite and the tholeiitic basalts from the Kromberg Formation. The andesitic basalts from this Formation consistently plot on the more evolved end of the tholeiitic trend, and correspond to the position of the Quartz Diorite from the Sterkspruit Intrusion. The tholeiites from the Tjakastad Subgroup (Smith, 1980), fall in a separate field at the high-Mg, (low-Zr) end of the individual trends, and show no affinity with the parental magma composition of the Sterkspruit Intrusion. Even though these tholeiites differ chemically, they all have similar tectonic settings to the Sterkspruit Intrusion. According to the Pearce and Cann (1973) classification of Ti-Zr-Y, they fall into the oceanic basalt field assigned to MORB, island-arc tholeiites and calc-alkaline basalts.

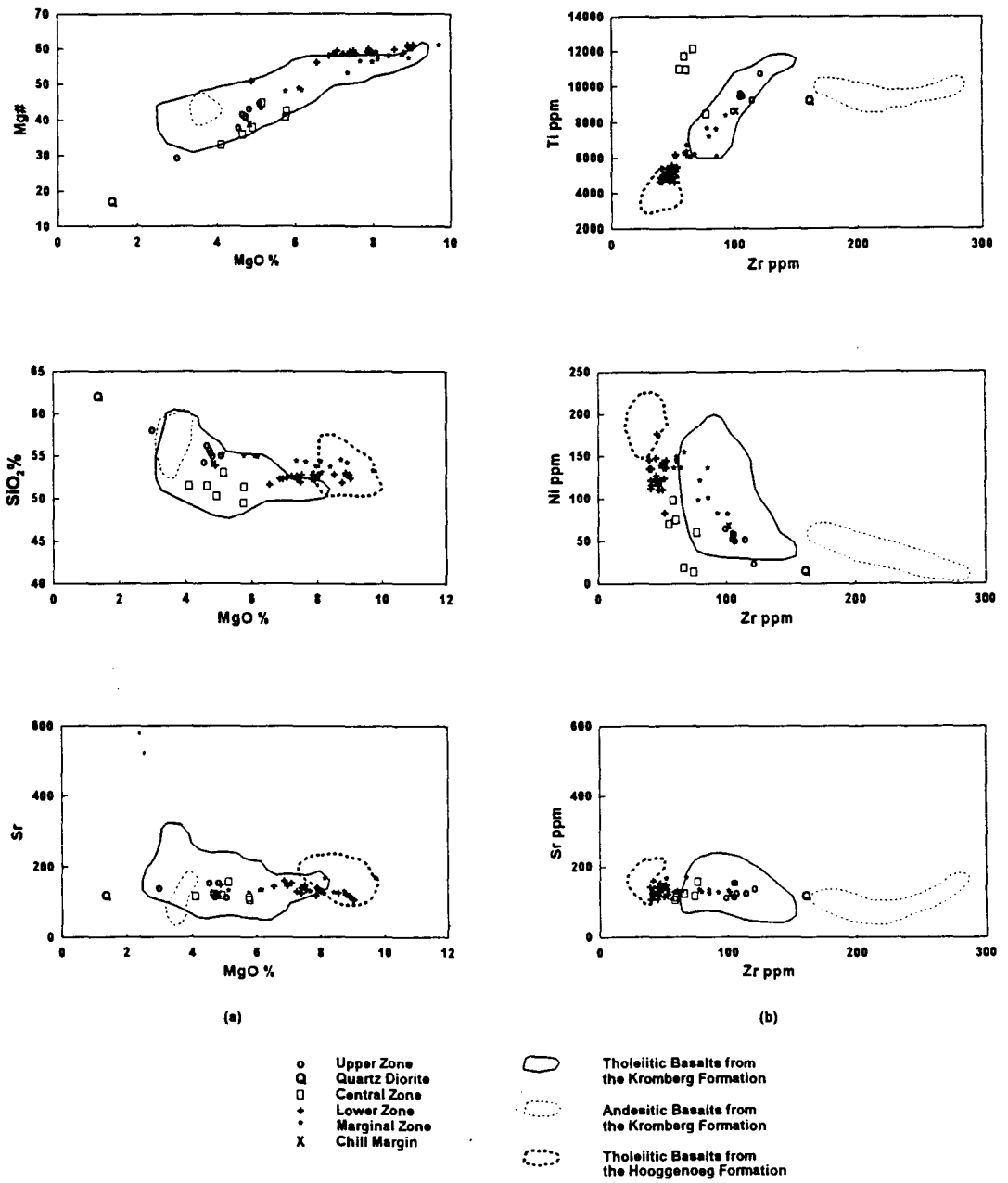


Figure 35: Bivariate diagrams of major oxides and trace elements plotted against (a) MgO and (b) Zr, comparing gabbros from the Sterkspruit Intrusion with tholeiitic basalts from the Onverwacht Group.

CHAPTER EIGHT
DISCUSSION

In the previous chapters the geology and petrography of the Sterkspruit Intrusion were described, and the intrusion classified geochemically. These descriptions and classifications have led to a characterisation of the intrusion and have shown the body to be distinct from most intrusive igneous rocks in the Barberton Mountain Land.

Layered ultramafic complexes are widespread in the Onverwacht Group, particularly the lower Tjakastad Subgroup, of the Archaean Barberton greenstone sequence. These complexes, of which the Stolzburg Complex is a typical example, comprise dunites, orthopyroxenites and harzburgites in their lower portions, with subordinate websterites, gabbros and anorthosites occurring higher in the body. In general, they are best developed along the north-western flank of the greenstone belt. The bulk composition of most of these complexes is peridotitic, very similar to the composition of the komatiitic extrusives found in the Onverwacht Group (Viljoen and Viljoen, 1970; Anhaeusser, 1985). The layered intrusions are thought to be comagmatic with these ultramafic volcanics. Gabbroic rocks, located in the upper portions of some complexes, are perceived to be fractionated residual liquids.

In contrast, the Sterkspruit Intrusion contains no ultramafic component, being comprised entirely of gabbroic and dioritic rock types. This feature is considered unusual because of its emplacement into mafic-to-ultramafic lavas of the Lower Ultramafic Unit of the Onverwacht Group. In addition, it lies in very close proximity to the Stolzburg Complex, which has a peridotitic bulk composition (Anhaeusser, 1985), in places

separated from this body by less than 100m. Because of these differences, a number of options for the emplacement of the Sterkspruit magma body can be considered, viz.:

1) the intrusion represents a younger, Proterozoic dyke or sill, which post-dated the granite plutonic phase and regional deformation;

2) it was emplaced as a hypabyssal equivalent of associated komatiitic and tholeiitic basalts;

3) it was emplaced as a high level intrusion into older greenstone volcanics, and is unrelated to these volcanics; or

4) the gabbroic body could represent the centre of a very thick komatiitic basalt lava flow.

The following discussion evaluates each of these possible models in the light of the geological and geochemical evidence.

With reference to the attitude of the body (dyke-like or sill-like), several features of the Sterkspruit Intrusion suggest that it was emplaced as a sill. Firstly, steep, northerly dipping, felsic stringers and rhythmic layering in the Lower Zone are construed as density-sorted layers formed by a combination of gravity settling of pyroxene and plagioclase cumulates, in-situ crystallisation and magmatic flow. Magmatic layers could also have been produced parallel to the margins of a dyke, or within its interior. The Binneringie Dyke in Western Australia shows vertical magmatic layering near to both margins, which McCall and Peers (1971) assumed to reflect the attitude of the main dyke. The core of this dyke is mostly massive and coarsely crystallised. In contrast, the Vandfaldsdalen Macrodyke in the Skaergaard region contains a central series of differentiated and subhorizontally layered gabbros in the interior of the dyke (White *et al.*,

1989). Neither the layering model for the Binneringie Dyke nor the Vandfaldsdalen Macrodyke, are consistent with the Sterkspruit Intrusion. In the first instance, layering would be expected along both margins, but in the Sterkspruit body, layering only occurs in the Lower Zone. In the second case, if layering formed horizontally in the magma chamber, then an explanation for its rotation to a subvertical attitude would be needed.

The second feature pointing towards a sill-like origin is the attitude of the layering, internal shear structures, veining and the margins of the intrusion, which are all subparallel to the regional strike direction in the southern portion of the Nelshoogte Schist Belt. The concordant attitude of this intrusion corresponds more to a sill than a dyke. In addition, the Sterkspruit Intrusion is subparallel to the Stolzburg Complex, which has a younging (facing) direction to the south.

Thirdly, the Sterkspruit Intrusion contains at least four gabbroic rock types which form a heterogeneous zonation across the body and also display an interpreted younging direction to the south. The Marginal and Lower Zones, forming the northern portion, consist of cumulate textured and layered gabbros. The Upper Zone in the south consists of a subophitic, quartz-rich gabbro with characteristic coarse, acicular, green amphiboles. The Central Zone gabbros are Ti-rich and could either be a separate magma pulse, or crystallised Ti-rich minerals late in the fractionation history of the cooling magma. A late stage differentiate, termed the Quartz Diorite zone, occurs between the Central and Upper Zones, approximately two thirds of the way up the intrusion. In a dyke-like intrusion, a certain amount of petrological homogeneity, from both borders towards the centre, would be expected. This is not the case across the Sterkspruit body.

Lastly, the geochemical variation across the body points to a sill-like magma chamber that was filled during a single event, or at the most, two intrusive pulses. The major oxides and trace elements depict a trend of crystallisation from the base of the chamber upwards and from the roof downwards, converging at the Quartz Diorite layer. The Lower Zone contains high Mg and Ni contents, and low concentrations of incompatible elements, typical of a cumulate-formed gabbro. The cumulate textures are only located within the northern part of the body, thus supporting the contention that this margin of the intrusion forms the base of a sill.

The factors mentioned above argue strongly for a sill-like intrusive origin. If this is the case, then the steeply dipping attitude of rhythmic layers in the Lower Zone need to be explained. From the evidence above, the northern margin of the Sterkspruit Intrusion forms the base to this body. This is compatible with the Stolzburg Complex which also has its base in the north. It is therefore postulated that the Sterkspruit Intrusion was emplaced into the komatiitic lavas prior to the regional deformation that affected the Barberton sequence following the granite intrusion phase. This body then underwent regional deformation along with the rocks forming the Nelshoogte Schist Belt and was rotated to a subvertical attitude. The present erosional surface, therefore, represents a cross section across the width of the body.

Further evidence for an older, Archaean age for the Sterkspruit Intrusion comes from the deuterically altered and metamorphosed mineral assemblages, which match those observed in the surrounding Onverwacht lavas and the Stolzburg Complex. The regional greenschist facies metamorphism that the Lower Zone gabbros have undergone is shown by the products of saussuritisation, fibrous uralite, actinolite/tremolite, epidote, zoisite, chlorite and albite. Higher up, the

Upper Zone quartz gabbros are comprised of acicular grains of green pleochroic amphibole, quartz and epidotised albitic plagioclase.

It has been established that extrusive equivalents to intrusive layered complexes are common. As examples from the Lower Onverwacht Group, Anhaeusser (1985) and Rodel (1993) correlated the Stolzburg Complex with the surrounding komatiitic lavas. Viljoen and Viljoen (1970) showed similarities between their Geluk-type komatiitic basalts and the bulk composition of the Canal differentiated body. These authors also found an association between their Badplaas-type komatiitic basalts and the mafic portions of the Ship Hill intrusion. By analogy, the Sterkspruit Intrusion parental magma composition (taken from the chill margin) should also show similarities with extrusive rocks.

The evolved quartz-normative tholeiitic magma composition from Sterkspruit bears no resemblance to the mafic-to-ultramafic lavas of the Nelshoogte Schist Belt. Therefore, the second option for the origin of the intrusion, mentioned above, is dispelled. This leaves option three above as being the most feasible, whereby the magma intruded into older greenstone volcanics of the Tjakastad Subgroup (Lower Onverwacht Group) prior to the completion of the Onverwacht Group volcanism. The affinity between the Sterkspruit magma composition and evolved tholeiitic basalt from the Geluk Subgroup (Upper Onverwacht Group), points to either a common tholeiitic magma source or a hypabyssal intrusion acting as a feeder to the extrusive rocks.

Possibility four above, follows ideas proposed by Cattell and Taylor (1990) for some gabbroic suites in Precambrian terrains. These authors described the lower parts of basaltic komatiitic flows having cumulate textures whilst the upper, spinifex-textured zones represent crystallisation downward from the flow tops. They also described thicker flows as having

a central gabbroic portion with lower MgO contents, in the range of 5 - 8%. This setting for the Sterkspruit Intrusion is rejected due to the great width of the intrusion relative to the interlayered komatiitic basalts and komatiite flows, and also because of the clear chill margin observed along the northern contact of the body.

The Sterkspruit Intrusion has been compared with the gabbroic portions of some layered complexes in eastern Mpumalanga Province. Similarities have also been found with tholeiitic intrusions from other parts of the world. The geological zonation and geochemical variation across the Sterkspruit body are consistent with those observed in other complexes such as the Skaergaard Intrusion, Mt Kilkenny sill and Usushwana Complex. The Sterkspruit Intrusion is, however, unique in its setting in the Lower Onverwacht Group when compared with the layered ultramafic complexes. The parental magma to the Sterkspruit gabbroic suite has an evolved, quartz normative, tholeiitic composition. In addition, quartz forms a high proportion of the mineral assemblage throughout the gabbro and diorite, a feature not commonly observed in mafic rocks from the Barberton greenstone sequence.

Bearing in mind all the arguments for the origin of the Sterkspruit Intrusion, the writers preferred model suggests that the magma was emplaced as a sill into the mafic-to-ultramafic lavas of the Tjakastad Subgroup. The subvertical layering in the Lower Zone and the geochemical variation herein recorded constrains the age of the intrusion to pre-regional deformation of the Nelshoogte Schist Belt, brought about by the granite plutonic phase at about 3.2Ga. In support of this age interpretation, the Sterkspruit gabbros bear little resemblance to the compositions of gabbroic suites from younger intrusions such as Usushwana, Uitkomst and pre-Bushveld sills. The gabbros have, however, geochemical affinities with tholeiitic and andesitic basalts from

the Kromberg Formation of the Geluk Subgroup. By analogy, the intrusion may have represented a high level magma chamber that acted as a feeder zone for tholeiitic lavas developed higher up in the greenstone sequence.

Possible problems relating the Sterkspruit Intrusion to tholeiites from the Kromberg Formation include the large distance (~40 km) between the intrusion and the type section of this Formation further to the east. However, it is feasible to assume that similar volcanic sequences may have existed at higher stratigraphic levels in the Nelshoogte area and that these higher units were removed by erosion or by structural influences.

The isotopic age of the Sterkspruit Intrusion needs to be determined to quantify its relationship with associated tholeiitic volcanics and to confirm the findings outlined above. This may present problems due to the high degree of alteration in the rocks and the superimposed greenschist facies metamorphism, as well as the scarcity of zircons or other mineral assemblages useful in geochronological studies.

CHAPTER NINE
CONCLUSIONS

1. The Sterkspruit Intrusion, which comprises mostly gabbroic rocks of subalkaline, tholeiitic affinity, intruded komatiitic basalts and komatiites of the Tjakastad Subgroup of the Lower Onverwacht Group in the Barberton greenstone belt. It is argued that this sill-like intrusion is of early Archaean age and, along with the surrounding Nelshoogte Schist Belt, was intruded by granitic rocks forming the Nelshoogte and Kaap Valley Plutons. These granitic plutons were emplaced 3.2Ga ago (Oosthuyzen, 1970; Kamo and Davis, 1991).

2. The length of the intrusion is approximately 8 km and averages 500 m in width. It has a concordant relationship with the surrounding mafic and ultramafic volcanic rocks, further exemplified by subparallel rhythmic layering, shear foliation and thin dilational veins. The rhythmic layering, along with felsic stringers, are well developed in parts of the Lower Zone and dip steeply to the north.

3. The Sterkspruit Intrusion has been subdivided into a Marginal Zone containing a chill margin, a Lower Zone comprising cumulate plagioclase and pyroxene, a Central Zone which is characterised by a high-Ti ferrogabbro, and an Upper Zone made up of a quartz-rich gabbro. A Quartz Diorite unit, interpreted to be a late differentiate or residual melt, was identified along Traverse 1 between the Central and Upper Zones. Compositional variations in the gabbroic suite were found to be consistent with fractionation of clinopyroxene, orthopyroxene and plagioclase.

4. The major mineral phases observed within the gabbroic rocks are albitic plagioclase, pyroxene, actinolite/hornblende, quartz, chlorite, epidote and leucoxene. Alteration, in the form of saussuritisation and albitisation of plagioclase and uralitisation of pyroxene, is especially prevalent in the Marginal and Lower Zones. Abundant carbonate alteration is found in the Quartz Diorite. This alteration can be ascribed to early sea-floor metamorphism which was subsequently superimposed by regional, burial metamorphism, resulting in the present greenschist metamorphic grade.

5. A fine-grained chill margin to the gabbro was observed at two localities on the northern contact of the body and provided what is considered to be a parental magma composition. This magma is quite evolved with relatively high SiO_2 (52.5 %), low MgO (4.8 %) and an Mg# of 42. A quartz-normative magma is indicated by the abundance of primary and interstitial quartz found throughout the gabbro body.

6. Major and trace element variations with height across the intrusion are typical of a layered sill with cumulate mineral phases forming in the lower portions of the body. MgO increases and incompatible trace element contents decrease upwards to the top of the cumulate Lower Zone, followed by a decrease in MgO and an increase in incompatible trace elements towards the Quartz Diorite at the centre of the intrusion. This trend of decreasing MgO and increasing incompatible trace elements is also observed from the roof of the chamber (Upper Zone) downwards towards the Quartz Diorite.

7. The Quartz Diorite, comprising abundant quartz, plagioclase, carbonate, chlorite and epidote, has very high SiO_2 (60.6%) and low MgO (1.4%). This unit could have been the residue which formed at the interface between advancing crystallisation fronts from the base and roof of the cooling magma chamber.

8. The Sterkspruit Intrusion has an interpreted younging direction from north to south, which corresponds to that observed in the adjacent Stolzburg Complex. This has implications for the regional structure of the Nelshoogte Schist Belt.

9. The Sterkspruit Intrusion, with its evolved, quartz-normative, tholeiitic composition, is considered unique in the lower or Tjakastad succession of the Onverwacht Group of the Barberton Sequence when compared to the more usual ultramafic layered complexes. This gabbroic intrusion has no chemical similarities with the mafic-to-ultramafic volcanic rocks into which it was intruded, nor with the komatiitic bulk composition of the Stolzburg Complex, which is located adjacent and subparallel to the Sterkspruit body.

10. The gabbroic composition of the Sterkspruit Intrusion has chemical similarities with tholeiitic and andesitic basalts from the Kromberg Formation of the Geluk Subgroup, as well as with some high-Ti tholeiites from the Hooggenoeg Formation. This intrusion could, therefore, have originated as a subvolcanic magma chamber and now represents a hypabyssal equivalent of associated tholeiitic basalts found stratigraphically higher up in the Onverwacht Group.

11. Incompatible trace element patterns plotted on multi-element diagrams are consistent with the Sterkspruit Intrusion having an oceanic island association. Discrimination diagrams suggest that the gabbroic suite displays an affiliation with plate margin, ocean-floor basalts.

12. The determination of isotope signatures and the use of a dating technique for gabbroic rocks from the Sterkspruit Intrusion are deemed necessary to equivocally compare this body with volcanic rocks from the surrounding Onverwacht Group and to resolve the age of emplacement of the Intrusion.

13. The Sterkspruit Intrusion and southern portion of the Nelshoogte Schist Belt were intruded by a set of northwest trending diabase dykes, termed the Sterkspruit Mafic Dyke Swarm. These dykes which are older than the Godwan Formation and Transvaal Supergroup, show strong intra-dyke chemical variation and can be subdivided into four groups. The dykes have a calc-alkaline affinity.

LIST OF REFERENCES

Allen, I.V.L. (1990). The geology and geochemistry of the Uitkomst layered complex, Eastern Transvaal. Unpubl. Honours Thesis. University of the Witwatersrand, Johannesburg, 51pp.

Anhaeusser, C.R. (1971). Cyclic volcanicity and sedimentation in the evolutionary development of Archaean greenstone belts of shield areas. Geol. Soc. Aust., Spec. Publ., 3, 57-70.

Anhaeusser, C.R. (1973). The Stolzburg differentiated ultramafic igneous complex, Barberton Mountain Land. Abstract, Fifteenth Congr. Geol. Soc. S. Afr., Bloemfontein, 69-72.

Anhaeusser, C.R. (1974). The geology of the Stolzburg layered ultramafic complex, Barberton Mountain Land, South Africa. Abstract, International conference on the "Geology and Geochemistry of the Oldest Precambrian Rocks", Redwood Falls, Minnesota, USA. 5pp. Plus: Geological map of a portion of the Nelshoogte Schist Belt and the Stolzburg layered ultramafic complex, Barberton Mountain Land, by C.R. Anhaeusser (1971).

Anhaeusser, C.R. (1975). The geological evolution of the primitive earth. Evidence from the Barberton Mountain Land. Inform. Circ. Econ. Geol. Res. Unit., Univ. Witwatersrand, Johannesburg, 98, 22pp.

Anhaeusser, C.R. (1976). The nature of chrysotile asbestos occurrences in Southern Africa: A review. Econ. Geol., 71, 96-116.

Anhaeusser, C.R. (1978). The geology and geochemistry of the Muldersdrift Ultramafic Complex and surrounding area, Krugersdorp District. Trans. Geol. Soc. S. Afr., 81, 193-203.

Anhaeusser, C.R. (1979). Rodingite occurrences in some Archaean ultramafic complexes in the Barberton Mountain Land, South Africa. Precambrian Res., 8, 49-76.

Anhaeusser, C.R. (1983). A contribution to the Archaean geology of southern Africa with particular reference to aspects involving metallogeny, granite-greenstone belt development and crustal evolution. DSc thesis (unpubl.), Univ. Witwatersrand, Johannesburg (2 volumes).

Anhaeusser, C.R. (1985). Archaean layered complexes in the Barberton Mountain Land, South Africa, 281-301. In: Ayres, L.D., Thurston, P.C., Card, K.D., and Weber, W., (eds.), Evolution of Archean Supracrustal Sequences. Geol. Assoc. Canada., Spec. Pap., 28, 380pp.

Anhaeusser, C.R. (1986). The geological setting of chrysotile asbestos occurrences in southern Africa, 359-376. In: Anhaeusser, C.R. and Maske, S. (eds.), Mineral Deposits of Southern Africa. I, Geol. Soc. S. Afr., Johannesburg.

Anhaeusser, C.R. and Viljoen, M.J. (1965). The base of the Swaziland System in the Barberton-Noordkaap-Louw's Creek area, Barberton Mountain Land. Inform. Circ. Econ. Geol. Res. Unit., Univ. Witwatersrand, Johannesburg, 25, 35pp.

Anhaeusser, C.R. and Robb, L.J (1981). Magmatic cycles and the evolution of the Archaean granitic crust in the Eastern Transvaal and Swaziland. Spec. Publ. Geol. Soc. Australia, 7, 457-467.

Anhaeusser, C.R., Mason, R., Viljoen, M.J., and Viljoen, R.P. (1969). A reappraisal of some aspects of Precambrian shield geology. Bull. Geol. Soc. Amer., 80, 2175-2200.

Arndt, N.T. and Nisbet, E.G. (1982). What is a komatiite?. In: Arndt, N.T. and Nisbet, E.G. (eds.), Komatiites. George Allen and Unwin, London, 526pp.

Barrie, C.T., Gorton, M.P., Naldrett, A.J. and Hart, T.R. (1991). Geochemical constraints on the petrogenesis of the Kamiskotia gabbroic complex and related basalts, western Abitibi Subprovince, Ontario, Canada. Precam. Res., 50, 173-199.

Bates, R.L. and Jackson, J.A. (1980). Glossary of Geology (2nd ed). American Geological Institute, 751pp.

Beswick, A.E (1982). Some geochemical aspects of alteration and genetic relations in komatiitic suites. In: Arndt, N.T. and Nisbet, E.G. (eds.), Komatiites. George Allen and Unwin, London, 526pp.

Bowes, D.R. (Ed.) (1989). The Encyclopedia of Igneous and Metamorphic Petrology. Van Nostrand Reinhold. New York, 666pp.

Byerly, G.R., Kroner, A., Lowe, D.R., Todt, W. and Walsh, M.M. (1996). Prolonged magmatism and time constraints for sediment deposition in the early Archaean Barberton greenstone belt: Evidence from the Upper Onverwacht and Fig Tree Groups. Precambrian Res., 78, 125-138.

Cattell, A.C. and Taylor, R.N. (1990). Archaean basic magmas, 11-39. In: Hall, R.P. and Hughes, D.J. (eds.), Early Precambrian Basic Magmatism. Blackie, Glasgow and London, 486pp.

Cloete, M. (1990). The metamorphic history of the Komati Formation (Barberton, South Africa) : a P-T-t path and its tectonic implications. In: Glover, J.E. and Ho, S.E. (compilers:). The Third International Archaean Symposium, Perth, 1990. Extended Abstracts Volume. Geoconferences (W.A) Inc., Perth, 121-123.

Cloete, M. (1991). An overview of metamorphism in the Barberton greenstone belt., 84-98. In: Ashwal, L.D. (ed.), Two Cratons and an Orogen - Excursion Guidebook and Review Articles. IGCP Project 280, Dept. of Geology, Univ. Witwatersrand, Johannesburg, 312pp.

Cloete, M. (1994). Aspects of volcanism and metamorphism of the Onverwacht Group lavas in the southwestern portion of the Barberton greenstone belt. PhD thesis (unpubl.), Univ. Witwatersrand, Johannesburg, 419pp.

Condie, K.C. (1981). Archaean greenstone belts. Developments in Precambrian Geology 3, Elsevier, Amsterdam, 434pp.

Condie, K.C. (1990). Geochemical characteristics of Precambrian basaltic greenstones, 40-55 In: Hall, R.P. and Hughes, D.J. (eds.), Early Precambrian Basic Magmatism. Blackie, Glasgow and London, 486pp.

Condie, K.C., Viljoen, M.J. and Kable, E.J.D. (1977). Effects of alteration on element distributions in Archaean tholeiites from the Barberton greenstone belt, South Africa. Contrib. Mineral. Petrol., 64, 75-89.

Condie, K.C., Bobrow, D.J. and Card, K.D. (1987). Geochemistry of Precambrian mafic dykes from the Southern Superior Province of the Canadian Shield, 95-108. In: Halls, H.C. and Fahrig, W.F. (eds.), Mafic Dyke Swarms. Geol. Ass. Canada. Spec. Paper, 34.

Conway, G.P. (1985). A geochemical study of tholeiitic metabasalts from the Barberton Mountain Land. Honours thesis (unpubl.), Univ. Cape Town, 50pp.

Davies, G., Cawthorn, R.G., Barton, J.M. Jr., and Morton, M. (1980). Parental magma to the Bushveld Complex. Nature, 287, 33-35.

Deer, W.A., Howie, R.A. and Zussman, J. (1982). An Introduction to the Rock-Forming Minerals. Longman, 528pp.

De Wit, M.J. (1982). Gliding and overthrust nappe tectonics in the Barberton greenstone belt. J. Struct. Geol., 4, 117-136.

De Wit, M.J. and Tredoux, M. (1987). PGE in the 3.5 Ga Jamestown Ophiolite Complex, Barberton greenstone belt, with implications for PGE distribution in simatic lithosphere, 319-342. In: Prichard, H.M., Potts, P.J., Bowels, J.F.W., and Cribb, S.J. (Eds.), Geoplat 1987, Elsevier Applied Science.

De Wit, M.J, Fripp, R.E.P. and Stanistreet, I.G. (1983). Tectonic and stratigraphic implications of new field observations along the southern part of the Barberton greenstone belt. Spec. Publ. Geol. Soc. S. Afr. 9, 21-29.

De Wit, M.J., Hart, R.A., and Hart, R.J. (1987a). The Jamestown Ophiolite Complex, Barberton Mountain Land: a section through 3.5 Ga oceanic crust. J. African Earth Sci., 6, (5), 681-730.

De Wit, M.J., Armstrong, R., Hart, R.J. and Wilson, A.H. (1987b). Felsic igneous rocks within the 3.3 to 3.5 Ga Barberton greenstone belt: High crustal level equivalents of the surrounding tonalite-trondhjemite terrain, emplaced during thrusting. Tectonics, 6, 529-549.

De Wit, M.J., Roering, C., Hart, R.J., Armstrong, R.A., De Ronde, C.E.J., Green, R.W.E., Tredoux, M., Peberdy, E. and Hart, R.A. (1992). Formation of an Archaean continent. Nature, 357, 533-537.

Evenson, N.M., Hamilton, P.J. and O'Nions, R.M. (1978). Rare earth abundances in chondritic meteorites. Geochim. Cosmochim. Acta., 42, 1199-1212.

Floyd, P.A. (1991). Oceanic Islands and Seamounts, 174-218. In: Floyd, P.A. (ed). Oceanic Basalts. Blackie, Van Nosrand Reinhold, 456pp.

Gibb, F.G.F. and Henderson, C.M.B. (1992). Convection and crystal settling in sills. Contrib. Mineral. Petrol., 109, 538-545.

Gibson, I.L., Madhurendra, N.S. and Fahrig, W.F. (1987). The geochemistry of the Mackenzie dyke swarm, Canada, 109-121. In: Halls, H.C. and Fahrig, W.F. (eds). Mafic Dyke Swarms. Geol. Assoc. Canada. Spec. Paper, 34.

Glikson, A.Y. and Jahn, B.M. (1985). REE and LIL elements, eastern Kaapvaal Shield, South Africa: Evidence of crustal evolution by 3-stage melting, 303-324. In: Ayres, L.D., Thurston, P.C., Card, K.D., and Weber, W. (eds.), Evolution of Archean Supracrustal Sequences. Geol. Assoc. Canada, Spec. Pap., 28, 380pp.

Goode, A.D.T. (1976). Small-scale primary cumulus igneous layering in the Kalka Layered Intrusion, Giles Complex, Central Australia. J. Petrol. 17(3), 379-397.

Hall, A.L. (1918). The geology of the Barberton gold mining district. Mem. Geol. Surv. S. Afr., 9, 347pp.

Hammerbeck, E.C.I. (1982). The geology of the Usushwana Complex and associated formations - South-Eastern Transvaal. Mem. Geol. Surv. S. Afr., 70, 119 pp.

Hawkesworth, C.J., Marsh, J.S., Duncan, A.R., Erlank, A.J. and Norry, M.J. (1984). The role of continental lithosphere in the generation of the Karoo volcanic rocks: Evidence from combined Nd- and Sr-isotope studies. Spec. Publ. Geol. Soc. S. Afr., 13, 341-354.

Hegner, A., Kroner, A. and Hofmann, A.W. (1984). Age and isotope geochemistry of the Archaean Pongola and Usushwana suites in Swaziland, southern Africa: a case for crustal contamination of mantle-derived magma. Earth Planet. Sci. Lett., 70, 267-279.

Henderson, P. (1984). General geochemical properties and abundances of the rare earth elements, 1-32. In: Henderson, P (ed.), Rare Earth Element Geochemistry. Developments in Geochemistry 2. Elsevier, Amsterdam.

Hess, P.C. (1989). Origins of Igneous Rocks. Harvard University Press, 336pp.

Hunter, D.R. and Reid, D.L. (1987). Mafic dyke swarms in southern Africa, 445-456. In: Halls, H.C. and Fahrig, W.F. (eds.), Mafic Dyke Swarms. Geol. Assoc. Canada. Spec. Pap., 34.

Hunter, R.H. and Sparks, R.S.J. (1987). The differentiation of the Skaergaard Intrusion. Contrib. Mineral. Petrol., 95, 451-461.

Irvine, T.N. (1982). Terminology for layered intrusions. J. Petrol., 23(2), 127-162.

Irvine, T.N. and Ridler, R.H. (1972). Ultramafic and gabbroic bodies. In: Goodwin, A.M. *et al*, The Superior Province, 553-575. In: Price, R.A. and Douglas, R.J.W. (eds.), Variations in Tectonic Styles in Canada. Geol. Assoc. Canada. Spec. Pap. 11.

Jahn, B-M., Gruau, G. and Glikson, A.Y. (1982). Komatiites of the Onverwacht Group: REE geochemistry, Sm/Nd age and mantle evolution. Contrib. Mineral. Petrol, 80, 25-40.

Jaques, A.L. (1976). An Archaean tholeiitic layered sill from Mt Kilkenny, Western Australia. J. Geol. Soc. Aust., 23, 157-168.

Jensen, L.S. (1976). A new cation plot for classifying sub-alkalic volcanic rocks. Ontario Division of Mines, Misc. Pap., 66.

Jolly, W.T. (1977). Relations between Archaean lavas and intrusive bodies of the Abitibi Greenstone Belt, Ontario, Quebec, 311-330. In: Baragar, W.R.A, Coleman, L.C. and Hall, J.M. (eds.), Volcanic Regimes in Canada : Geol. Assoc. Canada. Spec. Pap. 16.

Kamo, S.L. and Davis, D. (1991). A review of geochronology from the Barberton Mountain Land, 59-69. In: Ashwal, L.D. (ed.), Two Cratons and an Orogen - Excursion Guidebook and Review Articles. IGCP Project 280, Dept. of Geology, Univ. Witwatersrand, Johannesburg, 312pp.

Kenyon, A.K, Attridge, R.L, and Coetzee, G.L, (1986). The Uitkomst nickel-copper deposit, Eastern Transvaal, 1009-1017. In: Anhaeusser, C.R., and Maske, S. (eds.), Mineral Deposits of Southern Africa, I. Geol. Soc. S. Afr., Johannesburg.

Kuno, H. (1968). Differentiation of basalt magmas, 623-688. In: Hess, H.H. and Poldervaart, A. (eds.), Basalts. The Poldervaart treatise on rocks of basaltic composition. Vol. 2. Interscience, New York.

Lightfoot, P.C. and Naldrett, A.J. (1984). Chemical variation in the Insizwa Complex, Transkei, and the nature of the parent magma. Can. Mineral., 22, 111-123.

Lowe, D.R., Byerly, G.R., Ranson, B.L. and Nocita, B.W. (1985). Stratigraphic and sedimentological evidence bearing on structural repetition in early Archaean rocks of the Barberton greenstone belt, South Africa. Precambrian Res., 27, 165-186.

Maaloe, S. (1976). The zoned plagioclase of the Skaergaard Intrusion, East Greenland. J. Petrol., 17(3), 398-419.

MacDonald, G.A. and Katsura, T. (1964). Chemical compositions of Hawaiian lavas. J. Petrol., 5, 82-113.

MacLachlan, K. and Helmstaedt, H. (1995). Geology and geochemistry of an Archaean mafic dyke complex in the Chan Formation: basis for a revised plate-tectonic model of the Yellowknife greenstone belt. Can. J. Earth Sci., 32, 614-630.

Mandziuk, W.S., Brisbin, W.C. and Scoates, R.F.J. (1989). Igneous structures in the Falcon Lake Intrusive Complex, Southeastern Manitoba. Canadian Mineralogist., 27, 81-92.

McBirney, A.R. (1996). The Skaergaard Intrusion, 147-180. In: Cawthorn, R.G. (ed.), Layered Intrusions. Developments in Petrology 15. Elsevier, Amsterdam, 531pp.

McCall, G.J.H. and Peers, R. (1971). Geology of the Binneringie Dyke, Western Australia. Geologische Rundschau, 60, 1174-1263.

Menell, R.P, Brewer, T.H, Delve, J.R, and Anhaeusser, C.R. (1986). The Kalkkloof chrysotile asbestos deposit and surrounding area, Barberton Mountain Land, 427-435. In: Anhaeusser, C.R., and Maske, S. (eds.), Mineral Deposits of Southern Africa, I. Geol. Soc. S. Afr., Johannesburg.

Miller, J.D. and Ripley, E.M. (1996). Layered intrusions of the Duluth Complex, Minnesota, USA, 257-301. In: Cawthorn, R.G. (ed.), Layered Intrusions. Developments in Petrology 15. Elsevier, Amsterdam, 531pp.

Naslund, H.R. and McBirney, A.R. (1996). Mechanisms of formation of igneous layering, 1-43. In: Cawthorn, R.G. (ed.), Layered Intrusions. Developments in Petrology 15. Elsevier, Amsterdam, 531pp.

Norrish, K. and Hutton, J.T. (1969). An accurate X-ray spectrographic method for the analysis of a wide range of geological samples. Geochem. Cosmochim. Acta., 33, 431-453.

O'Nions, R.K. and Pankhurst, R.J. (1978). Early Archaean rocks and geochemical evolution of the Earth's crust. Earth Planet. Sci. Lett., 38, 211-236.

Oosthuyzen, E.J. (1970). The geochronology of a suite of rocks from the Granite terrain surrounding the Barberton Mountain Land. Ph.D. thesis (unpubl.), Univ. Witwatersrand, Johannesburg, 94pp.

Pearce, J.A. and Cann, J.R (1973). Tectonic setting of basic volcanic rocks determined using trace element analyses. Earth Planet. Sci. Lett., 19, 290-300.

Pearce, J.A. and Gale, G.H. (1977). Identification of ore deposition environment from trace element geochemistry of associated igneous host rocks. Geol. Soc. Spec. Publ., 7, 14-24.

Pospisek, P. (1991). A geochemical study of the Sterkspruit Gabbro, Eastern Transvaal. Honours thesis (unpubl.), Univ. Witwatersrand, Johannesburg, 74pp.

Ranson, B.L. and Byerly, G.R. (1983). Absence of mafic to felsic volcanic cycles in the Kromberg Formation, Upper Onverwacht Group, west limb of the Onverwacht anticline, Barberton Mountain Land, South Africa. Abstracts. Prog. Geol. Soc. Am., 15, 666pp.

Robb, L.J. (1977). The geology and geochemistry of the Archaean granite-greenstone terrane between Nelspruit and Bushbuckridge, Eastern Transvaal. MSc thesis (unpubl.), Univ. Witwatersrand, Johannesburg, 190pp.

Rodel, J.E. (1993). The petrography and geochemistry of the Stolzburg and Rosentuin layered ultramafic complexes, Barberton Mountain Land, Eastern Transvaal. MSc thesis (unpubl.), Univ. Witwatersrand, Johannesburg, 232pp.

Rollinson, H.R. (1993). Using Geochemical Data: Evaluation, Presentation, Interpretation. Longman, London, 352pp.

Sial, A.N., Oliveira, E.P. and Choudhuri, A. (1987). Mafic dyke swarms of Brazil, 467-481. In: Halls, H.C. and Fahrig, W.F. (eds.), Mafic Dyke Swarms. Geol. Assoc. Canada. Spec. Pap., 34.

Sharpe, M.R. (1981). Petrology and geochemistry of Pre-Bushveld and Waterberg mafic sills. Trans. geol. Soc. S. Afr., 84, 75-83.

South African Committee for Stratigraphy (SACS) (1980). Stratigraphy of South Africa. Part I (Comp. L.E. Kent). Lithostratigraphy of the Republics of South Africa, Namibia, Bophuthatswana, Transkei and Venda. Handbook, Geol. Surv. S. Afr., 8, 690pp.

Smith, H.S. (1980). Aspects of the geochemistry of Onverwacht Group lavas from the Barberton greenstone belt. Ph.D. thesis (unpubl.), Univ. of Cape Town, 425pp.

Smith, H.S. and Erlank, A.J. (1982). Geochemistry and petrogenesis of komatiites from the Barberton greenstone belt, South Africa. In: Arndt, N.T. and Nisbet, E.G. (eds.), Komatiites. George Allen and Unwin, London, 526pp.

Sun, S. and Nesbitt, R.W. (1978). Petrogenesis of Archaean ultrabasic and basic volcanics: evidence from REE's. Contrib. Mineral. Petrol., 65, 301-325.

Tankard, A.J., Jackson, M.P.A., Eriksson, K.A., Hobday, O.K., Hunter, D.R. and Minter, W.E.L. (1982). Crustal Evolution of Southern Africa. Springer-Verlag, New York, 523pp.

Thompson, R.N. (1982). British Tertiary volcanic province. Scott. J. Geol., 18, 49-107.

Thompson, R.N., Morrison, M.A., Dicken, A.P. and Hendry, G.L. (1983). Continental flood basalts. Arachnids rule OK?, 158-185. In: Hawkesworth, C.J. and Norry, M.J. (eds.) Continental Basalts and Mantle Xenoliths. Shiva, Nantwick.

Van Berkel, F. (1977). The geology of the farms Weltevreden 712JT, Weltevreden 697JT and part of Hilversum 696JT, Nelshoogte Schist Belt, Barberton Mountain Land. Unpubl. Rep., Dept. Geol. Univ. Natal, Pietermaritzburg.

Viljoen, M.J. and Viljoen, R.P. (1969a). An introduction to the geology of the Barberton granite-greenstone terrain. Upper Mantle Project. Spec. Publ. Geol. Soc. S. Afr., 2, 9-28.

Viljoen, R.P. and Viljoen, M.J. (1969b). The effects of metamorphism and serpentinisation on the volcanic and associated rocks of the Barberton region. Upper Mantle Project. Spec. Publ. Geol. Soc. S. Afr., 2, 29-53.

Viljoen, M.J. and Viljoen, R.P. (1969c). The geology and geochemistry of the lower ultramafic unit of the Onverwacht Group and a proposed new class of igneous rock. Upper Mantle Project. Spec. Publ. Geol. Soc. S. Afr., 2, 55-85.

Viljoen, R.P. and Viljoen, M.J. (1969d). The geology and geochemistry of the upper formations of the Onverwacht Group. Upper Mantle Project. Spec. Publ. geol. Soc. S. Afr., 2, 113-152.

Viljoen, R.P. and Viljoen, M.J. (1970). The geology and geochemistry of the layered ultramafic bodies of the Kaapmuiden area, Barberton Mountain Land. Spec. Publ. Geol. Soc. S. Afr., 1, 661-688.

Viljoen, M.J., Viljoen, R.P. and Pearton, T.N. (1982). The nature and distribution of Archaean komatiite volcanics in South Africa. In: Arndt, N.T. and Nisbet, E.G. (eds.), Komatiites. George Allen and Unwin, London, 526pp.

Visser, D.J.L. (Compiler) (1956). The geology of the Barberton area. Spec. Publ. Geol. Surv. S. Afr., 15, 253pp.

Visser, H.N. and Verwoerd, W.J. (Compilers) (1960). The geology of the country north of Nelspruit. Explan. Sheet 22, Geol. Surv. S. Afr., 22, 128pp.

Wager, L.R. and Brown, G.M. (1968). Layered Igneous Rocks. Edinburgh: Oliver and Boyd, 588pp.

Ward, J.H.W. (1995). Geology and metallogeny of the Barberton greenstone belt: a survey. J. Afr. Earth Sciences., 21(2), 213-240.

White, C.M., Geist, D.J., Frost, C.D. and Verwoerd, W.J. (1989) Petrology of the Vandfaldsdalen Macrodyke, Skaergaard Region, East Greenland. J. Petrol., 30 (2), 271-298.

Williams, D.A.C. and Furnell, R.G. (1979). Reassessment of part of the Barberton type area, South Africa. Precambrian Res., 9, 325-347.

Wuth, M. (1980). The geology and mineralisation potential of the Oorschot-Weltevreden schist belt, south-west of Barberton, Eastern Transvaal. MSc thesis (unpubl.), Univ. Witwatersrand, Johannesburg, 185pp.

Appendix A :

Table A1 : Whole-rock geochemical data of gabbros from the Sterkspruit Intrusion

Sample	SG1	SG2	SG3	SG4	SG5	SG8	SG11	SG12	SG13	SG14	SG15	SG16	SG17	SG18
wt %														
SiO2	51.64	49.93	51.80	49.62	53.83	51.89	52.96	50.58	54.12	51.23	51.17	50.96	52.66	52.79
TiO2	0.84	0.72	0.75	0.74	2.56	0.69	0.99	0.65	1.20	0.75	0.66	0.82	1.01	0.95
Al2O3	13.91	16.44	16.28	13.73	12.52	15.55	12.18	15.60	13.38	15.04	16.66	16.34	11.91	12.04
Fe2O3(t)	12.04	10.93	10.30	12.31	16.83	10.51	13.12	10.98	12.99	11.22	10.15	10.49	14.01	13.15
MnO	0.18	0.16	0.16	0.18	0.21	0.14	0.17	0.15	0.17	0.17	0.15	0.15	0.19	0.20
MgO	8.62	7.28	7.32	8.36	3.03	7.21	8.40	8.16	6.01	8.34	7.19	6.60	8.87	9.07
CaO	8.06	9.35	9.00	11.84	7.30	8.93	7.48	8.79	8.34	7.63	9.09	9.15	6.85	7.30
Na2O	1.70	1.58	1.74	0.87	2.14	0.98	2.51	1.08	1.79	1.55	1.16	1.56	1.16	1.96
K2O	0.13	0.12	0.40	0.71	0.42	0.10	0.11	0.18	0.08	0.31	0.26	0.06	0.36	0.32
P2O5	0.12	0.14	0.07	0.06	0.16	0.07	0.11	0.08	0.14	0.10	0.09	0.08	0.14	0.11
LOI	2.81	2.93	2.72	2.03	1.22	2.76	2.43	2.94	2.06	2.72	2.76	2.53	2.54	2.24
Total	100.05	99.59	100.53	100.45	100.22	98.82	100.45	99.18	100.28	99.06	99.32	98.74	99.69	100.12
FeO	8.85	8.04	7.57	9.05	12.38	7.73	9.65	8.07	9.55	8.25	7.46	7.71	10.30	9.67
Fe2O3	2.21	2.01	1.89	2.26	3.09	1.93	2.41	2.02	2.39	2.06	1.87	1.93	2.58	2.42
ppm														
Rb	13.42	11.94	24.86	47.03	38.63	10.60	9.78	13.28	10.12	18.43	14.86	7.59	19.21	18.31
Sr	98.11	100.61	131.62	110.67	99.92	97.41	72.02	85.40	87.11	93.46	109.61	107.04	69.06	79.45
Y	20.81	22.16	17.04	20.28	45.77	16.93	30.13	18.39	31.68	17.35	17.04	18.41	24.52	24.75
Zr	44.45	48.82	45.20	30.84	124.06	40.75	85.33	38.85	84.54	40.42	42.66	46.77	59.20	59.44
Nb	5.19	4.29	4.55	4.03	8.01	4.31	4.86	5.03	5.80	3.86	3.78	3.90	4.14	4.47
Co	45.72	45.83	38.04	44.49	32.44	36.60	49.38	39.96	40.60	41.63	37.00	37.29	44.09	45.08
Ni	133.94	124.42	114.68	103.97	2.72	109.22	129.67	123.06	81.54	120.89	102.93	96.53	129.78	131.63
Cu	34.09	154.12	52.17	13.37	17.33	56.39	61.46	16.90	67.40	63.79	32.13	15.54	20.34	64.04
Zn	90.46	87.01	69.18	74.19	103.94	73.56	113.93	75.38	94.82	72.83	76.54	63.56	111.91	118.22
Ba	17.00	8.18	27.42	56.11	21.95	9.18	11.90	7.35	8.26	29.96	18.12	11.26	51.14	43.89
Tl	0.63	0.64	0.65	0.75	2.24	0.57	0.84	0.60	0.93	0.64	0.57	0.69	0.76	0.74
V	243.57	227.57	217.62	322.66	143.85	210.47	264.17	216.85	317.04	235.58	208.44	243.66	286.01	270.69
Cr	299.10	182.33	194.90	37.34	0.00	215.45	264.26	215.89	132.47	252.86	184.12	171.31	269.39	272.84

Table A1 : Whole-rock geochemical data of gabbros from the Sterkspruit Intrusion

Sample	SG19	SG20	SG21	SG22	SG23	SG24	SG25	SG26	SG27	SG28	SG29	SG30	SG31	SG32
wt %														
SiO2	52.22	52.54	53.58	52.63	51.17	51.26	52.45	49.00	50.21	60.60	56.76	53.00	53.68	56.69
TiO2	0.66	1.01	1.40	0.99	0.72	0.73	0.92	1.73	2.21	1.43	1.69	1.47	1.49	1.43
Al2O3	15.04	14.48	12.75	11.89	15.31	16.09	16.68	13.92	12.95	11.55	12.42	12.98	13.17	12.41
Fe2O3(t)	10.75	12.12	14.87	13.95	11.76	10.52	9.73	16.37	16.80	12.68	14.46	15.17	12.89	13.77
MnO	0.17	0.20	0.16	0.20	0.15	0.17	0.14	0.17	0.20	0.18	0.20	0.24	0.25	0.17
MgO	8.22	5.37	4.76	8.92	8.07	7.23	4.88	4.93	4.11	1.36	3.02	4.56	4.83	4.46
CaO	7.78	9.83	7.68	7.08	8.64	9.16	11.47	10.13	9.21	5.93	7.21	8.88	9.23	5.29
Na2O	1.60	2.54	3.24	2.04	1.17	2.47	2.27	2.40	2.28	2.51	2.51	1.23	2.31	3.83
K2O	0.40	0.12	0.17	0.22	0.15	0.13	0.14	0.11	0.07	0.06	0.09	0.07	0.22	0.23
P2O5	0.11	0.13	0.18	0.11	0.07	0.10	0.13	0.09	0.14	0.31	0.22	0.17	0.18	0.20
LOI	2.69	1.85	1.79	2.30	2.89	2.73	1.72	2.16	1.91	3.63	1.85	2.04	2.02	1.90
Total	99.63	100.18	100.39	100.32	100.10	100.60	100.52	101.01	100.09	100.23	100.44	99.81	100.28	100.38
FeO	7.90	8.91	10.93	10.26	8.65	7.74	7.15	12.04	12.35	9.32	10.63	11.15	9.48	10.13
Fe2O3	1.98	2.23	2.73	2.56	2.16	1.93	1.79	3.01	3.09	2.33	2.66	2.79	2.37	2.53
ppm														
Rb	15.94	10.83	13.96	16.19	12.47	10.21	9.22	14.89	16.16	11.73	12.92	15.22	14.66	12.06
Sr	102.28	91.83	91.13	71.73	94.01	97.26	113.93	86.64	85.05	84.14	106.66	122.92	122.38	48.49
Y	18.14	27.71	37.63	24.50	18.38	16.71	22.97	24.19	31.68	67.61	50.04	40.24	43.60	48.30
Zr	46.55	63.96	84.31	61.12	48.75	41.75	51.49	55.16	74.25	161.38	121.58	105.04	106.25	115.36
Nb	4.22	5.08	5.84	5.50	4.74	3.79	4.19	4.59	6.12	9.68	7.95	6.59	7.06	7.31
Co	41.64	38.06	42.43	51.69	43.78	34.60	28.92	46.36	46.75	12.85	35.28	39.00	34.06	38.22
Ni	118.56	64.98	51.97	133.32	122.37	102.92	69.14	57.35	0.00	0.83	10.50	39.51	45.14	36.04
Cu	38.41	35.49	127.00	82.24	68.64	12.58	35.88	219.06	71.36	29.05	23.28	1.81	4.97	19.72
Zn	73.04	80.71	71.40	118.35	125.72	72.15	56.82	82.75	101.24	52.48	42.35	86.45	91.11	44.47
Ba	32.46	16.81	27.48	31.89	10.94	17.11	10.08	9.13	4.00	8.06	7.79	7.23	27.89	25.59
Tl	0.60	0.84	1.05	0.79	0.58	0.59	0.76	1.39	1.70	1.13	1.34	1.20	1.18	1.13
V	213.05	317.67	385.01	278.10	213.94	212.72	257.81	881.46	561.70	27.80	313.57	412.62	387.08	364.47
Cr	206.46	22.12	29.75	282.44	246.42	189.40	122.97	0.00	0.00	0.00	0.00	2.66	23.07	6.17

Table A1 : Whole-rock geochemical data of gabbros from the Sterksprult Intrusion

Sample	SG33	SG34	SG35	SG38	SG39	SG40	SG41	SG42	SG43	SG44	SG45	SG46	SG47	SG48
wt %														
SiO2	54.46	53.41	54.45	52.82	53.54	53.36	52.84	52.10	52.67	51.48	51.43	51.44	50.31	48.20
TiO2	1.41	1.31	1.40	1.34	1.32	1.27	1.07	0.89	0.87	0.76	0.67	0.82	0.76	1.72
Al2O3	13.05	13.57	13.19	13.81	13.16	13.30	12.47	12.65	13.73	14.60	15.61	15.53	16.02	13.55
Fe2O3(t)	13.58	13.18	13.75	15.38	14.11	13.17	13.66	12.88	12.41	11.47	10.71	10.85	10.53	16.98
MnO	0.16	0.18	0.20	0.22	0.20	0.22	0.21	0.22	0.19	0.15	0.16	0.18	0.15	0.17
MgO	4.66	6.05	4.75	4.84	5.12	5.75	7.35	8.40	7.66	7.88	7.87	7.53	6.53	5.76
CaO	6.93	6.70	7.93	7.21	7.56	7.17	7.91	7.27	7.76	8.42	8.37	8.78	9.30	7.83
Na2O	2.98	1.95	2.40	3.39	4.50	4.39	1.98	2.05	1.14	1.20	1.64	1.54	1.48	2.50
K2O	0.21	0.63	0.14	0.09	0.07	0.10	0.05	0.10	0.14	0.14	0.15	0.12	0.03	0.22
P2O5	0.20	0.17	0.20	0.16	0.20	0.22	0.13	0.12	0.12	0.09	0.07	0.07	0.10	0.12
LOI	1.70	2.37	2.10	1.46	1.43	1.42	2.30	2.75	2.46	2.68	2.82	2.85	3.91	1.93
Total	99.33	99.51	100.51	100.70	101.20	100.36	99.96	99.40	99.14	98.86	99.48	99.71	99.11	98.97
FeO	9.99	9.69	10.11	11.31	10.38	9.68	10.04	9.47	9.13	8.43	7.88	7.98	7.74	12.49
Fe2O3	2.50	2.42	2.53	2.83	2.59	2.42	2.51	2.37	2.28	2.11	1.97	1.99	1.94	3.12
ppm														
Rb	11.57	19.47	13.07	13.52	12.32	10.93	12.09	9.87	13.79	13.82	12.21	11.32	8.71	17.15
Sr	72.88	91.91	95.34	91.48	92.73	88.16	88.13	88.58	91.06	97.30	107.10	101.58	111.41	80.99
Y	41.44	37.58	39.52	34.83	39.12	43.92	31.04	25.52	24.28	19.49	17.74	18.73	24.09	26.72
Zr	108.58	99.43	106.11	101.73	100.67	92.56	79.41	61.57	64.26	52.99	39.49	49.29	50.01	60.39
Nb	6.15	6.34	6.25	6.49	7.44	6.28	5.76	4.56	5.54	4.97	4.38	4.71	4.58	5.42
Co	31.64	32.32	32.52	26.28	35.46	34.01	44.34	47.11	48.25	41.89	43.02	35.56	37.06	55.08
Ni	46.90	59.11	48.41	55.48	65.71	66.81	105.73	127.85	120.58	124.88	122.05	109.01	97.41	62.03
Cu	12.41	16.34	99.88	53.23	42.85	51.31	68.92	93.05	53.64	53.31	30.65	17.64	8.86	182.34
Zn	31.10	94.40	108.75	68.57	92.08	92.54	107.46	97.93	87.29	83.89	88.06	85.28	66.55	94.84
Ba	8.75	88.44	9.69	7.76	14.34	15.37	11.36	14.66	20.48	25.93	23.88	15.81	6.87	13.75
Tl	1.21	1.08	1.08	1.20	1.04	0.99	0.80	0.75	0.73	0.65	0.57	0.65	0.60	1.20
V	385.07	354.88	361.09	370.55	346.73	363.20	284.43	261.09	250.43	227.93	211.30	243.57	229.91	948.55
Cr	18.98	63.65	28.77	55.42	74.02	88.00	203.84	265.49	250.14	256.28	248.75	197.01	157.92	0.00

Table A1 : Whole-rock geochemical data of gabbros from the Sterkspruit Intrusion

Sample	SG49	SG50	SG51	SG52	SG53	SG54	SG55	SG56	SG57	SG58	SG59	SG60	SG61	SG63
wt %														
SiO2	51.74	50.09	50.23	54.08	54.94	54.47	53.80	54.62	53.02	54.01	54.37	59.64	53.95	52.26
TiO2	1.31	1.85	1.92	1.48	1.44	1.50	1.34	1.41	1.50	1.33	1.39	1.21	1.39	1.37
Al2O3	14.33	12.70	13.14	12.88	12.95	13.14	13.08	12.97	12.96	13.34	13.00	12.14	13.32	13.43
Fe2O3(t)	12.93	15.98	16.85	14.10	13.27	13.76	12.83	12.68	14.38	13.06	13.81	11.29	13.46	16.00
MnO	0.17	0.20	0.21	0.20	0.17	0.20	0.15	0.19	0.20	0.15	0.20	0.12	0.17	0.17
MgO	5.15	5.78	4.66	4.76	4.66	4.73	5.09	4.62	4.94	4.81	4.76	2.38	4.99	4.82
CaO	9.21	8.63	7.86	8.05	7.29	7.70	7.69	7.97	8.29	7.81	7.30	10.15	7.31	7.26
Na2O	2.22	1.42	3.08	2.33	3.05	1.39	1.92	3.07	1.05	2.60	2.11	0.00	2.03	2.24
K2O	0.12	0.18	0.12	0.08	0.12	0.08	0.31	0.17	0.07	0.23	0.11	0.01	0.09	0.10
P2O5	0.13	0.12	0.11	0.20	0.19	0.17	0.15	0.21	0.17	0.17	0.18	0.25	0.17	0.16
LOI	1.88	2.04	2.10	2.00	2.28	2.03	2.35	2.31	2.09	1.91	2.11	2.19	2.08	1.69
Total	99.20	98.99	100.28	100.14	100.36	99.16	98.70	100.22	98.67	99.41	99.33	99.38	98.85	99.50
FeO	9.51	11.75	12.39	10.37	9.76	10.12	9.43	9.32	10.57	9.60	10.15	8.30	9.90	11.76
Fe2O3	2.38	2.94	3.10	2.59	2.44	2.53	2.36	2.33	2.64	2.40	2.54	2.08	2.47	2.94
ppm														
Rb	12.13	17.02	17.88	12.90	12.92	10.82	13.85	12.38	13.46	13.73	13.06	10.20	11.61	14.38
Sr	124.70	73.75	91.06	92.90	93.81	82.74	82.06	79.12	86.49	80.33	78.90	195.98	86.87	117.27
Y	28.71	26.99	27.49	39.32	41.88	42.26	37.04	38.29	40.49	37.19	42.25	48.64	40.19	29.17
Zr	76.99	58.81	66.52	106.96	114.85	105.47	99.18	95.90	101.30	101.97	108.03	130.25	106.78	100.19
Nb	5.60	4.91	4.97	6.59	6.85	6.65	5.96	6.43	6.10	7.00	7.22	7.28	6.69	6.92
Co	31.04	46.40	39.61	35.38	30.07	32.80	34.76	27.02	32.12	39.19	31.98	21.78	36.67	33.26
Ni	46.70	85.09	5.47	37.18	38.66	46.07	51.71	41.27	49.82	56.35	51.65	10.80	49.99	64.26
Cu	43.84	127.49	92.21	33.02	5.25	14.39	32.41	12.91	15.70	101.87	96.95	101.82	58.52	105.44
Zn	77.13	107.34	101.78	91.10	73.82	80.61	71.01	65.98	112.16	77.68	109.84	43.53	79.29	92.46
Ba	7.97	15.45	26.87	0.92	20.72	16.00	10.12	27.19	8.26	6.42	18.87	-2.51	13.33	4.14
Tl	0.99	1.42	1.51	1.17	1.12	1.12	1.12	1.05	1.15	1.13	1.00	0.97	1.00	1.15
V	402.30	700.07	662.98	392.80	386.01	392.14	350.23	380.63	384.52	345.08	360.90	182.99	370.18	363.94
Cr	9.13	3.74	0.00	7.06	14.19	22.50	53.48	19.18	29.78	51.27	22.02	12.42	37.87	61.46

Table A1 : Whole-rock geochemical data of gabbros from the Sterksprult Intrusion

Sample	SG64	SG65	SG66	SG67	SG68	SG69	SG70	SG71	SG72	SG73
wt %										
SiO2	54.73	54.00	56.26	51.72	51.58	51.40	51.03	51.01	51.69	53.98
TiO2	1.25	1.32	1.27	0.44	0.70	0.70	0.73	0.66	0.86	1.35
Al2O3	13.32	13.26	12.81	10.35	14.26	13.75	15.02	14.71	13.67	13.57
Fe2O3(t)	13.05	12.77	11.74	11.87	11.79	12.28	11.28	11.56	12.47	14.33
MnO	0.19	0.14	0.15	0.11	0.18	0.17	0.15	0.15	0.16	0.17
MgO	5.49	5.68	5.44	10.54	8.65	9.20	8.02	8.66	8.46	4.72
CaO	8.68	7.43	7.73	10.58	8.02	7.77	8.57	8.17	7.37	6.52
Na2O	1.67	1.85	1.63	1.82	1.69	2.42	2.05	2.27	1.99	3.29
K2O	0.13	0.33	0.96	0.10	0.24	0.20	0.31	0.31	0.55	0.07
P2O5	0.19	0.18	0.16	0.06	0.01	0.10	0.10	0.10	0.11	0.16
LOI	1.38	2.23	1.94	1.30	2.29	2.57	2.32	2.58	2.43	1.53
Total	100.08	99.18	100.08	98.89	99.52	100.52	99.58	100.17	99.76	99.68
FeO	9.60	9.39	8.63	8.73	8.67	9.03	8.29	8.50	9.17	10.54
Fe2O3	2.40	2.35	2.16	2.18	2.17	2.26	2.07	2.13	2.29	2.63
ppm										
Rb	14.01	16.98	26.58	11.28	18.17	16.50	20.79	21.84	36.88	10.82
Sr	94.89	105.44	110.42	40.60	88.13	67.63	95.64	86.14	88.75	86.73
Y	39.29	37.66	34.91	19.57	18.40	18.66	18.46	17.93	22.48	36.29
Zr	96.05	102.42	97.13	45.55	38.25	45.95	39.02	43.23	50.45	103.65
Nb	7.54	6.40	5.62	5.10	4.47	5.33	4.26	4.17	5.14	6.91
Co	35.71	26.56	30.45	44.38	41.50	48.89	41.33	45.51	44.05	32.00
Ni	86.24	54.97	48.12	132.75	132.28	135.78	122.62	134.66	123.33	60.64
Cu	56.26	117.60	28.30	147.93	50.07	30.32	49.97	79.00	75.33	64.17
Zn	113.69	76.94	61.84	65.81	77.13	79.15	98.71	86.47	112.38	67.85
Ba	22.53	21.40	54.52	10.72	12.87	8.44	13.10	15.22	39.13	5.53
Tl	0.97	0.97	1.10	0.44	0.66	0.61	0.65	0.59	0.71	1.20
V	312.31	356.95	335.03	245.86	234.77	235.66	237.20	220.62	254.90	376.67
Cr	101.43	52.77	51.91	1262.85	257.08	254.44	231.09	241.10	256.57	58.30

Table A2 : Whole rock geochemical data from the Sterkspruit Mafic Dyke Swarm

Sample	SD1	SD2	SD3	SD4	SD5	SD6	SD7	SD8	SD9	SD10	SD11	SD12	SD13	SD14	SD15	SD16	SD17	SD18
Group	A	A	A	B	B	B	A	-	B	B	B	B	B	B	C	C	D	D
wt %																		
SiO_2	53.62	55.28	55.08	52.93	52.45	52.50	55.08	53.52	53.27	53.19	51.74	52.12	53.44	52.01	49.25	48.87	51.33	53.32
TiO_2	0.35	0.39	0.37	0.30	0.27	0.31	0.41	0.35	0.33	0.31	0.59	0.60	0.38	0.34	0.30	0.26	1.07	1.16
Al_2O_3	16.69	16.43	16.33	13.03	12.03	12.88	16.22	15.23	12.23	12.43	14.43	13.73	13.53	12.43	12.48	11.47	9.23	10.21
$Fe_2O_3(t)$	7.62	8.04	8.18	8.91	9.02	8.62	8.17	8.50	8.37	8.32	9.93	9.56	8.50	8.24	9.13	9.83	11.88	12.10
MnO	0.11	0.12	0.11	0.15	0.16	0.15	0.14	0.17	0.12	0.14	0.16	0.15	0.13	0.12	0.14	0.16	0.15	0.17
MgO	6.04	5.70	5.68	10.64	12.67	11.05	5.23	7.24	11.41	12.35	9.14	9.07	9.32	12.38	12.93	15.72	11.23	9.80
CaO	8.61	8.73	9.25	8.11	8.29	7.91	8.71	9.61	7.40	7.51	7.65	9.17	8.21	7.76	9.44	8.56	9.89	8.36
Na_2O	1.58	2.51	2.11	1.39	1.01	0.82	1.84	2.19	1.20	0.84	2.03	1.34	2.33	1.06	0.72	0.38	0.63	1.70
K_2O	2.42	2.07	1.66	1.89	1.25	1.83	1.60	1.27	1.59	1.57	1.56	1.47	1.43	1.29	0.99	0.73	0.77	1.18
P_2O_5	0.07	0.09	0.09	0.09	0.08	0.09	0.13	0.12	0.10	0.08	0.11	0.12	0.09	0.08	0.07	0.06	0.12	0.14
LOI	1.89	1.91	1.81	2.54	3.15	3.03	1.61	1.44	2.85	3.07	2.52	2.19	2.80	3.19	3.40	2.78	2.29	1.86
Total	98.99	101.27	100.66	99.97	100.37	99.20	99.12	99.61	98.88	99.79	99.86	99.52	100.17	98.91	98.84	98.81	98.60	99.99
FeO	5.82	6.14	6.24	6.80	6.89	6.58	6.24	6.49	6.39	6.35	7.58	7.30	6.49	6.29	6.97	7.50	9.07	9.24
Fe_2O_3	1.16	1.23	1.25	1.36	1.38	1.32	1.25	1.30	1.28	1.27	1.52	1.46	1.30	1.26	1.39	1.50	1.81	1.85
ppm																		
Rb	104.99	73.55	54.43	60.48	43.31	71.40	53.25	30.76	53.56	56.69	51.75	59.63	49.33	46.42	41.89	40.82	28.56	42.66
Sr	278.79	238.71	232.28	141.74	120.52	162.64	266.21	202.31	151.65	121.22	117.72	127.30	169.04	105.46	69.05	105.80	212.65	190.51
Y	19.44	18.92	17.60	19.69	16.77	20.01	18.70	20.36	15.71	15.99	20.42	18.15	18.13	14.84	14.21	13.00	20.65	21.66
Zr	89.32	95.51	93.44	95.19	85.07	90.10	102.87	104.05	79.33	77.45	103.99	87.14	93.41	73.54	48.24	45.59	124.75	134.61
Nb	7.04	7.48	7.46	8.28	8.31	7.75	7.21	8.11	8.06	6.74	7.27	5.66	8.08	6.54	4.60	4.01	7.80	7.95
Co	32.13	32.55	33.91	44.77	54.66	48.91	30.48	36.65	45.35	50.24	48.45	48.13	45.69	51.61	53.21	62.05	61.30	54.04
Ni	139.40	131.25	126.95	390.66	509.34	417.36	106.38	151.87	445.86	550.92	315.39	254.32	352.57	532.51	521.14	660.06	553.14	379.65
Cu	27.56	20.67	28.34	19.15	18.26	19.77	28.44	34.54	22.74	25.08	42.99	51.25	32.25	30.85	40.16	31.00	129.62	103.45
Zn	62.62	58.89	65.13	63.88	73.50	65.77	69.88	67.55	58.60	66.32	76.73	70.95	65.78	59.77	64.57	60.26	74.48	80.62
Ba	311.67	325.69	260.72	312.33	202.47	330.70	300.45	361.89	212.40	204.74	219.28	205.56	224.92	187.34	143.76	77.88	224.06	316.67
Tl	0.33	0.38	0.32	0.30	0.26	0.28	0.37	0.34	0.32	0.30	0.53	0.52	0.37	0.32	0.27	0.27	0.97	1.06
V	99.11	107.85	102.66	147.98	132.43	137.91	103.77	131.73	108.61	109.51	120.39	144.12	116.57	118.72	130.84	121.46	195.91	201.42
Cr	251.75	223.24	206.82	1010.73	1418.43	1128.73	170.17	293.99	1457.47	1640.52	711.76	957.74	1079.77	1418.70	1787.91	2260.53	1136.1	946.54
Tl/Zr	23	24	24	19	19	21	24	20	25	24	34	41	24	28	37	34	51	52
Tl/Y	108	124	126	91	97	93	131	103	126	116	173	198	126	137	127	120	311	321
Zr/Y	4.6	5.0	5.3	4.8	5.1	4.5	5.5	5.1	5.0	4.8	5.1	4.8	5.2	5.0	3.4	3.5	6.0	6.2
Zr/Nb	12.7	12.8	12.5	11.5	10.2	11.6	14.3	12.8	9.8	11.5	14.3	15.4	11.6	11.2	10.5	11.4	16.0	16.9
mg#	65	62	62	74	77	75	60	67	76	78	68	69	72	78	77	79	69	65

$Fe_2O_3(t)$: Total Fe as Fe_2O_3 FeO calculated using Fe2O3/FeO ratio = 0.2

mg# : 100 $[Mg^{2+}/ Mg^{2+} + Fe^{2+}]$

Table A3 : Whole-rock compositions of tholeiitic and andesitic basalts from the Kromberg Formation (Conway, 1985)

sample	GH4	GH5	GH6	GH9	GH10	GH11	GH12	GH13	GH14	GH16	GH17	GH18	GH22	GH30	GH31
	Tholeiitic Basalts														
wt %															
SiO_2	49.2	50.5	51.7	52.1	52.8	58.9	52.3	52.8	58.4	55.5	50.3	51.9	50.1	51.9	50.5
TiO_2	1.4	1.4	1.8	1.6	1.6	1.5	1.4	1.4	1.4	1.4	1.3	1	1.3	1.1	1.3
Al_2O_3	14.3	14	13.4	14.8	14.6	13.5	13.8	15.4	13.7	15	15.3	15.5	14.3	12.4	14.4
FeO	11.47	10.9	11.75	10.12	9.39	5.56	7.72	7.55	6.95	7.44	10.09	6.15	11.09	7.82	10.02
Fe_2O_3	3.57	3.39	3.66	3.15	2.92	1.73	2.4	2.35	2.16	2.32	3.14	1.92	3.45	2.43	3.12
MnO	0.2	0.2	0.2	0.2	0.2	0.2	0.2	0.2	0.2	0.2	0.2	0.2	0.2	0.1	0.2
MgO	5.92	5.36	4.41	5.2	6.3	2.7	4.7	4.3	4	3.9	4.6	6.7	5.4	6	6.1
CaO	8.6	8.9	5.4	7.2	4.6	5.4	7.4	5.7	5.2	6.5	9.2	6.1	11.1	12.3	8.2
Na_2O	2.07	2.6	3.74	2.21	1.84	3.03	3.09	3.66	3.62	4.07	3.77	1.95	0.77	4.19	3.43
K_2O	0.08	0.19	0.57	0.16	0.58	1.86	0.24	0.46	0.27	0.38	0.27	4.76	0.05	0.24	0.41
P_2O_5	0.16	0.16	0.22	0.16	0.18	0.18	0.16	0.16	0.16	0.16	0.14	0.07	0.14	0.12	0.14
LOI	2.7	2.3	1.8	3.4	4.9	4.8	5.6	4.7	3.2	2.2	2.1	3.5	2.8	1.9	2.1
Total	99.8	100.0	98.8	100.3	99.8	99.5	98.9	98.8	99.3	99.1	100.4	99.8	100.7	100.7	99.9
ppm															
Rb	2	5	13	4	16	38	5	10	5	6	5	78	2	3	6
Sr	133	137	41	180	93	122	160	139	65	78	104	91	156	56	85
Y	35	36	47	32	36	34	35	33	30	30	29	16	29	23	28
Zr	92	97	127	107	121	106	104	108	100	99	91	73	87	68	92
Nb	3.5	3.4	3.9	3.1	3.7	4.8	5.4	5.1	4.7	3.5	4.9	3.6	3.6	2.5	3.4
Co	63	55	53	45	41	54	41	37	38	37	49	70	61	47	60
Ni	129	113	55	81	72	104	44	47	41	49	65	153	65	115	111
Cu	127	164	128	194	103	169	166	165	149	4	82	6	68	5	29
Zn	123	114	101	127	93	138	111	146	91	95	86	89	87	39	62
Ba	11	32	29	24	61	120	20	37	35	21	23	320	19	24	53
V	381	391	459	319	320	317	343	346	334	333	335	330	307	258	314
Cr	134	115	20	125	98	90	12.3	13	11	12	45	355	15	157	84
Ti/Zr	92	86	86	88	78	83	80	79	81	82	85	83	89	93	85
Ti/Y	242	232	234	294	263	257	239	260	267	271	270	384	263	267	281
Zr/Y	2.6	2.7	2.7	3.3	3.4	3.1	3.0	3.3	3.3	3.3	3.1	4.6	3.0	3.0	3.3
Zr/Nb	26	29	33	35	33	22	19	21	21	28	19	20	24	27	27
Mg#	48	47	40	48	54	46	52	50	51	48	45	66	47	58	52

Table A3 : Whole-rock compositions of tholeiitic and andesitic basalts from the Kromberg Formation (Conway, 1985)

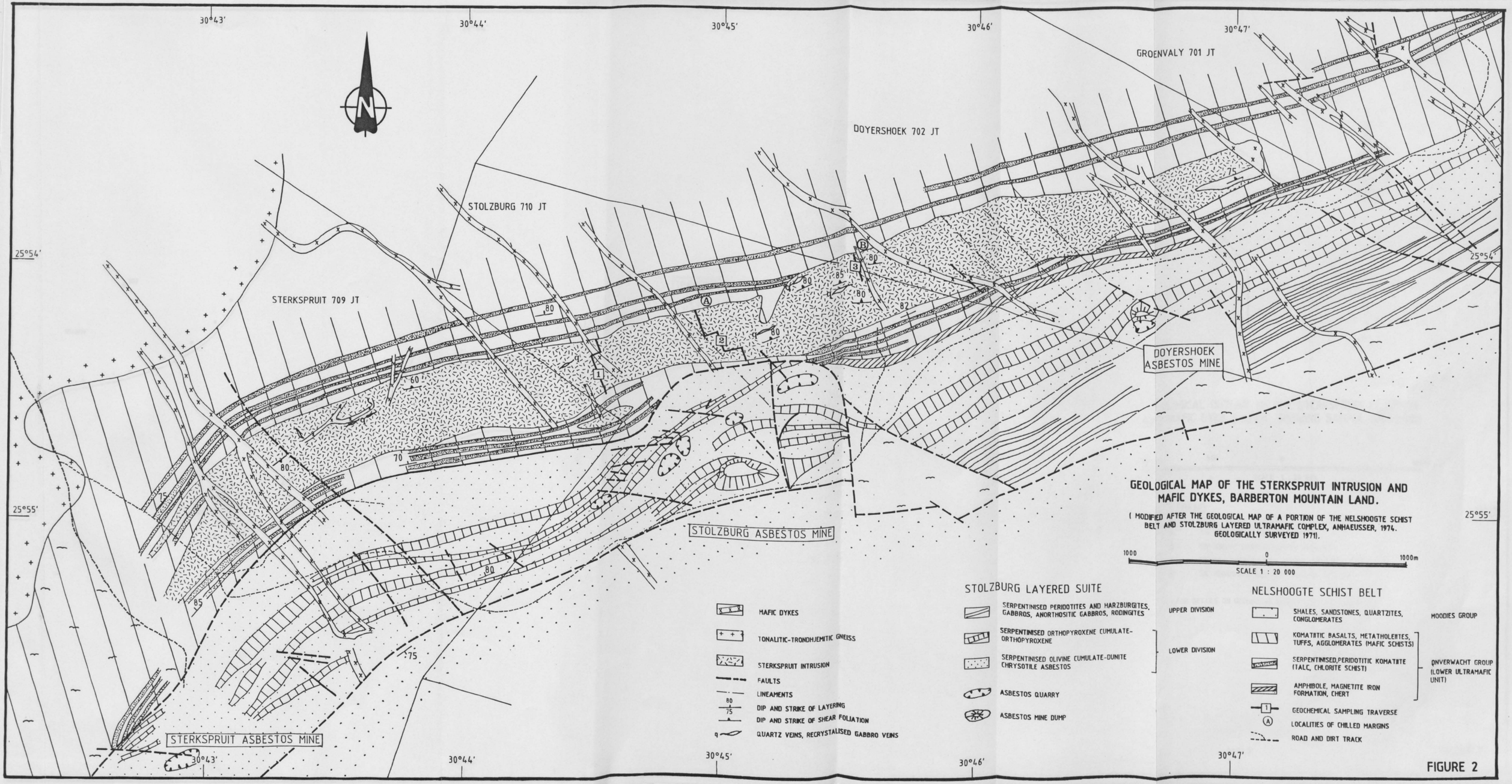
sample	GH32	GH37	GH39	GH42	GH46	GH47	GH48	GH49	GH50	GH100	GH101	GH102	GH29	GH43	GH53
	Tholeiitic Basalts												Andesitic Basalts		
wt %															
SiO_2	47.6	50	50.2	45.5	56.1	50.2	49	50.7	51	48	51.2	52	52.1	64	58.1
TiO_2	1.2	1.1	0.97	1.8	1.5	1	1.1	1.2	1.1	1.2	1.8	1.7	1.6	1.4	1.6
Al_2O_3	13.2	13.6	14.8	14.9	15	12.6	13	14.3	14.1	13.4	13.7	15.3	14.2	13.2	11.9
FeO	11.62	10.06	10.36	11.38	8.44	9.05	9.59	10.78	10.2	11.33	11.21	11.76	8.45	6.63	8.31
Fe_2O_3	3.62	3.13	3.22	3.54	2.63	2.82	2.99	3.36	3.18	3.53	3.49	3.66	2.63	2.07	2.59
MnO	0.2	0.2	0.2	0.2	0.1	0.2	0.2	0.2	0.2	0.2	0.2	0.2	0.2	0.1	0.2
MgO	5.5	8.2	7.8	6.4	4.4	7	9.3	6.1	3.4	4.9	3.9	5.8	3.65	3.61	4.06
CaO	9.1	7.2	5.16	5.2	2.7	8.5	8.9	7.1	8.1	10.7	7.1	2.9	9.58	1.3	5.6
Na_2O	1.88	2.17	2.54	2.37	3.64	1.71	0.09	3.16	1.96	0.95	2.88	2.29	4.7	3.5	2.53
K_2O	0.93	1.07	0.5	0.27	0.52	0.4	3.18	0.29	1.25	0.8	0.37	0.23	0.23	0.71	0.01
P_2O_5	0.13	0.12	0.1	0.21	0.16	0.13	0.13	0.13	0.12	0.17	0.19	0.19	0.23	0.29	0.52
LOI	4.7	2.8	3.1	6.7	4.1	5.9	2.7	2.2	5.1	4.8	3.8	3.1	2.2	2.4	4.5
Total	99.7	99.6	99.1	98.8	99.5	99.8	100.3	99.5	99.7	100.1	99.7	99.1	99.9	99.3	99.9
ppm															
Rb	17	17	9	9	7	9	72	6	27	12	15	4	3	9	–
Sr	507	136	109	36	42	126	177	154	270	369	181	97	76	26	138
Y	27	25	23	34	27	27	29	29	27	27	34	34	39	40	82
Zr	79	78	73	147	112	88	91	85	85	114	134	129	171	220	282
Nb	2.1	2.6	4	7.1	4.4	3.9	2.5	3.2	3.8	4.4	6.2	5.2	8.3	9.4	16.1
Co	69	63	72	44	56	64	62	62	62	78	68	54	45	32	30
Ni	51	132	80	26	98	148	176	73	36	131	32	48	48	25	-
Cu	65	98	98	45	128	89	80	63	66	112	20	94	127	54	12
Zn	98	91	121	188	120	86	90	102	105	89	85	126	46	148	88
Ba	184	144	43	18	60	40	325	18	115	179	45	44	22	61	6
V	230	290	246	351	346	276	292	292	276	223	315	319	251	94	126
Cr		174	60		17	253	300	39	9	13	3	14	10		
Ti/Zr	90	85	80	74	80	71	71	83	77	65	79	78	56	38	35
Ti/Y	264	263	255	318	336	230	223	247	242	273	313	295	244	208	119
Zr/Y	2.9	3.1	3.2	4.3	4.1	3.3	3.1	2.9	3.1	4.2	3.9	3.8	4.4	5.5	3.4
Zr/Nb	38	30	18	21	25	23	36	27	22	26	22	25	21	23	18
Mg#	46	59	57	50	48	58	63	50	37	44	38	47	44	49	47

Table A4 : Average Rare Earth Element Abundances in C1 Chondritic Meteorites (Evensen *et al.*, 1978)

Element	Chondrite ppm
La	0.24
Ce	0.64
Pr	0.1
Nd	0.47
Sm	0.15
Eu	0.06
Gd	0.2
Tb	0.04
Dy	0.25
Ho	0.06
Er	0.17
Tm	0.03
Yb	0.17
Lu	0.03

Table A5 : Chondrite normalised data used in the calculation of spider diagrams from Thompson (1982) and Hawkesworth *et al.* (1984)

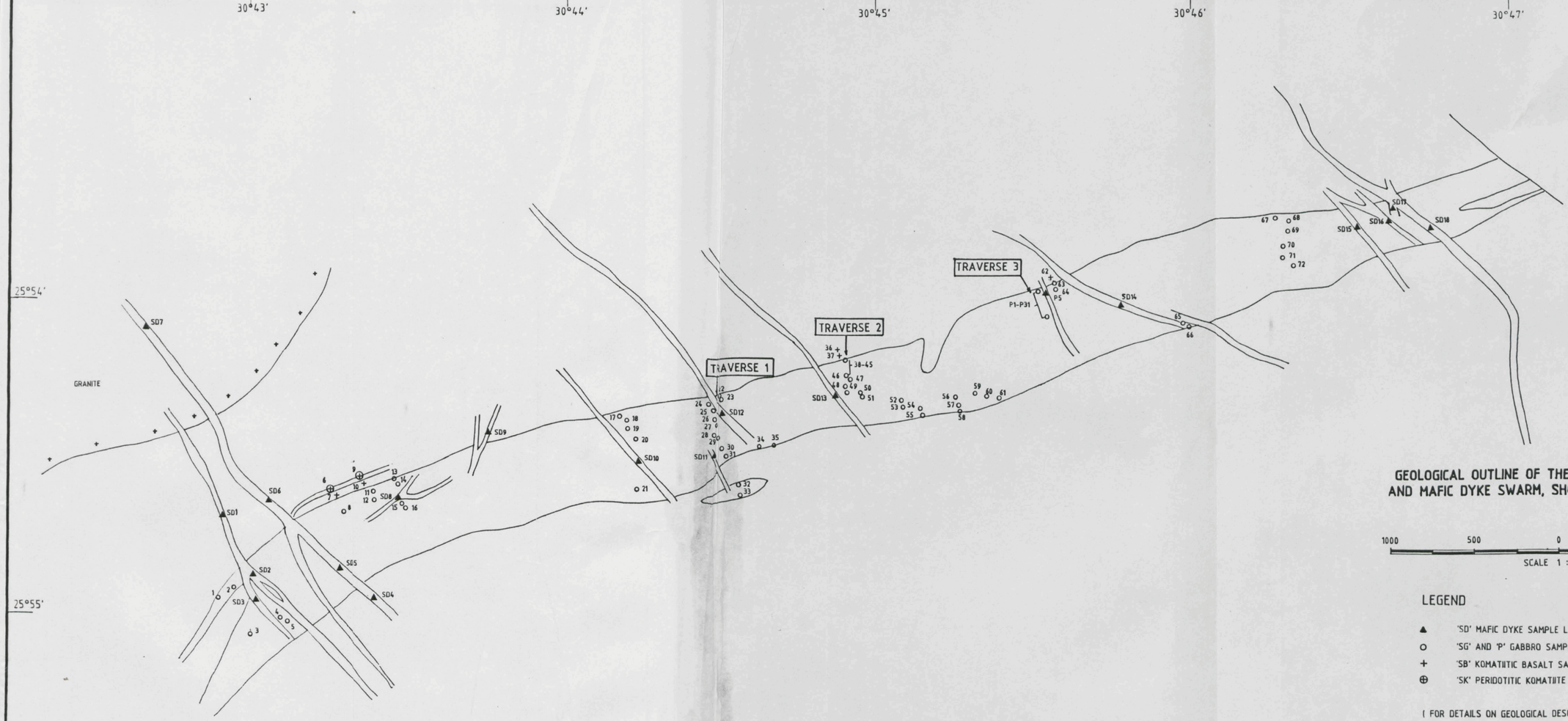
Element	Chondrite ppm
Ba	3.85
Rb	0.35
Th	0.04
K	120
Nb	0.35
Ta	0.02
La	0.33
Ce	0.87
Sr	11.8
Nd	0.63
P	46
Sm	0.2
Zr	6.84
Hf	0.2
Ti	620
Tb	0.05
Y	2
Tm	0.03
Yb	0.22



GEOLOGICAL MAP OF THE STERKSPRUIT INTRUSION AND MAFIC DYKES, BARBERTON MOUNTAIN LAND.

(MODIFIED AFTER THE GEOLOGICAL MAP OF A PORTION OF THE NELSHOOGTE SCHIST BELT AND STOLZBURG LAYERED ULTRAMAFIC COMPLEX, ANHAEUSSER, 1974. GEOLOGICALLY SURVEYED 1971).

FIGURE 2



GEOLOGICAL OUTLINE OF THE STERKSPRUIT INTRUSION AND MAFIC DYKE SWARM, SHOWING SAMPLE LOCALITIES

LEGEND

- ▲ 'SD' MAFIC DYKE SAMPLE LOCALITY
- o 'SG' AND 'P' GABBRO SAMPLE LOCALITY
- \+ 'SB' KOMATIITIC BASALT SAMPLE LOCALITY
- ⊕ 'SK' PERIDOTITIC KOMATIITE SAMPLE LOCALITY

(FOR DETAILS ON GEOLOGICAL DESCRIPTIONS SEE FIGURE 2)

FIGURE 3